

Recent developments in neuroimaging in mood disorders

Edited by

Jigar Jogia, Chien-Han Lai, Keita Watanabe
and Reiji Yoshimura

Published in

Frontiers in Psychiatry



FRONTIERS EBOOK COPYRIGHT STATEMENT

The copyright in the text of individual articles in this ebook is the property of their respective authors or their respective institutions or funders. The copyright in graphics and images within each article may be subject to copyright of other parties. In both cases this is subject to a license granted to Frontiers.

The compilation of articles constituting this ebook is the property of Frontiers.

Each article within this ebook, and the ebook itself, are published under the most recent version of the Creative Commons CC-BY licence. The version current at the date of publication of this ebook is CC-BY 4.0. If the CC-BY licence is updated, the licence granted by Frontiers is automatically updated to the new version.

When exercising any right under the CC-BY licence, Frontiers must be attributed as the original publisher of the article or ebook, as applicable.

Authors have the responsibility of ensuring that any graphics or other materials which are the property of others may be included in the CC-BY licence, but this should be checked before relying on the CC-BY licence to reproduce those materials. Any copyright notices relating to those materials must be complied with.

Copyright and source acknowledgement notices may not be removed and must be displayed in any copy, derivative work or partial copy which includes the elements in question.

All copyright, and all rights therein, are protected by national and international copyright laws. The above represents a summary only. For further information please read Frontiers' Conditions for Website Use and Copyright Statement, and the applicable CC-BY licence.

ISSN 1664-8714
ISBN 978-2-8325-4574-4
DOI 10.3389/978-2-8325-4574-4

About Frontiers

Frontiers is more than just an open access publisher of scholarly articles: it is a pioneering approach to the world of academia, radically improving the way scholarly research is managed. The grand vision of Frontiers is a world where all people have an equal opportunity to seek, share and generate knowledge. Frontiers provides immediate and permanent online open access to all its publications, but this alone is not enough to realize our grand goals.

Frontiers journal series

The Frontiers journal series is a multi-tier and interdisciplinary set of open-access, online journals, promising a paradigm shift from the current review, selection and dissemination processes in academic publishing. All Frontiers journals are driven by researchers for researchers; therefore, they constitute a service to the scholarly community. At the same time, the *Frontiers journal series* operates on a revolutionary invention, the tiered publishing system, initially addressing specific communities of scholars, and gradually climbing up to broader public understanding, thus serving the interests of the lay society, too.

Dedication to quality

Each Frontiers article is a landmark of the highest quality, thanks to genuinely collaborative interactions between authors and review editors, who include some of the world's best academicians. Research must be certified by peers before entering a stream of knowledge that may eventually reach the public - and shape society; therefore, Frontiers only applies the most rigorous and unbiased reviews. Frontiers revolutionizes research publishing by freely delivering the most outstanding research, evaluated with no bias from both the academic and social point of view. By applying the most advanced information technologies, Frontiers is catapulting scholarly publishing into a new generation.

What are Frontiers Research Topics?

Frontiers Research Topics are very popular trademarks of the *Frontiers journals series*: they are collections of at least ten articles, all centered on a particular subject. With their unique mix of varied contributions from Original Research to Review Articles, Frontiers Research Topics unify the most influential researchers, the latest key findings and historical advances in a hot research area.

Find out more on how to host your own Frontiers Research Topic or contribute to one as an author by contacting the Frontiers editorial office: frontiersin.org/about/contact

Recent developments in neuroimaging in mood disorders

Topic editors

Jigar Jogia — University of Birmingham, United Kingdom

Chien-Han Lai — National Yang-Ming University, Taiwan

Keita Watanabe — Kyoto Prefectural University, Japan

Reiji Yoshimura — University of Occupational and Environmental Health Japan,
Japan

Citation

Jogia, J., Lai, C.-H., Watanabe, K., Yoshimura, R., eds. (2024). *Recent developments in neuroimaging in mood disorders*. Lausanne: Frontiers Media SA.

doi: 10.3389/978-2-8325-4574-4

Table of contents

- 05 **Editorial: Recent developments in neuroimaging in mood disorders**
Keita Watanabe, Jigar Jogia and Reiji Yoshimura
- 08 **Gyrification patterns in first-episode, drug-naïve major depression: Associations with plasma levels of brain-derived neurotrophic factor and psychiatric symptoms**
Tomoya Natsuyama, Naomichi Okamoto, Keita Watanabe, Enkhmurun Chibaatar, Hirofumi Tesen, Gaku Hayasaki, Atsuko Ikenouchi, Shingo Kakeda and Reiji Yoshimura
- 18 **Stress-related reduction of hippocampal subfield volumes in major depressive disorder: A 7-Tesla study**
Judy Alper, Rui Feng, Gaurav Verma, Sarah Rutter, Kuang-han Huang, Long Xie, Paul Yushkevich, Yael Jacob, Stephanie Brown, Marin Kautz, Molly Schneider, Hung-Mo Lin, Lazar Fleysheer, Bradley N. Delman, Patrick R. Hof, James W. Murrough and Priti Balchandani
- 26 **Face-specific negative bias of aesthetic perception in depression: Behavioral and EEG evidence**
Zhitang Chen, Zhenghua Wang, Yuhua Shen, Suhua Zeng, Xiangyu Yang, Yifang Kuang, Zheng Dou, Lihui Wang and Weidong Li
- 35 **Amygdala's T1-weighted image radiomics outperforms volume for differentiation of anxiety disorder and its subtype**
Qingfeng Li, Wenzheng Wang and Zhishan Hu
- 46 **Volumetric assessment of individual thalamic nuclei in patients with drug-naïve, first-episode major depressive disorder**
Enkhmurun Chibaatar, Keita Watanabe, Naomichi Okamoto, Nasanbadrakh Orkhonselenge, Tomoya Natsuyama, Gaku Hayakawa, Atsuko Ikenouchi, Shingo Kakeda and Reiji Yoshimura
- 57 **Electrophysiological evidence for the characteristics of implicit self-schema and other-schema in patients with major depressive disorder: An event-related potential study**
Jia-yu Yao, Zi-wei Zheng, Yi Zhang, Shan-shan Su, Yuan Wang, Jing Tao, Yi-hua Peng, Yan-ru Wu, Wen-hui Jiang and Jian-yin Qiu
- 70 **Preliminary findings on the effect of childhood trauma on the functional connectivity of the anterior cingulate cortex subregions in major depressive disorder**
Bei Rong, Guoqing Gao, Limin Sun, Mingzhe Zhou, Haomian Zhao, Junhua Huang, Hanling Wang, Ling Xiao and Gaohua Wang
- 82 **The efficacy and cerebral mechanism of intradermal acupuncture for major depressive disorder: a study protocol for a randomized controlled trial**
Xiaoting Wu, Mingqi Tu, Nisang Chen, Jiajia Yang, Junyan Jin, Siying Qu, Sangsang Xiong, Zhijian Cao, Maosheng Xu, Shuangyi Pei, Hantong Hu, Yinyan Ge, Jianqiao Fang and Xiaomei Shao

- 92 **Abnormal dynamic functional network connectivity in patients with early-onset bipolar disorder**
Ziyi Hu, Chun Zhou and Laichang He
- 102 **Human emotion processing accuracy, negative biases, and fMRI activation are associated with childhood trauma**
Alexis A. Reisch, Katie L. Bessette, Lisanne M. Jenkins, Kristy A. Skerrett, Laura B. Gabriel, Leah R. Kling, Jonathan P. Stange, Kelly A. Ryan, Mindy Westlund Schreiner, Sheila E. Crowell, Erin A. Kaufman and Scott A. Langenecker



OPEN ACCESS

EDITED AND REVIEWED BY
Paul Stokes,
King's College London, United Kingdom

*CORRESPONDENCE
Keita Watanabe
✉ kw0928@koto.kpu-m.ac.jp

RECEIVED 16 January 2024
ACCEPTED 15 February 2024
PUBLISHED 28 February 2024

CITATION
Watanabe K, Jogia J and Yoshimura R (2024)
Editorial: Recent developments in
neuroimaging in mood disorders.
Front. Psychiatry 15:1371347.
doi: 10.3389/fpsyt.2024.1371347

COPYRIGHT
© 2024 Watanabe, Jogia and Yoshimura. This
is an open-access article distributed under the
terms of the [Creative Commons Attribution
License \(CC BY\)](#). The use, distribution or
reproduction in other forums is permitted,
provided the original author(s) and the
copyright owner(s) are credited and that the
original publication in this journal is cited, in
accordance with accepted academic
practice. No use, distribution or reproduction
is permitted which does not comply with
these terms.

Editorial: Recent developments in neuroimaging in mood disorders

Keita Watanabe^{1*}, Jigar Jogia² and Reiji Yoshimura³

¹Department of Radiology, Kyoto Prefectural University of Medicine, Kyoto, Japan, ²School of Psychology, University of Birmingham, Dubai, United Arab Emirates, ³Department of Psychiatry, University of Occupational and Environmental Health, Kitakyushu, Japan

KEYWORDS

mood disorder, major depressive disorder, neuroimaging, VBM, brain network

Editorial on the Research Topic

Recent developments in neuroimaging in mood disorders

MRI technology began to be used in hospitals in the 1980s. MRI has not only revolutionized the diagnosis of acute cerebral infarction and cerebral hemorrhage but has also increasingly been employed to visually assess neurodegenerative diseases. The 2000s saw a continuous improvement in MRI image quality. Along with the development of 3D T1-weighted imaging (T1WI) with a spatial resolution of 1-2mm iso voxel, the volumetric measurement of brain structures, such as the hippocampus, advanced from manual region of interest methods to automated measurements using neuroimaging software like FreeSurfer and FMRIB Software library (FSL) (1, 2). The technique of voxel-based morphometry using Statistical Parametric Mapping (SPM) (3), which evaluates brain structures on a voxel-by-voxel basis, also progressed the field further. Additionally, the advent of functional MRI allowed for real-time visualization of active brain regions. The development of diffusion tensor imaging not only visualized white matter tracts but also enabled their quantitative analysis. These technologies confirmed organic brain changes in mood disorders, including major depressive disorder and Bipolar disorder.

Currently, MRI and neuroimaging techniques continue to evolve. With the latest MRI models, ultra-high-resolution imaging of less than 1mm, specifically 7T MRI, marks a transformative era in precision psychiatry, thanks to its unparalleled spatial resolution and signal-to-noise ratio. This leap in technology allows for individualized examinations, capturing the nuances of single participants' brain structures and activities with great detail. The advanced capabilities of 7T MRI in detecting subtle neurobiological changes are guiding research towards individualized psychiatric treatment plans, based on the unique brain structure or connectivity patterns of individuals (4). A manuscript in this Research Topic, "Stress-related reduction of hippocampal subfield volumes in major depressive disorder: A 7-Tesla study", demonstrates that specific hippocampal subfield volumes, such as CA2/3, were reduced in people with major depressive disorder (MDD) compared to controls, and reductions in other subfields correlated with lifetime stressors (Alper et al.). The changes in specific hippocampal subfields may reflect underlying neurobiological characteristics of MDD, offering potential biomarkers for its diagnosis and for assessing treatment resistance.

While 7T MRI marks a technological advancement in MRI capabilities, the evolution of analysis techniques in 3T MRI systems is similarly advancing our ability to conduct detailed regional brain analyses (5). The features also include analyses dividing the cingulate gyrus and thalamus into subregions (6, 7). The study titled “*Amygdala’s T1-weighted image radiomics outperforms volume for differentiation of anxiety disorder and its subtype*” utilizes radiomics analysis to extract image features like texture and shape, aiming to detect subtle differences in amygdala impairments among anxiety disorder subtypes (Li et al.). Moreover, recent advances in cerebral cortical analysis introduced metrics (8), such as the Gyrification index and fractal coefficient, to evaluate the complexity of cortical structures, one example being the study “*Gyrification patterns in first-episode, drug-naïve major depression: Associations with plasma levels of brain-derived neurotrophic factor and psychiatric symptoms.*” (Natsuyama et al.). In addition to elucidating brain impairments in mood disorders, these new neuroimaging techniques are also expected to quantify therapeutic effects and provide deeper insights into the mechanisms of action of treatments. In “*The efficacy and cerebral mechanism of intradermal acupuncture for major depressive disorder: a study protocol for a randomized controlled trial,*” the protocol for a randomized controlled trial is described (Wu et al.). Utilizing the developed neuroimaging techniques, future research aims to validate the efficacy of intradermal acupuncture for major depressive disorder and elucidate its cerebral mechanism of action.

Resting-state functional MRI (fMRI) has also seen significant progress. The discovery of the three major networks - default mode network, salience network, and central executive network - in resting-state fMRI can be considered one of the most crucial advances in neuroscience since the 2000s (9). Initial analyses of Resting state functional MRI were based on the premise that connectivity during rest was constant, but recent research delves into the dynamic changes in connectivity (10). The study “*Abnormal dynamic functional network connectivity in people with early-onset bipolar disorder*” investigates the temporal changes in resting connectivity in early-onset bipolar disorder (Hu et al.). The authors reported people with early-onset BD had abnormal dynamic properties of brain functional network connectivity, which is indicative of unstable functional brain network connectivity. This was demonstrated through impaired coordination between cognitive and perceptual networks. Task-based fMRI has evolved, with a surge in studies using diverse cognitive tasks and emotional challenges.

In addition to MRI, there have been advancements in Electroencephalography (EEG) characterized by an increase in electrode count leading to higher resolution, as well as progress in cognitive tasks and emotional assignments. The study titled “*Electrophysiological Evidence for the Characteristics of Implicit Self-Schema and Other-Schema in Patients with Major Depressive Disorder: An Event-Related Potential Study*” investigated the neural correlates of self- and other-schemas in people with MDD (Yao et al.). The findings suggest that individuals with MDD exhibit distinct neural patterns, potentially reflecting a lack of positive self- and other-schemas and provide insights into the neural mechanisms underlying MDD, highlighting the importance of

considering both self- and other-schemas in understanding and treating the disorder. Moreover, the research “*Face-specific negative bias of aesthetic perception in depression: behavioral and EEG evidence*” delved into the bias in aesthetic judgments in individuals with depression (Chen et al.). The aesthetic evaluation of unattractive faces was associated with decreased N200 negativity in the depression compared to controls, whereas the evaluation of beautiful faces was linked with decreased brain synchronization at the theta band. These findings are important for suggested design and development of aesthetics-oriented schemes in assisting the clinical diagnosis and therapy of MDD.

The objective of our present topic theme, which focuses on recent developments in neuroimaging in mood disorders, is to gain deeper insights into the cerebral alterations in mood disorders using newly proposed neuroimaging techniques. The research in this Research Topic enhances our understanding of brain changes in mood disorders, potentially guiding future efforts to identify early biomarkers, understand the natural progression of mood disorders, and develop targeted interventions from the outset of diagnosis. Further, this Research Topic includes several studies on people with first-episode and drug-naïve MDD, highlighting the pivotal role of neuroimaging in this nascent and critical area of research. As neuroimaging technology advances, the importance of investigating first-episode and drug-naïve MDD becomes increasingly apparent, providing unique insights into the neurobiological underpinnings of the disorder before the potential confounding effects of treatment.

Author contributions

KW: Writing – original draft, Writing – review & editing. JJ: Writing – review & editing. RY: Writing – review & editing.

Acknowledgments

We thank Chien-Han Lai for their invaluable contributions and collaborative efforts as co-editors on this Research Topic.

Conflict of interest

The authors declare that the research was conducted in the absence of any commercial or financial relationships that could be construed as a potential conflict of interest.

Publisher’s note

All claims expressed in this article are solely those of the authors and do not necessarily represent those of their affiliated organizations, or those of the publisher, the editors and the reviewers. Any product that may be evaluated in this article, or claim that may be made by its manufacturer, is not guaranteed or endorsed by the publisher.

References

1. Jenkinson M, Beckmann CF, Behrens TE, Woolrich MW, Smith SM. FSL. *Neuroimage*. (2012) 62:782–90. doi: 10.1016/j.neuroimage.2011.09.015
2. Fischl B. FreeSurfer. *Neuroimage*. (2012) 62:774–81. doi: 10.1016/j.neuroimage.2012.01.021
3. Ashburner J. SPM: a history. *Neuroimage*. (2012) 62:791–800. doi: 10.1016/j.neuroimage.2011.10.025
4. Neuner I, Veselinović T, Ramkiran S, Rajkumar R, Schnellbaeher GJ, Shah NJ. 7T ultra-high-field neuroimaging for mental health: an emerging tool for precision psychiatry? *Trans Psychiatry*. (2022) 12:36. doi: 10.1038/s41398-022-01787-3
5. Iglesias JE, Augustinack JC, Nguyen K, Player CM, Player A, Wright M, et al. A computational atlas of the hippocampal formation using ex vivo, ultra-high resolution MRI: Application to adaptive segmentation of *in vivo* MRI. *Neuroimage*. (2015) 115:117–37. doi: 10.1016/j.neuroimage.2015.04.042
6. Saygin ZM, Kliemann D, Iglesias JE, van der Kouwe AJW, Boyd E, Reuter M, et al. High-resolution magnetic resonance imaging reveals nuclei of the human amygdala: manual segmentation to automatic atlas. *Neuroimage*. (2017) 155:370–82. doi: 10.1016/j.neuroimage.2017.04.046
7. Iglesias JE, Insausti R, Lerma-Usabiaga G, Bocchetta M, Van Leemput K, Greve DN, et al. A probabilistic atlas of the human thalamic nuclei combining ex vivo MRI and histology. *Neuroimage*. (2018) 183:314–26. doi: 10.1016/j.neuroimage.2018.08.012
8. Ruiz de Miras J, Costumero V, Belloch V, Escudero J, Ávila C, Sepulcre J. Complexity analysis of cortical surface detects changes in future Alzheimer's disease converters. *Hum Brain Mapp*. (2017) 38:5905–18. doi: 10.1002/hbm.23773
9. Menon V. Large-scale brain networks and psychopathology: a unifying triple network model. *Trends Cognit Sci*. (2011) 15:483–506. doi: 10.1016/j.tics.2011.08.003
10. Chang C, Glover GH. Time-frequency dynamics of resting-state brain connectivity measured with fMRI. *Neuroimage*. (2010) 50:81–98. doi: 10.1016/j.neuroimage.2009.12.011



OPEN ACCESS

EDITED BY

Panagiotis Ferentinos,
National and Kapodistrian University
of Athens, Greece

REVIEWED BY

Foteini Christidi,
National and Kapodistrian University
of Athens, Greece
Wenming Zhao,
The First Affiliated Hospital of Anhui
Medical University, China

*CORRESPONDENCE

Reiji Yoshimura
✉ yoshi621@med.uoeh-u.ac.jp

SPECIALTY SECTION

This article was submitted to
Mood Disorders,
a section of the journal
Frontiers in Psychiatry

RECEIVED 29 August 2022

ACCEPTED 06 December 2022

PUBLISHED 06 January 2023

CITATION

Natsuyama T, Okamoto N,
Watanabe K, Chibaatar E, Tesen H,
Hayasaki G, Ikenouchi A, Kakeda S
and Yoshimura R (2023) Gyrification
patterns in first-episode, drug-naïve
major depression: Associations with
plasma levels of brain-derived
neurotrophic factor and psychiatric
symptoms.
Front. Psychiatry 13:1031386.
doi: 10.3389/fpsy.2022.1031386

COPYRIGHT

© 2023 Natsuyama, Okamoto,
Watanabe, Chibaatar, Tesen, Hayasaki,
Ikenouchi, Kakeda and Yoshimura. This
is an open-access article distributed
under the terms of the [Creative
Commons Attribution License \(CC BY\)](#).
The use, distribution or reproduction in
other forums is permitted, provided
the original author(s) and the copyright
owner(s) are credited and that the
original publication in this journal is
cited, in accordance with accepted
academic practice. No use, distribution
or reproduction is permitted which
does not comply with these terms.

Gyrification patterns in first-episode, drug-naïve major depression: Associations with plasma levels of brain-derived neurotrophic factor and psychiatric symptoms

Tomoya Natsuyama¹, Naomichi Okamoto¹, Keita Watanabe²,
Enkhmurun Chibaatar¹, Hirofumi Tesen¹, Gaku Hayasaki¹,
Atsuko Ikenouchi^{1,3}, Shingo Kakeda⁴ and Reiji Yoshimura^{1*}

¹Department of Psychiatry, University of Occupational and Environmental Health, Kitakyushu, Japan, ²Open Innovation Institute, Kyoto University, Kyoto, Japan, ³Medical Center for Dementia, Hospital of University of Occupational and Environmental Health, Kitakyushu, Japan, ⁴Department of Radiology, Graduate School of Medicine, Hirosaki University, Hirosaki, Japan

Background and objectives: Cortical structural changes in major depressive disorder (MDD) are usually studied using a voxel-based morphometry approach to delineate the cortical gray matter volume. Among cortical structures, gyrification patterns are considered a relatively stable indicator. In this study, we investigated differences in gyrification patterns between MDD patients and healthy controls (HCs) and explored the association of gyrification patterns with plasma brain-derived neurotrophic factor (BDNF) levels and depressive symptoms in MDD patients.

Methods: We evaluated 79 MDD patients and 94 HCs and assessed depression severity in the patients using the 17-item Hamilton Depression Rating Scale (HAM-D). Blood samples of both groups were collected to measure plasma BDNF levels. Magnetic resonance imaging (MRI) data were obtained using three-dimensional fast-spoiled gradient-recalled acquisition. Differences in plasma BDNF levels between groups were examined using the Mann–Whitney U test. Principal component analysis and orthogonal partial least squares discriminant analysis (OPLS-DA) were conducted to investigate the gyrification patterns which were significantly different between the groups, i.e., those with variable importance in projection (VIP) scores of >1.5 and p -value < 0.05 in multiple regression analyses adjusted for age and sex. Finally, multiple regression analysis was performed on the selected gyrification patterns to examine their association with BDNF levels in the two groups and HAM-D in the patients.

Results: There were no significant differences in plasma BDNF levels between the groups. We found that 108 (71.0%) of 152 total local gyrification indices were MDD < HC. We identified 10 disease-differentiating factors based on critical gyrification features (VIP > 1.5 and *p*-value adjusted for age and sex < 0.05). However, we found no significant correlations between the 10 gyrification patterns and plasma BDNF levels and no interaction with group. Moreover, no significant correlations were observed between the local gyrification indices and HAM-D total scores.

Conclusion: These results suggest that abnormal early cortical neurodevelopment may mediate vulnerability to MDD, independent of plasma BDNF levels and depressive symptoms.

KEYWORDS

gyrification, major depression, brain-derived neurotrophic factor, gray matter, cerebral cortex

Introduction

Major depressive disorder (MDD) is a highly prevalent and debilitating mental disorder that affects more than 264 million people worldwide (1). Individuals with depression commonly experience dysfunctional symptoms, including undesirable mood, impaired concentration, and poor sleep quality, and—more importantly—these patients are at high risk (up to 15%) of suicide (2). Moreover, previous evidence shows that MDD is a risk factor for physical illnesses (3), and the most common comorbidities are chronic physical conditions such as cardiovascular and respiratory diseases, diabetes, arthritis, osteoporosis, and cancer (4). MDD is predicted to become the second major contributor to the general medical service burden by 2030 (5, 6). The pathophysiology of MDD is complex and no single model or mechanism can fully explain it. Growth and adaptation at the neuronal level is more broadly termed neuroplasticity, and it is presumably this cellular-level neuroplasticity that is altered by inflammation and hypothalamus-pituitary-adrenal axis dysfunction due to environmental stress. The process of neurogenesis is controlled by regulatory proteins. Animal studies have shown that limiting neurogenesis inhibits antidepressant effects and produces depression-like symptoms, especially in stressful situations. Thus, it has been suggested that neurogenesis promotes resilience to stress, which may be the basis for the clinical efficacy of antidepressants. Postmortem studies of MDD patients have demonstrated a loss of granule neurons in the dentate gyrus of untreated patients compared to treated and non-MDD patients. There are considerably more splitting neural progenitor cells in patients treated for MDD compared to untreated MDD and even non-MDD patients. These findings are consistent with mouse studies showing that antidepressants act by increasing

neurogenesis in the adult brain. In short, neuroplasticity plays an important role in the pathophysiology of MDD (7, 8).

Cortical gyrification, a forming process of cerebral cortex folds, begins between 10 and 15 weeks of fetal development. Cortical folding related to fetal and early postnatal neurodevelopmental processes is defined by the local gyrification index (LGI) (9). LGI quantifies the amount of cortex buried within the sulcal folds and represents the extent of cortical folding. It is expressed as the ratio of the entire outer cortical surface (superficial exposed area plus the area buried in the sulcus) to the superficial exposed area (10, 11). The index of each vertex is calculated by dividing the ossicular surface area by the corresponding outer surface area (12). LGI increases dramatically during the third trimester of pregnancy and peaks by age 2, then remains relatively constant throughout the rest of life (13–15). Cortical thickness and surface area mainly characterize the neuronal density and number and spacing of the cortical columns, respectively (16–18). Therefore, computing LGI, the pattern and degree of cortical folding, might be a more stable indicator for investigating abnormal neurodevelopmental patterns in MDD. Additionally, recent technological developments in 3D image reconstruction and surface morphometry have improved LGI measurement and gained wide acceptance in psychiatric research (19).

Abbreviations: BDNF, brain-derived neurotrophic factor; DSM-5, Diagnostic and Statistical Manual for Mental Disorders-5; HAM-D, Hamilton Depression Rating Scale; HC(s), healthy control(s); LGI(s), local gyrification index (indices); MDD, major depressive disorder; MRI, magnetic resonance imaging; OPLS-DA, orthogonal partial least squares discriminant analysis; PLS-DA, partial least squares discriminant analysis; VIP, variable importance in projection.

Voxel-based morphometry is a frequently used approach in MDD patients to assay cortical structural changes and to delineate the cortical gray matter volume. Considering many ongoing studies, researchers have identified several neuroanatomical changes in MDD, including widespread focal alterations in cortical thickness (20), surface area (21), and cortical gyrification (9). A large-scale meta-analysis demonstrated distributed cortical alterations that affected the orbitofrontal cortex, anterior and posterior cingulate cortex, insula, and temporal lobes (21). Additionally, MDD is considered a disorder of dysregulated neural networks, including irregularities in the neural connection (22, 23), rather than regional abnormalities (24). Thus, direct investigation of cortical thickness, surface area, and folding patterns—which reflect different biological factors—is better and more accurate in revealing the structural alterations in MDD (14, 15). Cortical folding related to fetal and early postnatal neurodevelopmental processes is defined by LGI (9, 10, 25, 26). Thus, computing LGI might be ideal for investigating abnormal neurodevelopmental patterns in MDD. Several studies have found different LGI in patients with MDD than in healthy controls (HCs) (27–29). Reports on changes in LGI in patients with MDD are inconsistent (9, 27–29), but have not largely explored the association with depressive symptoms.

Brain-derived neurotrophic factor (BDNF) is a neurotrophic factor that is essential for neuronal survival, growth, and maintenance in brain circuits involved in emotional and cognitive function (30). Several previous studies and meta-analyses have proved that BDNF is associated with brain neuroplasticity and is involved in the pathophysiology of MDD (31–33). Previous studies also demonstrated decreased plasma or serum levels of BDNF in patients with MDD (34, 35). Perhaps, even more important is the fact that reduced BDNF levels in patients with MDD can be restored by antidepressant therapies such as pharmacotherapy and psychological interventions. Although the relevance of BDNF for MDD is obvious, no studies have investigated the relationship between LGI and BDNF levels, which might be associated with synaptogenesis and neurogenesis. Moreover, recent reports demonstrated that the BDNF gene (Val66Met) was related to changes in gyrification in bipolar disorder (36). Another report indicated that autism spectrum disorder is associated with a distorted relationship between the Val66Met genotype and determinants of regional cortical surface area—cortical gyrification and/or sulcal positioning (37). From these previous findings, it can be postulated that BDNF secretion associated with Val66Met polymorphism may be related to cortical gyrification.

Thus, we investigated differences in gyrification patterns between first-episode, drug-naïve MDD patients and HCs. Moreover, we explored the relationship between cortical gyrification and plasma BDNF levels, which might be associated

with synaptogenesis and neurogenesis in both groups. We also explored the association between gyrification patterns and depressive symptoms in patients with MDD based on HAM-D scores.

Materials and methods

Participants

Patients were recruited from the Hospital of University of Occupational and Environmental Health in Kitakyushu, Japan. We conducted the full Structured Clinical Interview from the Diagnostic and Statistical Manual for Mental Disorders-5 (DSM-5) (38) for all participants to diagnose MDD and ensure that HCs did not currently fulfill the criteria for any psychiatric diseases. We also ensured that no HC had a history of serious medical and neurological diseases or a family history of major psychiatric or neurological diseases among their first-degree relatives. Although our study population overlaps in part with several of our previously published studies (39, 40), no study has analyzed the correlation between cortical gyrification, plasma BDNF levels, and psychiatric symptoms.

Clinical assessment and blood sampling

Depression severity was assessed using the 17-item Hamilton Depression Rating Scale (HAM-D) (41). A veteran psychiatrist with 35 years of clinical psychiatric experience assessed patients with MDD using a GRID-Hamilton Rating Scale for Depression (GRID-HAM-D-17 and -21) (42). Patients' blood samples were collected in regular tubes between 9:00 and 11:00 AM, and plasma samples were separated by centrifugation at 2000 rpm for 20 min. The separated plasma samples were stored at -80°C in silicone-coated tubes until analysis.

MRI acquisition

Magnetic resonance imaging data were obtained using a 3T MR system (Signa EXCITE 3T; GE Healthcare, Chicago, IL, US) with an 8-channel brain phased-array coil. Images were acquired using three-dimensional fast-spoiled gradient-recalled acquisition. The acquisition parameters were as follows: repetition time/echo time, 10/4.1 ms; flip angle, 10° ; field of view, 24 cm; and resolution, $0.9 \times 0.9 \times 1.2$ mm. All images were corrected for distortion due to gradient non-linearity using the “Grad Warp” software program.

<0.05 set as statistically significant. For correlation analyses, Bonferroni corrections were performed for those that reached statistical significance.

Ethical considerations

This study was conducted in accordance with the principles of the Declaration of Helsinki, and the relevant Ethics Committee approved the protocol. Informed consent was obtained from all participants, and we assigned each patient an arbitrary identification number to protect their privacy.

Results

Demographic data and clinical characteristics of participants

Demographic and clinical characteristics are shown in [Table 1](#). Differences in age and sex were observed.

LGIs in MDD and HC groups

LGIs in MDD and HC groups are shown in [Figure 1](#) and [Supplementary Table 1](#); 108 (71.0%) of the 152 LGIs measured in this study were MDD < HC.

Differences in plasma BDNF levels between MDD and HC groups

The median plasma BDNF level in the MDD group was 5.0 ng/mL [2.65–7.95], while the median in the HC group was 3.8 ng/mL [2.12–8.25]. There was no significant difference in plasma BDNF levels between the two groups ($p = 0.35$).

PCA and OPLS-DA

We evaluated all LGIs using PCA and created two-dimensional plots for the first and second principal components.

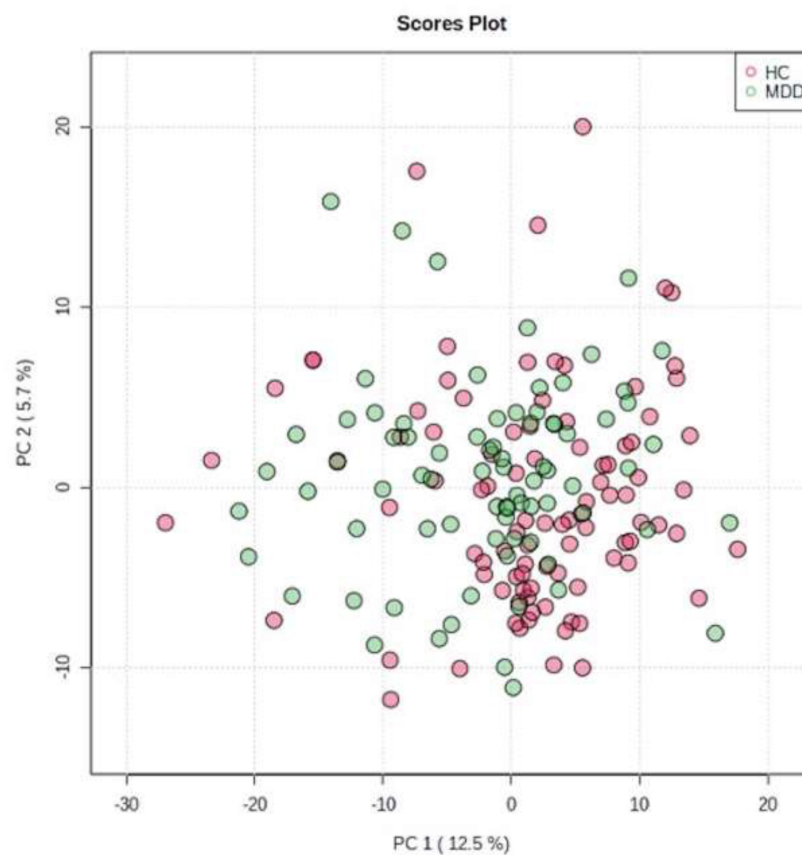


FIGURE 2

Principal component analysis (PCA). We evaluated all LGIs using PCA and created two-dimensional plots for the first and second principal components.

PCA separated MDD and HC groups by the first main component, as shown in [Figure 2](#).

To obtain further separation, we evaluated all LGIs using OPLS-DA and created two-dimensional plots. OPLS-DA showed a relatively clear separation from PCA between MDD and HC groups by the first principal component ([Figure 3](#)). OPLS model overview was as follows: p1 (R^2X : 0.035, R^2Y : 0.195, Q^2 : 0.019); o1(R^2X : 0.142, R^2Y : 0.238, Q^2 : -0.0307).

Variable importance in projection scores were extracted from this model (45). Essential features of differentially expressed LGIs were defined as $VIP > 1.5$. Differentially expressed LGIs in MDD and HC groups are shown in [Figure 4](#) and [Table 2](#). We finally detected 10 differentially expressed LGIs ($VIP > 1.5$ and p -value adjusted for age and sex < 0.05) between HC and MDD (i.e., *rS_circular_insula_inf*, *lUnknown*, *lS_circular_insula_inf*, *rUnknown*, *lG_oc-temp_med-Parahip*, *lG_temp_sup-Plan_polar*, *rG_oc-temp_med-Parahip*, *rG_temp_sup-Plan_polar*, *lG_cingul-Post-ventral*, and *rG_insular_short*).

Relationship between important features of differentially expressed LGIs and plasma BDNF levels

We showed the relationship between differentially expressed LGIs and plasma BDNF levels in HCs (see [Supplementary Table 2](#)) and patients with MDD (see [Supplementary Table 3](#)). We examined the correlation between plasma BDNF levels and 10 differentially expressed LGIs ($VIP > 1.5$ and p -value adjusted for age and sex < 0.05) using age and sex as confounding factors. However, we found no significant correlation between the LGIs and plasma BDNF at any location. In addition, BDNF showed no significant interaction between MDD and HC groups for the 10 LGIs (see [Supplementary Table 4](#)).

Correlation between HAM-D and LGI

We also examined the top 10 LGIs ($VIP > 1.5$ and p -value adjusted for age and sex < 0.05) and psychiatric symptoms

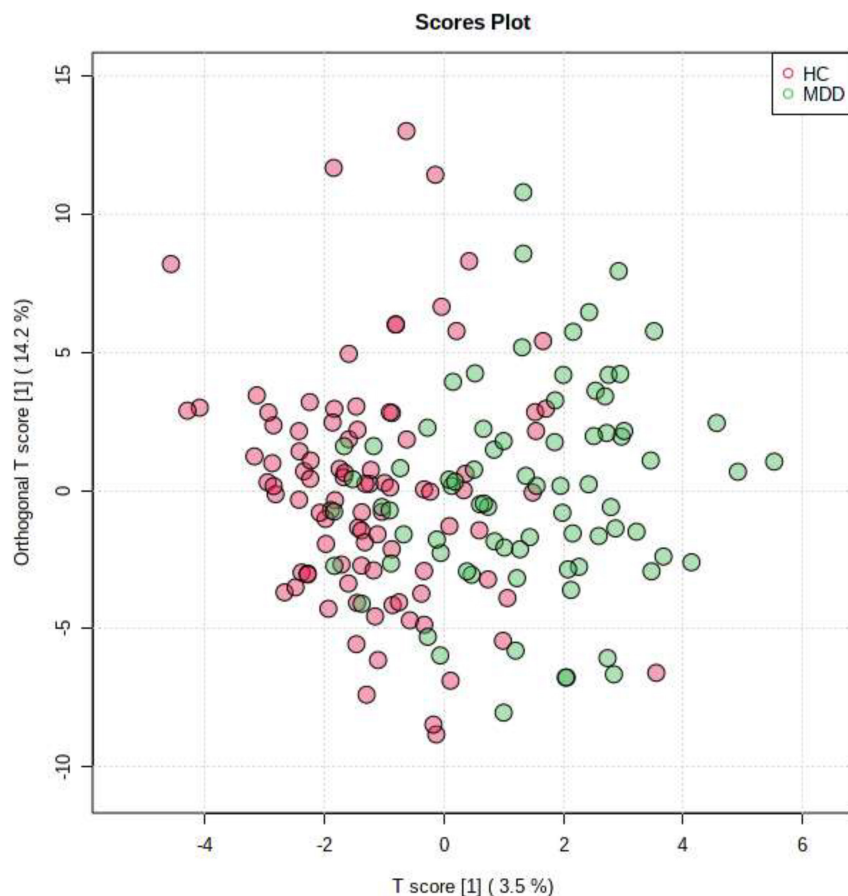


FIGURE 3

Orthogonal partial least squares discriminant analysis (OPLS-DA). OPLS-DA showed a relatively clear separation from PCA between patients in MDD group and HC group by the first principal component.

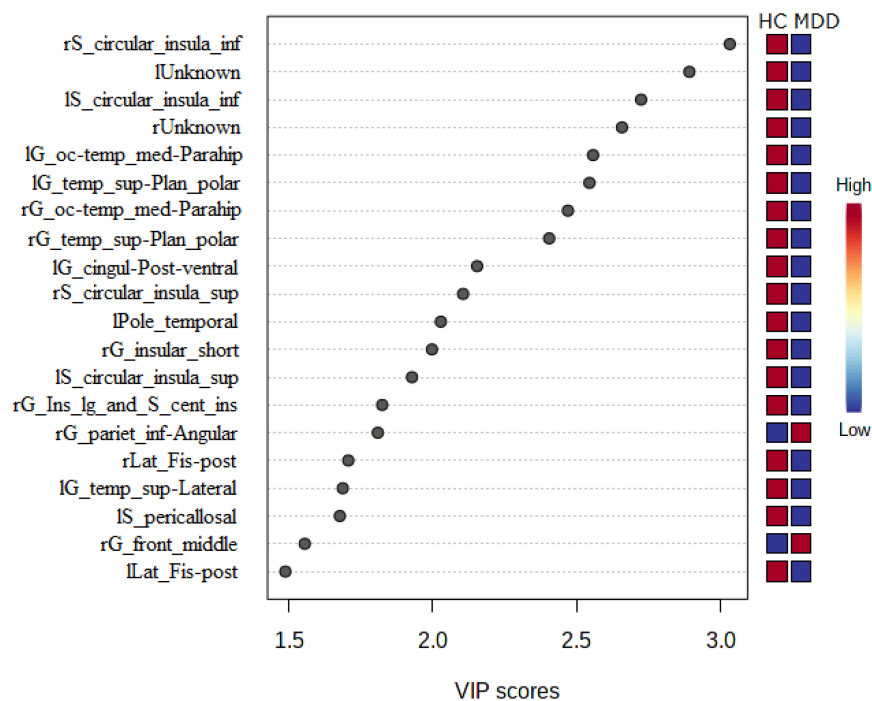


FIGURE 4

Relationship between expressed LGIs in MDD and HC groups. We showed the 20 significant features of differently expressed LGIs (VIP > 1.5) in MDD and HC groups. "l" and "r" attached to the beginning of the word mean "left" and "right".

using these top features. We found a statistically significant correlation between rG_temp_sup-Plan_polar and HAM-D (standard partial regression coefficient = 0.238, $p = 0.049$); however, no significant correlations were observed between LGI and HAM-D total scores after Bonferroni correction ($p = 0.49$) (see [Supplementary Table 5](#)).

Discussion

This study provides evidence of cortical gyrification pattern differences between first-episode, drug-naïve MDD patients and HCs. In this study, we found that 108 (71.0%) of the 152 total LGIs were MDD < HC. We then identified 10 disease-differentiating factors based on critical LGIs features (VIP > 1.5 and p -value adjusted for age and sex < 0.05), but found no significant correlation between LGIs and plasma BDNF level at any location. In addition, BDNF level showed no significant interaction between MDD and HC groups for the 10 determined LGIs.

Several previous studies have reported altered LGI in patients with MDD compared to HCs, including decreased LGI in the bilateral precuneus (23), bilateral mid-posterior cingulate, insula, orbital frontal cortices (orbitofrontal cortex), left anterior cingulate cortex (right anterior cingulate gyrus cortex), right temporal operculum (27), left lingual gyrus (left

lingual corpuscle), right posterior superior temporal sulcus (right superior temporal sulcus) (29) and precuneus, superior parietal gyrus, parahippocampal gyrus, middle frontal gyrus, and fusiform and right fusiform gyrus (46). There are also several reports supporting increased LGI in patients with MDD, including increased LGI in the frontal, cingulate, parietal, temporal, and occipital regions (9); right rostral anterior cingulate cortex and medial orbitofrontal cortex; frontal pole (28); left anterior cingulate; right precentral, supramarginal region; and left superior frontal gyrus (47). However, in this study, we found that 108 (71.0%) of the 152 LGIs were MDD < HC, supporting previous findings of a decreased LGI in patients with MDD.

Some studies have reported associations between cortical gyrification patterns and BDNF level. Cortical gyrification refers to the forming process of cerebral cortex folds. During the third trimester, the brain develops from a relatively smooth erect brain structure to one that more closely resembles adult brain morphology. LGI, a measure of the degree of cortical folding, increases dramatically during the third trimester of pregnancy but remains relatively constant throughout the rest of development (48). LGI peaks by age 2 and then gradually decreases with increasing age (15, 49). One study prospectively followed patients with bipolar disorder for 4 years and found that those with one or more BDNF Met alleles, indicating that decreased BDNF secretion produced a more significant

TABLE 2 Top 20 gyrification patterns (VIP > 1.5) in major depressive disorder (MDD) and healthy control (HC) groups.

	HC	MDD	<i>p</i> -value	Adjusted <i>p</i> -value
rS_circular_insula_inf	24.85 (2.43)	23.67 (2.51)	0.002	0.032
lUnknown	23.66 (1.37)	22.95 (1.36)	0.00089	0.037
lS_circular_insula_inf	25.70 (2.51)	24.31 (2.89)	0.00103	0.003
rUnknown	23.32 (1.45)	22.65 (1.27)	0.00153	0.035
lG_oc-temp_med-Parahip	25.64 (1.60)	24.74 (1.66)	0.000452	<0.001
lG_temp_sup-Plan_polar	22.58 (3.55)	20.83 (2.87)	0.000443	0.009
rG_oc-temp_med-Parahip	26.18 (1.62)	25.10 (1.50)	0.0000101	0.001
rG_temp_sup-Plan_polar	23.59 (3.17)	22.07 (2.82)	0.00109	0.005
lG_cingul-Post-ventral	28.7 (3.28)	27.08 (3.84)	0.00291	0.023
rS_circular_insula_sup	29.34 (1.82)	28.81 (1.71)	0.0514	0.15
lPole_temporal	28.56 (1.31)	28.02 (1.33)	0.00931	0.33
rG_insular_short	28.17 (2.87)	27.21 (2.89)	0.0292	0.014
lS_circular_insula_sup	29.20 (1.66)	28.69 (1.53)	0.0353	0.078
rG_Ins_lg_and_S_cent_ins	26.87 (3.06)	26.06 (3.27)	0.0999	0.46
rG_pariet_inf-Angular	28.94 (1.30)	29.35 (1.25)	0.0366	0.71
rLat_Fis-post	29.81 (1.43)	29.48 (1.55)	0.152	0.21
lG_temp_sup-Lateral	28.45 (1.28)	28.01 (1.55)	0.0455	0.27
lS_pericallosal	33.64 (2.13)	32.72 (2.86)	0.0188	0.38
rG_front_middle	29.17 (1.11)	29.33 (1.06)	0.345	0.99
lLat_Fis-post	30.26 (1.80)	30.01 (1.34)	0.315	0.21

P-value is adjusted for age and sex.

HC, healthy control; MDD, major depressive disorder; VIP, variable importance in projection.

reduction in LGI (36). Besides, the neuroplasticity in brain formation—including cortical gyrification in fetal sheep—is more critical in brain regions rich in BDNF expression (50).

Astrogenesis, gliogenesis, and angiogenesis may also be related to cortical gyrification. A recent study reported that localized astrogenesis plays an important role in gyrus formation in the gyrencephalic cerebral cortex. In functional genetic experiments using ferrets, reducing astrocyte numbers prevents gyrus formation in the cortex. Meanwhile, increasing astrocyte numbers in mice, which do not have cortical folds, can induce gyrus-like protrusions (51). Gliogenesis is also involved in the gyrification of the primate cerebrum (52). In summary, astrocytes—one of the microglia—might play a role in cortical gyrification. Fibroblast growth factor 2, which is a member of a large family of proteins that bind heparin and heparan sulfate and modulate the function of a wide range of cell types, stimulates the growth and development of angiogenesis, thus

contributing to the pathogenesis of several diseases including atherosclerosis, and is associated with cortical gyrification in the mouse brain (53). Taken together, astrogenesis, gliogenesis, and angiogenesis, whereas, neurogenesis might be associated with cortical gyrification in the brain.

Microglial activation plays a role in maintaining the delicate balance of BDNF release into neuronal synapses (54). Thus, BDNF secretion is considered to be influenced by astrocytes and glia, which might influence cortical gyrification. We did not, however, find an association between plasma BDNF level and LGI in this study. Therefore, plasma BDNF level may be independent of cortical gyrification. Additionally, it is controversial that plasma BDNF level reflects BDNF dynamics in the brain. These findings indicate that the association between cortical gyrification and BDNF level must still be further elucidated.

In addition, we focused on the association between gyrification patterns and depression severity. One study adjusted for age, sex, education level, and total cortical surface area reported positive correlations between LGI in the left caudal middle frontal cortex and Beck Depression Inventory scores (47). Another recent study examined correlations between the HAM-D and LGI in 22 cortical regions of patients with MDD but found no significance in the field (28). Yet another previous study reported an inverse correlation between LGI and HAM-D scores in the right inferior parietal, right postcentral, and left superior parietal lobes of patients with MDD (9). We also assessed the correlation between the top 10 gyrification patterns and psychiatric symptoms; however, we found no statistically significant correlations between LGI and HAM-D total scores.

This study had several limitations. First, the number of participants was small, and the age and sex distributions of the two groups were significantly different—a typical limitation of clinical research. In addition, we did not include education level or dominant arm in the analysis because of missing data. This may have resulted in insufficient statistical power to confirm our hypothesis. However, these differences in age and educational level may be somewhat acceptable considering that LGI peaks by age 2 and then remains relatively constant throughout one's life. In addition, we also statistically calculated age and sex-adjusted *p*-value. Due to the limited sample size, the statistical analysis also had several limitations. We could not replicate the results to determine the validity of the outcome. However, *a priori* dimensionality reduction techniques such as PCA and OPLS-DA were used to refine the variables in examining differences in gyration patterns between the MDD and HC groups, thus increasing the accuracy of the analysis. Another point to consider is that we conducted this study using a one-point cross-sectional method. Thus, whether there were any changes in LGI during the progression of MDD was not fully elucidated. Therefore, a longitudinal study is warranted in the future.

Conclusion

Predicated on previous publications, this is not the first study that investigated differences in cortical gyrification patterns between MDD and HC groups. The present study observed several gyrification patterns that cause differences in the disease predicated on essential features of and VIP scores and adjusted *p*-value. Of the 152 LGIs measured in this study, 108 were MDD < HC. Future large-scale studies with more participants would help to clarify the relationship between gyrification patterns and psychiatric symptoms.

Data availability statement

The raw data supporting the conclusions of this article will be made available by the authors, without undue reservation.

Ethics statement

The studies involving human participants were reviewed and approved by the Ethical Committee of University of Occupational and Environmental Health, Japan. The patients/participants provided their written informed consent to participate in this study.

Author contributions

TN, NO, KW, and RY conceived and designed the experiments. TN, NO, EC, HT, KW, and RY performed the experiments. TN, NO, EC, and KW analyzed the data. TN, NO, KW, EC, and RY composed the manuscript. TN, NO, EC, KW,

HT, GH, AI, SK, and RY provided expertise and edited the manuscript. All authors read the manuscript and were solely and jointly responsible for its content.

Acknowledgments

We thank Ms. Tomomi Ishiba for her help with blood sampling.

Conflict of interest

The authors declare that the research was conducted in the absence of any commercial or financial relationships that could be construed as a potential conflict of interest.

Publisher's note

All claims expressed in this article are solely those of the authors and do not necessarily represent those of their affiliated organizations, or those of the publisher, the editors and the reviewers. Any product that may be evaluated in this article, or claim that may be made by its manufacturer, is not guaranteed or endorsed by the publisher.

Supplementary material

The Supplementary Material for this article can be found online at: <https://www.frontiersin.org/articles/10.3389/fpsyt.2022.1031386/full#supplementary-material>

References

1. GBD 2017 Disease and Injury Incidence and Prevalence Collaborators. Global, regional, and national incidence, prevalence, and years lived with disability for 354 diseases and injuries for 195 countries and territories, 1990–2017: a systematic analysis for the Global Burden of Disease Study 2017. *Lancet*. (2018) 392:1789–858. doi: 10.1016/S0140-6736(18)32279-7
2. Alsaman R, Alansari B. Relationship of suicide ideation with depression and hopelessness. *Eur Psychiatry*. (2020) 33:S597. doi: 10.1016/j.eurpsy.2016.01.2228
3. Wulsin L, Vaillant G, Wells V. A systematic review of the mortality of depression. *Psychosom Med*. (1999) 61:6–17. doi: 10.1097/00006842-199901000-00003
4. Clarke D, Currie K. Depression, anxiety and their relationship with chronic diseases: a review of the epidemiology, risk and treatment evidence. *Med J Aust*. (2009) 190:S54–60. doi: 10.5694/j.1326-5377.2009.tb02471.x
5. Mathers C, Loncar D. Projections of global mortality and burden of disease from 2002 to 2030. *PLoS Med*. (2006) 3:e442. doi: 10.1371/journal.pmed.0030442
6. Lin J, Chen T, He J, Chung R, Ma H, Tsang H. Impacts of acupuncture treatment on depression: a systematic review and meta-analysis. *World J Psychiatry*. (2022) 12:169–86. doi: 10.5498/wjp.v12.i1.169
7. Malhi G, Mann J. Depression. *Lancet*. (2018) 392:2299–312. doi: 10.1016/S0140-6736(18)31948-2
8. Levy M, Boule F, Steinbusch H, van den Hove D, Kenis G, Lanfumey L. Neurotrophic factors and neuroplasticity pathways in the pathophysiology and treatment of depression. *Psychopharmacology*. (2018) 235:2195–220. doi: 10.1007/s00213-018-4950-4
9. Schmitgen M, Depping M, Bach C, Wolf N, Kubera K, Vasic N, et al. Aberrant cortical neurodevelopment in major depressive disorder. *J Affect Disord*. (2019) 243:340–7. doi: 10.1016/j.jad.2018.09.021
10. Zilles K, Armstrong E, Schleicher A, Kretschmann H. The human pattern of gyrification in the cerebral cortex. *Anat Embryol*. (1988) 179:173–9. doi: 10.1007/BF00304699
11. Zilles K, Palomero-Gallagher N, Amunts K. Development of cortical folding during evolution and ontogeny. *Trends Neurosci*. (2013) 36:275–84. doi: 10.1016/j.tins.2013.01.006
12. Schaer M, Cuadra M, Schmansky N, Fischl B, Thiran J, Eliez S. How to measure cortical folding from MR images: a step-by-step tutorial to compute local gyrification index. *J Vis Exp*. (2012) 59:e3417. doi: 10.3791/3417

13. Peng D, Shi F, Li G, Fralick D, Shen T, Qiu M, et al. Surface vulnerability of cerebral cortex to major depressive disorder. *PLoS One*. (2015) 10:e0120704. doi: 10.1371/journal.pone.0120704
14. Li G, Nie J, Wang L, Shi F, Lin W, Gilmore J, et al. Mapping region-specific longitudinal cortical surface expansion from birth to 2 years of age. *Cereb Cortex*. (2013) 23:2724–33. doi: 10.1093/cercor/bhs265
15. Li G, Wang L, Shi F, Lyall A, Lin W, Gilmore J, et al. Mapping longitudinal development of local cortical gyrification in infants from birth to 2 years of age. *J Neurosci*. (2014) 34:4228–38. doi: 10.1523/JNEUROSCI.3976-13.2014
16. Casanova M, Tillquist C. Encephalization, emergent properties, and psychiatry: a minicolumnar perspective. *Neuroscientist*. (2008) 14:101–18. doi: 10.1177/1073858407309091
17. Pontious A, Kowalczyk T, Englund C, Hevner R. Role of intermediate progenitor cells in cerebral cortex development. *Dev Neurosci*. (2008) 30:24–32. doi: 10.1159/000109848
18. la Fougère C, Grant S, Kostikov A, Schirrmacher R, Gravel P, Schipper H, et al. Where in-vivo imaging meets cytoarchitectonics: the relationship between cortical thickness and neuronal density measured with high-resolution [18F]flumazenil-PET. *Neuroimage*. (2011) 56:951–60. doi: 10.1016/j.neuroimage.2010.11.015
19. Sasabayashi D, Takayanagi Y, Takahashi T, Nemoto K, Furuichi A, Kido M, et al. Increased brain gyrification in the schizophrenia spectrum. *Psychiatry Clin Neurosci*. (2020) 74:70–6. doi: 10.1111/pcn.12939
20. Li Q, Zhao Y, Chen Z, Long J, Dai J, Huang X, et al. Meta-analysis of cortical thickness abnormalities in medication-free patients with major depressive disorder. *Neuropsychopharmacology*. (2020) 45:703–12. doi: 10.1038/s41386-019-0563-9
21. Schmaal L, Hibar D, Sämann P, Hall G, Baune B, Jahanshad N, et al. Cortical abnormalities in adults and adolescents with major depression based on brain scans from 20 cohorts worldwide in the ENIGMA Major Depressive Disorder Working Group. *Mol Psychiatry*. (2017) 22:900–9. doi: 10.1038/mp.2016.60
22. Kaiser R, Andrews-Hanna J, Wager T, Pizzagalli D. Large-scale network dysfunction in major depressive disorder: a meta-analysis of resting-state functional connectivity. *JAMA Psychiatry*. (2015) 72:603–11. doi: 10.1001/jamapsychiatry.2015.0071
23. Chen C, Liu Z, Xi C, Tan W, Fan Z, Cheng Y, et al. Multivariate structural covariance in first-episode major depressive disorder: a graph theoretical analysis. *J Psychiatry Neurosci*. (2022) 47:E176–85. doi: 10.1503/jpn.210204
24. Mulders P, van Eijndhoven P, Schene A, Beckmann C, Tendolcar I. Resting-state functional connectivity in major depressive disorder: a review. *Neurosci Biobehav Rev*. (2015) 56:330–44. doi: 10.1016/j.neubiorev.2015.07.014
25. Petanjek Z, Judas M, Kostović I, Uylings H. Lifespan alterations of basal dendritic trees of pyramidal neurons in the human prefrontal cortex: a layer-specific pattern. *Cereb Cortex*. (2008) 18:915–29. doi: 10.1093/cercor/bhm124
26. Petanjek Z, Judas M, Šimic G, Rasin M, Uylings H, Rakic P, et al. Extraordinary neoteny of synaptic spines in the human prefrontal cortex. *Proc Natl Acad Sci USA*. (2011) 108:13281–6. doi: 10.1073/pnas.1105108108
27. Zhang Y, Yu C, Zhou Y, Li K, Li C, Jiang T. Decreased gyrification in major depressive disorder. *Neuroreport*. (2009) 20:378–80. doi: 10.1097/WNR.0b013e3283249b34
28. Han K, Won E, Kang J, Kim A, Yoon H, Chang H, et al. Local gyrification index in patients with major depressive disorder and its association with tryptophan hydroxylase-2 (TPH2) polymorphism. *Hum Brain Mapp*. (2017) 38:1299–310. doi: 10.1002/hbm.23455
29. Long J, Xu J, Wang X, Li J, Rao S, Wu H, et al. Altered local gyrification index and corresponding functional connectivity in medication free major depressive disorder. *Front Psychiatry*. (2020) 11:585401. doi: 10.3389/fpsy.2020.585401
30. Kowiański P, Lietzau G, Czuba E, Waśkow M, Steliga A, Moryś J. BDNF. A Key Factor with Multipotent Impact on Brain Signaling and Synaptic Plasticity. *Cell Mol Neurobiol*. (2018) 38:579–93. doi: 10.1007/s10571-017-0510-4
31. Sen S, Duman R, Sanacora G. Serum brain-derived neurotrophic factor, depression, and antidepressant medications: meta-analyses and implications. *Biol Psychiatry*. (2008) 64:527–32. doi: 10.1016/j.biopsych.2008.05.005
32. Brunoni A, Lopes M, Fregni F. A systematic review and meta-analysis of clinical studies on major depression and BDNF levels: implications for the role of neuroplasticity in depression. *Int J Neuropsychopharmacol*. (2008) 11:1169–80. doi: 10.1017/S1461145708009309
33. Bocchio-Chiavetto L, Bagnardi V, Zanardini R, Molteni R, Nielsen M, Placentino A, et al. Serum and plasma BDNF levels in major depression: a replication study and meta-analyses. *World J Biol Psychiatry*. (2010) 11:763–73. doi: 10.3109/15622971003611319
34. Yoshimura R, Kishi T, Atake K, Katsuki A, Iwata N. Serum brain-derived neurotrophic factor, and plasma catecholamine metabolites in people with major depression: preliminary cross-sectional study. *Front Psychiatry*. (2018) 9:52. doi: 10.3389/fpsy.2018.00052
35. Kishi T, Yoshimura R, Ikuta T, Iwata N. Brain-derived neurotrophic factor, and major depressive disorder: evidence from meta-analyses. *Front Psychiatry*. (2018) 8:308. doi: 10.3389/fpsy.2017.00308
36. Mirakhor A, Moorhead T, Stanfield A, McKirdy J, Sussmann J, Hall J, et al. Changes in gyrification over 4 years in bipolar disorder and their association with the brain-derived neurotrophic factor valine(66) methionine variant. *Biol Psychiatry*. (2009) 66:293–7. doi: 10.1016/j.biopsych.2008.12.006
37. Raznahan A, Toro R, Proitsi P, Powell J, Paus T, Bolton P, et al. A functional polymorphism of the brain derived neurotrophic factor gene and cortical anatomy in autism spectrum disorder. *J Neurodev Disord*. (2009) 1:215–23. doi: 10.1007/s11689-009-9012-0
38. American Psychiatric Association. *Diagnostic and Statistical Manual of Mental Disorders*. 5th Edn. Washington, DC: American Psychiatric Association (2013).
39. Fujii R, Watanabe K, Okamoto N, Natsuyama T, Tesen H, Igata R, et al. Hippocampal volume and plasma brain-derived neurotrophic factor levels in patients with depression and healthy controls. *Front Mol Neurosci*. (2022) 15:857293. doi: 10.3389/fnmol.2022.857293
40. Tesen H, Watanabe K, Okamoto N, Ikenouchi A, Igata R, Konishi Y, et al. Volume of amygdala subregions and clinical manifestations in patients with first-episode, drug-naïve major depression. *Front Hum Neurosci*. (2022) 15:780884. doi: 10.3389/fnhum.2021.780884
41. Hamilton M. A rating scale for depression. *J Neurol Neurosurg Psychiatry*. (1960) 23:56–62. doi: 10.1136/jnnp.23.1.56
42. Depression Rating Scale Standardization Team [DRSST]. *GRID-HAMD-17, GRID-HAMD-21: Structured Interview Guide*. San Diego, CA: International Society for CNS Drug Development (2003).
43. Fischl B, van der Kouwe A, Destrieux C, Halgren E, Ségonne F, Salat D, et al. Automatically parcellating the human cerebral cortex. *Cereb Cortex*. (2004) 14:11–22. doi: 10.1093/cercor/bhg087
44. Trygg J, Wold S. Orthogonal projections to latent structures (O-PLS). *J Chemometr*. (2002) 16:119–28. doi: 10.1002/cem.695
45. Yang J, Chen T, Sun L, Zhao Z, Qi X, Zhou K, et al. Potential metabolite markers of schizophrenia. *Mol Psychiatry*. (2013) 18:67–78. doi: 10.1038/mp.2011.131
46. Depping M, Schmitgen M, Kubera K, Wolf R. Cerebellar contributions to major depression. *Front Psychiatry*. (2018) 9:634. doi: 10.3389/fpsy.2018.00634
47. Xiong G, Dong D, Cheng C, Jiang Y, Sun X, He J, et al. State-independent and -dependent structural alterations in limbic-cortical regions in patients with current and remitted depression. *J Affect Disord*. (2019) 258:1–10. doi: 10.1016/j.jad.2019.07.065
48. White T, Su S, Schmidt M, Kao C, Sapiro G. The development of gyrification in childhood and adolescence. *Brain Cogn*. (2010) 72:36–45. doi: 10.1016/j.bandc.2009.10.009
49. Cao B, Mwangi B, Passos I, Wu M, Keser Z, Zunta-Soares G, et al. Lifespan gyrification trajectories of human brain in healthy individuals and patients with major psychiatric disorders. *Sci Rep*. (2017) 7:511. doi: 10.1038/s41598-017-00582-1
50. Quezada S, van de Looij Y, Hale N, Rana S, Sizonenko S, Gilchrist C, et al. Genetic and microstructural differences in the cortical plate of gyri and sulci during gyrification in fetal sheep. *Cereb Cortex*. (2020) 30:6169–90. doi: 10.1093/cercor/bhaa171
51. Shinmyo Y, Saito K, Hamabe-Horiike T, Kameya N, Ando A, Kawasaki K, et al. Localized astrogenesis regulates gyrification of the cerebral cortex. *Sci Adv*. (2022) 8:eabi5209. doi: 10.1126/sciadv.abi5209
52. Rash B, Duque A, Morozov Y, Arellano J, Micali N, Rakic P. Gliogenesis in the outer subventricular zone promotes enlargement and gyrification of the primate cerebrum. *Proc Natl Acad Sci U.S.A.* (2019) 116:7089–94. doi: 10.1073/pnas.1822169116
53. Rash B, Tomasi S, Lim H, Suh C, Vaccarino F. Cortical gyrification induced by fibroblast growth factor 2 in the mouse brain. *J Neurosci*. (2013) 33:10802–14. doi: 10.1523/JNEUROSCI.3621-12.2013
54. Prowse N, Hayley S. Microglia and BDNF at the crossroads of stressor related disorders: towards a unique trophic phenotype. *Neurosci Biobehav Rev*. (2021) 131:135–63. doi: 10.1016/j.neubiorev.2021.09.018



OPEN ACCESS

EDITED BY
Keita Watanabe,
Kyoto University,
Japan

REVIEWED BY
Liza Van Eijk,
James Cook University,
Australia
Reiji Yoshimura,
University of Occupational and Environmental
Health Japan,
Japan

*CORRESPONDENCE
Judy Alper
✉ judy.alper@mssm.edu

SPECIALTY SECTION
This article was submitted to
Mood Disorders,
a section of the journal
Frontiers in Psychiatry

RECEIVED 03 October 2022
ACCEPTED 10 January 2023
PUBLISHED 02 February 2023

CITATION
Alper J, Feng R, Verma G, Rutter S, Huang K-H,
Xie L, Yushkevich P, Jacob Y, Brown S, Kautz M,
Schneider M, Lin H-M, Fleyscher L, Delman BN,
Hof PR, Murrough JW and
Balchandani P (2023) Stress-related reduction
of hippocampal subfield volumes in major
depressive disorder: A 7-Tesla study.
Front. Psychiatry 14:1060770.
doi: 10.3389/fpsyt.2023.1060770

COPYRIGHT
© 2023 Alper, Feng, Verma, Rutter, Huang, Xie,
Yushkevich, Jacob, Brown, Kautz, Schneider,
Lin, Fleyscher, Delman, Hof, Murrough and
Balchandani. This is an open-access article
distributed under the terms of the [Creative
Commons Attribution License \(CC BY\)](#). The
use, distribution or reproduction in other
forums is permitted, provided the original
author(s) and the copyright owner(s) are
credited and that the original publication in this
journal is cited, in accordance with accepted
academic practice. No use, distribution or
reproduction is permitted which does not
comply with these terms.

Stress-related reduction of hippocampal subfield volumes in major depressive disorder: A 7-Tesla study

Judy Alper^{1,2*}, Rui Feng³, Gaurav Verma¹, Sarah Rutter⁴,
Kuang-han Huang¹, Long Xie⁵, Paul Yushkevich⁵, Yael Jacob¹,
Stephanie Brown¹, Marin Kautz⁴, Molly Schneider⁴, Hung-Mo Lin⁶,
Lazar Fleyscher¹, Bradley N. Delman¹, Patrick R. Hof⁷,
James W. Murrough^{4,7} and Priti Balchandani¹

¹Department of Diagnostic, Molecular, and Interventional Radiology, Icahn School of Medicine at Mount Sinai, New York, NY, United States, ²Department of Biomedical Engineering, City College of New York, New York, NY, United States, ³Department of Neurosurgery, Icahn School of Medicine at Mount Sinai, New York, NY, United States, ⁴Department of Psychiatry, Icahn School of Medicine at Mount Sinai, New York, NY, United States, ⁵Department of Radiology, University of Pennsylvania, Philadelphia, PA, United States, ⁶Population Health Science and Policy Department, Icahn School of Medicine at Mount Sinai, New York, NY, United States, ⁷Nash Family Department of Neuroscience and Friedman Brain Institute, Icahn School of Medicine at Mount Sinai, New York, NY, United States

Background: Major depressive disorder (MDD) is a prevalent health problem with complex pathophysiology that is not clearly understood. Prior work has implicated the hippocampus in MDD, but how hippocampal subfields influence or are affected by MDD requires further characterization with high-resolution data. This will help ascertain the accuracy and reproducibility of previous subfield findings in depression as well as correlate subfield volumes with MDD symptom scores. The objective of this study was to assess volumetric differences in hippocampal subfields between MDD patients globally and healthy controls (HC) as well as between a subset of treatment-resistant depression (TRD) patients and HC using automatic segmentation of hippocampal subfields (ASHS) software and ultra-high field MRI.

Methods: Thirty-five MDD patients and 28 HC underwent imaging using 7-Tesla MRI. ASHS software was applied to the imaging data to perform automated hippocampal segmentation and provide volumetrics for analysis. An exploratory analysis was also performed on associations between symptom scores for diagnostic testing and hippocampal subfield volumes.

Results: Compared to HC, MDD and TRD patients showed reduced right-hemisphere CA2/3 subfield volume ($p=0.01$, $\eta^2=0.31$ and $p=0.3$, $\eta^2=0.44$, respectively). Additionally, negative associations were found between subfield volumes and life-stressor checklist scores, including left CA1 ($p=0.041$, $r^2=0.419$), left CA4/DG ($p=0.010$, $r^2=0.584$), right subiculum total ($p=0.038$, $r^2=0.354$), left hippocampus total ($p=0.015$, $r^2=0.134$), and right hippocampus total ($p=0.034$, $r^2=0.110$). Caution should be exercised in interpreting these results due to the small sample size and low power.

Conclusion: Determining biomarkers for MDD and TRD pathophysiology through segmentation on high-resolution MRI data and understanding the effects of stress on these regions can enable better assessment of biological response to treatment selection and may elucidate the underlying mechanisms of depression.

KEYWORDS

depression, hippocampus, magnetic resonance imaging, stress, subfields, ultrahigh field MRI

1. Introduction

Major depressive disorder (MDD) is a debilitating illness of high prevalence worldwide (1) that affects ~6.9% of the U.S. population annually. Current treatments for MDD are lacking due to limited treatment efficacy and significant lag time to onset of therapeutic benefit. Although several mechanisms for depression have been proposed in the literature (2–6), the pathophysiology underlying psychological dysfunction that characterizes the disease is still not clearly understood. Determining measurable neurobiological biomarkers for pathology in MDD may enable better assessment of biological response to treatment selection and timing, highly specific criteria for diagnosis by which to differentiate disease subtypes, and development of novel treatments targeting disease mechanisms. Elucidating the complex interactions between brain biomarkers and clinical characteristics of MDD would allow for greater integration of anatomical biomarkers in clinical diagnoses and treatments.

In addition to understanding the biological basis for MDD, further analysis is warranted to understand treatment-resistant depression (TRD), as there are many patients for whom no sufficient treatment exists (7). It is estimated that 20%–30% of patients with depression experience resistance to treatment (8), and TRD represents approximately half of the treatment costs for MDD overall (9).

A major brain structure known to be implicated in neuropsychiatric diseases is the hippocampus. For perspective, previous magnetic resonance imaging (MRI) studies have shown that structural abnormalities in the hippocampus are often found in post-traumatic stress disorder (10), Alzheimer's disease (11), and depression (12). Furthermore, meta-analyses of large datasets indicate hippocampal grey matter volume is commonly diminished in MDD (13, 14).

Anatomically, the hippocampus consists of cytoarchitecturally defined fields and includes Ammon's horn (and its four subdivisions, CA1–4), the dentate gyrus (DG), and the subiculum (SUB) (15). A variety of neuropsychiatric conditions may involve the hippocampus overall or may differentially involve various hippocampal subfields, as these regions are morphologically and functionally different from one another (16).

Animal studies (17, 18) as well as post-mortem analyses (19, 20) have confirmed that hippocampal subfields are differentially affected by neuropsychiatric diseases (15, 16) and have further reinforced an association between hippocampal subfield volume changes and MDD in humans (21–23). It is possible that volumetric reductions in subfield volumes result from deleterious neurotoxic effects of stress-related hormones on neurons and glial cells (24). Therefore, hippocampal subfield volumes may serve as sensitive biomarkers for the disease. While many studies in depression have been performed, there is still a lack of consistency in the reported subfields with significant findings and validation of existing findings is warranted (25).

MRI has been used to inspect hippocampal subfield volumes *in vivo* (26–30) at varying field strengths. Use of ultra-high field MRI scanners, such as those operating at 7-Tesla (7T), can allow for increased visualization of boundaries and delineation of subfields than conventional clinical strength scanners due to superior contrast and resolution

at 7T (31). These high-field advantages can reveal structural subtleties which are below the threshold of detectability at clinical field strengths (32). There is a limited number of 7T studies examining hippocampal subfields in MDD and their segmentation methods include either manual tracings (33) or automated segmentation with FreeSurfer version 6.0 (29, 34, 35). Manual hippocampal subfield segmentation is labor-intensive and can be difficult to reproduce across research centers (36). The applicability of automated segmentation of hippocampal subfields with FreeSurfer 6.0 has been validated on field strengths lower than 7T (up to 3T) and the atlas used was built from manual tracings in a cohort of elderly subjects, potentially limiting its applicability in studies with younger populations (37). Additionally, some of the subfield boundaries, including the CA4/GC-DG interface and the interfaces between the CA fields along the pyramidal layer of the hippocampus, cannot be clearly visualized in the training data used for the atlas in FreeSurfer 6.0. Overall, there is an ongoing challenge in hippocampal subfield MRI literature, such that there is large discrepancy and variability in subregion definitions and boundaries (25). The fact that there may be variability in subfield delineations warrants further analyses employing other segmentation methods, such as the trained automatic segmentation of hippocampal subfields (ASHS) software (38), to verify and validate results in the MDD cohort.

In this study, we evaluated differences in hippocampal subfield volumes between MDD patients and healthy controls, as well as between a subset of TRD patients and healthy controls. We also performed an exploratory analysis on associations between symptom scores for diagnostic testing, including the Montgomery-Asberg Depression Rating Scale (MADRS) and Life Stressor Checklist (LSC), and hippocampal subfield volumes. These analyses were enabled by acquisition of high-resolution data using 7T MRI and applying ASHS software to perform automated hippocampal subfield segmentation. ASHS is unique in that it has been validated on ultra-high field MRI data (36, 37) and allows for user-defined segmentation protocols through its training pipeline. We used manual hippocampal subfield tracings to generate a specialized 7T atlas for ASHS training to enable increased segmentation accuracy based on our high-resolution 7T data. To our knowledge, this study is the first to apply ASHS to 7T MDD data.

Investigation of hippocampal subfield volumes at higher field strengths using segmentation methods optimized for ultra-high field data can shed light on the accuracy and reproducibility of previous subfield findings in depression as well as association of subfield volumes and MDD symptom scores. Determining biomarkers for pathology in MDD through segmentation on high-resolution MRI data can ultimately enable better assessment of biological response to treatment selection and timing as well as development of novel treatments targeting disease mechanisms.

2. Methods

2.1. Subjects

A total of 63 subjects were included in this study (39 biologic males, 23 biologic females, and one other) including 35 MDD patients

(mean age 39.5 years, standard deviation 11.8 years, 20 males, 14 females, and one other) and 28 healthy controls (mean age 39.4 years, standard deviation 10.4 years, 19 males and 9 females). Age was not significantly different between groups ($p = 0.99$). All participants provided informed written consent prior to investigation. The protocol used was approved by the local Institutional Review Board, namely the Human Research Protection Program at the Icahn School of Medicine at Mount Sinai.

Prior to the MRI visit, a series of symptom questionnaires were administered to all participants by trained clinical raters. Included in these were the Structural Clinical Interview for DSM-IV Axis I Disorders (SCID) or the Structured Clinical Interview for DSM-5 Research Version (SCID-5), the Montgomery-Asberg Depression Rating Scale (MADRS; range 0–60; higher score indicates greater depression severity) and Life Stressor Checklist (LSC; range 0–30, higher score indicates greater number of exposures to stressful life events). Lifetime number of antidepressant failures were also collected. The demographic and clinical characteristics are presented in Table 1.

All subjects underwent MRI scanning at 7T (Magnetom, Siemens) under an approved protocol by the Institutional Review Board at the Icahn School of Medicine at Mount Sinai. To qualify for the study, MDD participants needed to have a current primary diagnosis of MDD based on clinical evaluation using the SCID or SCID-5. All MDD participants were antidepressant free for at least 4 weeks prior to study participation. Healthy control (HC) participants were also assessed using the SCID or SCID-5 and were excluded for any current or lifetime psychiatric conditions. Participants in both groups with a current diagnosis of obsessive-compulsive disorder, with alcohol or substance use disorder in the past year, or with a lifetime history of psychosis, neurological disease, or bipolar disorder were excluded. Participants with contraindications to 7T MRI were also excluded. TRD patients were defined as patients with a lifetime history of one or more anti-depressant failures. This is a non-standard definition for TRD and, therefore, results in this subset of patients would be considered very preliminary.

2.2. Image acquisition protocol

A 32-channel Nova Medical head coil was used to acquire brain images for segmentation. The 90-min imaging protocol included MP2RAGE (TR 6,000 ms, TI1 1,050 ms, TI2 3,000 ms, TE 5.06 ms, voxel $0.70 \times 0.70 \times 0.70 \text{ mm}^3$) and T_2 TSE (TR 9,000 ms, TE 69 ms, voxel $0.45 \times 0.45 \times 2 \text{ mm}^3$) scans acquired at a coronal oblique oriented perpendicular to the long axis of the hippocampus.

2.3. Hippocampal subfield segmentation

Prior to performing automated hippocampal subfield segmentation manual subfield tracings were performed using 3DSlicer software on high-resolution 7T T_2 -TSE images ($0.45 \times 0.45 \times 2 \text{ mm}^3$). The tracing method was guided and verified by an expert neuroanatomist (PH) and neuroradiologist (BD) and the segmentations were generated through the joint effort of two trained image analysts, including the following subfields: CA1, CA2/3, CA4/DG, subiculum, and pre-subiculum.

As ASHS performs hippocampal subfield segmentation based on existing brain atlases, the developers of the ASHS platform allowed for atlas building, which can enable increased segmentation accuracy based on advantages of a given set of data. Therefore, we used the manual tracings described above to generate a specialized 7T atlas for ASHS training.

The atlas contained manually-traced hippocampi on 7T images on a combined subset of 15 MDD patients and controls with no clinically significant, identifiable hippocampal abnormalities. The manually segmented subsample consisted of 6 females, with a mean age of 41.3 years and 9 males, with a mean age of 48.1 years. A left-right flip of each segmentation was performed, resulting in a total of 30 subjects for ASHS atlas training. The atlas was approved upon visual inspection by an expert neuroradiologist (BD) and neuroanatomist (PH).

Automated hippocampal subfield segmentation using the specialized 7T atlas for ASHS was applied to 7T MRI data on MDD patients and healthy controls. The subfields delineated by ASHS are the same as those segmented in the manual tracings used for training and included CA1, CA2/3, CA4/DG, subiculum, and pre-subiculum. High resolution T_1 and T_2 weighted images were used as inputs to perform optimal segmentation with ASHS.

2.4. Statistics

All hippocampal subfields were normalized to total brain volume provided by FreeSurfer version 6.0. For this normalization, each subfield volume was divided by the total brain volume of a given subject and multiplied by a scaling factor. We elected to combine the subiculum and presubiculum into one region (subiculum total) for analysis in order to overcome inconsistencies between methods in segmenting these regions (25). Because the data were not normally distributed, the nonparametric Mann-Whitney U -test was used to compare subfield volumes by group. Effect sizes (η^2) were also calculated. A proportional odds ordinal

TABLE 1 Demographic and clinical characteristics.

	MDD ($n = 35$)	HC ($n = 28$)	Value of p
Male (frequency, %)	20, 57.14%	19, 67.86%	0.46
Age, years (mean \pm SD)	39.46 \pm 11.77	39.43 \pm 10.35	0.99
Age at first episode (mean \pm SD)	18.46 \pm 14.07	–	–
Duration of current episode, months (mean \pm SD)	47.52 \pm 71.80	–	–
Number of antidepressant failures (mean \pm SD)	1.25 \pm 2.02 (32)	–	–
MADRS	22.94 \pm 11.93	0.50 \pm 1.07	2.58E-14*
LSC	5.15 \pm 4.35 (26)	2.32 \pm 2.13	0.0034*

MADRS, Montgomery-Asberg Depression Rating Scale; LSC, Life Stressor Checklist.

*Significant value of $p < 0.05$ for MDD group compared to HC group.

logistic regression model was also used to compare subfield volumes by group, controlling for age and biological sex. β values were also calculated. A multivariate ordinary least squares regression model was applied to predict symptom scores, specifically MADRS and LSC score, from hippocampal subfield volumes, controlling for age and biological sex. Effect sizes (*Cohen's* f^2) were also calculated. Significance was set at an α level of 0.05 for all tests. Correction for multiple comparisons was performed on all findings using adaptive false discovery rate (FDR) (39).

3. Results

The results of ASHS hippocampal subfield segmentation for one representative subject are shown in Figure 1.

3.1. Group comparisons of subfield volumes

3.1.1. Group comparison of subfield volumes in MDD patients and controls

The full set of results for this group comparison is shown in Tables 2A,B. Table 2A summarizes the results of the Mann–Whitney *U*-test and Table 2B summarizes the results of the proportional odds ordinal logistic regression model, controlling for age and biological sex. The volume of the CA2/3 subfield on the right side was found to be significantly smaller in patients compared to controls in Table 2A ($p=0.01$, $\eta^2=0.31$), as shown in Figure 2, and in Table 2B ($p=0.02$, $\beta=1.12$). No subfield was significant after correction for multiple comparisons using the adaptive FDR method.

3.1.2. Group comparison of subfield volumes in TRD subset and controls

The full set of results for this group comparison is shown in Tables 3A,B. Table 3A summarizes the results of the Mann–Whitney *U*-test on 13 TRD patients (eight males, five females) and 13 HC. Table 3B summarizes the results of the proportional odds ordinal logistic regression model, controlling for age and biological sex, on 13 TRD patients and 28 HC. The volume of the CA2/3 subfield on the right side was found to be significantly smaller in patients compared to controls in Table 3A ($p=0.03$, $\eta^2=0.44$), as shown in Figure 3, and in Table 3B ($p=0.01$, $\beta=-1.77$). The right CA2/3 subfield volume finding, identified through the proportional odds ordinal logistic regression model, was significant after correction for multiple comparisons ($p=0.04$) using the adaptive FDR method.

3.2. Regression analysis predicting symptom scores from subfield volumes

In a subset of 26 patients (14 males, 12 females) and 28 healthy controls (19 males, nine females) for which symptom scores were collected, linear regressions, with age and sex as covariates, were performed to assess the relationship between symptom scores and hippocampal subfield volumes.

The ASHS generated subfield volumes that had significance in association with LSC scores included left CA1 ($p=0.04$, $f^2=0.419$), left CA4/DG ($p=0.01$, $f^2=0.584$), and right subiculum total ($p=0.04$, $f^2=0.354$), all of which indicated a negative relationship between subfield volume and LSC score. Similarly, the left hippocampus total

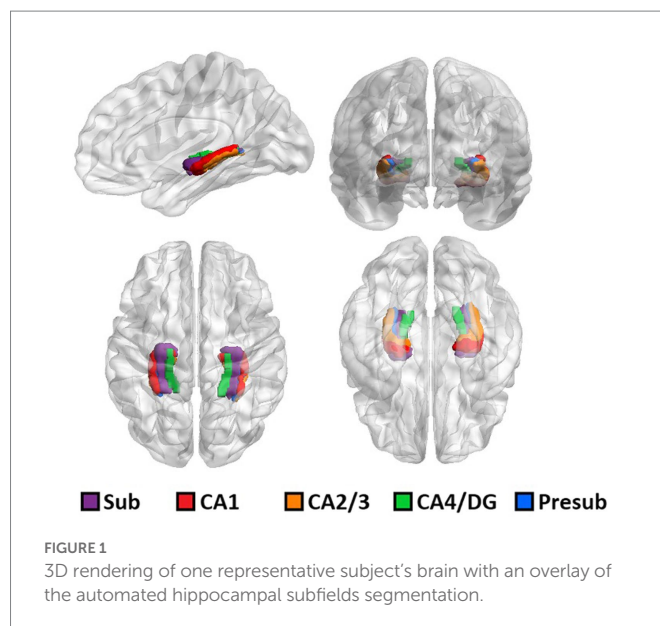


TABLE 2A Group differences in volumes between MDD patients and healthy controls.

Hippocampal subfield	Left hemisphere		Right hemisphere	
	Raw/Adj <i>p</i>	η^2	Raw/Adj <i>p</i>	η^2
CA1	0.62/0.79	0.06	0.75/0.75	0.04
CA2/3	0.08/0.38	0.22	0.01*/0.06	0.31
CA4/DG	0.69/0.79	0.05	0.16/0.36	0.18
Subiculum total	0.79/0.79	0.03	0.74/0.75	0.04
Hippocampus total	0.62/0.79	0.06	0.22/0.36	0.16

*Significant p -value < 0.05 in right hemisphere CA2/3 without correction for multiple comparisons. No subfield was significant after corrected for multiple comparisons by brain side using the adaptive false discovery method Mann–Whitney *U*-test; effect sizes $\eta^2 \geq 0.1$, $\eta^2 \geq 0.3$, and $\eta^2 \geq 0.5$ represent small, medium, and large effect sizes, respectively; ($n = 63$; 35 MDD, 28 HC).

TABLE 2B Group effect in volumes between MDD patients and healthy controls, adjusting for age and sex using proportional odds ordinal logistic regression model.

Hippocampal subfield	Left hemisphere		Right hemisphere	
	Raw/Adj <i>p</i>	β (SE)	Raw/Adj <i>p</i>	β (SE)
CA1	0.67/0.93	0.19 (0.44)	0.54/0.66	0.27 (0.45)
CA2/3	0.06/0.32	0.84 (0.45)	0.02*/0.08	1.12 (0.46)
CA4/DG	0.80/0.93	0.11 (0.44)	0.15/0.27	0.65 (0.45)
Subiculum total	0.93/0.93	−0.04 (0.44)	0.66/0.66	0.20 (0.44)
Hippocampus total	0.57/0.93	0.25 (0.45)	0.16/0.27	0.63 (0.45)

*Significant p -value < 0.05 in right hemisphere CA2/3 without correction for multiple comparisons. No subfield was significant after corrected for multiple comparisons by brain side using the adaptive false discovery method; ($n = 63$; 35 MDD, 28 HC).

volume ($p=0.02$, $f^2=0.134$) and right hippocampus total volume ($p=0.03$, $f^2=0.110$) were also significant in their negative association with LSC scores. Regression plots with ASHS software significant findings are shown in Figure 4. All significant findings survived multiple comparison correction with adaptive FDR. The full set of results for the

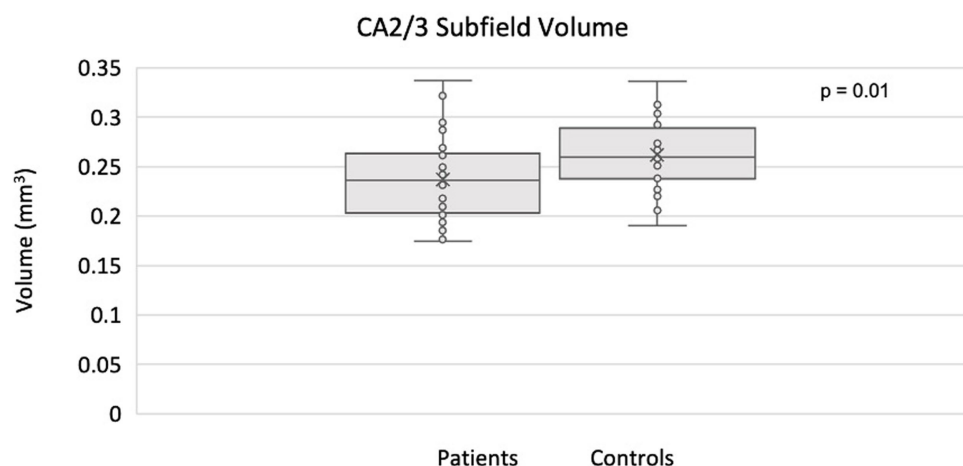


FIGURE 2

Smaller CA2/3 subfield volume in the right hippocampus of MDD patients compared to controls using ASHS.

TABLE 3A Group differences in volumes between TRD patients and healthy controls.

Hippocampal subfield	Left hemisphere		Right hemisphere	
	Raw/Adj p	η^2	Raw/Adj p	η^2
CA1	0.82/0.82	0.05	0.23/0.29	0.24
CA2/3	0.23/0.82	0.24	0.03*/0.13	0.44
CA4/DG	0.46/0.82	0.15	0.13/0.24	0.3
Subiculum total	0.78/0.82	0.06	0.82/0.82	0.05
Hippocampus total	0.59/0.82	0.11	0.15/0.24	0.29

*Significant p -value < 0.05 in right hemisphere CA2/3, corrected for multiple comparisons by brain side using the adaptive false discovery rate method, Mann–Whitney U -test; effect sizes $\eta^2 \geq 0.1$, $\eta^2 \geq 0.3$, and $\eta^2 \geq 0.5$ represent small, medium, and large effect sizes, respectively; ($n = 26$; 13 MDD, 13 HC).

TABLE 3B Group effect in volumes between TRD patients and healthy controls, adjusting for age and sex using proportional odds ordinal logistic regression model.

Hippocampal subfield	Left hemisphere		Right hemisphere	
	Raw/Adj p	β (SE)	Raw/Adj p	β (SE)
CA1	0.86/0.86	−0.11 (0.61)	0.28/0.35	−0.67 (0.28)
CA2/3	0.12/0.60	−0.97 (0.63)	0.01*/0.04*	−1.77 (0.66)
CA4/DG	0.81/0.86	−0.14 (0.61)	0.10/0.23	−1.02 (0.63)
Subiculum total	0.56/0.86	0.36 (0.61)	0.77/0.77	0.18 (0.61)
Hippocampus total	0.73/0.86	−0.21 (0.61)	0.14/0.23	−0.93 (0.62)

*Significant p -value < 0.05 in right hemisphere CA2/3, corrected for multiple comparisons by brain side using the adaptive false discovery rate method; ($n = 41$; 13 MDD, 28 HC).

associations between LSC scores and hippocampal subfields are shown in Table 4. The MADRS score and other symptom scores collected showed no significant association with subfield volumes.

4. Discussion

In this study, we used high-resolution 7T MRI data to train the ASHS software for hippocampal subfield segmentation and analyze

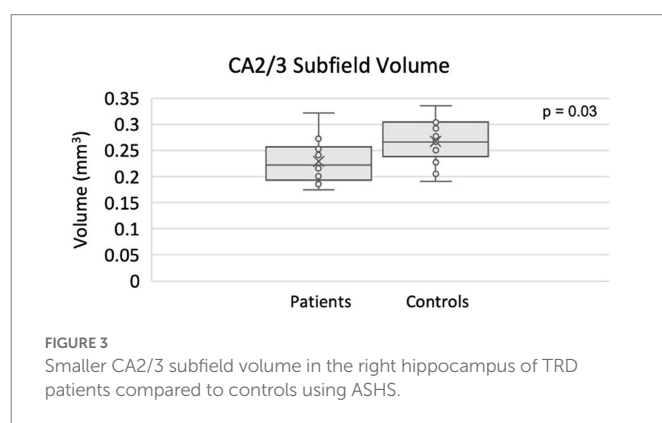


FIGURE 3

Smaller CA2/3 subfield volume in the right hippocampus of TRD patients compared to controls using ASHS.

hippocampal subfield volumes in depression. The analyses in this study involved group comparisons between MDD patients and healthy controls and between TRD patients and healthy controls, as well as regressions for prediction of symptom scores from hippocampal subfield volumes to probe the effects of stress on specific hippocampal domains.

4.1. Hippocampal subfield volume differences between patients and controls

Significant volumetric differences between MDD patients and controls were found in CA2/3 in the right hemisphere, with smaller volumes in patients, a pattern which is concordant with the literature on hippocampal subfield changes associated with stress-related disorders (40, 41). Pyramidal neurons in the CA fields are most susceptible to stress and increased cortisol levels (17, 40, 41) which induces neuronal damage, dendritic shrinkage, and reduced astrocyte density, which together may contribute to volume loss (41). This group-level finding persisted in the subset of TRD patients compared to healthy controls, suggesting that hippocampal abnormalities may be further pronounced in patients with resistance to antidepressants. Given the small sample size, however, this finding must be interpreted with caution and validated in a larger population.

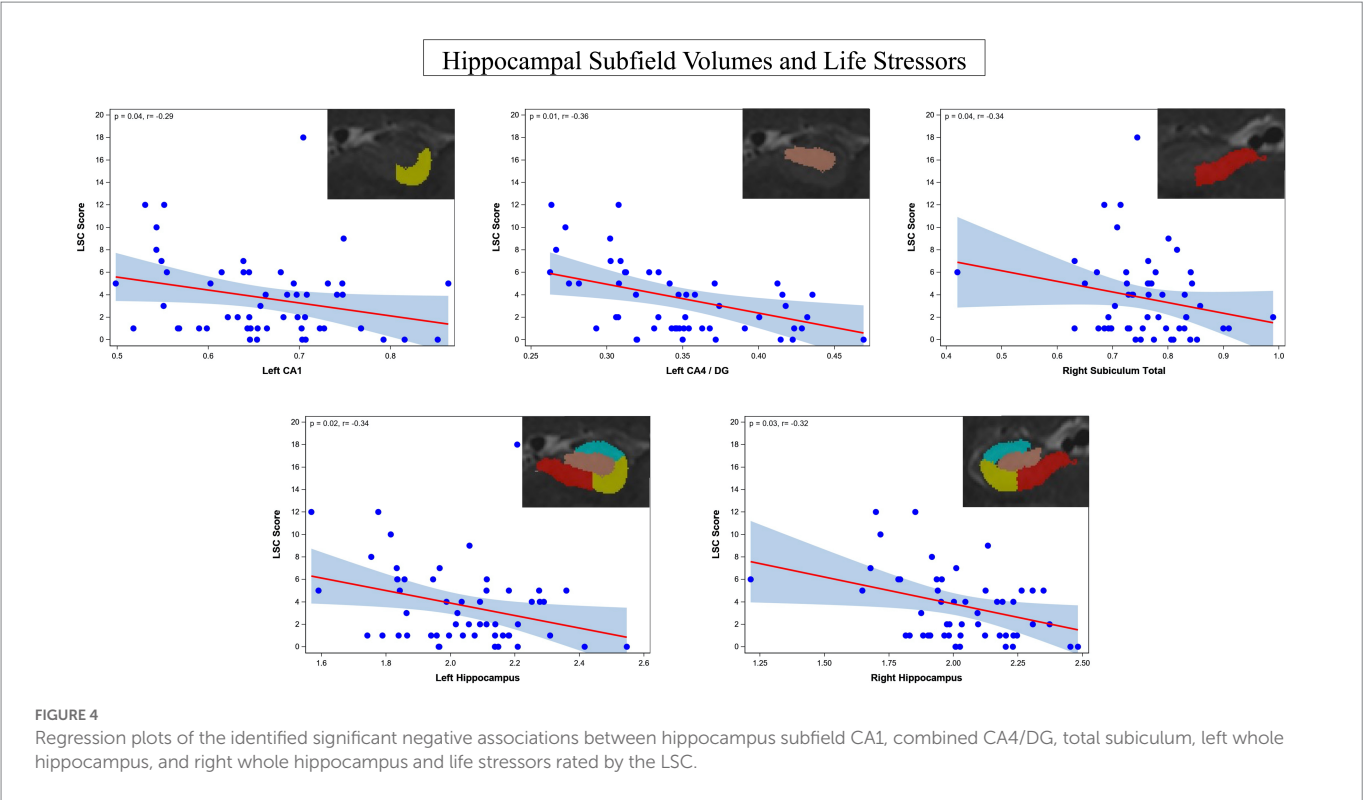


TABLE 4 Regression analysis findings for LSC score and hippocampal subfield volumes in MDD patients and healthy controls.

Hippocampal subfield	Left hemisphere		Right hemisphere	
	Raw/Adj <i>p</i>	Cohen's <i>f</i> ²	Raw/Adj <i>p</i>	Cohen's <i>f</i> ²
CA1	0.04*/0.04*	0.419	0.13/0.13	0.271
CA2/3	0.08/0.08	0.389	0.18/0.18	0.281
CA4/DG	0.01*/0.02*	0.584	0.14/0.14	0.696
Subiculum total	0.23/0.23	0.423	0.04*/0.04*	0.354
Hippocampus total	0.02*/0.02*	0.134	0.03*/0.04*	0.11

*Significant *p*-value < 0.05 in left hemisphere CA1 and CA4/DG, right hemisphere subiculum total, and hippocampus total in the left and right hemispheres, corrected for multiple comparisons by brain side using the adaptive false discovery method; local effect sizes $f^2 \geq 0.02$, $f^2 \geq 0.15$, and $f^2 \geq 0.35$ represent small, medium, and large effect sizes, respectively; (*n* = 54; 26 MDD, 28 HC).

4.2. Associations between hippocampal subfield volumes and LSC scores

Significant negative associations were found between LSC scores and subfield volumes, specifically left CA1, left CA4/DG, and right entire subiculum. Significant negative associations were also found between LSC and total hippocampal volume in the left and right hemispheres. Investigating associations between LSC score and hippocampal subfields in depression is important to understanding the effects of stress on the hippocampal anatomy, specifically dendritic shrinkage and other neurotoxic effects (24). These findings are concordant with the effects of stress on hippocampal anatomy, specifically affecting the CA fields (21).

4.3. Limitations and future directions

A limitation of this study is the small sample size. Despite this, significant differences were found between MDD patients and healthy

controls in this dataset, suggesting potential 7T benefits of resolving and identifying subtle structural changes in small subregions including hippocampal subfields. There were also a few subfields with medium to large effect sizes that showed a trend toward an association with MDD, such as the right CA2/3 in Table 2 and right CA4/DG in Table 4. We estimated the *post hoc* power for detecting the difference in right CA2/3 between the MDD patients and the healthy controls to be 43%, with a significance level (alpha) of 0.01 using the Wilcoxon Mann–Whitney test. Caution should be exercised in interpreting the results as low study power can lead to not only decreased likelihood of finding a true association but also overestimation of effect size and low reproducibility. Analysis with a larger sample size or performance of meta-analysis would be necessary to validate these findings (42).

In studying MDD and its relationship to different depression related symptoms, we found that hippocampal subfield CA2/3 was reduced in MDD patients compared to controls as well as in TDR patients versus controls and that reductions in CA1, CA4/DG, and subiculum correlated with lifetime stressors. Leveraging the benefits of ultrahigh field 7T MRI, including superior signal and resolution over

clinical field strength MRI, to investigate the hippocampus and its subfields and using a 7T-trained and validated automated segmentation software to that end, can enable overall enhanced detection of imaging markers for MDD and treatment-resistant MDD. Hippocampal subfield volumes may serve as imaging biomarkers for MDD, which may help design more targeted treatments for the disease in the future. Furthermore, we found that there is value in studying MDD and its relationship to different depression related symptoms, especially lifetime stressors, rather than analyzing depression as a binary diagnosis.

Data availability statement

The raw data supporting the conclusions of this article will be made available by the authors, without undue reservation.

Ethics statement

The studies involving human participants were reviewed and approved by Icahn School of Medicine at Mount Sinai. The patients/participants provided their written informed consent to participate in this study.

Author contributions

JA study design, acquisition of data, analysis and interpretation of data, and drafting of manuscript. RF acquisition of data through generating training segmentation data for atlas creation. GV imaging data acquisition and analysis by creating scripts for data extrapolation and for providing key figures. SR recruitment and acquisition of symptom score data, statistical analysis of data including choice of statistical test and results interpretation. K-hH, LX, and PY implementation of automated segmentation software and atlas creation. YJ statistical analysis of data including choice of statistical test and interpretation of results. SB data organization and statistical testing. MK and MS subject recruitment and acquisition of clinical data. H-ML statistical analysis methods chosen and interpretation of results. LF implementation of automated segmentation software. BD study conception and design and analysis and interpretation of data. PH study conception and design and provided training for atlas creation. JM study conception and design, acquisition of data, analysis and

interpretation of data. PB contributed substantially to study conception and design, acquisition of data, analysis and interpretation of data, and supervised the study. All authors contributed to the article and approved the submitted version.

Funding

This research was supported by funds NIH R01 MH109544 and R01HL116953. Icahn School of Medicine Capital Campaign, Translational and Molecular Imaging Institute and Department of Diagnostic, Molecular, and Interventional Radiology.

Acknowledgments

The Ehrenkranz Laboratory for Human Resilience, a component of the Depression and Anxiety Center for Discovery and Treatment at the Icahn School of Medicine at Mount Sinai, and by a generous gift from the Gottesman Foundation to Mount Sinai. CCNY Department of Biomedical Engineering.

Conflict of interest

PB is a named inventor on patents relating to magnetic resonance imaging (MRI) and RF pulse design. The patents have been licensed to GE Healthcare, Siemens AG, and Philips international.

The remaining authors declare that the research was conducted in the absence of any commercial or financial relationships that could be construed as a potential conflict of interest.

Publisher's note

All claims expressed in this article are solely those of the authors and do not necessarily represent those of their affiliated organizations, or those of the publisher, the editors and the reviewers. Any product that may be evaluated in this article, or claim that may be made by its manufacturer, is not guaranteed or endorsed by the publisher.

References

- Kessler, RC, Berglund, P, Demler, O, Jin, R, Koretz, D, Merikangas, KR, et al. The epidemiology of major depressive disorder: results from the National Comorbidity Survey Replication (NCS-R). *JAMA*. (2003) 289:3095–105. doi: 10.1001/jama.289.23.3095
- Small, SA, Schobel, SA, Buxton, RB, Witter, MP, and Barnes, CA. A pathophysiological framework of hippocampal dysfunction in ageing and disease. *Nat Rev Neurosci*. (2011) 12:585–601. doi: 10.1038/nrn3085
- Krishnan, V, and Nestler, EJ. The molecular neurobiology of depression. *Nature*. (2008) 455:894–902. doi: 10.1038/nature07455
- Hasler, G. Pathophysiology of depression: do we have any solid evidence of interest to clinicians? *World Psychiatry*. (2010) 9:155–61. doi: 10.1002/j.2051-5545.2010.tb00298.x
- Kakeda, S, Watanabe, K, Katsuki, A, Sugimoto, K, Igata, N, Ueda, I, et al. Relationship between interleukin (IL)-6 and brain morphology in drug-naïve, first-episode major depressive disorder using surface-based morphometry. *Sci Rep*. (2018) 8:1–9. doi: 10.1038/s41598-018-28300-5
- Tesen, H, Watanabe, K, Okamoto, N, Ikenouchi, A, Igata, R, Konishi, Y, et al. Volume of amygdala subregions and clinical manifestations in patients with first-episode, drug-naïve major depression. *Front Hum Neurosci*. (2022) 15:780884. doi: 10.3389/fnhum.2021.780884
- Murrough, JW, and Charney, DS. Is there anything really novel on the antidepressant horizon? *Curr Psychiatry Rep*. (2012) 14:643–9. doi: 10.1007/s11920-012-0321-8
- Rush, AJ, Trivedi, MH, Wisniewski, SR, Nierenberg, AA, Stewart, JW, Warden, D, et al. Acute and longer-term outcomes in depressed outpatients requiring one or several treatment steps: a STAR*D report. *Am J Psychiatr*. (2006) 163:1905–17. doi: 10.1176/ajp.2006.163.11.1905
- Greden, JF. The burden of disease for treatment-resistant depression. *J Clin Psychiatry*. (2001) 62:26–31.
- Sala, M, Perez, J, Soloff, P, Di Nemi, SU, Caverzasi, E, Soares, JC, et al. Stress and hippocampal abnormalities in psychiatric disorders. *Eur Neuropsychopharmacol*. (2004) 14:393–405. doi: 10.1016/j.euroneuro.2003.12.005
- Barnes, J, Ourselin, S, and Fox, NC. Clinical application of measurement of hippocampal atrophy in degenerative dementias. *Hippocampus*. (2009) 19:510–6. doi: 10.1002/hipo.20617
- Bremner, JD, Narayan, M, Anderson, ER, Staib, LH, Miller, HL, and Charney, DS. Hippocampal volume reduction in major depression. *Am J Psychiatr*. (2000) 157:115–8. doi: 10.1176/ajp.157.1.115
- Wise, T, Radua, J, Via, E, Cardoner, N, Abe, O, Adams, TM, et al. Common and distinct patterns of grey-matter volume alteration in major depression and bipolar

- disorder: evidence from voxel-based meta-analysis. *Mol Psychiatry*. (2017) 22:1455–63. doi: 10.1038/mp.2016.72
14. Schmaal, L, Veltman, DJ, van Erp, TG, Sämann, PG, Frodl, T, Jahanshad, N, et al. Subcortical brain alterations in major depressive disorder: findings from the ENIGMA major depressive disorder working group. *Mol Psychiatry*. (2016) 21:806–12. doi: 10.1038/mp.2015.69
 15. Duvernoy, HM. *The human hippocampus: Functional anatomy, vascularization and serial sections with MRI* Springer Science & Business Media (2005).
 16. Langston, RF, Stevenson, CH, Wilson, CL, Saunders, I, and Wood, ER. The role of hippocampal subregions in memory for stimulus associations. *Behav Brain Res*. (2010) 215:275–91. doi: 10.1016/j.bbr.2010.07.006
 17. Sapolsky, RM. Glucocorticoids and hippocampal atrophy in neuropsychiatric disorders. *Arch Gen Psychiatry*. (2000) 57:925–35. doi: 10.1001/archpsyc.57.10.925
 18. Sousa, N, Paula-Barbosa, MM, and Almeida, O. Ligand and subfield specificity of corticoid-induced neuronal loss in the rat hippocampal formation. *Neuroscience*. (1999) 89:1079–87. doi: 10.1016/S0306-4522(98)00311-X
 19. Stockmeier, CA, Mahajan, GJ, Konick, LC, Overholser, JC, Jurjus, GJ, Meltzer, HY, et al. Cellular changes in the postmortem hippocampus in major depression. *Biol Psychiatry*. (2004) 56:640–50. doi: 10.1016/j.biopsych.2004.08.022
 20. Rössler, M, Zarski, R, Bohl, J, and Ohm, TG. Stage-dependent and sector-specific neuronal loss in hippocampus during Alzheimer's disease. *Acta Neuropathol*. (2002) 103:363–9.
 21. Huang, Y, Coupland, NJ, Lebel, RM, Carter, R, Seres, P, Wilman, AH, et al. Structural changes in hippocampal subfields in major depressive disorder: a high-field magnetic resonance imaging study. *Biol Psychiatry*. (2013) 74:62–8. doi: 10.1016/j.biopsych.2013.01.005
 22. Malykhin, NV, Seres, MP, and Coupland, NJ. Structural changes in the hippocampus in major depressive disorder: contributions of disease and treatment. *J Psychiatry Neurosci: JPN*. (2010) 35:337–43. doi: 10.1503/jpn.100002
 23. Malykhin, N, and Coupland, N. Hippocampal neuroplasticity in major depressive disorder. *Neuroscience*. (2015) 309:200–13. doi: 10.1016/j.neuroscience.2015.04.047
 24. Liu, W, Ge, T, Leng, Y, Pan, Z, Fan, J, Yang, W, et al. The role of neural plasticity in depression: from hippocampus to prefrontal cortex. *Neural Plast*. (2017) 2017:1–11. doi: 10.1155/2017/6871089
 25. Yushkevich, PA, Amaral, RS, Augustinack, JC, Bender, AR, Bernstein, JD, Boccardi, M, et al. Quantitative comparison of 21 protocols for labeling hippocampal subfields and parahippocampal subregions in *in vivo* MRI: towards a harmonized segmentation protocol. *NeuroImage*. (2015) 111:526–41. doi: 10.1016/j.neuroimage.2015.01.004
 26. Malykhin, N, Lebel, RM, Coupland, NJ, Wilman, AH, and Carter, R, et al. *In vivo* quantification of hippocampal subfields using 4.7 T fast spin echo imaging. *NeuroImage*. (2010) 49:1224–30. doi: 10.1016/j.neuroimage.2009.09.042
 27. Wisse, L, Gerritsen, L, Zwanenburg, JJ, Kuijf, HJ, Luijten, PR, Biessels, GJ, et al. Subfields of the hippocampal formation at 7 T MRI: *in vivo* volumetric assessment. *NeuroImage*. (2012) 61:1043–9. doi: 10.1016/j.neuroimage.2012.03.023
 28. Mueller, SG, Schuff, N, Yaffe, K, Madison, C, Miller, B, and Weiner, MW. Hippocampal atrophy patterns in mild cognitive impairment and Alzheimer's disease. *Hum Brain Mapp*. (2010) 31:1339–47. doi: 10.1002/hbm.20934
 29. Brown, SS, Rutland, JW, Verma, G, Feldman, RE, Alper, J, Schneider, M, et al. Structural MRI at 7T reveals amygdala nuclei and hippocampal subfield volumetric association with major depressive disorder symptom severity. *Sci Rep*. (2019) 9:1–10.
 30. Katsuki, A, Watanabe, K, Nguyen, L, Otsuka, Y, Igata, R, Ikenouchi, A, et al. Structural changes in hippocampal subfields in patients with continuous remission of drug-naïve major depressive disorder. *Int J Mol Sci*. (2020) 21:3032. doi: 10.3390/ijms21093032
 31. Balchandani, P, and Naidich, T. Ultra-high-field MR neuroimaging. *Am J Neuroradiol*. (2015) 36:1204–15. doi: 10.3174/ajnr.A4180
 32. Pai, A, Marcuse, LV, Alper, J, Delman, BN, Rutland, JW, Feldman, RE, et al. Detection of hippocampal subfield asymmetry at 7T with automated segmentation in epilepsy patients with Normal clinical strength MRIs. *Front Neurol*. (2021) 12:682615. doi: 10.3389/fneur.2021.682615
 33. Wisse, LEM, Biessels, GJ, Stegenga, BT, Kooistra, M, Van Der Veen, PH, Zwanenburg, JJM, et al. Major depressive episodes over the course of 7 years and hippocampal subfield volumes at 7 tesla MRI: the PREDICT-MR study. *J Affect Disord*. (2015) 175:1–7. doi: 10.1016/j.jad.2014.12.052
 34. Kraus, C, Seiger, R, Pfabigan, DM, Sladky, R, Tik, M, Paul, K, et al. Hippocampal subfields in acute and remitted depression—an ultra-high field magnetic resonance imaging study. *Int J Neuropsychopharmacol*. (2019) 22:513–22. doi: 10.1093/ijnp/pyz030
 35. Tannous, J, Godlewska, BR, Tirumalaraju, V, Soares, JC, Cowen, PJ, and Selvaraj, S. Stress, inflammation and hippocampal subfields in depression: a 7 tesla MRI study. *Transl Psychiatry*. (2020) 10:1–7. doi: 10.1038/s41398-020-0759-0
 36. Wisse, LE, Kuijf, HJ, Honingh, AM, Wang, H, Pluta, JB, Das, SR, et al. Automated hippocampal subfield segmentation at 7T MRI. *Am J Neuroradiol*. (2016) 37:1050–7. doi: 10.3174/ajnr.A4659
 37. Giuliano, A, Donatelli, G, Cosottini, M, Tosetti, M, Retico, A, and Fantacci, ME. Hippocampal subfields at ultra high field MRI: an overview of segmentation and measurement methods. *Hippocampus*. (2017) 27:481–94. doi: 10.1002/hipo.22717
 38. Yushkevich, PA, Pluta, JB, Wang, H, Xie, L, Ding, SL, Gertje, EC, et al. Automated volumetry and regional thickness analysis of hippocampal subfields and medial temporal cortical structures in mild cognitive impairment. *Hum Brain Mapp*. (2015) 36:258–87. doi: 10.1002/hbm.22627
 39. Blanchard, G, and Roquain, É. Adaptive false discovery rate control under Independence and dependence. *J Mach Learn Res*. (2009) 10, 2837–2871.
 40. Travis, SG, Coupland, NJ, Hegadoren, K, Silverstone, PH, Huang, Y, Carter, R, et al. Effects of cortisol on hippocampal subfields volumes and memory performance in healthy control subjects and patients with major depressive disorder. *J Affect Disord*. (2016) 201:34–41. doi: 10.1016/j.jad.2016.04.049
 41. Saur, L, Baptista, PPA, Bagatini, PB, Neves, LT, de Oliveira, RM, Vaz, SP, et al. Experimental post-traumatic stress disorder decreases astrocyte density and changes astrocytic polarity in the CA1 hippocampus of male rats. *Neurochem Res*. (2016) 41:892–904. doi: 10.1007/s11064-015-1770-3
 42. Button, KS, Ioannidis, J, Mokrysz, C, Nosek, BA, Flint, J, Robinson, ES, et al. Power failure: why small sample size undermines the reliability of neuroscience. *Nat Rev Neurosci*. (2013) 14:365–76. doi: 10.1038/nrn3475



OPEN ACCESS

EDITED BY

Chien-Han Lai,
National Yang-Ming University,
Taiwan

REVIEWED BY

Yosuke Morishima,
University of Bern,
Switzerland
Yixuan Ku,
Sun Yat-sen University, China

*CORRESPONDENCE

Weidong Li
✉ liwd@sjtu.edu.cn
Lihui Wang
✉ lihui.wang@sjtu.edu.cn

SPECIALTY SECTION

This article was submitted to
Mood Disorders,
a section of the journal
Frontiers in Psychiatry

RECEIVED 19 November 2022

ACCEPTED 18 January 2023

PUBLISHED 06 February 2023

CITATION

Chen Z, Wang Z, Shen Y, Zeng S, Yang X,
Kuang Y, Dou Z, Wang L and Li W (2023) Face-
specific negative bias of aesthetic perception in
depression: Behavioral and EEG evidence.
Front. Psychiatry 14:1102843.
doi: 10.3389/fpsy.2023.1102843

COPYRIGHT

© 2023 Chen, Wang, Shen, Zeng, Yang, Kuang,
Dou, Wang and Li. This is an open-access
article distributed under the terms of the
[Creative Commons Attribution License \(CC BY\)](https://creativecommons.org/licenses/by/4.0/).
The use, distribution or reproduction in other
forums is permitted, provided the original
author(s) and the copyright owner(s) are
credited and that the original publication in this
journal is cited, in accordance with accepted
academic practice. No use, distribution or
reproduction is permitted which does not
comply with these terms.

Face-specific negative bias of aesthetic perception in depression: Behavioral and EEG evidence

Zhitang Chen^{1,2,3}, Zhenghua Wang⁴, Yuhua Shen⁴, Suhua Zeng^{1,2,3},
Xiangyu Yang^{1,2,3}, Yifang Kuang^{1,2,3}, Zheng Dou^{1,2,3}, Lihui Wang^{2,5,6*}
and Weidong Li^{1,2,3,5,6*}

¹Bio-X Institutes, Key Laboratory for the Genetics of Development and Neuropsychiatric Disorders, School of Life Sciences and Biotechnology, Shanghai Jiao Tong University, Shanghai, China, ²Institute of Psychology and Behavioral Science, Shanghai Jiao Tong University, Shanghai, China, ³WLA Laboratories, World Laureates Association, Shanghai, China, ⁴The Fourth People's Hospital of Wuhu, Wuhu, Jiangsu, China, ⁵Shanghai Key Laboratory of Psychotic Disorders, Shanghai Mental Health Center, Shanghai Jiao Tong University School of Medicine, Shanghai, China, ⁶Shanghai Center for Brain Science and Brain-Inspired Intelligence Technology, Shanghai, China

Introduction: Symptoms of depression are associated with the dysfunction of neural systems such as the emotion, reward system, and the default mode network. These systems were suggested by the model of neuroaesthetics as key contributions to aesthetic experience, leading to the prediction of atypical aesthetic orientation in depression. Here we investigated the aesthetic characteristics of depression and the corresponding neural underpinnings.

Methods: Fifty-two (25 depression patients, 27 healthy controls) participants were asked to make aesthetic judgments on faces and landscapes in an electroencephalographic (EEG) experiment.

Results: Our results indicate that relative to the controls, the depression tended to give ugly judgments and refrained from giving beautiful judgments, which was observed only for faces but not for landscapes. We also found that the face-induced component N170 was more negative in the depression group than the control group for ugly and neutral faces. Moreover, the aesthetic evaluation of ugly faces was associated with decreased N200 negativity in the depression group than in the control group, while the evaluation of beautiful faces was associated with decreased brain synchronization at the theta band.

Discussion: These results suggested a face-specific negative aesthetic bias in depression which can help to design and develop aesthetics-oriented schemes in assisting the clinical diagnosis and therapy of depression.

KEYWORDS

depression, face, aesthetic bias, electroencephalography, neuroaesthetics

1. Introduction

When people have a depressive episode, the visual world seems to lose its color. What was beautiful may look flat or even ugly. What was enjoyed or assigned value stops being pleasurable or worth living for. In accordance with the two core clinical symptoms “depressed mood” and “loss of interest or pleasure in nearly all activities” (i.e., anhedonia) (1), great effort has been made to reveal the cognitive and neural mechanisms of the affective and the motivational abnormalities in depression. On the affective aspect, depressive populations exhibit biased cognitive processing for negative information against positive information (2). At the neural level, the processing of negative

information in depression is accompanied by hyperactivity in the limbic areas such as the amygdala, and aberrant activity in the prefrontal cortex (3). On the motivational aspect, depressive populations show insensitivity to reward stimuli and impaired ability to pursue rewarding behaviors, underlined by hypoactivity in the striatum and the prefrontal cortex (4).

While the affective and motivational characteristics of depression have been well documented, little is known about the aesthetic characteristics of depression. The aesthetic experience, which covers both the affective and motivational components, is linked to both the emotional and reward circuits in the brain (i.e., the emotion-valuation system) (5). A growing body of studies has shown that the aesthetic perception of various stimuli consistently activated the orbitofrontal cortex (6–9), an area crucially involved in both emotion and reward processing (10). Of note, the dysfunction of OFC has been suggested as responsible for both the bias for negative emotion and the anhedonia in depression (11–13). Moreover, depression is also characterized by pathological self-referential processes (i.e., depressive rumination) related to the dysfunction of the default mode network (DMN) (14). In parallel, the DMN was active during aesthetic appreciation and was suggested to reflect the internal processing evoked by the appreciated stimuli (15, 16). Therefore, the aesthetic orientation and the corresponding neural underpinnings may provide an integrated signature of the multidimensional symptoms of depression.

In the present study, we asked if people with clinically diagnosed depression have aesthetic abnormalities that can be probed with both behavioral and electroencephalographic (EEG) techniques. For this purpose, in an EEG experiment, we asked both depression and the healthy controls to make aesthetic judgments on faces and landscapes, stimuli commonly used in recent neuroaesthetic studies (17). Based on the negative emotional bias and the anhedonia in depression, we predicted that the depression group would tend to give ‘non-beautiful’ judgments on stimuli that agreed to be beautiful by healthy people. At the neural level, it has been shown in previous studies that the aesthetic experience engaged both the perceptual activity and the prefrontal activity in the brain. For instance, viewing beautiful faces enhanced the activity in the fusiform face area (FFA) (18, 19) and the OFC (9). In terms of EEG evidence, the well-known face-specific component N170 (20) was modulated by the aesthetic properties such as facial attractiveness (21) and emotion (22). A frontal negativity was elicited by the stimuli only in the aesthetic task (aesthetic judgment), but not in the perceptual task (symmetry judgment) (23). We hence expected that the biased aesthetic tendency in depression would be underlined by the corresponding EEG activities over the occipital and frontal regions.

2. Method

2.1. Participants

Sample size was determined by the sample size in recent studies on neuroaesthetics ($N=21-24$, (7, 15, 19)), the availability of the recruited participants and the inclusion–exclusion criteria. Twenty-five depressive patients and 27 healthy controls (Table 1) participated in the EEG experiment. Patients were recruited from the outpatient clinics of the Fourth People's Hospital of Wuhu. Diagnosis was performed by licensed psychiatrists using structured interview following DSM-V (24). Patients were included if they met the criteria of depression according to the structured interview. Patients were excluded if they met the criteria of

TABLE 1 Demographic and clinical characteristics of participants (mean \pm SD).

	Control	Depression	Statistics
Gender (F/M)	14/13	14/11	$p=0.76$
Age (years)	24 ± 5.27	25.48 ± 6.42	$p=0.37$
BDI score	6.37 ± 5.32	24.32 ± 10.30	$p<0.001$
Education (years)	15.63 ± 3.88	14.32 ± 1.65	$p=0.71$
Medication(Y/N)	0/27	23/2	

BDI, Beck Depression Inventory-II (21-item).

schizophrenia, schizoaffective disorder, bipolar disorder, or anxiety disorder as the primary diagnosis. Patients were also excluded if their age lied outside the range of 18–40 years old. The healthy controls were recruited *via* internet-based advertisement and was screened for current and the history of psychiatric and neurological disorders. All participants had normal or corrected-to-normal vision. In addition to the clinical interview, both groups filled out the 21-item Beck Depression Inventory (25) prior to the experiment. Informed consent was obtained from all participants prior to the experiment. This study was approved by the Institutional Review Board for Human Research Protections of Shanghai Jiao Tong University (B20200111).

2.2. Materials

Pictures were selected based on the aesthetic judgments from an independent group of healthy participants who did not take part in the EEG experiment. For the rating, thirty healthy participants (14 females, 25.93 ± 2.53 years old; 16 males 25.86 ± 3.11 years old) were recruited and made aesthetic judgement (beautiful, neutral vs. ugly) on a total of 267 pictures (72 landscape pictures, 99 male face pictures and 96 female pictures) collected from the internet. Prior to the aesthetic task, pictures were preprocessed such that they had the same visual resolution (72 pixels per inch), and the same size for each type (Landscape: $12^\circ \times 7.3^\circ$ of visual angle, Face: $6^\circ \times 8^\circ$ of visual angle). The background of each face was kept white. We used 50% as the threshold to decide the valence of the picture in the way that a picture was assigned to a specific valence category (e.g., beautiful) if more than 50% of the participants made the corresponding aesthetic judgment (e.g., more than 50% of participants gave the “beautiful” response). Within each valence category, the pictures were ranked based on the proportion of agreement, and 66 pictures were selected based on the rankings for the main experiment. For faces, there were 44 “beautiful” pictures, 44 “ugly” pictures, and 44 neutral pictures, with an equal amount (i.e., 22 pictures) of female and male faces under each of the three valence types. For landscape, there were 22 pictures under each valence type.

2.3. Experimental procedure

The formal experiment was conducted in a sound-attenuated room. Participants were seated in front of a monitor with an eye-to-monitor distance of 60 cm. Stimuli were presented at the center of a black background (Figure 1). At the beginning of each trial, a white cross was presented for a random interval of 0.25–0.5 s. A picture was then presented and remained on the screen for 2 s. Participants were asked to pay attention to the picture and evaluate the aesthetic valence of the picture. After the offset of the picture, the judgment frame was presented

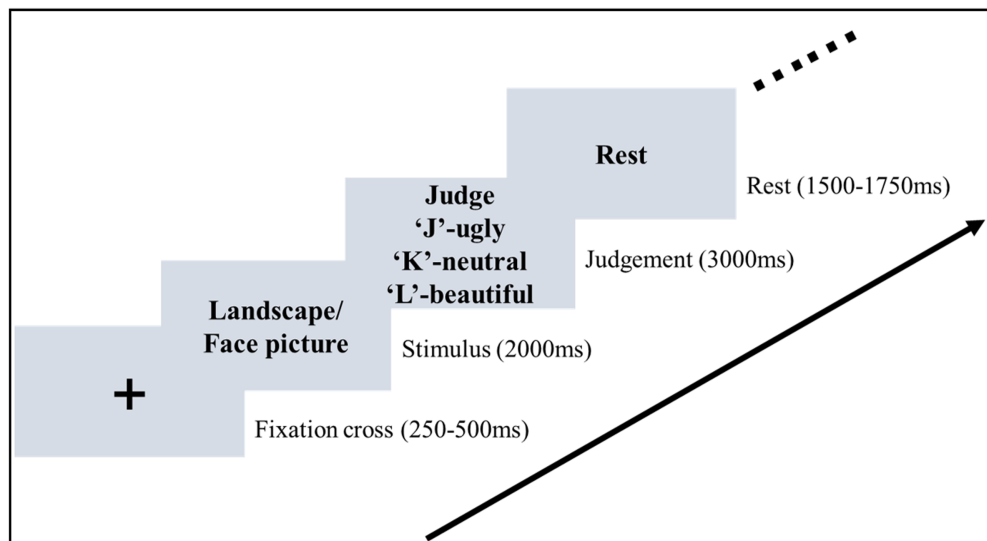


FIGURE 1

Stimuli sequence of the aesthetic judgment task. In the stimulus stage, participants were asked to pay attention to the picture and then evaluate the aesthetic valence in the judgement stage.

for 3 s. During the presentation of the judgment frame, the mapping between the three aesthetic valences and the response key was shown on the screen. Participants were required to press the key to make the aesthetic judgment (beautiful, neutral, vs. ugly). They were required to give a response within 3 s. The judgment frame was then replaced by the text “Rest” on the screen, indicating the end of the current trial. This rest frame was presented for a random interval of 1.5–1.75 s.

The 132 face pictures and 66 landscape pictures were mixed and pseudo-randomly assigned to 3 blocks of equal length, with each block including 22 male faces, 22 female faces, and 22 landscapes. Within each block, the 66 pictures were mixed and presented in random order. To ensure statistical power, each picture was presented twice and there were 6 blocks in total, with the first presentation in the first 3 blocks and the second presentation in the last 3 blocks. There was a break between every two blocks, which lasted 5–10 min. Participants were asked to avoid body movement and to reduce eye blinks during the task to minimize artifacts.

2.4. Statistical analysis of behavioral data

Per each participant and each experimental condition, the perceptual discriminability d' and the response bias β and judgement criterion c were calculated based on the signal detection theory (26). Specifically, an aesthetic response was identified as Hit if it was consistent with the picture valence (e.g., an “ugly” response was given to an “ugly” picture), and a response was identified as False Alarm (FA) if it was inconsistent with the picture valence (e.g., an ugly response was given to a beautiful or a neutral picture). The perceptual discriminability d' was then calculated using the formula $d' = Z(\text{Hit rate}) - Z(\text{FA rate})$, and the response bias β was calculated using the formula $\beta = \exp. (d' * c)$, where $c = -(Z(\text{Hit rate}) + Z(\text{FA rate}))/2$. A 2(Group: depression vs. control) * 2(Picture type: face vs. landscape) * 3(Picture valence: beautiful, ugly, vs. neutral) repeated-measures ANOVA was, respectively, conducted on d' , β and c , with Group included as the between-subjects factor and Picture type and Picture Valence as the within-subject factors.

Further separate ANOVAs and t tests were performed following an interaction that involved group. The Greenhouse–Geisser correction

was used to compensate for sphericity violations and the Bonferroni method was used for correcting multiple comparisons. A threshold of $\alpha = 0.05$ was used to decide statistical significance.

Reaction times (RTs) were calculated as the time of response relative to the onset of the judgement frame and were averaged across all trials for each experimental condition. The same 2 * 2 * 3 ANOVA was also performed on the mean RTs.

2.5. EEG recording and preprocessing

EEG signals were recorded with a NeuSen W332 system (Neuracle, China). Thirty-two Ag/AgCl scalp electrodes were placed according to the international 10/20 system. The impedance of each channel was kept below 5k Ω . The ground electrode was located at the FPz and the reference at the Cz. EEG signals were recorded with a sampling frequency of 1,000 Hz. A notch filter with 50 Hz was adopted to remove power frequency interference during data acquisition. Data were analyzed with EEG-toolbox (27). In the pre-processing stage, the offline raw data was amplified with a 0.5–100 Hz band-pass filter, down-sampled at 500 Hz/channel, and then re-referenced by the common average reference. Independent component analysis (ICA) algorithm was then used to remove the artifacts. Trials with peak-to-peak deflections exceeding $\pm 100 \mu\text{V}$ were also excluded from data analysis.

2.6. Event-related potential analysis of EEG data

For each trial, data were segmented from –200 to 1,000 ms relative to the picture onset. Baseline corrections were applied to the interval of –200 to 0 ms relative to the picture onset. We focused on the occipital region over the visual cortex to examine if the aesthetic judgment was reflected by the perceptual processing, and the frontal region to assess how the aesthetic judgment was reflected by high-level cognitive processing. For this purpose, the channels (PO3, PO4, O1, Oz, O2) over the occipital region were grouped into a cluster, and the channels (FP1, FP2, F3, Fz, F4) over

the frontal region were grouped into a cluster. For each cluster, the ERP times courses were averaged across all channels within the current cluster and averaged across all trials in a specific condition.

Given that face pictures and landscape pictures may induce distinct ERP components (e.g., face-specific N170), the statistical analysis was performed separately for faces and landscapes. The time range of each component was decided based on the peak amplitude. Specifically, the peak amplitude of each component was identified at the group level in each of the 6 conditions. For each component in each condition, the mean amplitude was calculated by averaging 100 ms centered at the peak point ((28); see [Supplementary Table S1](#) for the time point of peak amplitude). For each picture type (Face and Landscape) and each cluster, the mean amplitude was entered into a 2(Group: depression vs. control) * 3(Picture valence: beautiful, ugly, vs. neutral) ANOVA. Only the occipital N170 and the frontal N200 were involved in the negative aesthetic bias (see results). The full ERP results are reported in [Supplementary material](#).

For each of the two regions, the latencies of the first ERP component ([Supplementary Table S2](#)) were identified for each condition using the jackknife method (29). Considering the potential temporal correlation of the EEG waves, we performed the statistical analysis only on the latency of the first component. Latencies were also submitted to 2(Group: depression vs. control) * 3(Picture valence: beautiful, ugly, vs. neutral) ANOVA.

2.7. Time-frequency analysis of EEG data

For each trial, data were first subjected to a Butterworth bandpass filter (3rd order, 0.5–45 Hz), and then segmented from –500 to 2000 ms relative to the picture onset. The short-time Fourier transform (STFT, frequency range: 0.5–45 Hz, step = 1 Hz) with a Gaussian-tapered window (500 ms) was used to calculate the event-related spectral perturbations (ERSPs). The mean power in a baseline period (–500 to 0 ms relative to picture onset) was subtracted from each spectral estimate to produce the baseline-corrected ERSPs. The statistical testing was also focused on the occipital and frontal regions. To obtain ERSPs that related to the aesthetic evaluation, data were collapsed over all conditions for the occipital and the frontal region. Here we collapsed data over Face and Landscape conditions because there was no prior hypothesis for face-specific brain oscillations. To achieve unbiased statistical analysis, we firstly identified the oscillatory activities that involved the picture evaluation across groups, picture types, and valence types. For each region, a one-sample t-test was conducted for each cell of the ERSPs matrix, and cluster-based permutation testing (1,000 permutations, alpha level = 0.05) was used to correct multiple comparisons (30). Then, power amplitudes in each condition were extracted from the time-frequency clusters (see results for the significant clusters) that reached significance and were submitted to a 2(Group: depression vs. control) * 3(Picture valence: beautiful, ugly, vs. neutral) ANOVA for Face and Landscape, respectively. Only the frontal theta was involved in the negative aesthetic bias (see results). The full time-frequency results are reported in [Supplementary material](#).

3. Results

3.1. Behavioral results

The 2(Group: depression vs. control) * 2(Picture type: face vs. landscape) * 3(Picture valence: beautiful, neutral vs. ugly) ANOVA on

response bias (measured by β) showed a three-way interaction, $F(2, 100) = 6.447$, $p = 0.002$, $\eta^2_p = 0.114$ (see [Supplementary material](#) for full ANOVA results). For Face, a separate 2 * 3 ANOVA with group as the between-subjects factor and valence as the within-subject factor showed a main effect of valence $F(1.448, 72.384) = 21.007$, $p < 0.001$, $\eta^2_p = 0.296$, with increased response bias from neutral to ugly, and from ugly to beautiful faces, all $p < 0.033$ (Bonferroni-corrected). Importantly, there was an interaction between group and valence, $F(1.448, 72.384) = 5.435$, $p = 0.013$, $\eta^2_p = 0.098$. This interaction was due to that the response bias for ugly faces was stronger in depression than the controls, $t(50) = 2.286$, $p = 0.027$, Cohen's $d = 0.635$, 95% CI = [0.221, 3.425], whereas response bias for beautiful faces was weaker in depression than the controls, $t(50) = 2.100$, $p = 0.041$, Cohen's $d = 0.583$, 95% CI = [0.087, 3.920] ([Figure 2B](#)). However, the decision bias for neutral faces did not differ between the two groups, $t < 1$. For Landscape, neither the main effect of group nor the interaction between group and valence reached significance, both $F < 1$. The same pattern was observed in both genders ([Supplementary Figure S1](#)). In all, the depressive group showed a stronger reaction bias towards ugly face.

The ANOVA on perceptual sensitivity (measured by d') showed higher perceptual discriminability for ugly pictures than for beautiful pictures, and higher perceptual discriminability for beautiful pictures than for neutral pictures, $F(2, 100) = 319.004$, $p < 0.001$, $\eta^2_p = 0.864$, and $p < 0.001$ with Bonferroni-corrected comparisons ([Figure 2C](#)). The perceptual discriminability was higher for Landscape than for Face, $F(1, 50) = 50.263$, $p < 0.001$, $\eta^2_p = 0.501$. Also, the three-way interaction was significant, $F(1.549, 77.459) = 3.408$, $p = 0.050$, $\eta^2_p = 0.064$.

The ANOVA on judgement criterion (measured by c) showed a three-way interaction, $F(2, 100) = 3.773$, $p = 0.026$, $\eta^2_p = 0.07$. For Face, a separate 2 * 3 ANOVA showed a main effect of valence $F(2, 100) = 16.789$, $p < 0.001$, $\eta^2_p = 0.251$, with increased criterion from ugly to beautiful, and from neutral to beautiful faces, all $p < 0.001$ (Bonferroni-corrected). Also, there was an interaction between group and valence, $F(2, 100) = 4.799$, $p = 0.010$, $\eta^2_p = 0.088$, which was due to that the judgement criterion for ugly faces was weaker in depression than the controls, $t(50) = 2.540$, $p = 0.014$, Cohen's $d = 0.705$, 95% CI = [0.061, 0.518], whereas criterion for beautiful faces was stronger in depression than the controls, $t(50) = 2.424$, $p = 0.019$, Cohen's $d = 0.673$, 95% CI = [0.061, 0.647]. However, the criterion for neutral faces did not differ between the two groups, $t < 1$. For Landscape, neither the main effect of group nor the interaction between group and valence reached significance, both $p > 0.173$. ([Figure 2D](#)). The ANOVA on RTs did not show any significant effect that involved Group, all $p > 0.079$ ([Figure 2A](#)). The hit and false alarm rate of beautiful, neutral, and ugly were shown in [Table 2](#).

3.2. ERP results

The depression group showed generally longer ERP latencies than the controls, all $p < 0.001$ ([Figure 3A](#), [Supplementary Table S2](#)). For Face, the amplitude of the N170 component over the occipital region was more negative in depression than the controls, $F(1, 50) = 6.313$, $p = 0.015$, $\eta^2_p = 0.112$ ([Figure 3B](#)). There was also an interaction between group and valence, $F(1.737, 86.863) = 3.925$, $p = 0.029$, $\eta^2_p = 0.073$: the N170 was more negative in depression than the controls for ugly faces, $t(50) = 2.787$, $p = 0.007$, Cohen's $d = 0.774$, 95% CI = [0.565, 3.479] and neutral faces, $t(50) = 2.670$, $p = 0.010$,

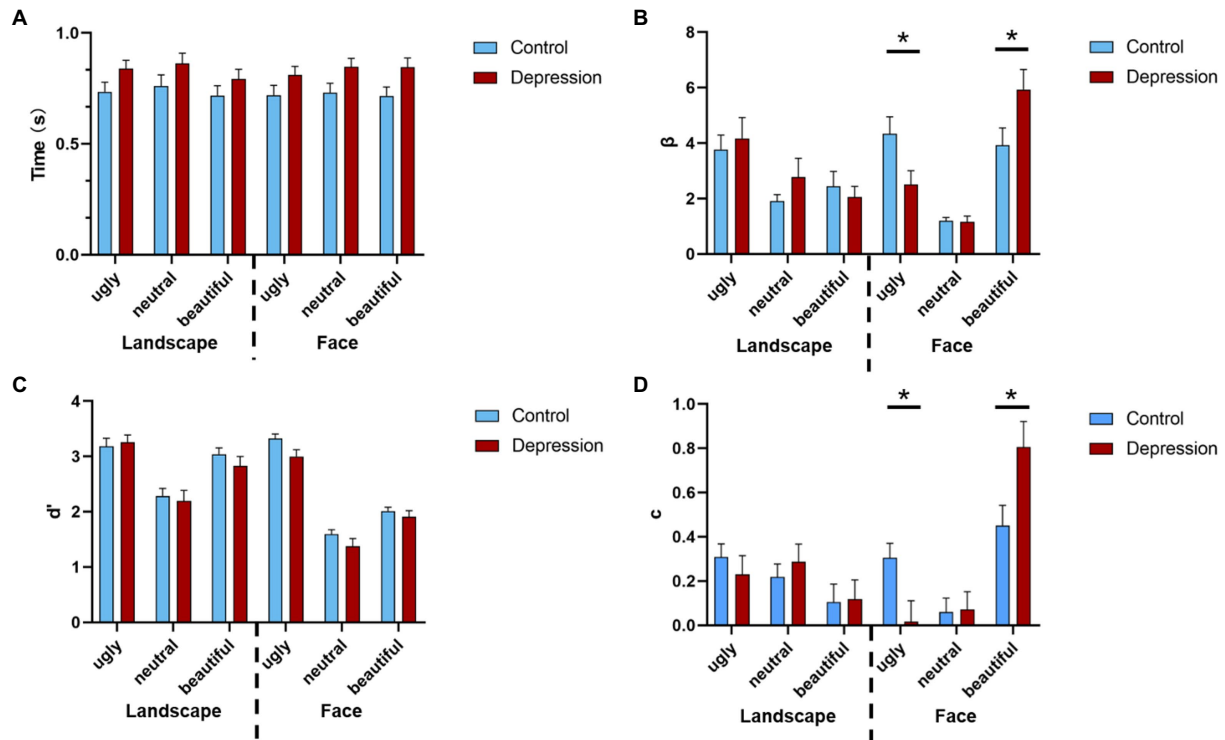


FIGURE 2

(A) The reaction times (RT) of the aesthetic judgments are shown as a function of the stimuli type, valence, and group. Error bars indicate standard errors. (B) The response bias is shown as a function of stimuli type, valence, and group. (C) The perceptual sensitivity is shown as a function of stimuli type, valence, and group, and (D) the judgement criterion is shown as a function of stimuli type, valence, and group. Error bars indicate standard errors. * indicates a significant difference.

TABLE 2 The hit and false alarm rate under different respond of participants (mean±SD).

		Landscape			Face		
		Ugly	Neutral	Beautiful	Ugly	Neutral	Beautiful
Hit rate	control	0.88 ± 0.12	0.79 ± 0.13	0.89 ± 0.11	0.89 ± 0.08	0.74 ± 0.13	0.68 ± 0.18
	depression	0.90 ± 0.08	0.74 ± 0.19	0.86 ± 0.19	0.90 ± 0.08	0.70 ± 0.19	0.54 ± 0.23
False alarm rate	control	0.04 ± 0.05	0.10 ± 0.08	0.07 ± 0.06	0.03 ± 0.04	0.21 ± 0.10	0.10 ± 0.07
	depression	0.05 ± 0.08	0.11 ± 0.12	0.08 ± 0.07	0.11 ± 0.15	0.24 ± 0.10	0.06 ± 0.06

Cohen's $d = 0.741$, 95% CI = [0.450, 3.183], but not for beautiful faces, $t(50) = 1.89$, $p = 0.065$. In the depression group, there was a main effect of valence, $F(2, 48) = 6.071$, $p = 0.004$, $\eta^2_p = 0.202$, with more negative N170 to ugly faces ($p = 0.087$) and neutral faces ($p = 0.016$) than beautiful face, but no difference between ugly and neutral faces, $p > 0.999$ (Bonferroni-corrected). In the control group, however, the main effect of valence was not significant, $F(2, 52) = 1.975$, $p = 0.149$.

The amplitude of the N200 component over the frontal region showed an interaction between group and valence, $F(2, 100) = 4.095$, $p = 0.020$, $\eta^2_p = 0.076$ (Figure 3C). Further tests showed that the N200 was less negative in depression than the controls regardless of valence, all $p < 0.004$. In the depression group, there was a main effect of valence, $F(2, 48) = 6.392$, $p = 0.003$, $\eta^2_p = 0.210$, with less negative N200 to ugly faces than to neutral faces, $p = 0.007$, but no difference between ugly and beautiful faces, $p = 0.132$, or between neutral and beautiful faces, $p = 0.512$ (Bonferroni-corrected). By contrast in the control group, the

main effect of valence did not reach significance, $F < 1$. Other ERP components did not show any interaction that involved Group for Face (Supplementary material).

No interaction that involved Group was observed for Landscape (Supplementary material).

3.3. EEG oscillation

The ERSPs over the frontal region and the occipital region were shown in Figure 4A, whereas only the frontal theta oscillation was involved in the aesthetic bias. For Face, the ANOVA on the frontal theta oscillation showed that the main effect of group was not significant, $F(1, 50) = 2.318$, $p = 0.134$. Both the main effect of valence, $F(1.75, 87.514) = 3.283$, $p = 0.049$, $\eta^2_p = 0.062$, and the interaction between valence and group, $F(1.75, 87.514) = 3.277$, $p = 0.049$, $\eta^2_p = 0.062$, were significant. The theta synchronization was weaker in the depression

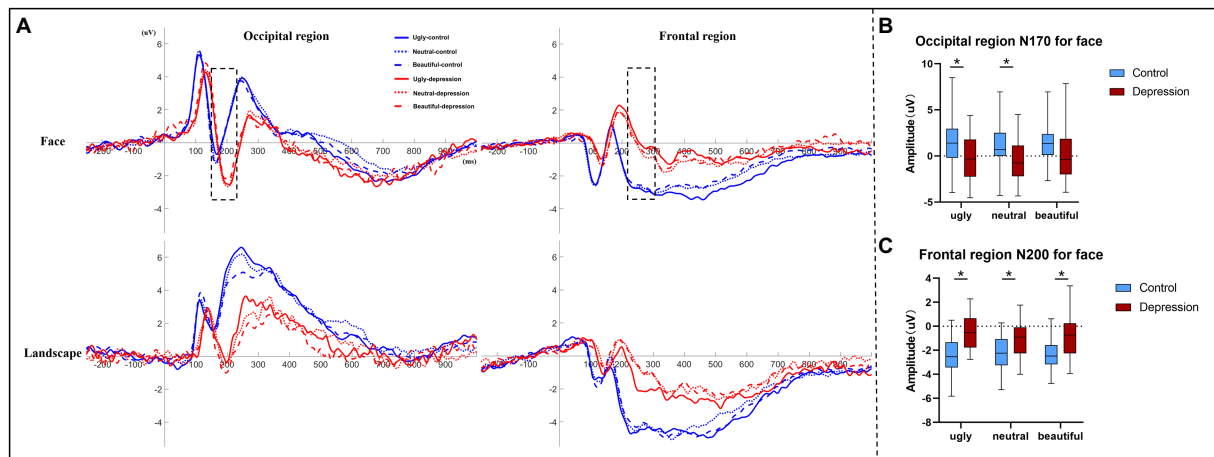


FIGURE 3

(A) Event-related potentials (ERP) averaged over the occipital region and the frontal region, respectively, are shown as a function of stimuli type, valence, and group. Only the two ERP components (occipital N170 and frontal N200) marked by dotted lines showed a significant interaction between group and valence. (B) The amplitudes of face-evoked occipital N170 are shown as a function of valence and group, and (C) the amplitudes of frontal N200 evoked by faces are shown as a function of valence and group. The error bars indicate the range of the amplitude values. The upper and lower boundaries of the colored square indicate the upper and lower quartiles of the amplitudes, and the black horizontal lines indicate the median of the amplitudes. * indicates a significant difference.

group than in the control group for beautiful faces, $t(44.247) = 2.382$, $p = 0.022$, Cohen's $d = 0.650$, 95% CI = [0.065, 0.779], but not for ugly $t(43.102) = 1.235$, $p = 0.224$, or neutral faces, $t < 1$. In the depression group, there was a main effect of valence, $F(2, 48) = 6.578$, $p = 0.003$, $\eta^2_p = 0.215$, with lower synchronization to beautiful faces than ugly ($p = 0.011$) and neutral faces ($p = 0.017$), but no difference between neutral and ugly faces, $p > 0.999$ (Bonferroni-corrected) (Figure 4B). By contrast in the control group, the main effect of valence did not reach significance, $F < 1$. The topographical distributions of the theta-power change extracted from the significant time-frequency range for faces was shown in Figure 4C. The oscillatory activity at other bands did not show interaction that involved Group for Face (Supplementary material).

No interaction that involved Group was observed for Landscape (Supplementary material).

4. Discussion

In the present study, we investigated the aesthetic preference and the corresponding neural underpinnings in depression. The behavioral results showed a response bias and judgement criterion for faces but not for landscapes in depression. Specifically, relative to the control group, the depression group tended to give “ugly” judgments and were more conservative in giving “beautiful” judgments. The bias for negative judgment (i.e., ugly) while against positive judgment (i.e., beautiful) in depression was accompanied by enhanced N170 over the occipital cortex, decreased N200, and theta oscillation over the prefrontal cortex. These results convergingly point to a face-specific negative bias of aesthetic perception in depression.

As the response bias and judgment criteria reflect the strictness of the criteria used by the participants to judge the stimulus, that is, the greater β and c values represent the stricter judgment criteria. Compared with the control group, the depressed group showed significant abnormal criteria in judging the ugly and beautiful face, which meant that the depressed group had a negative bias specific to the face. Some

studies on the response bias of depressed patients show that an overall increase in bias towards identifying emotions which appeared to be largely driven by results for mood-relevant emotions (31). The study on negative emotional bias in depression reports both increased attention and facilitated processing of negative stimuli, and reduced discrimination and withdrawal or avoidance from them (32). Although Lynn et al. reported that perceivers with poor sensitivity (d') exhibited more extreme bias (c) than did perceivers with better sensitivity (33), we did not see a significant effect that involved group in sensitivity in our results, which may be related to methodology and the type and context of stimulus presentation. In addition, we did not find any significant effect related to group in RTs. The overall response time of the depression group was higher than that of the healthy group, which was consistent with the results of Anderson et al. (31), indicating that the impact of task difficulty could be ignored.

The negative aesthetic bias that specific to face in depression shown here raised the social origin of depression. While the cognitive model of depression highlighted the cognitive bias such as biased attention for negative information not exclusively social, the social-oriented model emphasized the interpersonal dysfunction such as interpersonal vulnerability and social difficulty (34). A recent study showed that face sensitivity was predicted by social cognition capabilities in healthy populations whereas was predicted by perceptual capabilities in major depressive disorder (35). Thus, the interpersonal dysfunctions in depression can sensitize the processing or reaction to social stimuli (e.g., faces) than non-social stimuli (e.g., landscapes), leading to a more pronounced bias.

The occipital N170 has been shown as a sensitive perceptual component to faces, with more negative amplitude to emotional faces than to neutral faces (22), and more negative amplitude to faces with higher attractiveness (21, 36). The face-induced N170 was also found to be more negative in depression than the controls for both emotional and neutral faces, indicating generally enhanced perceptual processing of faces in depression (37). Consistent with this result, here the ERP results showed more negative N170 during face processing in depression than

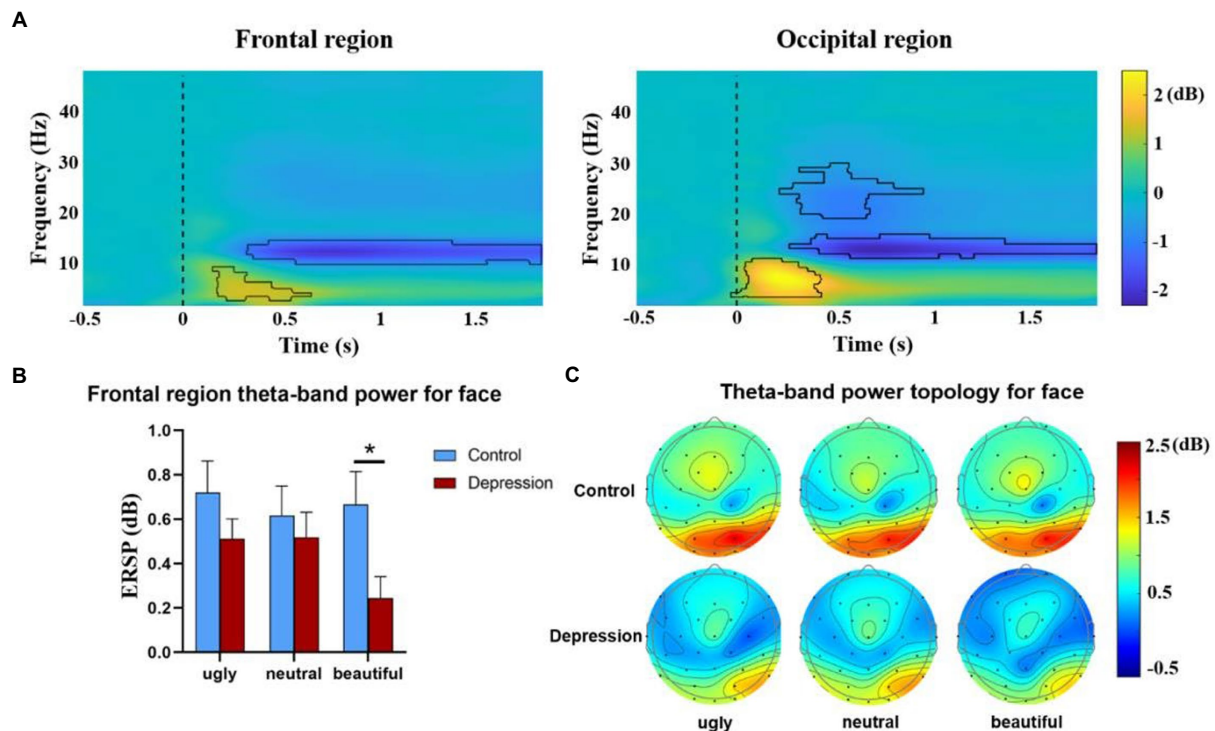


FIGURE 4

(A) The event-related spectral perturbations (ERSPs) over the frontal region (left panel) and the occipital region (right panel) were collapsed over stimuli type, valence and group, and are shown as a function of frequency and time. The areas marked by black lines indicate the time-frequency clusters that showed significant power changes relative to baseline. The 0-time point (marked by dotted lines) refers to the onset of the picture. (B) The ERSPs extracted from the frontal theta (the significant time-frequency range shown in (A) for faces are shown as a function of valence and group). Error bars indicate standard errors. *Indicates a significant difference, and (C) the topographical distributions of the theta-power change extracted from the significant time-frequency range for faces (only for illustration).

the controls. Importantly, the degree of the enhanced N170 in depression increased from beautiful faces to neutral and ugly faces, a pattern echoed well with the decision bias of the aesthetic judgment, suggesting that the aesthetic evaluation modulates the perceptual representations of the encountered stimuli (18, 19).

The frontal N200 has been suggested as reflecting the initial affective reaction or contagion regardless of the emotional valence of the perceived stimuli (38, 39). For instance, the frontal N200 induced by faces conveying positive or negative emotion showed less negative amplitude than the N200 induced by neutral faces (40). Moreover, the frontal N200 was not restrictively involved in the processing of or reaction to face emotion, but also in face attractiveness, showing less negative amplitude to attractive faces than unattractive faces (41). Collectively, the frontal N200 may reflect the affective engagement of face processing, with less negative amplitude signaling higher affective engagement. Here the frontal N200 was generally less negative in the depression group than in the control group in the presence of all face stimuli. This result, along with the overall more negative occipital N170, suggested higher affective engagement in face processing in the depression group than in the controls. Importantly, ugly faces induced the least negative amplitude in depression, suggesting a biased affective engagement in ugly faces than in neutral and beautiful faces.

An alternative account could have been that the frontal N200 simply signaled the cognitive engagement rather than affective engagement in the aesthetic evaluation, as frontal N200 was often observed in tasks that required cognitive control (42). For instance, the frontal N200 was more

negative when the presented stimuli contained incompatible information than when there was no incompatible information (42). On the contrary to this pattern, the frontal N200 showed less negative amplitude during high (vs. low) empathetic reactions to faces (39, 40). The opposite patterns of frontal N200 may reflect the external versus the internal processing, with more negative amplitude when the external processing was more dominant (e.g., during cognitive control) whereas less negative when the internal processing was more dominant (e.g., during affective reaction). This notion was supported by the current results that, relative to the control group, the frontal N200 was generally less negative in the depression group, who had a biased internal self-referential processing over external processing (14). Relative to beautiful and neutral faces, ugly faces in our experiment may concur with the negative self-referential information in depression and hence evoked the least negative N200.

As the frontal N200, the frontal theta oscillation was also found to be involved in both cognitive control and affective processing. On the one hand, the frontal theta was suggested as the source of the frontal N200 in cognitive control, with stronger synchronization in coping with high (vs. low) demand of control (28, 43). This account could be ruled out here as the frontal theta showed a different pattern from N200. Firstly, an overall group difference regardless of aesthetic valence was observed for N200 but not for theta synchronization. Secondly, while the decreased frontal N200 in depression manifested during the aesthetic evaluation of ugly faces, the desynchronized frontal theta oscillation in depression manifested during the aesthetic evaluation of beautiful faces. On the other hand, the frontal theta has been repeatedly found to show strong

synchronization to stimuli with high emotional intensity (44). There are also findings that the theta synchronization was specifically associated with positive emotion (45, 46). In a more relevant study, greater theta synchronization was observed for the preferred face than the non-preferred face (47), which could originate from the activity in OFC (48). Along this line, the lowered theta synchronization, together with the behavioral bias against the positive judgment in depression, might be related to the lack of interest or the loss of pleasure in beautiful faces that are otherwise rewarding for healthy people.

One might argue that the negative aesthetic bias for face in depression could be simply due to the biased recognition of facial expressions in depression. It has been shown that depressive populations tended to perceive neutral expressions as negative (49) and had difficulty correctly identifying positive expressions (50). It should be noted, however, that the aesthetic experience of a face cannot be equal to the emotion identification of the face stimulus. While a neutral stimulus can be identified as sad, the sadness or sorrow conveyed by the stimulus can nevertheless be perceived as beautiful at the same time (51). In other words, a face with negative expression does not necessarily induce negative aesthetic experiences.

According to the recent models of neuroaesthetics, the emotion-valuation system and the DMN that supports self-referential processing are key contributors to the aesthetic experience (5). It is well-established that these systems are dysfunctional in depression, with manifestations such as the bias for negative emotion, the insensitivity to reward, and the ruminative thinking, as well as aberrance in the corresponding neural circuits (4, 13). Such dysfunctions could in combination lead to abnormal aesthetic orientation in depression. Specifically, in the present study, the insensitivity to reward and the dominance of negative over positive emotion may bias the perceptual processing away from the beautiful faces and result in a high threshold for “beautiful” judgments. The negative self-image and the dominance of internal over external processing may bias the perceptual processing of ugly faces and result in a low threshold for “ugly” judgments.

Taken together, the face-specific negative bias of aesthetic perception observed here, along with the EEG signatures, may be an integrated consequence of the multidimensional dysfunctions in depression.

Data availability statement

The original contributions presented in the study are included in the article/Supplementary material, further inquiries can be directed to the corresponding authors.

Ethics statement

The studies involving human participants were reviewed and approved by Institutional Review Board for Human Research Protections of Shanghai Jiao Tong University (B20200111). The patients/participants provided their written informed consent to participate in this study.

References

1. Bell, CC. DSM-IV: diagnostic and statistical manual of mental disorders. *JAMA*. (1994) 272:828–9. doi: 10.1001/jama.1994.03520100096046
2. Gotlib, IH, and Joormann, J. Cognition and depression: current status and future directions. *Annu Rev Clin Psychol*. (2010) 6:285–312. doi: 10.1146/annurev-clinpsy.121208.131305
3. Disner, SG, Beevers, CG, Haigh, EA, and Beck, AT. Neural mechanisms of the cognitive model of depression. *Nat Rev Neurosci*. (2011) 12:467–77. doi: 10.1038/nrn3027
4. Pizzagalli, DA. Depression, stress, and anhedonia: toward a synthesis and integrated model. *Annu Rev Clin Psychol*. (2014) 10:393–423. doi: 10.1146/annurev-clinpsy-050212-185606

Author contributions

WL conceived the project. WL and LW supervised the study. ZC and ZD constructed the paradigm with faces and landscapes and collected data. ZW, YS, and SZ recruited the hospital samples. XY and YK recruited the healthy samples. ZC and LW analyzed data and wrote the first draft. All authors contributed to the article and approved the submitted version.

Funding

This study is supported by Shanghai Education Commission Research and Innovation Program (2019-01-07-00-02-E00037), a Ministry Key Project (GW0890006), Shanghai Municipal Commission of Science and Technology Program (21dz2210100), “111” Program of Higher Education Discipline Innovation, and Shanghai Jiao Tong University Scientific and Technological Innovation Funds (B18034). LW was supported by the National Natural Science Foundation of China (32271086), and the Shanghai Sailing Program (20YF1422100).

Acknowledgments

The authors thank Hui Xu and Yuan Xia for help with the recruitment of the participant.

Conflict of interest

The authors declare that the research was conducted in the absence of any commercial or financial relationships that could be construed as a potential conflict of interest.

Publisher's note

All claims expressed in this article are solely those of the authors and do not necessarily represent those of their affiliated organizations, or those of the publisher, the editors and the reviewers. Any product that may be evaluated in this article, or claim that may be made by its manufacturer, is not guaranteed or endorsed by the publisher.

Supplementary material

The Supplementary material for this article can be found online at: <https://www.frontiersin.org/articles/10.3389/fpsy.2023.1102843/full#supplementary-material>

5. Chatterjee, A, and Vartanian, O. Neuroaesthetics. *Trends Cogn Sci.* (2014) 18:370–5. doi: 10.1016/j.tics.2014.03.003
6. Brown, S, Gao, X, Tisdelle, L, Eickhoff, SB, and Liotti, M. Naturalizing aesthetics: brain areas for aesthetic appraisal across sensory modalities. *NeuroImage.* (2011) 58:250–8. doi: 10.1016/j.neuroimage.2011.06.012
7. Ishizu, T, and Zeki, S. Toward a brain-based theory of beauty. *PLoS One.* (2011) 6:e21852. doi: 10.1371/journal.pone.0021852
8. Jacobsen, T, Schubotz, RI, Höfel, L, and Cramon, DYV. Brain correlates of aesthetic judgment of beauty. *NeuroImage.* (2006) 29:276–85. doi: 10.1016/j.neuroimage.2005.07.010
9. Kawabata, H, and Zeki, S. Neural correlates of beauty. *J Neurophysiol.* (2004) 91:1699–705. doi: 10.1152/jn.00696.2003
10. O'Doherty, J, Kringelbach, ML, Rolls, ET, Hornak, J, and Andrews, C. Abstract reward and punishment representations in the human orbitofrontal cortex. *Nat Neurosci.* (2001) 4:95–102. doi: 10.1038/82959
11. Dichter, GS, Kozink, RV, McClernon, FJ, and Smoski, MJ. Remitted major depression is characterized by reward network hyperactivation during reward anticipation and hypoactivation during reward outcomes. *J Affect Disord.* (2012) 136:1126–34. doi: 10.1016/j.jad.2011.09.048
12. Frodl, T, Bokde, AL, Scheuerecker, J, Lisiecka, D, Schoepf, V, Hampel, H, et al. Functional connectivity bias of the orbitofrontal cortex in drug-free patients with major depression. *Biol Psychiatry.* (2010) 67:161–7. doi: 10.1016/j.biopsych.2009.08.022
13. Rolls, ET. A non-reward attractor theory of depression. *Neurosci Biobehav Rev.* (2016) 68:47–58. doi: 10.1016/j.neubiorev.2016.05.007
14. Sheline, YI, Barch, DM, Price, JL, Rundle, MM, Vaishnavi, SN, Snyder, AZ, et al. The default mode network and self-referential processes in depression. *Proc Natl Acad Sci U S A.* (2009) 106:1942–7. doi: 10.1073/pnas.081268610
15. Cela-Conde, CJ, García-Prieto, J, Ramasco, JJ, Mirasso, CR, Bajo, R, Munar, E, et al. Dynamics of brain networks in the aesthetic appreciation. *Proc Natl Acad Sci U S A.* (2013) 110:10454–61. doi: 10.1073/pnas.1302855110
16. Vessel, EA, Starr, GG, and Rubin, N. Art reaches within: aesthetic experience, the self and the default mode network. *Front Neurosci.* (2013) 44:2899–906. doi: 10.1016/j.neuropsychologia.2006.06.020
17. Cela-Conde, CJ, Agnati, L, Huston, JP, Mora, F, and Nadal, M. The neural foundations of aesthetic appreciation. *Prog Neurobiol.* (2011) 94:39–48. doi: 10.1016/j.pneurobio.2011.03.003
18. Chatterjee, A, Thomas, A, Smith, SE, and Aguirre, GK. The neural response to facial attractiveness. *Neuropsychology.* (2009) 23:135–43. doi: 10.1037/a0014430
19. Yang, T, Formuli, A, Paolini, M, and Zeki, S. The neural determinants of beauty. *Eur J Neurosci.* (2022) 55:91–106. doi: 10.1111/ejn.15543
20. Eimer, M, Kiss, M, and Nicholas, S. Response profile of the face-sensitive N170 component: a rapid adaptation study. *Cereb Cortex.* (2010) 20:2442–52. doi: 10.1093/cercor/bhp312
21. Han, S, Liu, S, Gan, Y, Xu, Q, Xu, P, Luo, Y, et al. Repeated exposure makes attractive faces more attractive: neural responses in facial attractiveness judgement. *Neuropsychologia.* (2020) 139:107365. doi: 10.1016/j.neuropsychologia.2020.107365
22. Sprengelmeyer, R, and Jentsch, I. Event related potentials and the perception of intensity in facial expressions. *Neuropsychologia.* (2006) 44:2899–906. doi: 10.1016/j.neuropsychologia.2006.06.020
23. Jacobsen, T, and Höfel, L. Descriptive and evaluative judgment processes: behavioral and electrophysiological indices of processing symmetry and aesthetics. *Cogn Affect Behav Neurosci.* (2003) 3:289–99. doi: 10.3758/CABN.3.4.289
24. Appointment, M. A. Diagnostic and statistical manual of mental disorders. *Text Revision.* (2000) 189:39–44. doi: 10.1007/978-0-387-78665-0_5485
25. Dozois, DJ, Dobson, KS, and Ahnberg, JL. A psychometric evaluation of the Beck depression inventory–II. *Psychol Assess.* (1998) 10:83–9. doi: 10.1037/1040-3590.10.2.83
26. Snodgrass, JG, and Corwin, J. Perceptual identification thresholds for 150 fragmented pictures from the Snodgrass and Vanderwart picture set. *Percept Mot Skills.* (1988) 67:3–36. doi: 10.2466/pms.1988.67.1.3
27. Delorme, A, and Makeig, S. EEGLAB: an open source toolbox for analysis of single-trial EEG dynamics including independent component analysis. *J Neurosci Methods.* (2004) 134:9–21. doi: 10.1016/j.jneumeth.2003.10.009
28. Wang, L, Chang, W, Krebs, RM, Boehler, CN, Theeuwes, J, and Zhou, X. Neural dynamics of reward-induced response activation and inhibition. *Cereb Cortex.* (2019) 29:3961–76. doi: 10.1093/cercor/bhy275
29. Kiesel, A, Miller, J, Jolicœur, P, and Brisson, B. Measurement of ERP latency differences: a comparison of single-participant and jackknife-based scoring methods. *Psychophysiology.* (2008) 45:250–74. doi: 10.1111/j.1469-8986.2007.00618.x
30. Maris, E, and Oostenveld, R. Nonparametric statistical testing of EEG-and MEG-data. *J Neurosci Methods.* (2007) 164:177–90. doi: 10.1016/j.jneumeth.2007.03.024
31. Anderson, IM, Shippen, C, Juhasz, G, Chase, D, Thomas, E, Downey, D, et al. State-dependent alteration in face emotion recognition in depression. *Br J Psychiatry Suppl.* (2011) 198:302–8. doi: 10.1192/bjp.bp.110.078139
32. Gollan, JK, Pane, HT, McCloskey, MS, and Coccaro, EF. Identifying differences in biased affective information processing in major depression. *Psychiatry Res.* (2008) 159:18–24. doi: 10.1016/j.psychres.2007.06.011
33. Lynn, SK, and Barrett, LE. “Utilizing” signal detection theory. *Psychol Sci.* (2014) 25:1663–73. doi: 10.1177/0956797614541991
34. Hammen, C. Risk factors for depression: an autobiographical review. *Annu Rev Clin Psychol.* (2018) 14:1–28. doi: 10.1146/annurev-clinpsy-050817-084811
35. Kubon, J, Sokolov, AN, Popp, R, Fallgatter, AJ, and Pavlova, MA. Face tuning in depression. *Cereb Cortex.* (2021) 31:2574–85. doi: 10.1093/cercor/bhaa375
36. Marzi, T, and Viggiano, M. When memory meets beauty: insights from event-related potentials. *Biol Psychol.* (2010) 84:192–205. doi: 10.1016/j.biopsycho.2010.01.013
37. Yin, G, Zhao, L, and Li, H. The early stage of face detection in patients with major depressive disorder: an ERP study. *Neuroreport.* (2019) 30:939–44. doi: 10.1097/WNR.0000000000001305
38. Decety, J, Lewis, KL, and Cowell, JM. Specific electrophysiological components disentangle affective sharing and empathic concern in psychopathy. *J Neurophysiol.* (2015) 114:493–504. doi: 10.1152/jn.00253.2015
39. Fan, Y, and Han, S. Temporal dynamic of neural mechanisms involved in empathy for pain: an event-related brain potential study. *Neuropsychologia.* (2008) 46:160–73. doi: 10.1016/j.neuropsychologia.2007.07.023
40. McCrackin, SD, and Itier, RJ. Feeling through another's eyes: perceived gaze direction impacts ERP and behavioural measures of positive and negative affective empathy. *NeuroImage.* (2021) 226:117605. doi: 10.1016/j.neuroimage.2020.117605
41. Jin, J, Fan, B, Dai, S, and Ma, Q. Beauty premium: event-related potentials evidence of how physical attractiveness matters in online peer-to-peer lending. *Neurosci Lett.* (2017) 640:130–5. doi: 10.1016/j.neulet.2017.01.037
42. Folstein, JR, and Van Petten, C. Influence of cognitive control and mismatch on the N2 component of the ERP: a review. *Psychophysiology.* (2008) 45:152–70. doi: 10.1111/j.1469-8986.2007.00602.x
43. Cavanagh, JF, and Frank, MJ. Frontal theta as a mechanism for cognitive control. *Trends Cogn Sci.* (2014) 18:414–21. doi: 10.1016/j.tics.2014.04.012
44. Güntekin, B, and Başar, E. A review of brain oscillations in perception of faces and emotional pictures. *Neuropsychologia.* (2014) 58:33–51. doi: 10.1016/j.neuropsychologia.2014.03.014
45. Aftanas, L, and Golocheikine, S. Human anterior and frontal midline theta and lower alpha reflect emotionally positive state and internalized attention: high-resolution EEG investigation of meditation. *Neurosci Lett.* (2001) 310:57–60. doi: 10.1016/S0304-3940(01)02094-8
46. Aftanas, LI, Lotova, NV, Koshkarov, VI, Makhnev, VP, Mordvintsev, YN, and Popov, SA. Non-linear dynamic complexity of the human EEG during evoked emotions. *Int J Psychophysiol.* (1998) 28:63–76. doi: 10.1016/S0167-8760(97)00067-6
47. Lindsen, JP, Jones, R, Shimojo, S, and Bhattacharya, J. Neural components underlying subjective preferential decision making. *NeuroImage.* (2010) 50:1626–32. doi: 10.1016/j.neuroimage.2010.01.079
48. Kim, H, Adolphs, R, O'Doherty, JP, and Shimojo, S. Temporal isolation of neural processes underlying face preference decisions. *Proc Natl Acad Sci U S A.* (2007) 104:18253–8. doi: 10.1073/pnas.0703101104
49. Gollan, JK, McCloskey, M, Hoxha, D, and Coccaro, EF. How do depressed and healthy adults interpret nuanced facial expressions? *J Abnorm Psychol.* (2010) 119:804–10. doi: 10.1037/a0020234
50. Csukly, G, Telek, R, Filipovits, D, Takács, B, Unoka, Z, and Simon, L. What is the relationship between the recognition of emotions and core beliefs: associations between the recognition of emotions in facial expressions and the maladaptive schemas in depressed patients. *J Behav Ther Exp Psychiatry.* (2011) 42:129–37. doi: 10.1016/j.jbtep.2010.08.003
51. Sachs, ME, Damasio, A, and Habibi, A. The pleasures of sad music: a systematic review. *Front Hum Neurosci.* (2015) 9:404. doi: 10.3389/fnhum.2015.00404



OPEN ACCESS

EDITED BY

Keita Watanabe,
Kyoto University, Japan

REVIEWED BY

Kai Wu,
South China University of Technology, China
Weizhao Lu,
Shandong First Medical University, China

*CORRESPONDENCE

Zhishan Hu
✉ huzhishan@me.com

[†]These authors have contributed equally to this work and share first authorship

SPECIALTY SECTION

This article was submitted to
Mood Disorders,
a section of the journal
Frontiers in Psychiatry

RECEIVED 07 November 2022

ACCEPTED 06 February 2023

PUBLISHED 24 February 2023

CITATION

Li Q, Wang W and Hu Z (2023) Amygdala's
T1-weighted image radiomics outperforms
volume for differentiation of anxiety disorder
and its subtype. *Front. Psychiatry* 14:1091730.
doi: 10.3389/fpsy.2023.1091730

COPYRIGHT

© 2023 Li, Wang and Hu. This is an
open-access article distributed under the terms
of the [Creative Commons Attribution License](https://creativecommons.org/licenses/by/4.0/)
(CC BY). The use, distribution or reproduction
in other forums is permitted, provided the
original author(s) and the copyright owner(s)
are credited and that the original publication in
this journal is cited, in accordance with
accepted academic practice. No use,
distribution or reproduction is permitted which
does not comply with these terms.

Amygdala's T1-weighted image radiomics outperforms volume for differentiation of anxiety disorder and its subtype

Qingfeng Li^{1†}, Wenzheng Wang^{1†} and Zhishan Hu^{1,2*}

¹Shanghai Mental Health Center, Shanghai Jiao Tong University School of Medicine, Shanghai, China,

²State Key Laboratory of Cognitive Neuroscience and Learning, Beijing Normal University, Beijing, China

Introduction: Anxiety disorder is the most common psychiatric disorder among adolescents, with generalized anxiety disorder (GAD) being a common subtype of anxiety disorder. Current studies have revealed abnormal amygdala function in patients with anxiety compared with healthy people. However, the diagnosis of anxiety disorder and its subtypes still lack specific features of amygdala from T1-weighted structural magnetic resonance (MR) imaging. The purpose of our study was to investigate the feasibility of using radiomics approach to distinguish anxiety disorder and its subtype from healthy controls on T1-weighted images of the amygdala, and provide a basis for the clinical diagnosis of anxiety disorder.

Methods: T1-weighted MR images of 200 patients with anxiety disorder (including 103 GAD patients) as well as 138 healthy controls were obtained in the Healthy Brain Network (HBN) dataset. We extracted 107 radiomics features for the left and right amygdala, respectively, and then performed feature selection using the 10-fold LASSO regression algorithm. For the selected features, we performed group-wise comparisons, and use different machine learning algorithms, including linear kernel support vector machine (SVM), to achieve the classification between the patients and healthy controls.

Results: For the classification task of anxiety patients vs. healthy controls, 2 and 4 radiomics features were selected from left and right amygdala, respectively, and the area under receiver operating characteristic curve (AUC) of linear kernel SVM in cross-validation experiments was 0.6739 ± 0.0708 for the left amygdala features and 0.6403 ± 0.0519 for the right amygdala features; for classification task for GAD patients vs. healthy controls, 7 and 3 features were selected from left and right amygdala, respectively, and the cross-validation AUCs were 0.6755 ± 0.0615 for the left amygdala features and 0.6966 ± 0.0854 for the right amygdala features. In both classification tasks, the selected amygdala radiomics features had higher discriminatory significance and effect sizes compared with the amygdala volume.

Discussion: Our study suggest that radiomics features of bilateral amygdala potentially could serve as a basis for the clinical diagnosis of anxiety disorder.

KEYWORDS

anxiety disorder, generalized anxiety disorder, magnetic resonance imaging, amygdala, radiomics

1. Introduction

As a common brain and behavioral disorder (1), anxiety disorder manifests primarily as excessive fear, worry and avoidance, leading to severe emotional distress, physical illness, cognitive, and behavioral impairments, which further impairs social functioning and quality of life (2). Generalized anxiety disorder (GAD) is a common subtype of anxiety disorder, which is characterized by chronic, excessive anxiety, and worry accompanied by somatic symptoms such as restless, muscle tension, cardiopalmus, and sleep disturbance. The diagnosis of anxiety disorder and its subtypes mainly bases on the presenting symptom, which is subjective and is heavily influenced by the experience of psychiatrist. Biomarkers from neuroimaging, genetics, neurochemistry, and neurophysiology are in critical need for more precise identification of patients with anxiety disorder.

Amygdala plays an important role in the development of anxiety disorder and its subtypes (3, 4). A resting state fMRI study found that adult GAD patients exhibited decreased amygdala sub-regions functional connectivity with the cingulate gyrus insula (5). In addition, numerous structural MR imaging studies have revealed alterations in the volume of the amygdala and its microstructures in patients with anxiety disorder and its subtypes (6–10).

The T1-weighted structural magnetic resonance (MR) imaging is necessary for the spatial registration of other MRI scan. Using the T1-weighted MR imaging only as a biomarker for mental disorders would save a lot of time. Radiomics is a candidate technique to achieve this. Radiomics uses different automated feature extraction algorithms to transform medical images to multi-dimensional advanced quantitative imaging features with high throughput (11, 12). It can be used to explore inherent relationships between image features and clinical diagnosis and symptom presentation. Radiomics was first used in the evaluation of tumor-like diseases (13, 14), and has recently been applied to investigate neurodegenerative diseases (15–18) and psychiatric disorders (19–22).

The T1-weighted MR images are also suitable for radiomics analysis. Previous studies have reported that radiomics features of T1-weighted MR images can be used to distinguish mental disorders such as schizophrenia (19), panic disorder (23), Parkinson's disease with depression (24), and temporal lobe epilepsy (25). Yet, to the best of our knowledge, this technique has not been used for the detection of anxiety disorders.

In this study, we performed radiomic analysis on the high-resolution T1-weighted MR images of bilateral amygdala. Using radiomics features of bilateral amygdala extracted from T1-weighted MR images, we aim to evaluate their feasibility in differentiating anxiety disorders and one of its subtypes (i.e., GAD) from the healthy population.

2. Material and methods

2.1. Dataset

We analyzed dataset from Child Mind Institute Healthy Brain Network (HBN) (26). The HBN protocol consists of four 3-h sessions collecting general information, behavioral measures,

diagnostic assessments, and neuroimaging data. Details of the data acquisition were provided in HBN webpages.¹ Psychiatric diagnoses were assessed and reported by clinicians according to DSM-5 criteria (27). Among 2,743 subjects in release 1–9 with T1-weighted MR images, we restricted inclusion to participants with diagnosis of anxiety disorder. These patients were further categorized into separation anxiety, specific phobia, GAD, social anxiety and other specified anxiety disorders. Considering the sample size, we selected GAD as a typical subtype of anxiety disorder for our study. After the data quality control (see “Processing” section), 338 participants with 138 healthy controls (HC), 200 patients with anxiety disorders (include 103 GAD patients) were included for further analysis. We randomly sampled 2/3 of the above data into training set and the rest as test set. Feature selection were performed on the training set, and the test set was used as independent validation data to avoid data leakage (Table 1). Note that feature selection, and subsequent machine learning experiments were performed independently for the Anxiety vs. HC and GAD vs. HC tasks.

2.2. Processing

Quality control using Computational Anatomy Toolbox 12 (CAT12) (28) was performed on T1-weighted MR images. CAT 12 includes various image quality control options, include image resolution, noise, bias field, and weighted overall image quality. Subjects with weighted overall image quality scores of “C+” or lower level were excluded. The remained images were further pre-processed using the standard FreeSurfer recon-all pipeline (version 6.0.0) (29). A probabilistic subcortical structure atlas (i.e., aseg atlas) (30) was used to generate an automated segmentation of bilateral amygdala in native space. The segmentation results were checked by visual inspection.

2.3. Radiomics feature extraction

The workflow of our study is shown in Figure 1. PyRadiomics (version 3.0.1) (31), an open-access Python toolkit, was used to extract radiomics features. Radiomics features were calculated using T1-weighted images of left or right amygdala, respectively, which included 18 first-order statistics features, 14 3D shape-based features, 24 gray level co-occurrence matrix (GLCM) features, 16 gray level run length matrix (GLRLM) features, 16 gray level size zone matrix (GLSZM) features, five neighboring gray tone difference matrix (NGTDM) features and 14 gray level dependence matrix (GLDM) features (Supplementary Table 7). In specific, the first-order statistics describes the distribution of voxel intensities within the image region defined by the mask through commonly used and basic metrics. 3D shape-based features are descriptors of the 3D size and shape of the ROI, i.e., amygdala, which are independent from the gray-level intensity distribution in the ROI. GLCM obtains the co-occurrence matrix by counting the

1 http://fcon_1000.projects.nitrc.org/indi/child/healthy_brain_network

TABLE 1 Demographics of participants.

	Training set				Test set			Training set				Test set		
	Anxiety disorder	HC	p-value	Anxiety disorder	HC	p-value		GAD	HC	p-value	GAD	HC	p-value	
Number of subjects	129	96	-	71	42	-		73	96	-	30	42	-	
Age (mean \pm std)	11.415 \pm 2.838	12.087 \pm 3.564	0.1311 ^a	12.066 \pm 3.297	12.008 \pm 2.605	0.9228 ^a		12.488 \pm 3.813	11.415 \pm 2.838	0.0386 ^a	12.549 \pm 2.88	12.008 \pm 2.605	0.4145 ^a	
Gender (male/female)	70/59	46/50	0.5884 ^b	34/37	17/25	0.8585 ^b		42/31	46/50	0.6384 ^b	15/15	17/25	1.0 ^b	
Site (SI/RU/CUNY/CBIC)	13/53/4/59	28/41/1/26	0.6944 ^b	9/26/4/32	18/17/0/7	0.7743 ^b		7/26/3/37	28/41/1/26	0.6404 ^b	3/12/2/13	18/17/0/7	0.8661 ^b	

STD, standard deviation; ^ap-value was calculated using two-sample student's t-test; ^bp-value was calculated using Chi-square test.

probability of the occurrence of pixel pairs in different directions and displacement vectors. It describes the complexity of the lesion, the level variation, and the degree of texture thickness (32, 33). GLRLM obtains the length matrix by calculating the probability of the pixels appearing repeatedly in succession with different directions and displacement vectors, and describes the complexity of the lesion, the level variation and the degree of texture thickness (34). GLSZM quantifies gray level zones in an image (a gray level zone is defined as the number of connected voxels that share the same gray level intensity) (35). NGTDM quantifies the difference between a gray value and the average gray value of its neighbors (36). LDM quantifies gray level dependencies in an image (a gray level dependency is defined as the number of connected voxels that are dependent on the center voxel) (37).

2.4. Statistical analysis

2.4.1. Feature selection

The range of radiomics features were rescaled *via* z-score normalization. Feature selection was performed on the training dataset from the left and right amygdala, respectively, using the least absolute shrinkage and selection operator (LASSO) regression model with 10-fold cross-validation (Figure 2).

2.4.2. General linear model

Group differences regarding the selected features were tested on the test data. Age, gender and total intracranial volume (TIV) information were also modeled into the GLM. In addition, the volume of the amygdala was also involved in group-wise comparison as a reference to assess the effect of radiomics features. The *p*-values were corrected using Benjamini-Hochberg false discovery rate (FDR) correction method. Further Cohen's *d* (38) was used to measure the effect size of the difference between patients and HC groups.

2.4.3. Machine learning

Further, linear kernel support vector machine (SVM) (39), a classic machine learning model was used to classify the diagnostic groups. In addition, to verify the performance of radiomics features on different machine learning algorithms, we also used four other effective algorithms, including Radial Basis Function (RBF) kernel SVM, random forest (40), extreme gradient boosting (XGBoost) (41), and Gradient Boosting Decision Tree (GBDT) (42). Details of the parameters of the above algorithms are shown in Table 2. For the radiomics features and volume metric, we also further tried to train models by combining features from the left and right amygdala to verify whether such operation could improve the classification performance. In specific, we used 5-fold cross-validation approach for model validation, and models were trained and tested using the abovementioned selected radiomics features. The model performance was evaluated by the area under curve (AUC) of the receiver operator curve (ROC) for the classification of diagnostic groups.

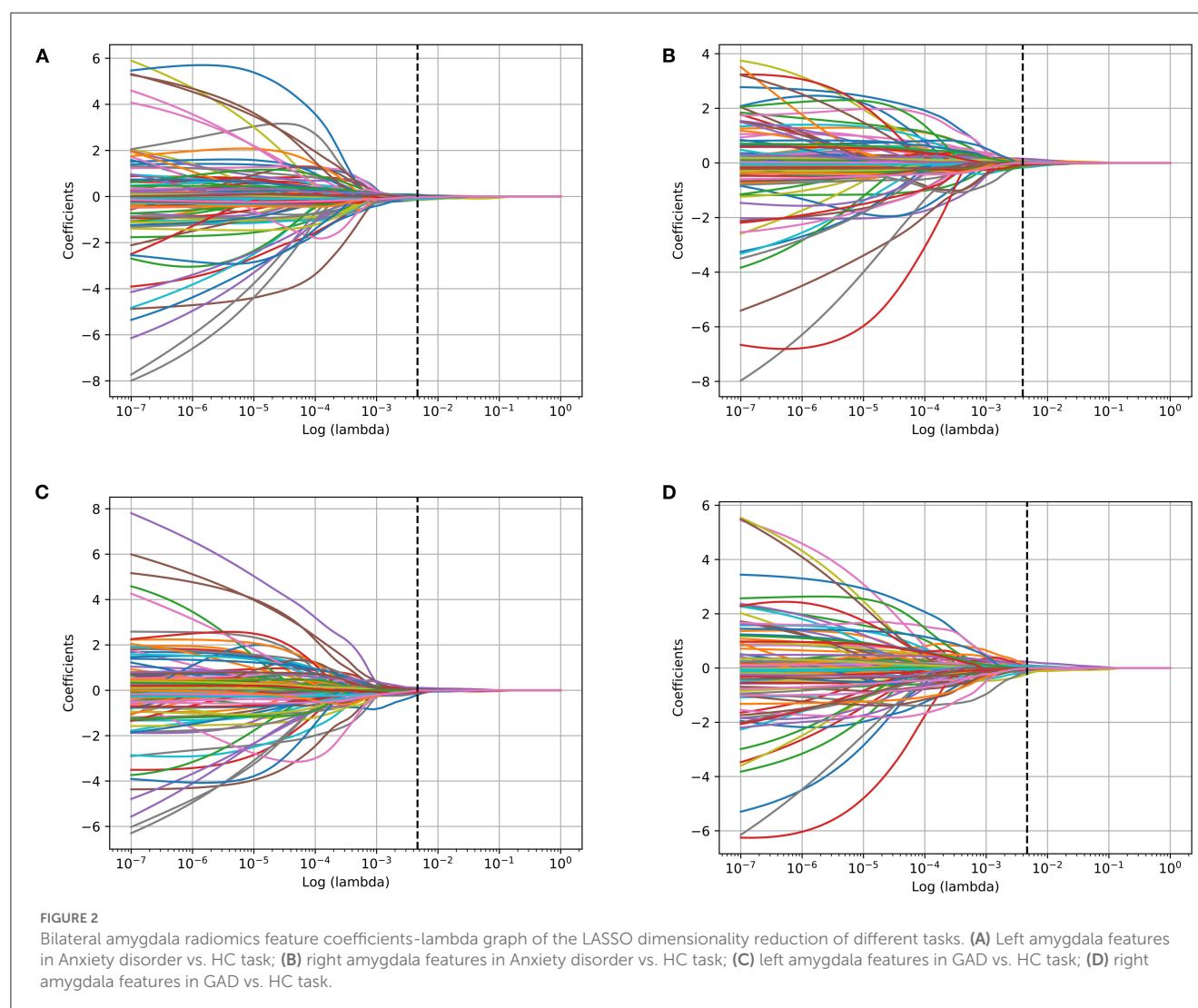
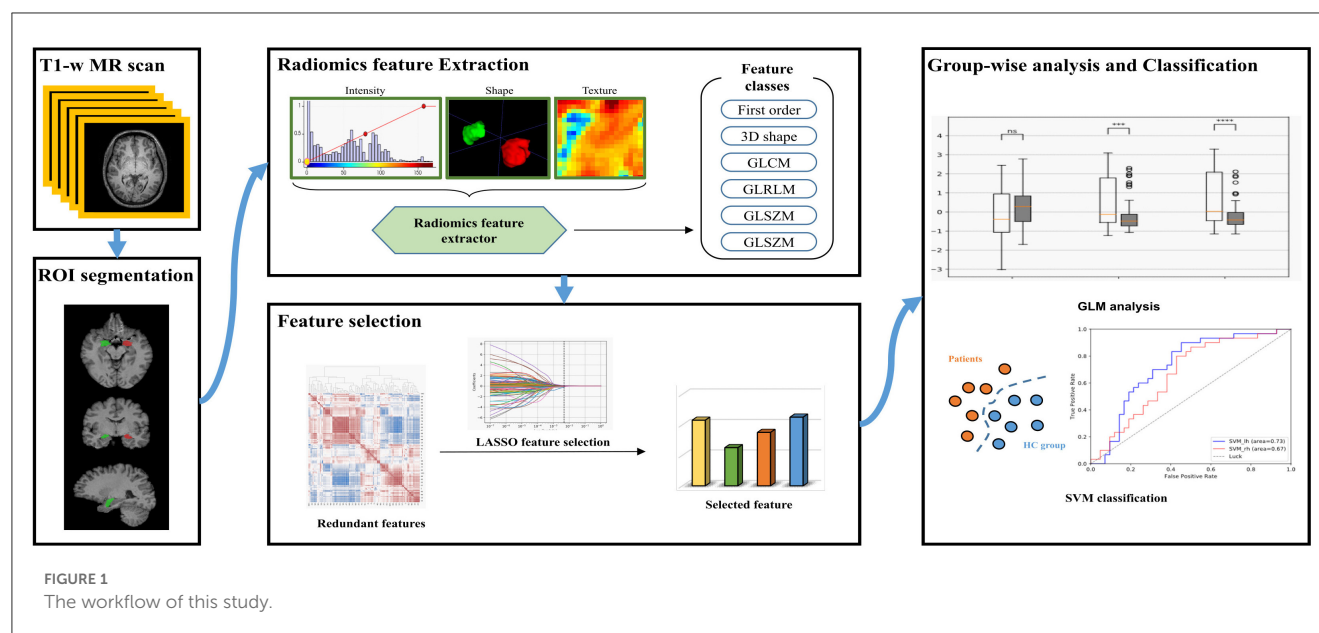


TABLE 2 Details of the parameters of the used machine learning algorithms.

Algorithm	Parameter name	Parameter setting
Linear kernel SVM	C	1
	Kernel	Linear kernel
	Tolerance	1e-3
RBF kernel SVM	C	1
	Kernel	RBF kernel
	Tolerance	1e-3
Random forest	Estimators number	100
	Criterion	Gini index
	Minimal sample split	2
	Minimal samples leaf	1
XGBoost	Base score	0.5
	Gamma	0
	Learning rate	0.1
	Maximum depth	10
	Estimators number	100
GBDT	Loss	Deviance
	Learning rate	0.1
	Estimators number	100
	Criterion	Friedman mean squared error

SVM, support vector machine; RBF, Radial basis function; XGBoost, extreme gradient boosting; GBDT, Gradient boosting decision tree (GBDT).

3. Results

3.1. Anxiety disorder vs. HC radiomics feature analysis

Using 10-fold LASSO regression model, we selected 2-dimensional features (i.e., small dependence emphasis and small dependence high gray level emphasis) for the left amygdala, and 4-dimensional features (i.e., maximum 2D diameter column, interquartile range, small dependence emphasis, and gray level non-uniformity normalized) for the right amygdala.

3.2. Anxiety disorder vs. HC radiomics feature group-wise comparison

For left amygdala, results of group-wise comparison reveals that there were significant differences between anxiety disorder patients and HC group on two selected radiomics features (Figure 3A). As a comparison, no significant difference in left amygdala volume was found between anxiety disorder patients and HC group. The absolute values of the effect sizes of the two radiomics features were also larger than the amygdala volume. For the right amygdala, three radiomics features (i.e., interquartile range, small dependence emphasis, and gray level non-uniformity normalized)

and amygdala volume were significantly different between anxiety disorder patients and HC group, and results of the interquartile range and small dependence emphasis was more significant than amygdala volume in group-wise comparison (Figure 3B). In addition, the values of the effect size of the interquartile range, small dependence emphasis, and gray level non-uniformity normalized were also larger than the amygdala volume (Table 3).

3.3. Anxiety disorder vs. HC classification

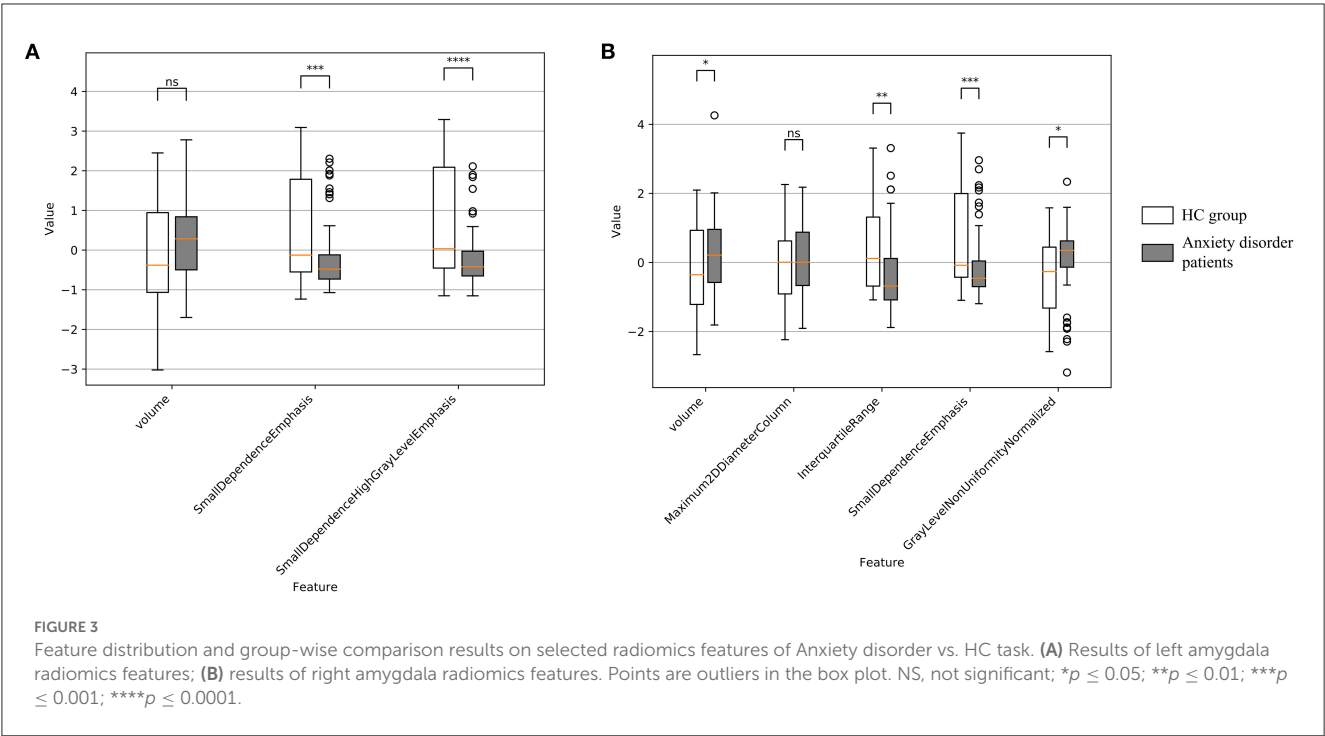
Results of cross-validation experiments showed that the linear kernel SVM models trained separately using selected left/right amygdala radiomics features achieved the classification of anxiety disorder vs. HC. Specifically, SVM trained using two-dimension left amygdala radiomics features achieved classification AUC of 0.6739, and the SVM model trained using four-dimension right amygdala radiomics features achieved classification AUC of 0.6403 (Figures 4A, B, Supplementary Tables 1, 2). For the left/right amygdala, the classification performance of various machine learning algorithms trained with radiomics features were higher than the performance of classifiers trained with amygdala volume (Figures 4A, B, D, E, Supplementary Tables 1–4). Combining features from the left and right amygdala to train machine learning models did not result in a significant improvement in classification performance, but the performance of machine learning models trained by combining radiomics features were still higher than the performance of models trained by combining volume metrics (Figures 4C, F, Supplementary Tables 5, 6).

3.4. GAD vs. HC radiomics feature analysis

7-dimensional features (i.e., maximum 2D diameter column, mean absolute deviation, cluster prominence, cluster tendency, small dependence high gray level emphasis, short run high gray level emphasis, and small area high gray level emphasis) for the left amygdala, and three-dimensional features (i.e., maximum 2D diameter column, interquartile range, and cluster tendency) for the right amygdala were selected using 10-fold LASSO regression model.

3.5. GAD vs. HC radiomics feature group-wise comparison

For left amygdala, results of group-wise comparison reveals that there were significant differences between anxiety disorder patients and HC group on 4 selected radiomics features (i.e., mean absolute deviation, small dependence high gray level emphasis, short run high gray level emphasis, and small area high gray level emphasis) (Figure 5A). As a comparison, no significant difference in left amygdala volume was found between anxiety disorder patients and HC group. The absolute values of the effect sizes of five radiomics features (i.e., mean absolute deviation, cluster prominence, small dependence high gray level emphasis, short run high gray level emphasis, and small area high gray level emphasis) were also larger



than the amygdala volume. For the right amygdala, two radiomics features (i.e., maximum 2D diameter column, and interquartile range) and amygdala volume were significantly different between anxiety disorder patients and HC group (Figure 5B). In addition, the value of the effect size of the interquartile range was larger than the amygdala volume (Table 4).

3.6. GAD vs. HC classification

Results showed that the SVM models trained separately using selected left/right amygdala radiomics features achieved the classification of anxiety disorder vs. HC. Specifically, SVM trained using seven-dimension left amygdala radiomics features achieved classification AUC of 0.6755, and the SVM model trained using three-dimension right amygdala radiomics features achieved classification AUC of 0.6966, which were higher than the performance of classifiers trained with amygdala volume (Figures 6A, B, D, E, Supplementary Tables 1–4). Combining features from the left and right amygdala to train machine learning models did not result in a significant improvement in classification performance, but the performance of machine learning models trained by combining radiomics features were still higher than the performance of models trained by combining volume metrics (Figures 6C, F, Supplementary Tables 5, 6).

4. Discussion

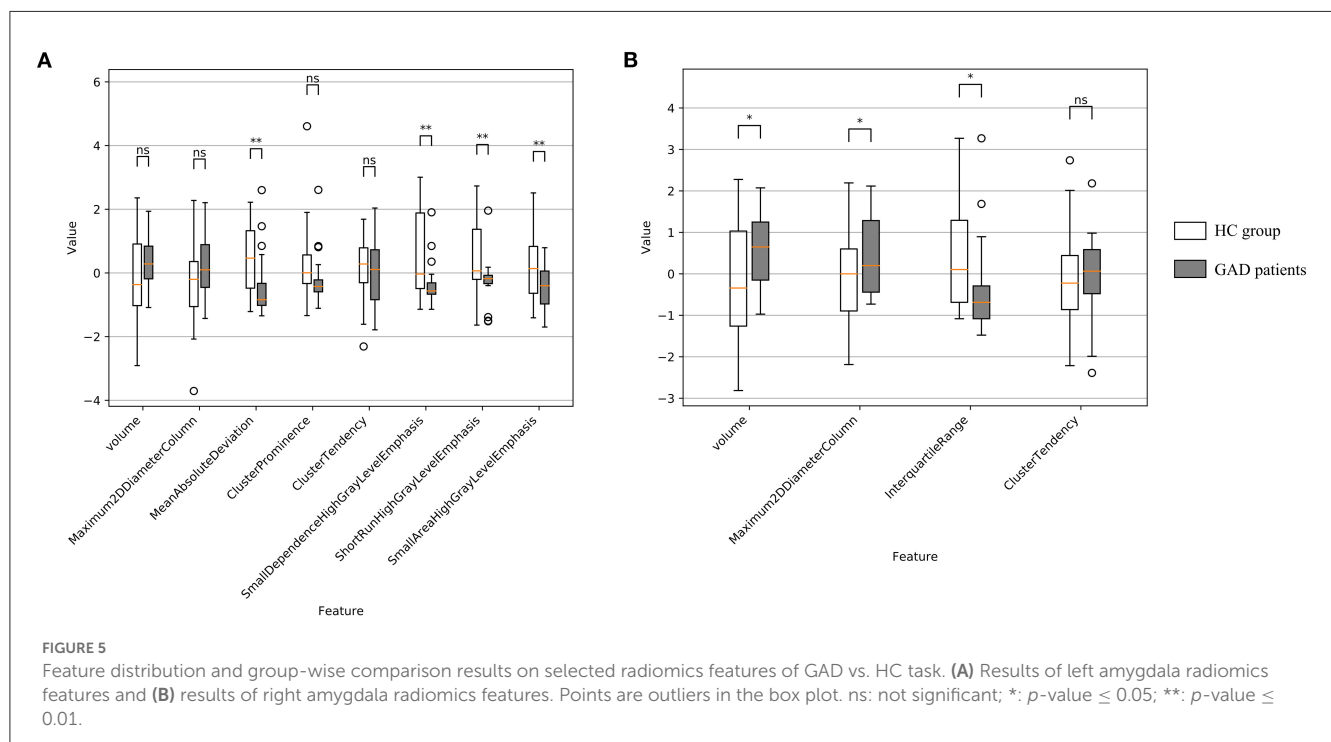
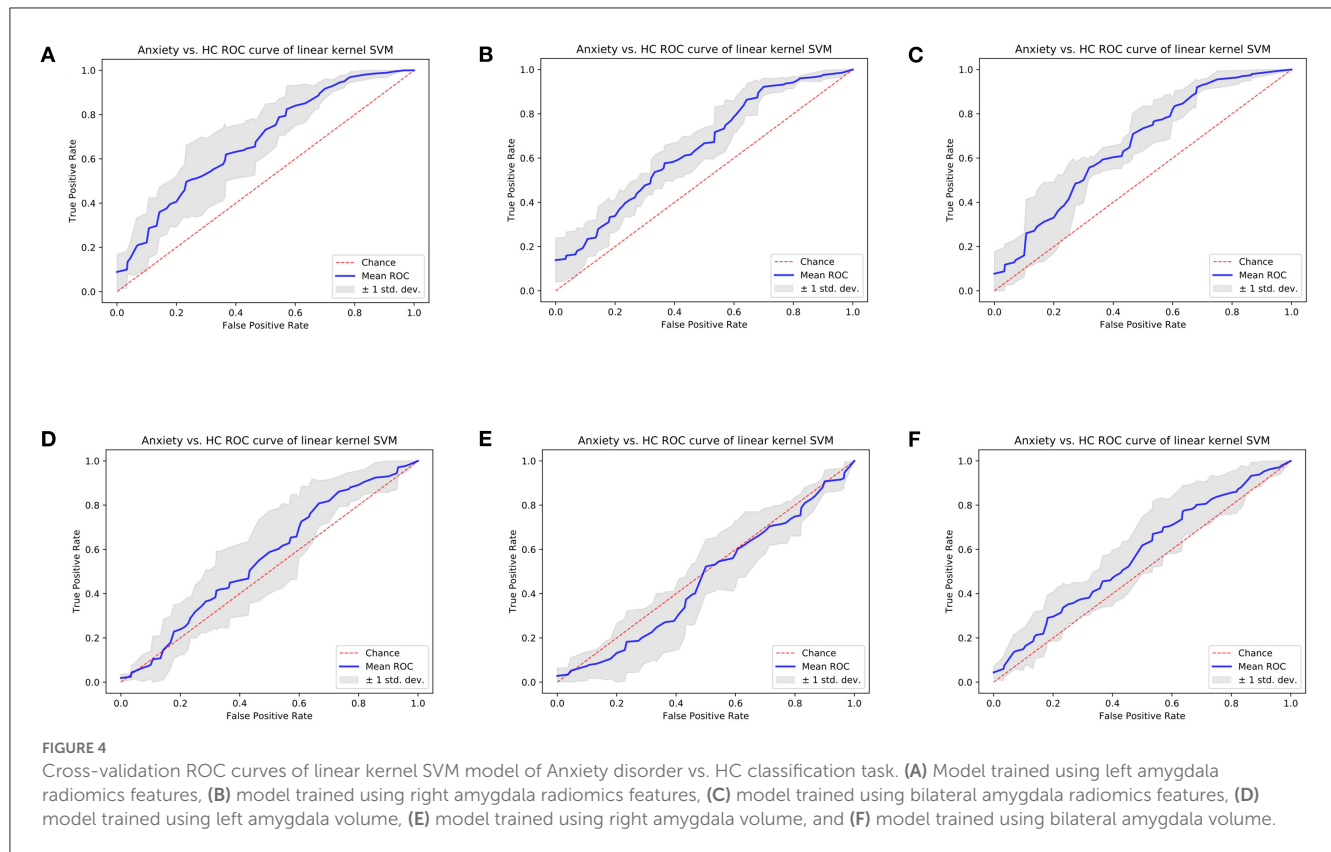
Our study indicated that patients with anxiety disorders and GAD showed abnormalities in the left/right amygdala radiomics features compared with the HC group. Group-wise comparison revealed that abnormalities of some radiomics features were more

TABLE 3 Effect sizes of selected radiomics features and bilateral amygdala volume in anxiety disorder vs. HC task.

Hemisphere	Feature class	Feature name	Effect size
Left	Volume	Amygdala volume	0.3392
	GLDM	Small dependence emphasis	0.7587
		Small dependence high gray level emphasis	0.9016
Right	Volume	Amygdala volume	0.42
	3D shape	Maximum 2D diameter column	0.3146
	First order	Interquartile range	0.6028
	GLDM	Small dependence emphasis	0.8085
	GLRLM	Gray level non-uniformity normalized	0.4667

significant than amygdala volume. Our study is a prospective research to evaluate the feasibility of differentiating anxiety disorders and one of its subtypes (i.e., GAD) from the healthy population using radiomics features of bilateral amygdala extracted from T1-weighted MR images.

Radiomics analysis has been applied to some neural psychiatric disorders. A study has found that radiomics features extracted from the hippocampus structure reflect high-order imaging patterns and heterogeneity characteristics of microstructure in hippocampus in AD patients (43). A radiomics study of autism spectrum disorder has found significant differences in the texture



features in the right hippocampus, corpus callosum, cerebellar white matter, and left choroid plexus between patients and controls (44). However, radiomics studies of anxiety disorder and its subtypes using T1-weighted structural MR images are still

lacking. Structural MR imaging studies have revealed alterations in the volume of the amygdala in patients with anxiety disorder and its subtypes (6–9). In our study, we used radiomics technique to further analyze the abnormalities of the amygdala

TABLE 4 Effect sizes of selected radiomics features and bilateral amygdala volume in GAD vs. HC task.

Hemisphere	Feature class	Feature name	Effect size
Left	Volume	Amygdala volume	0.4783
	3D shape	Maximum 2D diameter column	0.4421
	First order	Mean absolute deviation	0.9455
	GLCM	Cluster prominence	0.5997
		Cluster tendency	0.2273
	GLDM	Small dependence high gray level emphasis	0.9212
	GLRLM	Short run high gray level emphasis	0.801
Right	GLSZM	Small area high gray level emphasis	0.7675
	Volume	Amygdala volume	0.6312
	3D shape	Maximum 2D diameter column	0.5661
	First order	Interquartile range	0.757
	GLCM	Cluster tendency	0.1039

in anxiety disorders and its subtype (i.e., GAD). Radiomics features selected by LASSO regression model reflect the gray value distribution, spatial heterogeneity, texture characteristics and other microstructural information.

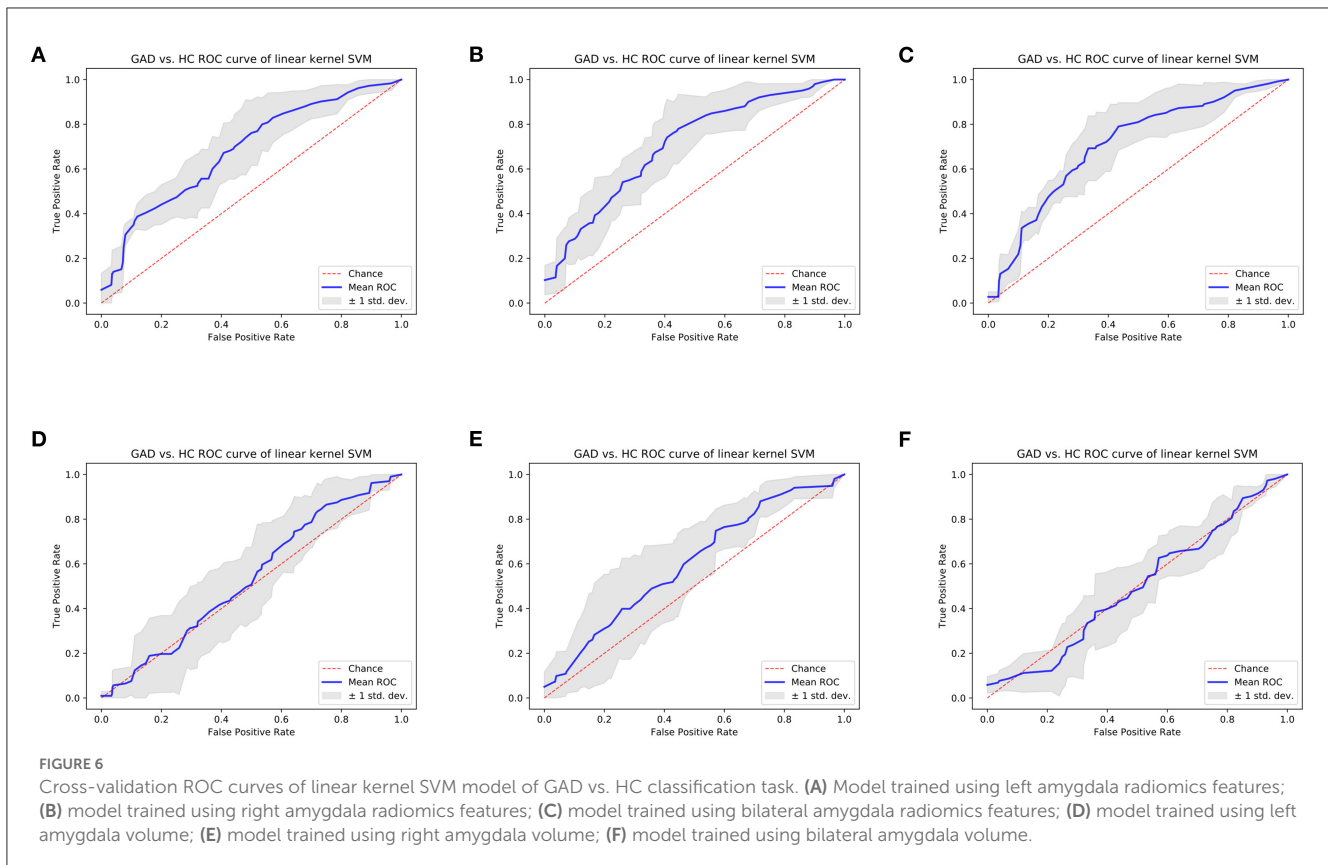
For anxiety disorders, there were 2 selected radiomics features of left amygdala, i.e., small dependence emphasis and small dependence high gray level emphasis are GLDM parameters. According to existing study (37), gray level dependency is defined as the number of connected voxels that are dependent on the center voxel, and small dependence emphasis is a measure of the distribution of small dependencies, with a lower value indicative of greater dependence and more homogeneous textures of left amygdala of anxiety disorder patients compared with HC group. Small dependence high gray level emphasis measures the joint distribution of small dependence with higher gray-level values, with a lower value indicating a smaller concentration of high gray-level values in the image. For right amygdala, there were 4 selected radiomics features, including maximum 2D diameter column, interquartile range, small dependence emphasis, and gray level non-uniformity normalized. Maximum 2D diameter (Column) is defined as the largest pairwise Euclidean distance between ROI surface mesh vertices in the row-slice (usually the coronal) plane. Interquartile range is defined as difference between 25th and 75th percentile of the gray level intensity within the ROI. Gray level non-uniformity normalized measures the variability of gray-level intensity values in the image, with a greater value indicating a smaller similarity in intensity values. The above features indicate structural and textural heterogeneity in the right amygdala in patients with anxiety disorder.

For GAD, seven radiomics features of left amygdala were selected, including maximum 2D diameter column, mean absolute

deviation, cluster prominence, cluster tendency, small dependence high gray level emphasis, short run high gray level emphasis, and small area high gray level emphasis. Mean absolute deviation is the mean distance of all intensity values from the mean value of the gray level intensity values within the ROI. Cluster prominence and cluster tendency are GLCM parameters (32). A lower values of cluster prominence implies less asymmetry of the GLCM, and cluster tendency is a measure of groupings of voxels with similar gray-level values. Short run high gray level emphasis measures the joint distribution of shorter run lengths with higher gray-level values (34), with a lower value indicating a smaller concentration of high gray-level values in the image. Small area high gray level emphasis measures the proportion in the image of the joint distribution of smaller size zones with higher gray-level values, with a lower value indicating a smaller proportion of higher gray-level values of small size zone in the image (35). For right amygdala, there were 3 selected features, i.e., maximum 2D diameter column, interquartile range, and cluster tendency. These features extracted from the left/right amygdala structure reflect high-order imaging patterns and heterogeneity characteristics of microstructure in amygdala in GAD patients.

It is worth noting that significant results in group-wise comparison were not observed on some LASSO-selected radiomics features (e.g., maximum 2D diameter column of right amygdala and cluster tendency of bilateral amygdala). As a machine learning method, LASSO integrates each feature dimension to assess feature importance, while the statistical method of group-wise comparison performs hypothesis testing independently for a specific feature dimension. Therefore, the possible reason for the above experimental results is that certain features that do not differ significantly between patients and healthy people are important for the machine learning task. The above reason can also explain the experimental results related to volume metrics. Although right amygdala volume was significantly different in both Anxiety vs. HC and GAD vs. HC group comparisons (Figures 3B, 5B), satisfactory classification results could not be obtained from machine learning classifiers that trained using right amygdala volume (Figures 4E, 6F, Supplementary Tables 4, 6). This may due to the fact that such differences may not necessarily valid for training machine learning models, e.g., SVM.

Existing studies have used radiomics features for machine learning-based neuropsychiatric disorders classification. A study (20) identified 30 radiomics features of corpus callosum to differentiate participants with schizophrenia from HCs using Bayesian optimized model. Another study (45) used texture features based on GLCM to separate autism spectrum disorder and development control subjects using SVM and random forest classifiers. In a recent study (46), logistic regression analysis was performed to build classification models based on amygdala radiomics features for Alzheimer's disease and amnesic mild cognitive impairment, and achieved an AUC of 0.93 for AD vs. NC classification, an AUC of 0.84 for AD vs. aMCI classification, and an AUC of 0.80 for aMCI vs. NC classification. However, there are still lack of studies on radiomics-based anxiety disorder-related classification. In our study, SVM classification experiments have demonstrated that selected radiomics features of the left/right amygdala can be used to separate patients with anxiety disorder and GAD from HC group, and using radiomics features of amygdala



for classification is better than using amygdala volume. In addition, for both anxiety disorder vs. HC and GAD vs. HC classification tasks, SVM classifiers trained using radiomics features of left amygdala achieved higher AUC than that of right amygdala, which implies that the microstructural changes associated with anxiety are greater in the left amygdala compared with the right amygdala.

Exist studies have revealed alterations in the volume of the amygdala in patients with anxiety disorder and its subtypes. Research on amygdala subregional structure suggests that microstructural information of amygdala is also associated with anxiety-related disorders (10). Radiomics features could reflect high-order imaging patterns and heterogeneity characteristics of microstructure in bilateral amygdala. According to group-wise comparison experiments, the differences between patients and HC group in most selected radiomics features were more significant than the amygdala volume. In addition, the absolute values of the effect sizes of most selected radiomics features were larger than the amygdala volume. Our study suggests bilateral amygdala radiomics features could serve as more effective neuroimaging biomarkers, compared with amygdala volume, for identifying patients with anxiety disorders and GAD.

There were several limitations in our study. Firstly, there are many subtypes of anxiety disorder, including social anxiety, separation anxiety, etc. Limited by sample size, only GAD was selected as an example for anxiety disorder subtype in our study.

Secondly, a complete 1:1 match in age, sex and site ratio had not been achieved. In future works, we will collect data of other anxiety disorder subtypes scanned from multiple scanners, and further evaluate relationship between amygdala radiomics features and behavioral information.

In summary, our study observed that compared with amygdala volume, bilateral amygdala radiomics features could serve as more effective neuroimaging biomarkers for identifying patients with anxiety disorders and GAD. Moreover, we used machine learning method to evaluate the feasibility of differentiating patients of anxiety disorders and GAD from the healthy people using radiomics features of bilateral amygdala extracted from T1-weighted MR images, thus providing effective biomarkers for the clinical diagnosis of anxiety disorders.

Data availability statement

Publicly available datasets were analyzed in this study. This data can be found at: Child Mind Institute Healthy Brain Network (HBN) dataset: http://fcon_1000.projects.nitrc.org/indi/cmi_healthy_brain_network.

Ethics statement

The studies involving human participants were reviewed and approved by Chesapeake Institutional Review Board. Written

informed consent to participate in this study was provided by the participants' legal guardian/next of kin.

Author contributions

QL, WW, and ZH designed the experiments and drafted and reviewed the manuscript. QL and WW performed the experiments and analyzed the data and interpreted the results. All the authors read and approved the final version of the manuscript.

Funding

This study was funded by the National Natural Science Foundation of China (62007002) and 2021 Shanghai Mental Health Center Hospital Level Key Projects (2021zd02).

Acknowledgments

We thank Mr. Yang Hu for his thoughtful comments and assistance with our experiments.

References

- Vos T, Lim SS, Abbafati C, Abbas KM, Abbasi M, Abbasifard M, et al. Global burden of 369 diseases and injuries in 204 countries and territories, 1990–2019: a systematic analysis for the global burden of disease study 2019. *Lancet*. (2020) 396:1204–22. doi: 10.1016/S0140-6736(20)30925-9
- Duval ER, Javanbakht A, Liberzon I. Neural circuits in anxiety and stress disorders: a focused review. *Ther Clin Risk Manag*. (2015) 11:115. doi: 10.2147/TCRM.S48528
- Walker LC. A balancing act: the role of pro- and anti-stress peptides within the central amygdala in anxiety and alcohol use disorders. *J Neurochem*. (2021) 157:1615–43. doi: 10.1111/jnc.15301
- Lau JY, Goldman D, Buzas B, Hodgkinson C, Leibenluft E, Nelson E, et al. BDNF gene polymorphism (Val66Met) predicts amygdala and anterior hippocampus responses to emotional faces in anxious and depressed adolescents. *Neuroimage*. (2010) 53:952–61. doi: 10.1016/j.neuroimage.2009.11.026
- Liu WJ, Yin DZ, Cheng WH, Fan MX, You MN, Men WW, et al. Abnormal functional connectivity of the amygdala-based network in resting-state FMRI in adolescents with generalized anxiety disorder. *Med Sci Monit*. (2015) 21:459–67. doi: 10.12659/MSM.893373
- De Bellis MD, Casey BJ, Dahl RE, Birmaher B, Williamson DE, Thomas KM, et al. A pilot study of amygdala volumes in pediatric generalized anxiety disorder. *Biol Psychiatry*. (2000) 48:51–7. doi: 10.1016/S0006-3223(00)00835-0
- Milham MP, Nugent AC, Drevets WC, Dickstein DS, Leibenluft E, Ernst M, et al. Selective reduction in amygdala volume in pediatric anxiety disorders: a voxel-based morphometry investigation. *Biol Psychiatry*. (2005) 57:961–6. doi: 10.1016/j.biopsych.2005.01.038
- Baur V, Hänggi J, Jäncke L. Volumetric associations between uncinate fasciculus, amygdala, trait anxiety. *BMC Neurosci*. (2012) 13:4. doi: 10.1186/1471-2202-13-4
- Donnici C, Long X, Dewey D, Letourneau N, Landman B, Huo Y, et al. Prenatal and postnatal maternal anxiety and amygdala structure and function in young children. *Sci Rep*. (2021) 11:4019. doi: 10.1038/s41598-021-83249-2
- Qin S, Young CB, Duan X, Chen T, Supekar K, Menon V. Amygdala subregional structure and intrinsic functional connectivity predicts individual differences in anxiety during early childhood. *Biol Psychiatry*. (2014) 75:892–900. doi: 10.1016/j.biopsych.2013.10.006
- Kumar V, Gu Y, Basu S, Berglund A, Eschrich SA, Schabath MB, et al. Radiomics: the process and the challenges. *Magn Reson Imaging*. (2012) 30:1234–48. doi: 10.1016/j.mri.2012.06.010
- Gillies RJ, Kinahan PE, Hricak H. Radiomics: images are more than pictures, they are data. *Radiology*. (2016) 278:563–77. doi: 10.1148/radiol.2015151169
- Zhou M, Scott J, Chaudhury B, Hall L, Goldof D, Yeom KW, et al. Radiomics in brain tumor: image assessment, quantitative feature descriptors, machine-learning approaches. *AJNR Am J Neuroradiol*. (2018) 39:208–16. doi: 10.3174/ajnr.A5391
- Liu Z, Wang S, Dong D, Wei J, Fang C, Zhou X, et al. The applications of radiomics in precision diagnosis and treatment of oncology: opportunities and challenges. *Theranostics*. (2019) 9:1303. doi: 10.7150/thno.30309
- Feng Q, Ding Z. MRI radiomics classification and prediction in Alzheimer's disease and mild cognitive impairment: a review. *Curr Alzheimer Res*. (2020) 17:297–309. doi: 10.2174/1567205017666200303105016
- Feng Q, Chen Y, Liao Z, Jiang H, Mao D, Wang M, et al. Corpus callosum radiomics-based classification model in Alzheimer's disease: a case-control study. *Front Neurol*. (2018) 9:618. doi: 10.3389/fneur.2018.00618
- Chaddad A, Desrosiers C, Niazi T. Deep radiomic analysis of MRI related to Alzheimer's disease. *IEEE Access*. (2018) 6:58213–21. doi: 10.1109/ACCESS.2018.2871977
- Zhao K, Ding Y, Han Y, Fan Y, Alexander-Bloch AF, Han T, et al. Independent and reproducible hippocampal radiomic biomarkers for multisite Alzheimer's disease: diagnosis, longitudinal progress and biological basis. *Sci Bull*. (2020) 65:1103–13. doi: 10.1016/j.scib.2020.04.003
- Park YW, Choi D, Lee J, Ahn SS, Lee SK, Lee SH, et al. Differentiating patients with schizophrenia from healthy controls by hippocampal subfields using radiomics. *Schizophr Res*. (2020) 223:337–44. doi: 10.1016/j.schres.2020.09.009
- Bang M, Eom J, An C, Kim S, Park YW, Ahn SS, et al. An interpretable multiparametric radiomics model for the diagnosis of schizophrenia using magnetic resonance imaging of the corpus callosum. *Transl Psychiatry*. (2021) 11:462. doi: 10.1038/s41398-021-01586-2
- Wang Y, Sun K, Liu Z, Chen G, Jia Y, Zhong S, et al. Classification of unmedicated bipolar disorder using whole-brain functional activity and connectivity: a radiomics analysis. *Cereb Cortex*. (2020) 30:1117–28. doi: 10.1093/cercor/bhz152
- Zhang B, Liu S, Liu X, Chen S, Ke Y, Qi S, et al. Discriminating subclinical depression from major depression using multi-scale brain functional features: a radiomics analysis. *J Affect Disord*. (2022) 297:542–52. doi: 10.1016/j.jad.2021.10.122
- Bang M, Park YW, Eom J, Ahn SS, Kim J, Lee SK, et al. An interpretable radiomics model for the diagnosis of panic disorder with or without agoraphobia using magnetic resonance imaging. *J Affect Disord*. (2022) 305:47–54. doi: 10.1016/j.jad.2022.02.072
- Li XN, Hao DP, Qu MJ, Zhang M, Ma AB, Pan XD, et al. Development and validation of a plasma FAM19A5 and MRI-based radiomics model for prediction of

Conflict of interest

The authors declare that the research was conducted in the absence of any commercial or financial relationships that could be construed as a potential conflict of interest.

Publisher's note

All claims expressed in this article are solely those of the authors and do not necessarily represent those of their affiliated organizations, or those of the publisher, the editors and the reviewers. Any product that may be evaluated in this article, or claim that may be made by its manufacturer, is not guaranteed or endorsed by the publisher.

Supplementary material

The Supplementary Material for this article can be found online at: <https://www.frontiersin.org/articles/10.3389/fpsy.2023.1091730/full#supplementary-material>

- parkinson's disease and parkinson's disease with depression *Front Neurosci.* (2021) 15:795539. doi: 10.3389/fnins.2021.795539
25. Park YW, Choi YS, Kim SE, Choi D, Han K, Kim H, et al. Radiomics features of hippocampal regions in magnetic resonance imaging can differentiate medial temporal lobe epilepsy patients from healthy controls. *Sci Rep.* (2020) 10:19567. doi: 10.1038/s41598-020-76283-z
 26. Alexander LM, Escalera J, Ai L, Andreotti C, Febre K, Mangone A, et al. An open resource for transdiagnostic research in pediatric mental health and learning disorders. *Sci Data.* (2017) 4:170181. doi: 10.1038/sdata.2017.181
 27. Regier DA, Kuhl EA, Kupfer DJ. The DSM-5: classification and criteria changes. *World Psychiatry.* (2013) 12:92–8. doi: 10.1002/wps.20050
 28. Gaser C, Dahnke R, Thompson PM, Kurth F, Luders E. CAT-a computational anatomy toolbox for the analysis of structural MRI data. *BioRxiv.* (2022). doi: 10.1101/2022.06.11.495736
 29. Fischl B. FreeSurfer. *Neuroimage.* (2012) 62:774–81. doi: 10.1016/j.neuroimage.2012.01.021
 30. Fischl B, Salat DH, Busa E, Albert M, Dieterich M, Haselgrove C, et al. Whole brain segmentation: automated labeling of neuroanatomical structures in the human brain. *Neuron.* (2002) 33:341–55. doi: 10.1016/S0896-6273(02)00569-X
 31. Van Griethuysen JJ, Fedorov A, Parmar C, Hosny A, Aucoin N, Narayan V, et al. Computational radiomics system to decode the radiographic phenotype. *Cancer Res.* (2017) 77:e104–7. doi: 10.1158/0008-5472.CAN-17-0339
 32. Haralick RM, Shanmugam K, Dinstein IH. Textural features for image classification. In: *IEEE Transactions on Systems, Man, and Cybernetics.* (1973). p. 610–21. doi: 10.1109/TSMC.1973.4309314
 33. Park S, Kim B, Lee J, Goo JM, Shin YG. GGO nodule volume-preserving nonrigid lung registration using GLCM texture analysis. *IEEE Trans Biomed Eng.* (2011) 58:2885–94. doi: 10.1109/TBME.2011.2162330
 34. Tang X. Texture information in run-length matrices. *IEEE Trans Image Process.* (1998) 7:1602–9. doi: 10.1109/83.725367
 35. Thibault G, Fertil B, Navarro C, Pereira A, Cau P, Levy N, et al. Shape and texture indexes application to cell nuclei classification. *Intern J Pattern Recognit Artif Intell.* (2013) 27:1357002. doi: 10.1142/S0218001413570024
 36. Amadasun M, King R. Textural features corresponding to textural properties. *IEEE Trans Syst Man Cyber.* (1989) 19:1264–74. doi: 10.1109/21.44046
 37. Sun C, Wee WG. Neighboring gray level dependence matrix for texture classification. *Comp Vis Graph Image Process.* (1983) 23:341–52. doi: 10.1016/0734-189X(83)90032-4
 38. Fritz CO, Morris PE, Richler JJ. Effect size estimates: current use, calculations, and interpretation. *J Exp Psychol Gen.* (2012) 141:2–18. doi: 10.1037/a0024338
 39. Cortes C, Vapnik V. Support-vector networks. *Mach Learn.* (1995) 20:273–97. doi: 10.1007/BF00994018
 40. Breiman L. Random forests. *Mach Learn.* (2001) 45:5–32. doi: 10.1023/A:1010933404324
 41. Chen T, Guestrin C. Xgboost: a scalable tree boosting system. In: *Proceedings of the 22nd ACM Sigkdd International Conference on Knowledge Discovery and Data Mining.* San Francisco, CA (2016). p. 785–94. doi: 10.1145/2939672.2939785
 42. Friedman JH. Greedy function approximation: a gradient boosting machine. *Ann Stat.* (2001) 29:1189–232. doi: 10.1214/aos/1013203451
 43. Feng Q, Wang M, Song Q, Wu Z, Jiang H, Pang P, et al. Correlation between hippocampus MRI radiomic features and resting-state intrahippocampal functional connectivity in Alzheimer's disease. *Front Neurosci.* (2019) 13:435. doi: 10.3389/fnins.2019.00435
 44. Chaddad A, Desrosiers C, Toews M. Multi-scale radiomic analysis of sub-cortical regions in MRI related to autism, gender and age. *Sci Rep.* (2017) 7:45639. doi: 10.1038/srep45639
 45. Chaddad A, Desrosiers C, Hassan L, Tanougast C. Hippocampus and amygdala radiomic biomarkers for the study of autism spectrum disorder. *BMC Neurosci.* (2017) 18:52. doi: 10.1186/s12868-017-0373-0
 46. Feng Q, Niu J, Wang L, Pang P, Wang M, Liao Z, et al. Comprehensive classification models based on amygdala radiomic features for Alzheimer's disease and mild cognitive impairment. *Brain Imaging Behav.* (2021) 15:2377–86. doi: 10.1007/s11682-020-00434-z



OPEN ACCESS

EDITED BY

Nuno Madeira,
University of Coimbra, Portugal

REVIEWED BY

João Valente Duarte,
University of Coimbra, Portugal
Taro Kishi,
Fujita Health University, Japan

*CORRESPONDENCE

Reiji Yoshimura
✉ yoshi621@med.uoeh-u.ac.jp

SPECIALTY SECTION

This article was submitted to
Mood Disorders,
a section of the journal
Frontiers in Psychiatry

RECEIVED 26 January 2023

ACCEPTED 06 March 2023

PUBLISHED 22 March 2023

CITATION

Chibaatar E, Watanabe K, Okamoto N,
Orkhonselenge N, Natsuyama T, Hayakawa G,
Ikenouchi A, Kakeda S and Yoshimura R (2023)
Volumetric assessment of individual thalamic
nuclei in patients with drug-naïve,
first-episode major depressive disorder.
Front. Psychiatry 14:1151551.
doi: 10.3389/fpsy.2023.1151551

COPYRIGHT

© 2023 Chibaatar, Watanabe, Okamoto,
Orkhonselenge, Natsuyama, Hayakawa,
Ikenouchi, Kakeda and Yoshimura. This is an
open-access article distributed under the terms
of the [Creative Commons Attribution License](https://creativecommons.org/licenses/by/4.0/)
(CC BY). The use, distribution or reproduction
in other forums is permitted, provided the
original author(s) and the copyright owner(s)
are credited and that the original publication in
this journal is cited, in accordance with
accepted academic practice. No use,
distribution or reproduction is permitted which
does not comply with these terms.

Volumetric assessment of individual thalamic nuclei in patients with drug-naïve, first-episode major depressive disorder

Enkhmurun Chibaatar¹, Keita Watanabe², Naomichi Okamoto¹,
Nasanbadrakh Orkhonselenge³, Tomoya Natsuyama¹,
Gaku Hayakawa¹, Atsuko Ikenouchi¹, Shingo Kakeda⁴ and
Reiji Yoshimura^{1*}

¹Department of Psychiatry, University of Occupational and Environmental Health, Kitakyushu, Japan,

²Open Innovation Institute, Kyoto University, Kyoto, Japan, ³Department of Second Internal Medicine, University of Occupational and Environmental Health, Kitakyushu, Japan, ⁴Department of Radiology, Graduate School of Medicine, Hiroshima University, Hiroshima, Japan

Introduction: Despite the previous inconsistent findings of structural and functional abnormalities of the thalamus in patients with major depressive disorder (MDD), the disruption of the thalamic nuclei in the pathophysiology of this disorder has not yet been adequately studied. Therefore, we investigated the volumetric changes of thalamic subregions and their nuclei in drug-naïve, first-episode MDD patients. We also investigated the association between HAM-D scores, a clinical scale frequently used to evaluate the severity of depression and thalamic nuclei volumes in MDD patients.

Methods: This study included 76 drug-naïve MDD patients and an equal number of healthy subjects. Magnetic resonance imaging (MRI) data were obtained using a 3T MR system and thalamic nuclei volumes were evaluated using FreeSurfer ver.7.11. The volumetric differences were compared by one-way analysis of covariance (ANCOVA) and to ensure that effects were not accounted for by other factors, age, sex, and ETICV variables were included as covariates.

Results: We observed significant volume reductions of the left whole thalamus ($p < 0.003$) and several thalamic nuclei mostly on the left side in the MDD group compared with healthy controls (HCs). Furthermore, we have revealed weak negative correlations between several thalamic nuclei volumes and HAM-D total and subscale scores.

Discussion: This is the first research study to investigate alterations of the various thalamic nuclei volumes in MDD patients compared with HCs. Moreover, we first analyzed the association between individual thalamic nuclei volumes and HAM-D subscale scores. Though our study may be restricted at certain levels, especially by the demographic difference between the two groups, they possibly contribute at a preliminary level to understanding the thalamic structural changes at its subregions in patients with drug-naïve, first-episode MDD.

KEYWORDS

major depressive disorder, thalamus, thalamic nuclei volumes, subregional difference, structural MRI

1. Introduction

Major depressive disorder (MDD) is a highly devitalizing mental disease that is common, with a high lifetime prevalence of approximately 15–20% (1). Patients with MDD are bothered by irritable and empty feelings, loss of pleasure or interest, impaired cognitive function, and, most importantly, thoughts of death or suicide (2). Specific structural alterations in brain regions and circuits, including the cortico-striato-thalamo-cortical (CSTC) circuit, have been reported as pathophysiological models of MDD that explain impairments in emotional and cognitive processes (3, 4). Among the brain regions that show deterioration and involvement in the circuit, the thalamus has been a prominent topic because of its extensive connections with other areas and its critical roles in cognitive impairment (5, 6). Although the thalamus is formed into functionally segregated nuclei, each with distinct anatomical locations and physiological functions (7–9), disruption of the thalamic nuclei in MDD patients has not yet been adequately studied.

Recent structural magnetic resonance imaging (MRI) studies have revealed inconsistent findings regarding the thalamic structure in patients with first-episode MDD. While most of the studies have shown a reduced volume in the bilateral thalami (10–14) or the left thalamus (15, 16), other meta-analyses observed increased thalamic volumes in patients with MDD (17, 18). As a volumetric change in the whole thalamus does not inform us about the functional significance of the cognitive and emotional processes underlying the pathophysiology of MDD, only one study has investigated thalamic subregions in the context of MDD. Choi et al. reported contractions in the medial and lateral nuclei in participants with MDD compared with participants in the control group (19). However, a more comprehensive segmentation study of the thalamus is required to identify the potential role of specific thalamic nuclei in the pathophysiology of MDD. Determining whether specific nuclei primarily drive thalamic differences could pinpoint specific circuits more affected in MDD, providing a potential avenue for targeted treatment strategies.

In vivo estimation of thalamic nuclei volumes could be challenging because of the limited contrast of most structural MRI images, which affects the accurate delineation of the internuclear borders. However, recent advances in automated thalamic segmentation have allowed unbiased large-scale volumetric analysis of individual nuclei. For instance, a probabilistic atlas presented by Iglesias et al. (20) enabled automatic segmentation of the thalamus into 25 specific nuclei using *ex vivo* brain MRI, histological data, and an *in vivo* MRI segmentation atlas.

In the present study, we applied this method to investigate volumetric differences in six different thalamic subregions (anterior, lateral, ventral, intralaminar, medial, and posterior) between drug-naïve patients with MDD in their first episode and healthy controls (HCs). We also investigated the association between HAMD-17 scores, a clinical scale frequently used to evaluate the severity of depression, and thalamic nuclei volumes in patients with MDD. As this is the first study of volumetric differences within various nuclei of the thalamus in the context of MDD and all nuclei can be potentially relevant from a functional perspective, we did not postulate an *a priori* hypothesis regarding which nuclei show differences.

2. Materials and methods

2.1. Participants

Seventy-six drug-naïve MDD patients (34 males, 42 females) and seventy-six healthy subjects (50 males, 26 females) participated in this study (Table 1). All patients with MDD were recruited from the inpatient and outpatient clinics of the Department of Psychiatry at the University of Occupational and Environmental Health (UOEH) Hospital, according to the following criteria: (1) newly diagnosed with MDD based on standard criteria of the Diagnostic and Statistical Manual of Mental Disorders–5 (DSM-V); (2) scored equal to or more than 14 on the 17-items Hamilton Rating Scale for Depression (HAMD-17); (3) did not use antidepressants or other psychiatric drugs; and (4) had no previous history of medical illness, neurological, or psychiatric disorders. Healthy subjects were recruited from the community through advertisements according to the following criteria: (1) had never been diagnosed with any psychiatric disorders according to the Structured Clinical Interview for DSM Disorders (SCID), and (2) had no family history of a serious medical or neuropsychiatric disorder among their first-degree relatives. All participants provided written informed consent after the study procedure was explained. The study protocol was approved by the Ethics Committee of the UOEH and was conducted in accordance with the Declaration of Helsinki.

2.2. Hamilton rating scale for depression

Hamilton Rating Scale for Depression HAMD-17 items were divided into the following subcategories: core (items 1, 2, 7, 8, 10, and 13), sleep (items 4 and 6), activity (items 7 and 8), psychic (items 9 and 10), and somatic anxiety (items 11 and 13), similar to our previous work (21, 22).

TABLE 1 Demographic and clinical characteristics of patients with MDD and healthy controls.

Characteristics	Patients with MDD (n = 76)	Healthy controls (n = 76)
Age	53.71 ± 17.07	35.66 ± 12.07
Gender		
Male (n, %)	34 (44.74%)	50 (65.79%)
Female (n, %)	42 (55.26%)	26 (34.21%)
ETICV (mm ³ ± SD)	15.21 × 10 ⁵ ± 1.74 × 10 ⁵	15.89 × 10 ⁵ ± 1.36 × 10 ⁵
HAMD-17 total score	22.45 ± 6.283	–
HAMD-17 subscale score		
Core (0–22)	10.18 ± 3.56	–
Sleep (0–4)	2.43 ± 1.13	–
Activity (0–8)	3.82 ± 1.51	–
Psychic (0–8)	2.78 ± 1.28	–
Anxiety (0–6)	2.71 ± 1.20	–

Values represent the mean ± SD unless otherwise stated. MDD, major depressive disorder; ETICV, estimated total intracranial cavity volume; HAMD-17, 17 items hamilton depression rating scale.

2.3. Structural MRI acquisition

Magnetic resonance imaging data were obtained using a 3T MR system (Signa EXCITE 3T; GE Healthcare, Waukesha, WI, USA) with an 8-channel brain phased-array coil. Images were acquired using three-dimensional fast-spoiled gradient-recalled acquisition (3D-FSPGR). The acquisition parameters were as follows: repetition time/echo time, 10/4.1 msec; flip angle, 10°; field of view, 24 cm; resolution, 0.9 mm × 0.9 mm × 1.2 mm. All images were corrected for image distortion due to gradient non-linearity using the “Grad Warp” software program (23).

2.4. Image processing (thalamic segmentation)

FreeSurfer ver.7.11 (24) was used to evaluate the volume of thalamic subregions. This fully automated segmentation technique for thalamic nuclei is based on a prior probabilistic atlas and a Bayesian modeling approach (20). The bilateral thalami were generated in each subject for 25 nuclei in six different regions (Figure 1) and the whole thalamus. The left and right substructures were analyzed separately. Furthermore, the estimated intracranial volume was also calculated using “Aseg segmentation.”

2.5. Statistical analyses

All statistical analyses were performed using IBM SPSS Statistics (version 26.0; SPSS Inc., Chicago, IL, USA). We performed independent *t*-tests and χ^2 tests to compare the

demographic and clinical data between patients with MDD and HCs. To investigate the volumetric differences, a one-way analysis of covariance (ANCOVA) was used to ensure that the effects were not accounted for by other factors; age, sex, and ETICV variables were included as covariates. The assumptions of normal distribution, linearity, and homogeneity of variance were tested and verified. The Bonferroni’s correction method was used for multiple comparisons. To examine the association between thalamic nuclei volumes and HAMD-17 scores, we performed a partial correlation analysis with age, sex, and ETICV as covariates. Results were considered statistically significant at $p < 0.05$.

3. Results

3.1. Demographic and clinical data

The demographic and clinical characteristics of patients with MDD and HCs are shown in Table 1. Significant differences ($p < 0.05$) were observed between the groups in age, sex, and estimated total intracranial volume (ETICV). However, these variables were used as covariates to eliminate their effects in further analyses. Table 1 also showed HAM-D total and subscale scores in the MDD group. Notably, all patients with MDD were in the first episode and were medication-free.

3.2. Volumetric analysis

Table 2 shows the thalamic volume as a whole and the individual nuclei. The right thalamic volume was not different

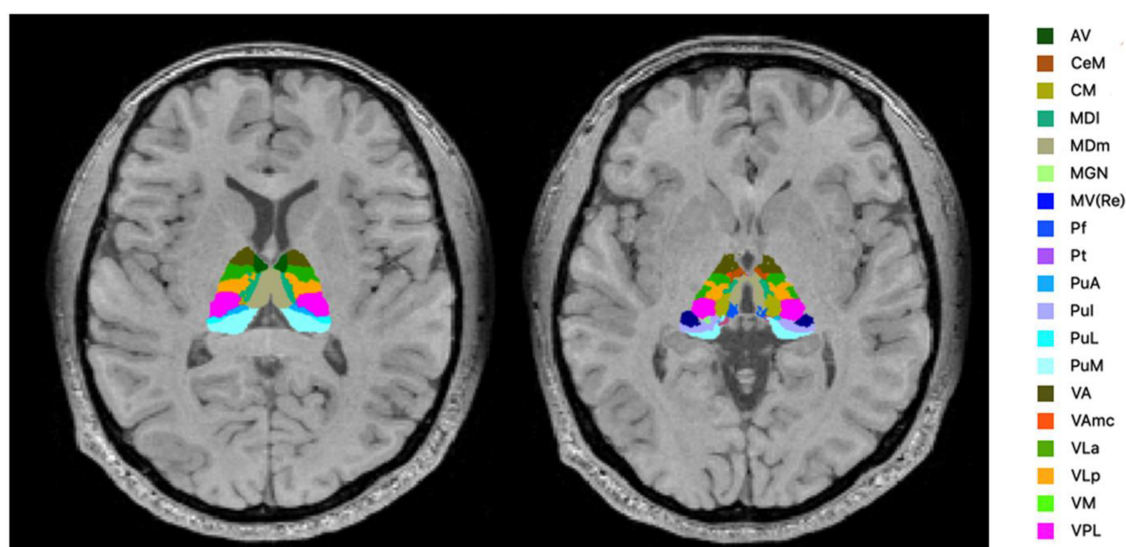


FIGURE 1

Segmentation of the thalamic nuclei. The example of probabilistic segmentation (not all segmentations are shown) of the thalamus generated by FreeSurfer ver.7.11 (23). Anterior region: AV, anteroventral. Intralaminar region: CeM, central medial; CM, centromedian; Pf, Parafascicular; medial region: MDI, mediodorsal lateral parvocellular; MDm, mediodorsal medial magnocellular; MV-re, medial ventral reuniens; Pt, paratenial. Posterior region: MGN, medial geniculate; PuA, pulvinar anterior; Pul, pulvinar inferior; PuL, pulvinar lateral; PuM, pulvinar medial. Ventral region: VA, ventral anterior; VAmc, ventral anterior magnocellular; VLa, ventral lateral anterior; VLp, ventral lateral posterior; VM, ventromedial; VPL, ventral posterolateral.

TABLE 2 Differences in thalamic nuclei volumes between patients with MDD and healthy control.

Thalamic nucleus	Patients with MDD (n = 76)		Healthy controls (n = 76)		F	p-value
	Mean, mm ³	SD, mm ³	Mean, mm ³	SD, mm ³		
Left whole thalamus	6425.39	865.44	7293.72	795.60	8.91	0.003*
Right whole thalamus	6493.89	805.46	7170.51	747.52	2.88	0.092
Anterior						
Left-AV	137.96	23.19	151.09	24.50	2.73	0.101
Right-AV	145.07	26.32	158.22	25.36	3.10	0.080
Lateral						
Left-LD	24.31	7.47	32.71	8.04	13.84	<0.001*
Right-LD	28.44	8.57	33.91	8.60	1.69	0.195
Left-LP	124.01	24.66	141.73	19.73	3.09	0.081
Right-LP	117.41	24.75	134.81	20.77	2.63	0.107
Ventral						
Left-VA	404.61	68.30	449.40	61.21	2.44	0.121
Right-VA	377.08	60.65	421.18	54.23	1.97	0.162
Left-VAmc	31.89	5.93	36.36	4.83	5.05	0.026*
Right-VAmc	32.16	5.73	36.01	4.67	1.40	0.238
Left-VLa	636.55	103.85	701.07	90.93	3.37	0.069
Right-VLa	612.95	96.15	672.73	88.98	1.34	0.248
Left-VLp	835.66	126.17	922.67	112.70	4.66	0.033*
Right-VLp	799.73	118.25	882.43	111.00	2.04	0.155
Left-VPL	892.78	142.20	984.15	137.13	4.51	0.035*
Right-VPL	844.68	127.75	935.08	127.83	2.55	0.112
Left-VM	23.57	3.93	26.51	3.93	5.49	0.020*
Right-VM	22.71	3.71	25.01	3.55	1.19	0.278
Intralaminar						
Left-CeM	66.41	13.52	73.25	12.26	1.34	0.249
Right-CeM	70.38	14.87	75.53	11.52	0.32	0.572
Left-CL	38.84	8.04	45.76	9.20	4.84	0.029*
Right-CL	40.96	9.48	46.35	10.92	0.85	0.359
Left-Pc	3.54	0.61	4.07	0.57	6.20	0.014*
Right-Pc	3.84	0.69	4.47	0.63	4.69	0.032*
Left-CM	250.08	44.34	279.85	40.62	4.31	0.040*
Right-CM	241.02	39.88	264.69	41.00	1.19	0.276
Left-Pf	59.70	11.09	67.40	10.21	3.18	0.077
Right-Pf	61.66	12.35	67.57	13.85	0.95	0.332
Medial						
Left-Pt	7.44	1.13	8.13	1.16	4.88	0.029*
Right-Pt	7.35	1.13	8.08	1.05	2.34	0.128
Left-MV-re	11.64	3.30	13.77	3.24	1.28	0.260
Right-Mv-re	11.92	3.71	13.79	3.40	0.14	0.706
Left-MDm	678.72	153.81	828.76	119.61	6.39	0.013*
Right-MDm	683.59	130.05	814.32	129.87	4.09	0.045*
Left-MDI	242.05	48.06	292.95	45.27	6.48	0.012*
Right-MDI	247.92	50.93	291.45	52.47	1.81	0.181

(Continued)

TABLE 2 (Continued)

Thalamic nucleus	Patients with MDD (<i>n</i> = 76)		Healthy controls (<i>n</i> = 76)		<i>F</i>	<i>p</i> -value
	Mean, mm ³	SD, mm ³	Mean, mm ³	SD, mm ³		
Posterior						
Left-LGN	275.52	55.69	313.47	55.25	5.09	0.026*
Right-LGN	267.60	59.66	304.56	53.34	2.29	0.132
Left-MGN	118.09	22.45	126.93	21.94	0.00	0.989
Right-MGN	120.01	25.67	128.33	23.17	0.04	0.841
Left-L-Sg	24.70	7.74	28.56	7.36	0.10	0.749
Right-L-Sg	19.76	7.44	23.17	8.03	1.24	0.267
Left-PuA	184.25	32.09	215.47	34.22	5.57	0.020*
Right-PuA	200.68	29.13	218.36	24.58	0.11	0.739
Left-PuM	939.24	169.40	1087.96	195.19	3.52	0.062
Right-PuM	1062.58	156.02	1135.65	146.29	0.00	0.947
Left-PuL	192.74	38.20	213.04	45.61	4.28	0.040*
Right-PuL	219.68	46.29	215.71	49.36	0.13	0.717
Left-PuI	221.10	46.93	248.66	53.71	2.20	0.140
Right-PuI	254.70	49.88	259.09	53.25	0.03	0.873

AV, anteroventral; LD, laterodorsal; LP, lateral posterior; VA, ventral anterior; VAmc, ventral anterior magnocellular; VLa, ventral lateral anterior; VLp, ventral lateral posterior; VPL, ventral posterolateral; VM, ventromedial; CeM, central medial; CL, central lateral; Pc, paracentral; CM, centromedian; Pf, parafascicular; Pt, paratenial; MV-re, medial ventral reunions; MDm, mediodorsal medial magnocellular; MDI, mediodorsal lateral parvocellular; LGN, lateral geniculate; MGN, medial geniculate; L-Sg, limitans supragenulate; PuA, pulvinar anterior; PuM, pulvinar medial; PuL, pulvinar lateral; PuI, pulvinar inferior. The *F* and *p*-values were obtained using a one-way analysis of covariance (ANCOVA) adjusted for age, sex, and estimated total intracranial cavity volume (ETICV) as covariates. The Bonferroni's correction was applied, **p* < 0.05.

between the two groups of patients with MDD and HCs; in contrast, the left thalamus was significantly different ($p < 0.003$). Regarding individual nuclei, significant differences were detected in 16 nuclei belonging to five regions, including the lateral, ventral, intralaminar, medial, and posterior regions, in which we found volume reductions in patients with MDD. Intergroup volumetric changes showing significance are summarized in Figures 2, 3. We found a significant bilateral volumetric decrease in the Pc nuclei of the intralaminar regions (L: $p = 0.01$; R: $p = 0.03$) and MDm nuclei of the medial regions (L: $p = 0.01$; R: $p = 0.05$). We also observed significant volumetric reductions in several nuclei of the left thalamus. Specifically, Left-LD ($p < 0.001$) in the lateral region, left VAmc ($p = 0.03$), left VLp ($p = 0.03$), left VPL ($p = 0.04$), and left VM ($p = 0.02$) in the ventral region, left CL ($p = 0.03$), left CM ($p = 0.04$) in the intralaminar region, left Pt ($p = 0.03$), and left MDI ($p = 0.01$) in the medial region. Last of all, left-LGN ($p = 0.03$), left-PuA ($p = 0.02$), and left-PuL ($p = 0.04$) in the posterior region.

3.3. Correlation analysis

The results of partial correlation analyses between affected nuclei volume and depression severity, as assessed by the HAMD-17 score, are shown in Figure 4. We found that the HAMD-17 total score was negatively correlated with the volume of the left thalamus ($r = -0.232$, $p = 0.05$), VAmc (L: $r = -0.262$, $p = 0.03$), and PuA ($r = -0.241$, $p = 0.04$) in the left thalamus, and Pc ($r = -0.293$, $p = 0.01$) in the right thalamus. Moreover, we assessed the relationship between affected nuclei and HAMD-17 subscale scores. Only three nuclei showed a negative correlation. The right

Pc was correlated with the core score ($r = -0.267$, $p = 0.02$), and the left-PuA was associated with the core ($r = -0.243$, $p = 0.04$) and activity scores ($r = -0.247$, $p = 0.04$). Interestingly, only the right-MDm was negatively correlated with core ($r = -0.270$, $p = 0.02$), sleep ($r = -0.274$, $p = 0.02$), activity ($r = -0.309$, $p = 0.01$), and anxiety ($r = -0.306$, $p = 0.01$) scores.

4. Discussion

In the present study, volumetric changes in various nuclei in six different regions of the bilateral thalami were investigated in medication-free, first-episode MDD patients relative to HCs. We observed significant volume reductions in the left thalamus and several thalamic nuclei, mainly on the left side, in the MDD group. Furthermore, we revealed weak negative correlations between several thalamic nuclei volumes and the HAMD-17 total and subscale scores.

As emerging perspectives on the thalamus and its role in the neuropathology of depression, several studies have investigated thalamic volume in patients with MDD. Following the earliest study that reported significant bilateral thalamic volume reduction in female subjects diagnosed with MDD (10), assorted studies have confirmed this result in different subjects with MDD (11–14, 19), including older adults (10, 14), patients with mild symptoms (13), and drug naïve MDD patients (19). In this study, we found thalamic volume contraction only on the left side, which is consistent with some volumetric studies in recent years (15, 16). However, these studies have several limitations compared to our research. They analyzed the thalamus as a whole or segmented it into

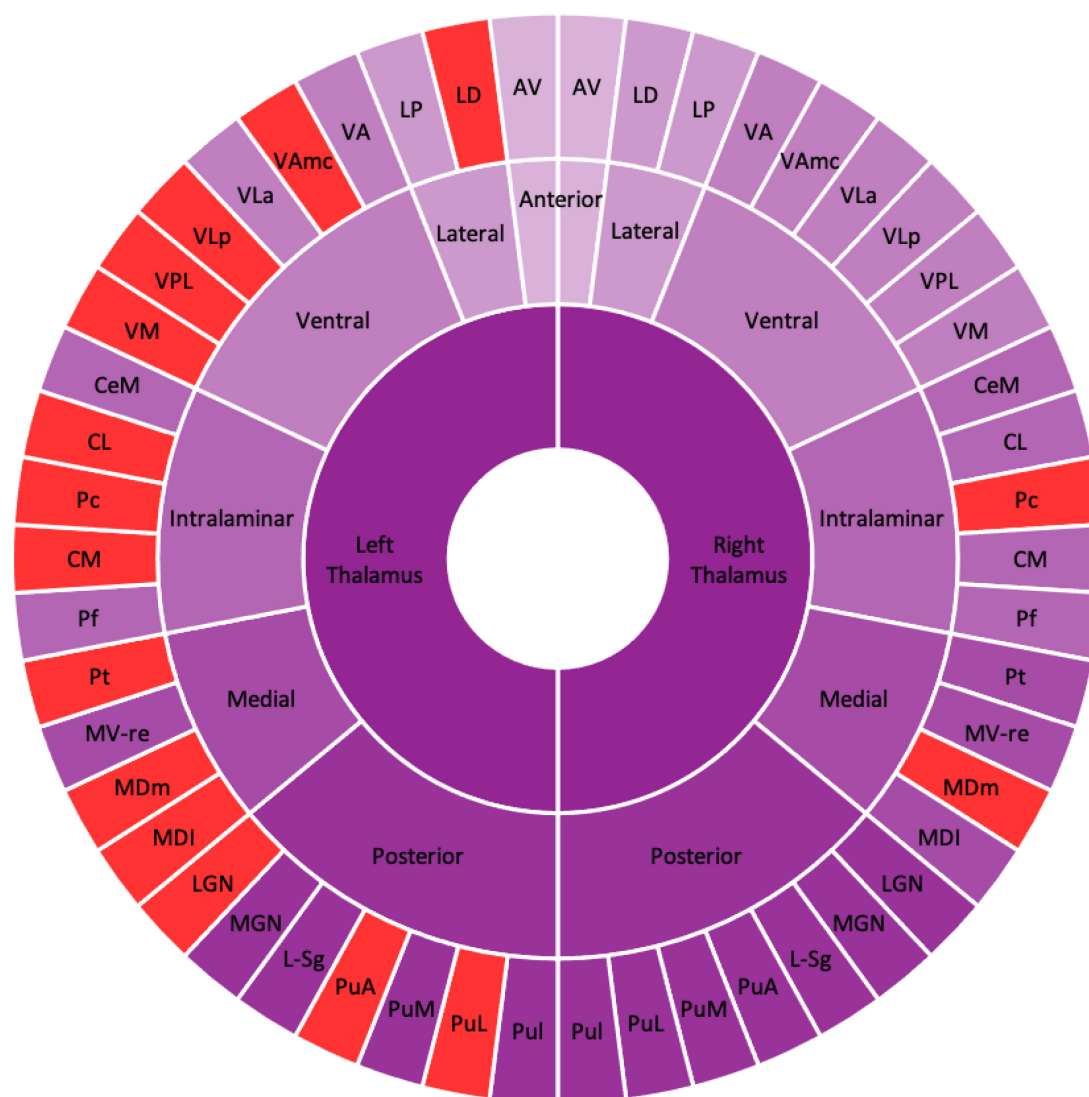


FIGURE 2

Schematic figure of the altered thalamic nuclei. Schematic illustration of altered thalamic nuclei. The nuclei in the red represent the significant volume alteration in patients with MDD as compared with HCs. The figure shows the left thalamic nuclei are significantly reduced compared with the right thalamic nuclei. AV, anteroventral; LD, laterodorsal; LP, lateral posterior; VA, ventral anterior; VAmc, ventral anterior magnocellular; VLa, ventral lateral anterior; VLp, ventral lateral posterior; VPL, ventral posterolateral; VM, ventromedial; CeM, central medial; CL, central lateral; Pc, paracentral; CM, centromedian; Pf, parafascicular; Pt, paratenial; MV-re, medial ventral reunions; MDm, mediodorsal medial magnocellular; MDI, mediodorsal lateral parvocellular; LGN, lateral geniculate; MGN, medial geniculate; L-Sg, limitans suprageniculate; PuA, pulvinar anterior; PuM, pulvinar medial; PuL, pulvinar lateral; PuI, pulvinar inferior.

subregions while we investigated the alterations of 25 individual thalamic nuclei volumes. Even so, previous meta-analyses that enrolled drug-naïve MDD patients revealed significantly increased gray matter volume in the thalamus (17, 18), contradictory to our findings. All participants with MDD in our study were medication-free, and in their first episode, like those in the meta-analyses, their average age was higher (53.7) compared with MDD patients in the previous studies. Therefore, these opposing results of increased volumetric changes in the thalamus may be specifically related to the patient's age and could reflect early thalamic hyperfunction (14).

According to thalamic nuclei functions, some nuclear groups are known as relay stations. They receive specific and well-defined motor and sensory information inputs and project them to the

brain cortex. Previous functional studies have reported that the lateral and ventral nuclei of the thalamus process motor and somatosensory information and support alertness and arousal in humans (25–27), as well as in rodents (28). The importance of the posterior region, especially the LGN, was also reported in a recent meta-analysis (29). In the present study, we found significant reductions in LD nuclei in the lateral region, VAmc, VLp, VPL, and VM nuclei in the ventral region, and LGN in the posterior region of the left thalamus in patients with MDD compared to HCs. Given that physical pain and psychomotor retardation or agitation often present symptoms of MDD (30, 31), we assumed that contractions in these nuclei could be related to the above-mentioned somatic symptoms. However, further functional and connectivity studies are required to provide further insight.

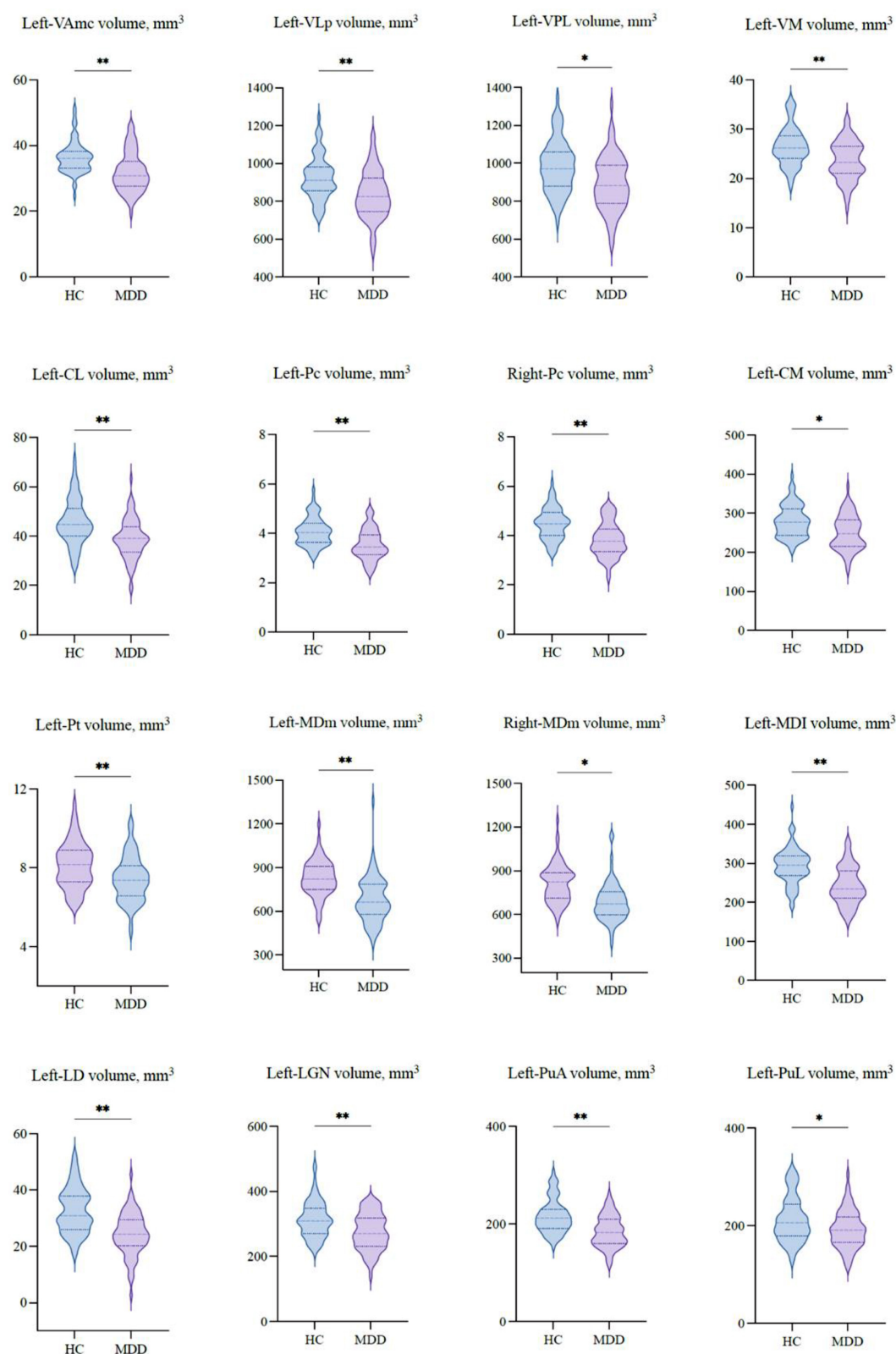


FIGURE 3

The volumetric differences of thalamic nuclei between MDD patients and HCs. Significant volume differences between groups. p -values were obtained using a one-way analysis of covariance (ANCOVA) adjusted for age, sex, and estimated total intracranial cavity volume (ETICV) as covariates. The Bonferroni's correction was applied, $*p < 0.05$ and $**p < 0.03$.

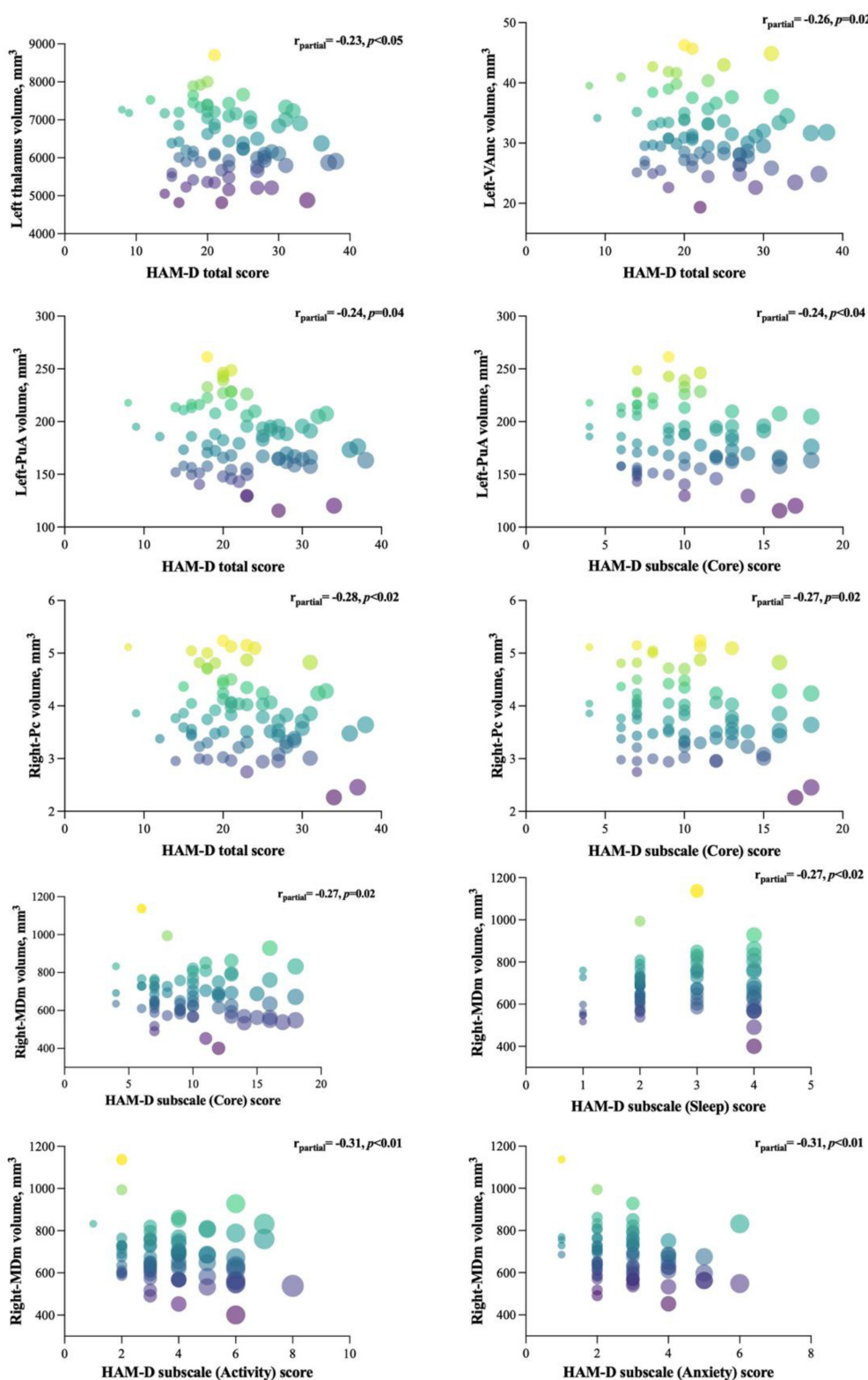


FIGURE 4

Significant correlations between the affected nuclei volume and HAM-D-17 total and subscale scores. The figure represents the correlation between affected nuclei volume and depression severity, as assessed by the HAM-D-17 score.

Intralaminar nuclei, known as “non-specific” nuclei of the thalamus, seem to be broadly connected with the entire cortex and globally activate it (32). In the current study, we found that patients

with MDD had significantly decreased intralaminar nuclei of the CL and CM in the left thalamus and Pc in the bilateral thalamus. However, it is not clear whether volume reductions in these nuclei

play a crucial role in MDD, and the concept that intralaminar nuclei can facilitate some depression symptoms is consistent with the findings of previous studies indicating that lesions to the intralaminar nuclei lead to attention diminishment. For example, Van Der Werf et al. (33) reported that damage to this area elicits complex attention deficits. Furthermore, other findings detailed the contribution of rostral intralaminar nuclei, together with CL, Pc, and CM, to extended cognitive and behavioral functions (34–36). Relating to the major depression symptoms of insufficient concentration and indecisiveness, our results of depletion in rostral intralaminar nuclei, specifically Pc nuclei in the bilateral thalamus in MDD patients, consistently support prior outcomes, such as the influence of cognitive processes (37), impairment of working memory (38), and attentional engagement of sensory events (35). Thus, our findings suggest that alterations in these rostral intralaminar nuclei could be related to depression-related arousal, awareness, and attention deficits in patients with MDD.

Among the thalamus parts that showed differences in patients with MDD, the medial and pulvinar have been the regions of interest because of their significant interconnection with the prefrontal cortex and other subcortical structures. The results of the study of many neuropsychiatric disorders reported changes in these regions of the thalamus, particularly in obsessive-compulsive disorder (OCD) (39, 40), psychosis (41), schizophrenia (42, 43), and Parkinson's disease (44). As for depression, few studies have investigated the structural (19) and functional (45) alterations of medial and pulvinar regions in MDD patients. Although the results of these previous studies were consistent with the outcomes of our research, none of them investigated detailed structural changes in the different nuclei of the thalamus. In particular, the mediodorsal (MD) nuclei and pulvinar nuclei (Pu). MD, one of the largest nuclei of the thalamus, is primarily involved in emotional, cognitive, and behavioral processing and is often impaired in depression (1). We found altered MDm, Pt, and MDI nucleus volumes in the current study. Above all, only the MDm nucleus showed differences on both sides of the thalamus, whereas the remaining two were on the left side. Given that the MD nuclei or its medial part physiologically interact with the prefrontal cortex during cognitive function (46) and emotion regulation (24), our findings suggest that alterations in the MD nuclei could be directly related to emotional and behavioral failure in MDD through involvement in the orbitofrontal circuit. Indeed, we observed volume reductions in the PuA and PuL nuclei of the left thalamus. Pu, the largest nuclear mass, is involved in executive function and emotional processing (47). Moreover, its circuit with the cortex predicts cognition in many psychiatric disorders, including schizophrenia (48) and psychosis (41).

Similarly, it showed a positive response to antidepressant treatment (49, 50). The Pu nuclei also play a role in attention (51), indicating that it could influence the dysfunctional cognition process and abnormal emotional behaviors accompanying MDD; whether the relationship between depression and structural changes in the thalamic nuclei in MDD remains a critical argument that requires further specifically designed approaches.

We also investigated the correlations between the HAMD-17 total and subscale scores and the affected thalamic nuclei volumes in patients with MDD. We found a weak negative correlation between the left thalamus and HAMD-17 total score, which supports previous reports of an association between thalamic volume and depression severity (52). Moreover, in

the left thalamus, VAmc and PuA nuclei were negatively associated with evaluation scores. These findings suggest that the nuclei of the ventral and posterior regions of the thalamus are negatively correlated with depression severity, suggesting their involvement in the anterior cingulate-prefrontal circuit (53). Regarding HAMD-17 subscale scores, the PuA nucleus of the left thalamus and Pc and MDm nuclei of the right thalamus showed a weak negative correlation with the core score, which might suggest their role in the core symptoms of depression, including depressed mood, loss of energy, and difficulty with memory and attention (45). Interestingly, only the right MDm nucleus was negatively correlated with sleep, activity, and anxiety scores. As the MDm nuclei have extensive efferent and afferent connections with the prefrontal cortex, motor cortex, basal ganglia, and amygdala, this result suggests that structural changes in the MDm nuclei may be relevant for explaining MDD symptoms, which are poorly understood (54). In support of this proposal, future studies will benefit from using longitudinal approaches that investigate the functional and structural relationships between specific thalamic nuclei and the clinical symptoms of MDD.

To the best of our knowledge, this is the first MDD study to investigate alterations in the volumes of various thalamic nuclei compared with HCs. Moreover, we first analyzed the association between individual thalamic nuclei volumes and HAMD-17 subscale scores. Nevertheless, this study had several limitations that should be addressed. First, we used a cross-sectional design, which makes it challenging to investigate the causal association between structural changes and clinical features. Second, we enrolled a relatively small sample without age and sex matching, limiting the generalizability of our results. Even though the analysis was statistically adjusted, demographic indicators between the two groups were different. Therefore, to understand the role of different regions of the thalamus in the pathophysiology of depression, longitudinal studies with larger age- and gender-matched sample sizes are required. Third, we did not investigate detailed clinical data, including handedness, educational year, age of onset, and duration of illness, which might have influenced the volumetric changes we reported. Finally, the present volumetric study did not point to functional abnormalities or neuronal plasticity associated with depression; thus, additional work is required to elucidate alternative explanations for the connections between structural and functional pathology and depressive symptoms.

5. Conclusion

In summary, our findings showed a reduction in the volume of the left thalamus in medication-free patients with MDD. The volumetric data of specific thalamic nuclei also showed alterations, mainly on the left side. In addition, our results also highlight the relationship between thalamic nuclei volume and the severity of clinical symptoms, suggesting an association between volumetric alteration of various nuclei in the thalamus relevant to the clinical outcome of depression. Although these findings may be restricted to certain levels, they may contribute to understanding brain structural changes in MDD and highlight the need for further investigation.

Data availability statement

The raw data supporting the conclusions of this article will be made available by the authors, without undue reservation.

Ethics statement

The studies involving human participants were reviewed and approved by the Ethics Committee of the University of Occupational and Environmental Health, Japan. The patients/participants provided their written informed consent to participate in this study.

Author contributions

EC, KW, SK, and RY: study conception and design. KW, NOk, TN, GH, AI, SK, and RY: data collection. EC, KW, and NOr: analysis and interpretation of results. EC: draft manuscript

preparation. All authors reviewed the results and approved the final version of the manuscript.

Conflict of interest

The authors declare that the research was conducted in the absence of any commercial or financial relationships that could be construed as a potential conflict of interest.

Publisher's note

All claims expressed in this article are solely those of the authors and do not necessarily represent those of their affiliated organizations, or those of the publisher, the editors and the reviewers. Any product that may be evaluated in this article, or claim that may be made by its manufacturer, is not guaranteed or endorsed by the publisher.

References

- Malhi G, Mann J. Depression. *Lancet*. (2018) 392:2299–312. doi: 10.1016/S0140-6736(18)31948-2
- Otte C, Gold S, Penninx B, Pariante C, Etkin A, Fava M, et al. Major depressive disorder. *Nat Rev Dis Primers*. (2016) 2:16065. doi: 10.1038/nrdp.2016.65
- Peters S, Dunlop K, Downar J. Cortico-striatal-thalamic loop circuits of the salience network: a central pathway in psychiatric disease and treatment. *Front Syst Neurosci*. (2016) 10:104. doi: 10.3389/fnsys.2016.00104
- Zhang F, Peng W, Sweeney J, Jia Z, Gong Q. Brain structure alterations in depression: psychoradiological evidence. *CNS Neurosci Ther*. (2018) 24:994–1003. doi: 10.1111/cns.12835
- Zacková L, Jáni M, Brázdil M, Nikolova Y, Marešková K. Cognitive impairment and depression: meta-analysis of structural magnetic resonance imaging studies. *Neuroimage Clin*. (2021) 32:102830. doi: 10.1016/j.nicl.2021.102830
- Yang C, Xiao K, Ao Y, Cui Q, Jing X, Wang Y. The thalamus is the causal hub of intervention in patients with major depressive disorder: evidence from the Granger causality analysis. *NeuroImage Clin*. (2022) 37:103295. doi: 10.1016/j.nicl.2022.103295
- Sherman S. The thalamus is more than just a relay. *Curr Opin Neurobiol*. (2007) 17:417–22. doi: 10.1016/j.conb.2007.07.003
- Phillips J, Kambi N, Redinbaugh M, Mohanta S, Saalman Y. Disentangling the influences of multiple thalamic nuclei on prefrontal cortex and cognitive control. *Neurosci Biobehav Rev*. (2021) 128:487–510. doi: 10.1016/j.neubiorev.2021.06.042
- Roy D, Zhang Y, Halassa M, Feng G. Thalamic subnetworks as units of function. *Nat Neurosci*. (2022) 25:140–53. doi: 10.1038/s41593-021-00996-1
- Kim MJ, Hamilton JP, Gotlib IH. Reduced caudate gray matter volume in women with major depressive disorder. *Psychiatry Res*. (2008) 164:114–22. doi: 10.1016/j.psychres.2007.12.020
- Bora E, Harrison B, Davey C, Yücel M, Pantelis C. Meta-analysis of volumetric abnormalities in cortico-striatal-pallidal-thalamic circuits in major depressive disorder. *Psychol Med*. (2012) 42:671–81. doi: 10.1017/S0033291711001668
- Nugent A, Davis R, Zarate C, Drevets W. Reduced thalamic volumes in major depressive disorder. *Psychiatry Res*. (2013) 213:179–85. doi: 10.1016/j.psychres.2013.05.004
- Webb C, Weber M, Mundy E, Killgore W. Reduced gray matter volume in the anterior cingulate, orbitofrontal cortex and thalamus as a function of mild depressive symptoms: a voxel-based morphometric analysis. *Psychol Med*. (2014) 44:2833–43. doi: 10.1017/S0033291714000348
- Ancelin M, Carrière I, Artero S, Maller J, Meslin C, Ritchie K, et al. Lifetime major depression and grey-matter volume. *J Psychiatry Neurosci*. (2019) 44:45–53. doi: 10.1503/jpn.180026
- Du M, Wu Q, Yue Q, Li J, Liao Y, Kuang W, et al. Voxelwise meta-analysis of gray matter reduction in major depressive disorder. *Prog Neuropsychopharmacol Biol Psychiatry*. (2012) 36:11–6. doi: 10.1016/j.pnpbp.2011.09.014
- Lu Y, Liang H, Han D, Mo Y, Li Z, Cheng Y, et al. The volumetric and shape changes of the putamen and thalamus in first episode, untreated major depressive disorder. *NeuroImage Clin*. (2016) 11:658–66. doi: 10.1016/j.nicl.2016.04.008
- Zhao Y, Du M, Huang X, Lui S, Chen Z, Liu J, et al. Brain grey matter abnormalities in medication-free patients with major depressive disorder: a meta-analysis. *Psychol Med*. (2014) 44:2927–37. doi: 10.1017/S0033291714000518
- Peng W, Chen Z, Yin L, Jia Z, Gong Q. Essential brain structural alterations in major depressive disorder: a voxel-wise meta-analysis on first episode, medication-naïve patients. *J Affect Disord*. (2016) 199:114–23. doi: 10.1016/j.jad.2016.04.001
- Choi K, Han K, Kim H, Kim A, Kang W, Kang Y, et al. Comparison of shape alterations of the thalamus and caudate nucleus between drug-naïve major depressive disorder patients and healthy controls. *J Affect Disord*. (2020) 264:279–85. doi: 10.1016/j.jad.2020.01.011
- Iglesias J, Insausti R, Lerma-Usabiaga G, Bocchetta M, Van Leemput K, Greve D, et al. A probabilistic atlas of the human thalamic nuclei combining ex vivo MRI and histology. *NeuroImage*. (2018) 183:314–26. doi: 10.1016/j.neuroimage.2018.08.012
- Igata N, Kakeda S, Watanabe K, Ide S, Kishi T, Abe O, et al. Voxel-based morphometric brain comparison between healthy subjects and major depressive disorder patients in Japanese with the s/s genotype of 5-HTTLPR. *Sci Rep*. (2017) 7:3931. doi: 10.1038/s41598-017-04347-8
- Tesen H, Watanabe K, Okamoto N, Ikenouchi A, Igata R, Konishi Y, et al. Volume of amygdala subregions and clinical manifestations in patients with first-episode, drug-naïve major depression. *Front Hum Neurosci*. (2021) 15:780884. doi: 10.3389/fnhum.2021.780884
- Jovicich J, Czanner S, Greve D, Haley E, Van Der Kouwe A, Gollub R, et al. Reliability in multi-site structural MRI studies: effects of gradient non-linearity correction on phantom and human data. *NeuroImage*. (2006) 30:436–43. doi: 10.1016/j.neuroimage.2005.09.046
- Fischl B. FreeSurfer. *NeuroImage*. (2012) 62:774–81. doi: 10.1016/j.neuroimage.2012.01.021
- Johansen-Berg H, Behrens T, Sillery E, Ciccarelli O, Thompson A, Smith S, et al. Functional-anatomical validation and individual variation of diffusion tractography-based segmentation of the human thalamus. *Cereb Cortex*. (2005) 15:31–9. doi: 10.1093/cercor/bhh105
- Kumar V, van Oort E, Scheffler K, Beckmann C, Grodd W. Functional anatomy of the human thalamus at rest. *NeuroImage*. (2017) 147:678–91. doi: 10.1016/j.neuroimage.2016.12.071

27. Honnorat N, Saranathan M, Sullivan E, Pfefferbaum A, Pohl K, Zahr N. Performance ramifications of abnormal functional connectivity of ventral posterior lateral thalamus with cerebellum in abstinent individuals with alcohol use disorder. *Drug Alcohol Depend.* (2021) 220:108509. doi: 10.1016/j.drugalcdep.2021.108509
28. Tlamsa A, Brumberg J. Organization and morphology of thalamocortical neurons of mouse ventral lateral thalamus. *Somatosens Mot Res.* (2010) 27:34–43. doi: 10.3109/08990221003646736
29. Wu W, Howard D, Sibille E, French L. Differential and spatial expression meta-analysis of genes identified in genome-wide association studies of depression. *Transl Psychiatry.* (2021) 11:8. doi: 10.1038/s41398-020-01127-3
30. Sobin C, Sackeim H. Psychomotor symptoms of depression. *Am J Psychiatry.* (1997) 154:4–17. doi: 10.1176/ajp.154.1.4
31. Trivedi M. The link between depression and physical symptoms. *Prim Care Companion J Clin Psychiatry.* (2004) 6:12–6.
32. Groenewegen H, Berendse H. The Specificity of the 'nonspecific' Midline and intralaminar thalamic Nuclei. *Trends Neurosci.* (1994) 17:52–7. doi: 10.1016/0166-2236(94)90074-4
33. Van Der Werf Y, Scheltens P, Lindeboom J, Witter M, Uylings H, Jolles J. Deficits of memory, executive functioning and attention following infarction in the thalamus; a study of 22 cases with localised lesions. *Neuropsychologia.* (2003) 41:1330–44. doi: 10.1016/S0028-3932(03)00059-9
34. Schiff N. Central thalamic contributions to arousal regulation and neurological disorders of consciousness. *In Ann N Y Acad Sci.* (2008) 1129:105–18. doi: 10.1196/annals.1417.029
35. Schiff N, Shah S, Hudson A, Nauvel T, Kalik S, Purpura K. Gating of attentional effort through the central thalamus. *J Neurophysiol.* (2013) 109:1152–63. doi: 10.1152/jn.00317.2011
36. Cover K, Mathur B. Rostral intralaminar thalamus engagement in cognition and behavior. *Front Behav Neurosci.* (2021) 15:652764. doi: 10.3389/fnbeh.2021.652764
37. Vertes R, Linley S, Hoover W. Limbic circuitry of the midline thalamus. *Neurosci Biobehav Rev.* (2015) 54:89–107. doi: 10.1016/j.neubiorev.2015.01.014
38. Mair R, Hembrook J. Memory enhancement with event-related stimulation of the rostral intralaminar thalamic nuclei. *J Neurosci.* (2008) 28:14293–300. doi: 10.1523/JNEUROSCI.3301-08.2008
39. Jung J, Park H, Kim T, Park I, Moon S, Lho S, et al. Smaller volume of posterior thalamic nuclei in patients with obsessive-compulsive disorder. *NeuroImage Clin.* (2021) 30:102686. doi: 10.1016/j.nicl.2021.102686
40. Weeland C, Vriend C, van der Werf Y, Huyser C, Hillegers M, Tiemeier H, et al. Thalamic subregions and obsessive-compulsive symptoms in 2,500 children from the general population. *J Am Acad Child Adolesc Psychiatry.* (2022) 61:321–30. doi: 10.1016/j.jaac.2021.05.024
41. Huang A, Rogers B, Sheffield J, Jalbrzikowski M, Anticevic A, Blackford J, et al. Thalamic nuclei volumes in psychotic disorders and in youths with psychosis spectrum symptoms. *Am J Psychiatry.* (2020) 177:1159–67. doi: 10.1176/appi.ajp.2020.19101099
42. Takahashi T, Tsugawa S, Nakajima S, Plitman E, Chakravarty M, Masuda F, et al. Thalamic and striato-pallidal volumes in schizophrenia patients and individuals at risk for psychosis: a multi-atlas segmentation study. *Schizophr Res.* (2022) 243:268–75. doi: 10.1016/j.schres.2020.04.016
43. Perez-Rando M, Elvira UKA, García-Martí G, Gadea M, Aguilar EJ, Escarti MJ, et al. Alterations in the volume of thalamic nuclei in patients with schizophrenia and persistent auditory hallucinations. *NeuroImage Clin.* (2022) 35:103070. doi: 10.1016/j.nicl.2022.103070
44. Bhome R, Zarkali A, Thomas G, Iglesias J, Cole J, Weil R. Thalamic white matter macrostructure and subnuclei volumes in Parkinson's disease depression. *NPJ Parkinsons Dis.* (2022) 8:2. doi: 10.1038/s41531-021-00270-y
45. Kang L, Zhang A, Sun N, Liu P, Yang C, Li G, et al. Functional connectivity between the thalamus and the primary somatosensory cortex in major depressive disorder: a resting-state fMRI study. *BMC Psychiatry.* (2018) 18:339. doi: 10.1186/s12888-018-1913-6
46. Ouhas Z, Fleming H, Mitchell A. Cognitive functions and neurodevelopmental disorders involving the prefrontal cortex and mediodorsal thalamus. *Front Neurosci.* (2018) 12:33. doi: 10.3389/fnins.2018.00033
47. Hakamata Y, Sato E, Komi S, Moriguchi Y, Izawa S, Murayama N, et al. The functional activity and effective connectivity of pulvinar are modulated by individual differences in threat-related attentional bias. *Sci Rep.* (2016) 6:34777. doi: 10.1038/srep34777
48. Mitelman S, Byne W, Kemether E, Hazlett E, Buchsbaum M. Correlations between volumes of the pulvinar, centromedian, and mediodorsal nuclei and cortical Brodmann's areas in schizophrenia. *Neurosci Lett.* (2006) 392:16–21. doi: 10.1016/j.neulet.2005.08.056
49. Tadayonnejad R, Ajilore O, Mickey B, Crane N, Hsu D, Kumar A, et al. Pharmacological modulation of pulvinar resting-state regional oscillations and network dynamics in major depression. *Psychiatry Res Neuroimaging.* (2016) 252:10–8. doi: 10.1016/j.pscychresns.2016.04.013
50. Kraus C, Klöbl M, Tik M, Auer B, Vanicek T, Geissberger N, et al. The pulvinar nucleus and antidepressant treatment: dynamic modeling of antidepressant response and remission with ultra-high field functional MRI. *Mol Psychiatry.* (2019) 24:746–56. doi: 10.1038/s41380-017-0009-x
51. Saalman Y, Pinski M, Wang L, Li X, Kastner S. The pulvinar regulates information transmission between cortical areas based on attention demands. *Science.* (2012) 337:753–6. doi: 10.1126/science.1223082
52. Li H, Song S, Wang D, Tan Z, Lian Z, Wang Y, et al. Individualized diagnosis of major depressive disorder via multivariate pattern analysis of thalamic SMRI features. *BMC Psychiatry.* (2021) 21:415. doi: 10.1186/s12888-021-03414-9
53. Haber S, Calzavara R. The cortico-basal ganglia integrative network: the role of the thalamus. *Brain Res Bull.* (2009) 78:69–74. doi: 10.1016/j.brainresbull.2008.09.013
54. Grill W. Exploring the thalamus and its role in cortical function. 2nd ed. In: Sherman S, Guillery R III editors. *Index.* Cambridge, MA: MIT Press (2007). XXIII+484 p. doi: 10.1086/519647



OPEN ACCESS

EDITED BY

Reiji Yoshimura,
University of Occupational and Environmental
Health, Japan

REVIEWED BY

Jessica R. Gilbert,
National Institute of Mental Health (NIH),
United States
Pengfei Xu,
Beijing Normal University, China

*CORRESPONDENCE

Wen-hui Jiang
✉ jwh_0303@163.com
Jian-yin Qiu
✉ jianyin_qiu@163.com

†These authors share first authorship

SPECIALTY SECTION

This article was submitted to
Mood Disorders,
a section of the journal
Frontiers in Psychiatry

RECEIVED 24 December 2022

ACCEPTED 27 March 2023

PUBLISHED 11 April 2023

CITATION

Yao J-y, Zheng Z-w, Zhang Y, Su S-s, Wang Y,
Tao J, Peng Y-h, Wu Y-r, Jiang W-h and
Qiu J-y (2023) Electrophysiological evidence
for the characteristics of implicit self-schema
and other-schema in patients with major
depressive disorder: An event-related
potential study.
Front. Psychiatry 14:1131275.
doi: 10.3389/fpsyt.2023.1131275

COPYRIGHT

© 2023 Yao, Zheng, Zhang, Su, Wang, Tao,
Peng, Wu, Jiang and Qiu. This is an
open-access article distributed under the terms
of the [Creative Commons Attribution License](https://creativecommons.org/licenses/by/4.0/)
(CC BY). The use, distribution or reproduction
in other forums is permitted, provided the
original author(s) and the copyright owner(s)
are credited and that the original publication in
this journal is cited, in accordance with
accepted academic practice. No use,
distribution or reproduction is permitted which
does not comply with these terms.

Electrophysiological evidence for the characteristics of implicit self-schema and other-schema in patients with major depressive disorder: An event-related potential study

Jia-yu Yao[†], Zi-wei Zheng[†], Yi Zhang, Shan-shan Su,
Yuan Wang, Jing Tao, Yi-hua Peng, Yan-ru Wu, Wen-hui Jiang*
and Jian-yin Qiu*

Shanghai Mental Health Center, Shanghai Jiao Tong University School of Medicine, Shanghai, China

Background: The significance of implicit self-schema and other-schema in major depressive disorder (MDD) is highlighted by both cognitive theory and attachment theory. The purpose of the current study was to investigate the behavioral and event-related potential (ERP) characteristics of implicit schemas in MDD patients.

Methods: The current study recruited 40 patients with MDD and 33 healthy controls (HCs). The participants were screened for mental disorders using the Mini-International Neuropsychiatric Interview. Hamilton Depression Rating Scale-17 and Hamilton Anxiety Rating Scale-14 were employed to assess the clinical symptoms. Extrinsic Affective Simon Task (EAST) was conducted to measure the characteristics of implicit schemas. Meanwhile, reaction time and electroencephalogram data were recorded.

Results: Behavioral indexes showed that HCs responded faster to positive self and positive others than negative self ($t = -3.304, p = 0.002$, Cohen's $d = 0.575$) and negative others ($t = -3.155, p = 0.003$, Cohen's $d = 0.549$), respectively. However, MDD did not show this pattern ($p > 0.05$). The difference in other-EAST effect between HCs and MDD was significant ($t = 2.937, p = 0.004$, Cohen's $d = 0.691$). The ERP indicators of self-schema showed that under the condition of positive self, the mean amplitude of LPP in MDD was significantly smaller than that in HCs ($t = -2.180, p = 0.034$, Cohen's $d = 0.902$). The ERP indexes of other-schema showed that HCs had a larger absolute value of N200 peak amplitude for negative others ($t = 2.950, p = 0.005$, Cohen's $d = 0.584$) and a larger P300 peak amplitude for positive others ($t = 2.185, p = 0.033$, Cohen's $d = 0.433$). The above patterns were not shown in MDD ($p > 0.05$). The comparison between groups found that under the condition of negative others, the absolute value of N200 peak amplitude in HCs was larger than that in MDD ($t = 2.833, p = 0.006$, Cohen's $d = 1.404$); under the condition of positive others, the P300 peak amplitude ($t = -2.906, p = 0.005$, Cohen's $d = 1.602$) and LPP amplitude ($t = -2.367, p = 0.022$, Cohen's $d = 1.100$) in MDD were smaller than that in HCs.

Conclusion: Patients with MDD lack positive self-schema and positive other-schema. Implicit other-schema might be related to abnormalities in both the early

automatic processing stage and the late elaborate processing stage, while the implicit self-schema might be related only to the abnormality in the late elaborate processing stage.

KEYWORDS

major depressive disorder (MDD), implicit schemas, self-schema, other-schema, event-related potential

1. Introduction

Major depressive disorder (MDD), a common mood disorder with approximately 350 million patients worldwide (1), has become an important global public health problem with high incidence, relapse, and suicide rates. Symptoms such as self-denial, self-deprecation, interpersonal avoidance, and high interpersonal sensitivity are key features in depression (2).

The abnormalities of implicit schemas are considered by cognitive theory and attachment theory to be the core issues of MDD. Schemas refer to the internal cognitive structure based on which individuals select, process, and organize information. Schemas are usually implicit and are activated in response to stressful events, especially interpersonal ones (3). According to Beck (4), MDD patients are characterized by negative views of self, others, and the world. Among them, the views of self-include representations and beliefs about the past, present, and future associated with oneself, i.e., self-schema, also known as self-representation. The belief about others is other-schema, also known as other-representation. Bowlby's attachment theory emphasizes that in MDD patients, the other-schema that plays a central role is the representation of those with whom the individual has intimate relationships, such as parents and partners (5).

Most previous studies explored the characteristic of explicit self-schema in MDD through Self-Referential Encoding Task (SRET). They found that MDD patients perceived negative words as more appropriate for describing themselves, whereas healthy controls (HCs) perceived the opposite (6–8). However, since SRET asks subjects to judge whether the adjectives presented describe themselves, it is vulnerable to expectancy effects. Furthermore, because the explicit and implicit self-schemas are incongruent in MDD patients (9), some studies have investigated the implicit self-schema through Implicit Association Test (IAT) and Go/No-go Association Task (GNAT) with reaction time (RT) as the main behavioral index. Nevertheless, the findings remain controversial. For example, both Risch et al. (10) and Romero et al. (11) found that MDD had a more negative implicit self-schema than HCs, while others found different results (12–15). Moreover, only a few researchers have investigated the other-schema in MDD patients. However, both cognitive theory and attachment theory emphasize the significance of both self-schema and other-schema in MDD, especially the other-schema toward parents and partners, making it essential to explore the characteristic of the other-schema in this population. To the best of our knowledge, only the study conducted by Yao et al. (16) revealed the presence of positive self-schema and other-schema in HCs, while MDD patients lacked positive self-schema and had negative other-schema of parents and partners.

In their study, External Affect Simon Task (EAST) was conducted, which offered an advantage over other paradigms since it can simultaneously measure both self-schema and other-schema (17). However, they did not explore the detailed cognitive processes since only RT was analyzed.

Event-Related Potential (ERP) has a higher temporal resolution than behavioral indexes, allowing for a more detailed exploration of cognitive processes. N200, P300, and late positive potential (LPP) are ERP components associated with neural activity patterns of implicit schemas, though the findings varied widely. N200 is a negative wave with a frontal scalp distribution that peaks around 250–350 ms after stimulus onset (18) and is associated with conflict monitoring and response inhibition (19). A study by Wu et al. (20) on healthy college students suggested that when negative words were paired with self-words, subjects showed a greater absolute value of N200 peak, suggesting that the pairing of negative words and self-words was inconsistent with subjects' implicit attitudes, i.e., the presence of a positive self-schema in HCs. However, similar results were not found in another study (21). P300 is a positive wave that peaks around 300–400 ms after stimulus onset over parietal sites and is related to the allocation of attention and cognitive resources (19). Some studies consider LPP and P300 as the same component, thus referring to the wave appearing at 300–400 ms or before 600 ms as early LPP (15, 22), and the wave appearing after 600 ms over the centro-parietal scalp as late LPP (15, 19, 23). Late LPP is related to the degree of arousal and delicate processing of stimuli (8, 24). Both Auerbach et al. (6) and Dainer-Best et al. (25) combined P300, LPP and SRET, but found different results. The former study found that MDD showed greater P300 and LPP amplitudes in the negative self condition, while HCs showed the opposite pattern (6). This suggested that MDD patients not only assigned more attention to the negative self, but also processed the negative self in more detail. However, in the study by Dainer-Best et al. (25), no significant results for LPP amplitudes were found. Notably, Auerbach et al.'s (6) study only included female adolescent MDD patients, and MDD sample in Dainer-Best et al.'s (25) study was not clinically diagnosed, but assessed only by telephone interview. Additionally, Grundy et al. (26) found that subjects with low self-esteem had a greater P300 amplitude in the positive self condition. Given that MDD patients is often accompanied by low self-esteem, further clarification of the neural activity pattern of the self-schema is needed. Furthermore, although several studies have involved the neural activity of other-schema, they have focused on HCs and have not yielded consistent conclusions. For example, Chen et al. (27) found that HCs had a greater P300 amplitude in the positive others condition than in the negative others condition, whereas Wu et al. (20) found the opposite results.

Therefore, the current study aimed to explore the neural activity patterns of both implicit self-schema and other-schema in MDD by combining EAST and ERP. For behavioral indexes, it was hypothesized that HCs responded to positive self-words and positive other-words more quickly. For ERP components, we hypothesized that in HCs, the absolute value of N200 peak amplitude was greater in the negative self condition and negative others condition, whereas the P300 amplitudes and the LPP amplitudes were greater in the negative self and negative others condition. However, MDD would show reduced or reversed patterns compared to HCs.

2. Materials and methods

2.1. Participants

All subjects with MDD were recruited from outpatients of Shanghai Mental Health Center from September 2021 to October 2022. All enrolled patients were evaluated with the following inclusion and exclusion criteria. (1) Inclusion criteria: (a) meeting the diagnosis of MDD in the Diagnostic and Statistical Manual of Mental Disorders (DSM), Fifth Edition; (b) currently in a depressive episode; (c) scoring ≥ 17 on the 17-item Hamilton Depression Rating Scale (HAMD-17) and scoring ≤ 21 on the 14-item Hamilton Anxiety Rating Scale (HAMA-14); (d) meeting the diagnosis of depression in the Mini-International Neuropsychiatric Interview (MINI) and without any psychotic symptoms; (e) at least a junior high school education level; (f) 18–55 years old; (g) not receiving medication and systematic psychotherapy in the last 6 months; (h) with sufficient audiovisual level to complete the study. (2) Exclusion criteria: (a) currently presence of serious physical disease; (b) history of brain injury; (c) meeting the diagnosis of other mental disorders in MINI; (d) presence of serious suicide attempts; (e) inability to complete the study due to other problems such as mental retardation.

All HCs were age-matched and gender-matched adults recruited from the community through advertisement from May 2022 to August 2022. All enrolled HCs were evaluated with the following inclusion and exclusion criteria. (1) Inclusion criteria: (a) no history of any mental disorders; (b) no history of any mental disorders across three family generations; (c) scoring < 7 on both HAMD-17 and HAMA-14; (d) at least a junior high school education level; (e) 18–55 years old; (f) with sufficient audiovisual level to complete the study; (2) Exclusion criteria: (a) currently presence of serious physical disease; (b) history of brain injury.

According to previous studies (6), a medium effect size was assumed in the current study, which required a minimum of 50 participants (25 in each group) (28). 40 MDD patients and 33 HCs met the corresponding inclusion and exclusion criteria and were included in the current study.

This study has been approved by the Ethics Committee of Shanghai Mental Health Center (2021ky-122). All participants have signed the informed consent.

2.2. Measures and procedure

All subjects were interviewed with MINI, HAMD-17, and HAMA-14 to assess their clinical symptoms and determine whether the inclusion criteria were met. Among them, MINI was designed to screen for mental disorders based on DSM-4. HAMD-14 was used to access anxiety symptoms, with higher scores indicating more severe anxiety symptoms. HAMD-17 was employed to access depressive symptoms including low mood, weight loss, somatic symptoms and so on. A HAMD-17 score of less than 7 was classified as no depressive symptoms, 7–16 as mild, 17–24 as moderate and more than 24 as severe.

Based on IAT, EAST was developed by De Houwer (17), which can measure self-schema and other-schema at the same time. Participants were asked to press the “F” or “J” keys according to the valence of attribute words or the color of object words presented on the screen. Consistent with a previous study (16), attribute words were printed in white, including positive words and negative words. Object words were printed in blue or green, including self-words and other-words. For each trial, a fixation was presented in the center of the screen for 500 ms. To avoid the influence of subjects’ anticipation of the upcoming word on ERP components, a blank screen with a duration of 150–250 ms appeared before the stimulus onset. After the stimulus was onset, subjects were asked to respond as quickly as possible. Once they pressed the “F” or “J” key, an inter-stimulus interval was presented for 2,000 ms to avoid the effect of the next trial on the late ERP components of the previous trial (Figure 1).

There were two practice blocks and six formal blocks in EAST. The first block consisted of eight positive words and eight negative words. Participants were asked to press the “F” key for negative words and the “J” key for positive words, assigning negative and positive attributes to the “F” and “J” keys, respectively. The second practice block consisted of four self-words and four other-words, each repeated twice in blue and green. In this block, participants were asked to press the “F” key for words in green, and the “J” key for words in blue, assigning negative attributes to green and positive attributes to blue. The formal blocks included six conditions (blue self-words, blue other-words, green self-words, green other-words, white positive words, and white negative words). To ensure that there were enough trials for ERP analysis, the number of trials in the formal blocks was increased from 144 trials in the original task (16) to 360 trials, with 60 trials in each block presented with randomization. The instruction of formal blocks combined the instructions of the two practice blocks, with responses based on valence if the words were white, or based on colors if the words were blue or green.

To avoid fatigue effects, there was a 30-s rest period between two blocks. The task was programmed by E-Prime 3.0, through which RT and accuracy were recorded.

2.3. Electroencephalography (EEG) data recordings and preprocessing

EEG data were acquired during EAST using ANT Neuro system with 64 scalp sites. The sampling rate was 500 Hz, and the impedance of each electrode was below 10 k Ω . The online

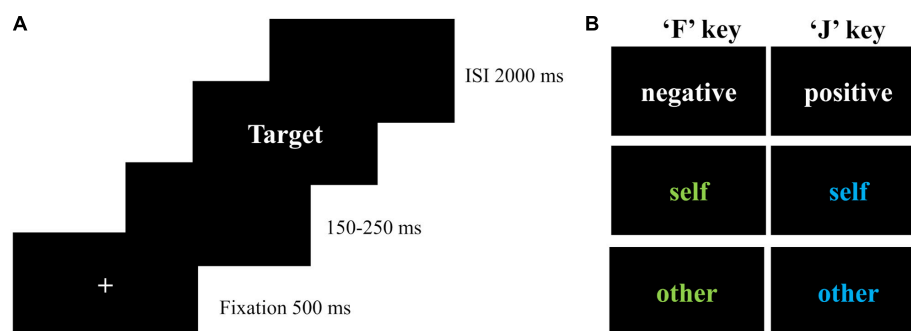


FIGURE 1

Extrinsic affective Simon task. (A) Flowchart of each trial; (B) conditions in EAST; ISI, inter-stimulus interval; self-words included I, myself, me, and self (“我”、“自己”、“本人”、“自我” in Chinese). Other-words included dad, mom, partner, and lover (“爸爸”、“妈妈”、“伴侣”、“恋人” in Chinese). Positive words included nice, warm, lovely, kind, excellent, and capable (“美好的”、“温暖的”、“善良的”、“善良的”、“优秀的”、“能干的”). Negative words included terrible, incompetent, useless, evil, lame, and disgusting (“糟糕的”、“无能的”、“没用的”、“罪恶的”、“差劲的”、“讨厌的”).

reference electrode was CPz, and the offline reference electrodes were M1 and M2.

EEGLAB toolbox in Matlab 2013b was used to preprocess the EEG data. There were seven steps of preprocessing. (1) locating the channels with international standard 10-20 system; (2) filtering the data with a bandpass in the range of 0.1–30 Hz; (3) segmenting the data in the range of 200 ms before stimulus onset to 1,000 ms after post-stimulus and epochs with incorrect answers were removed; (4) the data of 200 ms pre-stimulus were used for baseline correction; (5) re-referencing the data to M1 and M2 electrodes; (6) independent component analysis was used to remove artifacts such as eye movements; and (7) removing epochs with amplitudes at any electrode sites exceeding $\pm 80 \mu\text{V}$.

2.4. Statistical analyses

To compare the demographic and clinical differences between MDD patients and HCs, independent *t*-test was used for continuous variables such as age, HAMD-17 and HAMA-14. For categorical variables (i.e., gender and education level), chi-square test or Fisher's exact test was employed. To ensure the comparability of our results with previous studies, the method of processing RT outliers was consistent with previous studies (16, 17). Specifically, RTs below 300 ms and RTs above 3,000 ms were taken as 300 ms and 3,000 ms, respectively. The average proportion of this kind of trials was 0.23% across all participants and conditions, with a range of 0–1.68%. There were six indexes in EAST, four of which were the average RTs in the four conditions (i.e., positive self, negative self, positive others and negative others). The other two indexes were the self-EAST effect (RT for negative self condition minus RT for positive self condition) and the other-EAST effect (RT for positive others condition minus RT for negative others condition). A higher EAST effect indicated a more positive self-schema or other-schema. As we aimed to focus on the characteristics of self-schema and other-schema separately, rather than on their relationships, 2 (valence: positive/negative) $\times 2$ (group: MDD/Hc) repeated measures analysis of variances (RMANOVAs) were performed on RT for self-words and other-words, respectively. To compare the differences in self-EAST effect

and other-EAST effect between groups, an independent sample *t*-test was employed with Bonferroni correction. SPSS 22.0 was used to perform the above analysis.

After visual inspection of the grand averaged waveforms and topographic maps of the current study, along with previous studies (15, 18, 19, 23), we analyzed three ERP components with the following time windows and electrodes. (1) The peak amplitude and latency of N200 (250–350 ms) were calculated across Fz, F1, F2, F3, and F4. (2) The peak amplitude and latency of P300 (300–400 ms) were calculated across Pz, P1, P2, P3, P4, CP1, CP2, CP3, and CP4. (3) The mean amplitude of LPP (600–1,000 ms) was calculated across Cz, C1, C2, C3, and C4. Similar to the analysis of RT, 2 (valence: positive/negative) $\times 2$ (group: MDD/HCs) RMANOVAs were performed for self-words and other-words, respectively. Greenhouse–Geisser correction was conducted if the sphericity test was violated. The significant level was 0.05. R 4.0.2 with “bruceR” package was used to perform the above analysis.

3. Results

3.1. Demographic and clinical characteristics

A total of 40 MDD patients and 33 HCs were included in the study. No significant differences were observed in age ($t = -0.604$, $p = 0.106$), gender ($X^2 = 0.031$, $p = 0.861$), and education level ($p = 0.644$). Among them, chi-square test was conducted on gender and Fisher's exact test was conducted on education level given that 50% cells had an expected count less than 5. The scores of MDD patients were significantly higher than those of HCs in HAMD-17 ($t = -32.035$, $p < 0.001$), and HAMA-14 ($t = -18.928$, $p < 0.001$) (Table 1).

3.2. Behavioral outcomes

Table 2 shows the RTs of MDD patients and HCs in different conditions. For self-schema, the main effect of group ($F = 11.905$, $p < 0.001$, $\eta^2p = 0.144$) and valence ($F = 6.335$,

TABLE 1 Demographic and clinical characteristics of MDD and HCs.

	HCs (<i>n</i> = 33)	MDD (<i>n</i> = 40)	χ^2/t	<i>p</i>
Age (M ± SD)	28.15 ± 9.11	29.28 ± 6.76	−0.604	0.106
Gender (<i>n</i>)			0.031	0.861
Male	8	9		
Female	25	31		
Education level (<i>n</i>)			/	0.644
Middle school	1	3		
College	32	37		
HAMD-17 (M ± SD)	2.21 ± 1.65	20.90 ± 3.21	−32.035	<0.001
HAMA-14 (M ± SD)	1.06 ± 1.37	15.08 ± 4.43	−18.928	<0.001

MDD, major depressive disorder; HCs, healthy controls; M, mean; SD, standard deviation.

$p = 0.014$, $\eta^2p = 0.082$) were significant, but the interaction effect ($F = 2.147$, $p = 0.147$, $\eta^2p = 0.029$) was not significant. However, the exploratory analysis found that HCs responded significantly faster to the positive self-words than to the negative self-words ($t = -2.690$, $p = 0.009$, Cohen's $d = 0.472$), whereas no difference was found between negative self-words and positive self-words in MDD patients ($t = -0.782$, $p = 0.437$, Cohen's $d = 0.125$). In addition, HCs responded faster to both positive self-words ($t = 3.700$, $p < 0.001$, Cohen's $d = 2.458$) and negative self-words ($t = 3.101$, $p = 0.003$, Cohen's $d = 2.111$) than MDD patients. For other-schema, the main effect of group ($F = 11.339$, $p = 0.001$, $\eta^2p = 0.138$) and the interaction effect ($F = 8.625$, $p = 0.004$, $\eta^2p = 0.108$) were significant, while the main effect of valence ($F = 3.460$, $p = 0.067$, $\eta^2p = 0.046$) was not significant. *Post hoc* analysis found that the RT for positive other-words was significantly greater than that for negative other-words in HCs ($t = -3.240$, $p = 0.002$, Cohen's $d = 0.568$). And still, no difference was found between negative other-words and positive other-words in MDD patients ($t = 0.801$, $p = 0.426$, Cohen's $d = -0.127$). Moreover, HCs responded faster to both positive other-words ($t = 3.750$, $p < 0.001$, Cohen's $d = 2.882$) and negative other-words ($t = 2.895$, $p = 0.005$, Cohen's $d = 2.186$) than MDD patients (Figure 2). Independent sample *t*-test was performed on self-EAST effect and other-EAST effect. Though both the self-EAST effect (HCs: 29.36 ± 45.83 ; MDD: 6.96 ± 63.61) and other-EAST effect (HCs: 29.60 ± 53.89 ; MDD: -6.64 ± 51.30) of HCs were greater than that of MDD, only the difference of other-EAST effect was significant (other-EAST effect: $t = 2.937$, $p = 0.008$, Cohen's $d = 0.691$; self-EAST effect: $t = 1.465$, $p = 0.294$, Cohen's $d = 0.398$) (Figure 2).

TABLE 2 RTs of MDD and HCs in EAST.

		Positive		Negative	
		M ± SD	95% CI of M	M ± SD	95% CI of M
HCs	Self-words	591.11 ± 115.42	[550.184, 632.037]	617.47 ± 120.64	[574.694, 660.251]
	Other-words	594.54 ± 113.09	[554.439, 634.637]	624.14 ± 126.39	[579.326, 668.955]
MDD	Self-words	728.54 ± 185.72	[669.142, 787.936]	735.50 ± 189.05	[675.041, 795.962]
	Other-words	744.73 ± 205.69	[678.951, 810.517]	738.09 ± 194.62	[675.848, 800.331]

MDD, major depressive disorder; HCs, healthy controls; RT, reaction time; EAST, External Affect Simon Task; M, mean; SD, standard deviation; CI, confidence interval.

3.3. ERP outcomes

Six MDD patients and seven HCs were excluded due to excessive artifacts in more than half of their trials. The EEG data of four MDD patients were not acquired due to equipment problems. Thus, twenty-six HCs and thirty MDD patients were included in the analysis of ERP outcomes. To clarify whether the results of demographic characteristics and behavioral indicators were consistent for the complete sample and the sample included in the ERP analysis, the above statistical analyses were conducted again on the sample included in the ERP analysis. The results were presented in the [Supplementary material](#) and were consistent with the results of the complete sample described above. For ERP outcomes, RMANOVA was performed for self-words and other-words, respectively.

3.3.1. Comparison of the ERP differences of self-words between MDD and HCs

For the peak amplitude of N200, the main effect of valence ($F = 1.311$, $p = 0.257$, $\eta^2p = 0.024$) and interaction effect ($F = 0.222$, $p = 0.640$, $\eta^2p = 0.004$) were not significant, but the main effect of group was significant ($F = 4.670$, $p = 0.035$, $\eta^2p = 0.080$). Regarding the latency of N200, the main effect of valence ($F = 3.045$, $p = 0.087$, $\eta^2p = 0.053$) and group ($F = 1.754$, $p = 0.191$, $\eta^2p = 0.031$) was not significant, whereas the interaction was significant ($F = 4.420$, $p = 0.040$, $\eta^2p = 0.076$). *Post hoc* analysis showed that in HCs, the latency of positive self-words was significantly greater than that of negative self-words ($t = 2.628$, $p = 0.011$, Cohen's $d = 0.520$), but no significant difference was found in MDD ($t = -0.262$, $p = 0.794$, Cohen's $d = 0.048$). Additionally, the latency of negative self-words in MDD was greater than that in HCs ($t = 2.211$, $p = 0.031$, Cohen's $d = 0.604$), and no group difference was found in the positive self conditions ($t = 0.126$, $p = 0.900$, Cohen's $d = 0.035$) (Figures 3, 4; Table 3).

For the peak amplitude of P300, the main effect of valence ($F = 0.026$, $p = 0.873$, $\eta^2p = 0.000$) and interaction ($F = 0.000$, $p = 0.993$, $\eta^2p = 0.000$) were not significant, but the main effect of group was significant ($F = 6.369$, $p = 0.015$, $\eta^2p = 0.105$). In terms of the latency of P300, no significant results were found ($p > 0.05$) (Figures 5, 6; Table 3).

For the mean amplitude of LPP, the main effect of valence ($F = 0.153$, $p = 0.697$, $\eta^2p = 0.003$) and the interaction were not significant ($F = 0.302$, $p = 0.585$, $\eta^2p = 0.006$). The main effect of group was marginally significant ($F = 3.965$, $p = 0.052$, $\eta^2p = 0.068$). However, the exploratory analysis found that the mean amplitude in the positive self condition was significantly smaller in MDD than that in HCs ($t = -2.180$, $p = 0.034$, Cohen's

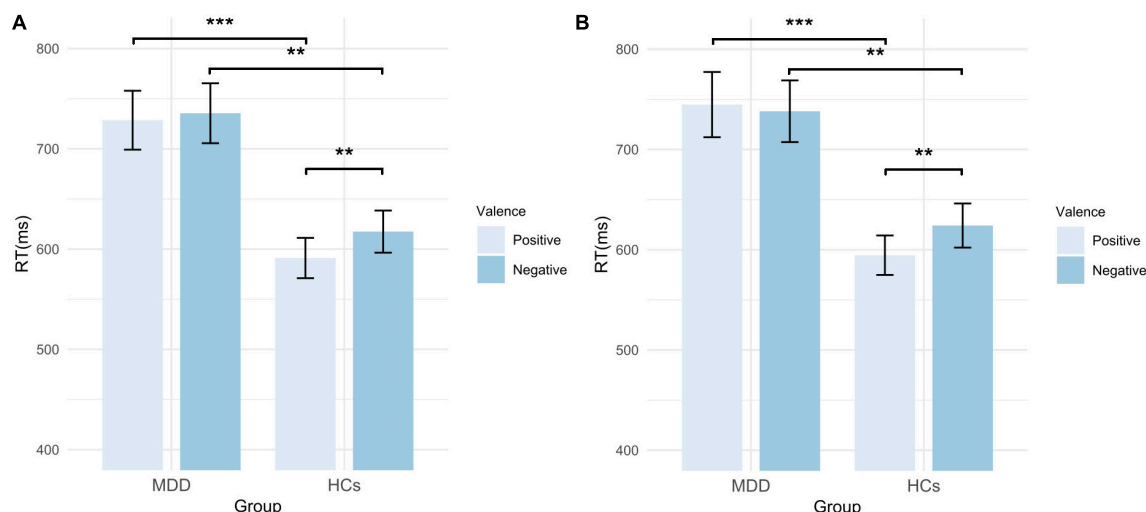


FIGURE 2

RTs of MDD patients and HCs in EAST. (A) RTs of self-words; (B) RTs of other-words. MDD, major depressive disorder; HCs, healthy controls; RT, reaction time; EAST, External Affect Simon Task; error bars represent the standard error. ** $p < 0.01$; *** $p < 0.001$.

$d = 0.902$), while no significant group difference was found in the negative self condition ($t = -1.640$, $p = 0.107$, Cohen's $d = 0.754$) (Figures 7, 8; Table 3).

3.3.2. Comparison of the ERP differences of other-words between MDD and HCs

For the peak amplitude of N200, valence main effect ($F = 4.487$, $p = 0.039$, $\eta^2p = 0.077$), group main effect ($F = 5.060$, $p = 0.029$, $\eta^2p = 0.086$) and the interaction ($F = 4.838$, $p = 0.032$, $\eta^2p = 0.082$) was significant. *Post hoc* analysis found that in HCs, the absolute value of N200 peak amplitude in the negative others condition was greater than that in the positive others condition ($t = 2.950$, $p = 0.005$, Cohen's $d = 0.584$). However, no significant results were observed in MDD ($t = -0.060$, $p = 0.953$, Cohen's $d = 0.011$). Moreover, HCs had a greater absolute value of N200 peak amplitude in the negative others condition than MDD ($t = 2.833$, $p = 0.006$, Cohen's $d = 1.404$), and no group difference was found in the positive others condition ($t = -1.543$, $p = 0.129$, Cohen's $d = 0.809$). In terms of the latency of N200, no significant results were found ($p > 0.05$) (Figures 3, 4; Table 3).

For the peak amplitude of P300, the main effect of valence was not significant ($F = 0.954$, $p = 0.333$, $\eta^2p = 0.017$), but the main effect of group ($F = 5.636$, $p = 0.021$, $\eta^2p = 0.095$) and the interaction effect was significant ($F = 4.940$, $p = 0.030$, $\eta^2p = 0.084$). *Post hoc* analysis showed that in HCs, the peak amplitude of positive other-words was greater ($t = 2.185$, $p = 0.033$, Cohen's $d = 0.433$), while no such difference was found in MDD ($t = -0.914$, $p = 0.365$, Cohen's $d = 0.168$). In addition, the peak amplitude of positive other-words in MDD was smaller than that in HCs ($t = -2.906$, $p = 0.005$, Cohen's $d = 1.602$). Regarding the latency of P300, no significant results were found ($p > 0.05$) (Figures 5, 6; Table 3).

For the mean amplitude of LPP, the main effect of valence ($F = 0.028$, $p = 0.868$, $\eta^2p = 0.001$) and the interaction effect were not significant ($F = 1.331$, $p = 0.254$, $\eta^2p = 0.024$), but the main effect of group was significant ($F = 4.381$, $p = 0.041$, $\eta^2p = 0.075$).

Exploratory analysis found that the amplitude of positive other-words in MDD was smaller than that in HCs ($t = -2.367$, $p = 0.022$, Cohen's $d = 1.100$), while no significant difference was found in the negative others condition ($t = -1.652$, $p = 0.104$, Cohen's $d = 0.788$) (Figures 7, 8; Table 3).

4. Discussion

By combining EAST and ERP, the current study investigated the behavioral and neural activity characteristics associated with implicit self-schema and implicit other-schema in MDD. HCs responded faster to positive self-words and positive other-words, while MDD patients did not. Besides, the absolute value of N200 peak amplitude was greater and the P300 peak amplitude was smaller under the negative others condition in HCs compared with MDD patients. Additionally, MDD patients showed smaller LPP amplitudes than HCs in positive self condition and positive others conditions. These results suggested that neural reactivities related to self-schema and other-schema might be altered in MDD.

Compared to negative self-words, HCs responded faster to positive self-words, indicating a closer association between positive attributes and their self-representations. This suggested the existence of positive self-schema in HCs. However, MDD patients did not show this pattern, indicating a lack of positive self-schema. This finding is consistent with some previous studies (10, 16, 19). Nevertheless, Franck et al. (12) used IAT but did not find differences in self-schema between currently depressed patients and HCs. Grundy et al. (26) suggested that this could be due to the confusion between self-schema and other-schema in IAT. Specifically, IAT contains two conditions: positive self condition and negative self condition. The former condition involves pressing the same key (e.g., F) for self-words and positive words, and pressing another key (e.g., J) for other-words and negative words. The latter condition involves pressing the same key (e.g., F) for self-words and negative words, and pressing another key (e.g., J) for

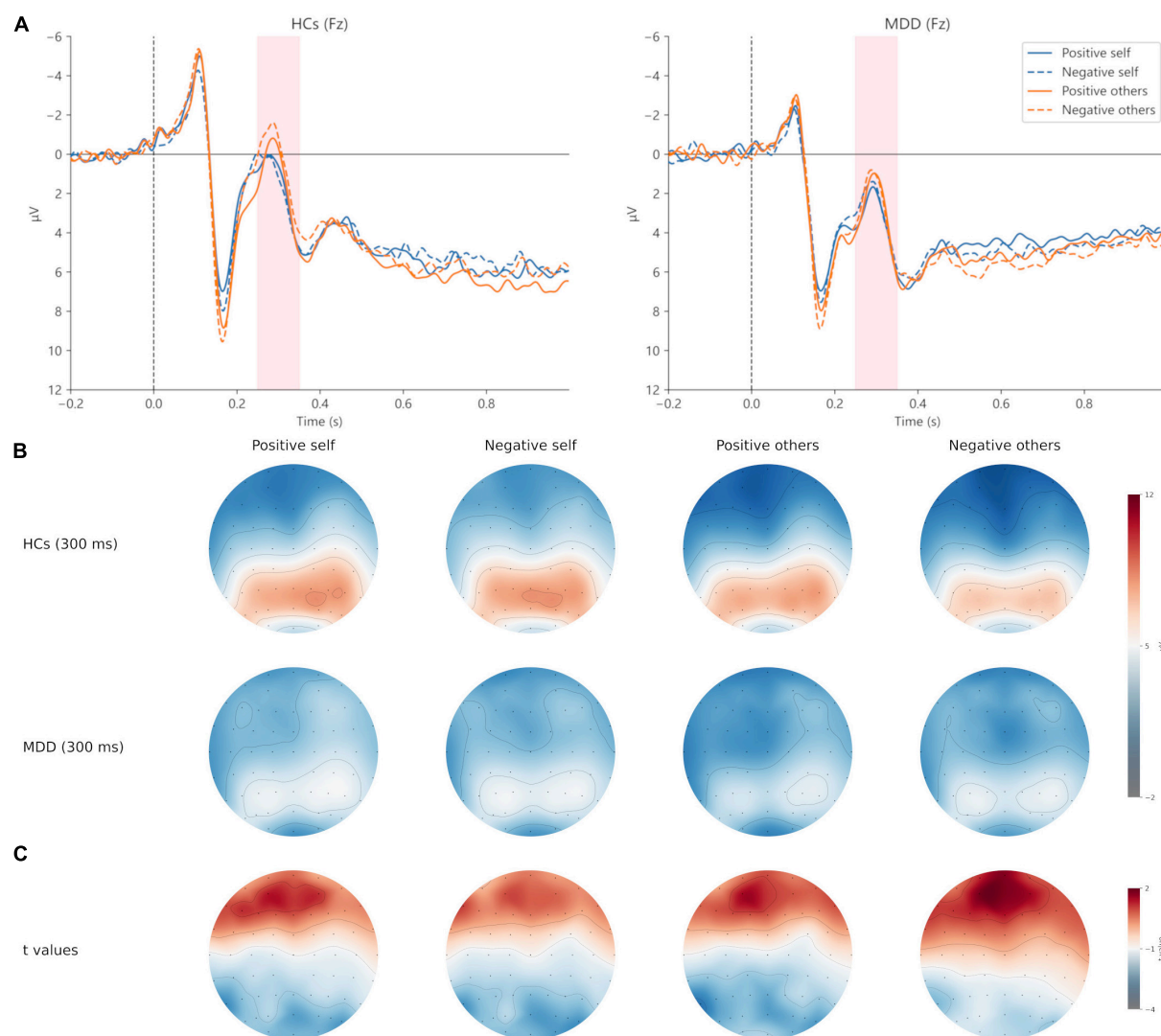


FIGURE 3

Grand averages (A) of N200 (250–350 ms) at Fz electrodes under positive self (blue solid lines), negative self (blue dashed lines), positive others (orange solid lines), and negative others (orange dashed lines) condition. Topographic maps of N200 at 300 ms (B) under four conditions. Topographic distribution of t values for N200 between MDD and HCs (C) under four conditions. MDD, major depressive disorder; HCs, healthy controls.

other-words and positive words. Therefore, in IAT, the RTs under the positive self condition actually includes the effect of positive self and negative others. Meanwhile, the RTs under negative self condition includes the effect of both negative self and positive others. Since in EAST, object words are presented in different colors and colors are paired with attributes, it can distinguish between self-schema and other-schema effectively.

The RT of positive other-words was smaller than negative other-words in HCs, while no such effect was found in MDD. Moreover, HCs had significantly greater effect of other-EAST than MDD patients. Thus, MDD patients showed a more negative other-schema than HCs. Previous studies have paid less attention to the characteristics of other-schema in MDD and the findings remain controversial. Wu et al. (21) used GNAT and found that HCs responded faster to trials in the negative others condition than to trials in the positive others condition, suggesting the presence of a negative other-schema in HCs. Additionally, Jiang et al. (19)

also used GNAT and found that MDD patients had a negative other-schema, but the RT of HCs in the negative others condition was smaller than that of MDD participants, indicating that the other-schema in MDD was more positive than that in HCs. The discrepancies may be due to the other-words used in these studies, which were words that did not refer to a specific object, such as “not me,” “he,” “she,” “others,” etc. Nevertheless, it is worth noting that the other-schema that plays a key role in MDD is the representation of those with whom the individual has intimate relationships, such as parents and partners (29–31). Similar to the present study, the other-words used in Yao et al.’s (16) study were words such as parents and lovers, and they also found that the other-schema in MDD was more negative than that in HCs. However, MDD participants in Yao et al.’s (16) study showed a negative other-schema, whereas in the present study, they only showed a lack of positive other-schema. This difference may relate

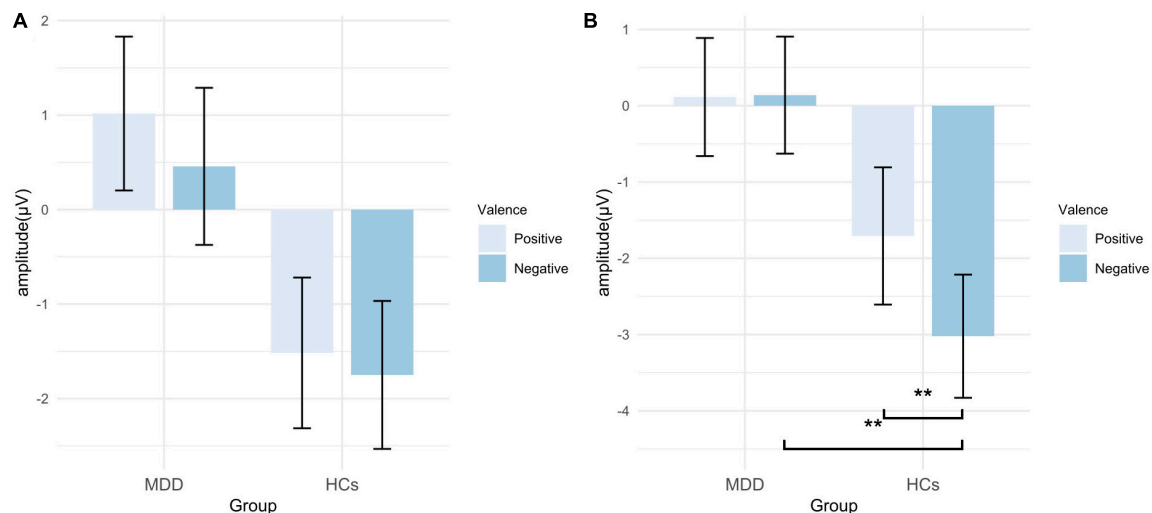


FIGURE 4
Peak amplitude of N200 in EAST. **(A)** Amplitudes of self-words; **(B)** amplitudes of other-words. MDD, major depressive disorder; HCs, healthy controls; EAST, External Affect Simon Task; error bars represent the standard error. $**p < 0.01$.

TABLE 3 The N200, P300, and LPP of MDD and HCs in EAST ($M \pm SD$).

			Positive		Negative	
			Latency (ms)	Peak/Mean amplitude (μV)	Latency (ms)	Peak/Mean amplitude (μV)
N200	HCs	Self-words	284.92 \pm 28.84	-1.52 \pm 4.07	272.00 \pm 26.30	-1.75 \pm 3.99
		Other-words	283.23 \pm 25.07	-1.71 \pm 4.59	278.15 \pm 24.46	-3.02 \pm 4.12
	MDD	Self-words	285.80 \pm 23.20	1.02 \pm 4.46	287.00 \pm 24.44	0.46 \pm 4.55
		Other-words	290.00 \pm 18.20	0.11 \pm 4.24	288.67 \pm 21.52	0.14 \pm 4.20
P300	HCs	Self-words	320.92 \pm 38.33	6.53 \pm 4.45	321.31 \pm 38.78	6.48 \pm 4.59
		Other-words	317.46 \pm 33.16	6.21 \pm 4.27	314.46 \pm 32.16	5.27 \pm 4.68
	MDD	Self-words	330.93 \pm 41.79	3.53 \pm 4.70	331.13 \pm 42.36	3.49 \pm 4.42
		Other-words	321.73 \pm 37.65	2.74 \pm 4.60	320.60 \pm 37.48	3.11 \pm 4.64
LPP	HCs	Self-words	/	5.69 \pm 3.42	/	5.65 \pm 3.46
		Other-words	/	6.36 \pm 3.21	/	6.00 \pm 3.31
	MDD	Self-words	/	3.79 \pm 3.09	/	4.06 \pm 3.72
		Other-words	/	4.20 \pm 3.56	/	4.46 \pm 3.64

MDD, major depressive disorder; HCs, healthy controls; M, mean; SD, standard deviation.

to the practice effect caused by the increase in the number of trials (32).

Regarding the neural activity patterns of self-schema, although no significant difference was found in N200 and P300, an exploratory analysis of LPP amplitudes showed that MDD patients showed smaller LPP amplitudes than HCs in positive self condition. Since LPP reflects the degree of elaborate processing of stimuli (8, 24), it indicates that MDD patients process positive self-words less elaborately than HCs. Therefore, the above results preliminarily revealed that the abnormal self-schema in MDD patients was only related to the late stage of elaborate processing, which was in line with some existing evidence. For example, Chen et al. (27) using IAT did not find any difference in N200 amplitudes of HCs under the positive and negative self conditions. Allison et al. (22) using SRET found no difference in P300 amplitudes.

In addition, Lou et al. (15) also focused on P300 (early LPP) and LPP (late LPP), and significant results were found only for LPP amplitudes. LPP has been considered as a neurophysiological marker of depression (33) and reflects the top-down processes of anterior cingulate cortex (ACC) and prefrontal cortex (PFC) (34). In the process of processing self-related information, ACC involves the identification of motivationally salient stimuli and PFC involves the emotional reappraisal and memory consolidation (34). Compared to HCs, MDD patients showed hyperactivation of PFC and ACC (35, 36), which are associated with self-esteem and depression (36). Therefore, the abnormality of self-schema in MDD may be related to the dysregulated self-cognition and abnormal processing of emotional stimuli based on ACC and PFC. More detailed exploration with functional magnetic resonance imaging (fMRI) will be necessary.

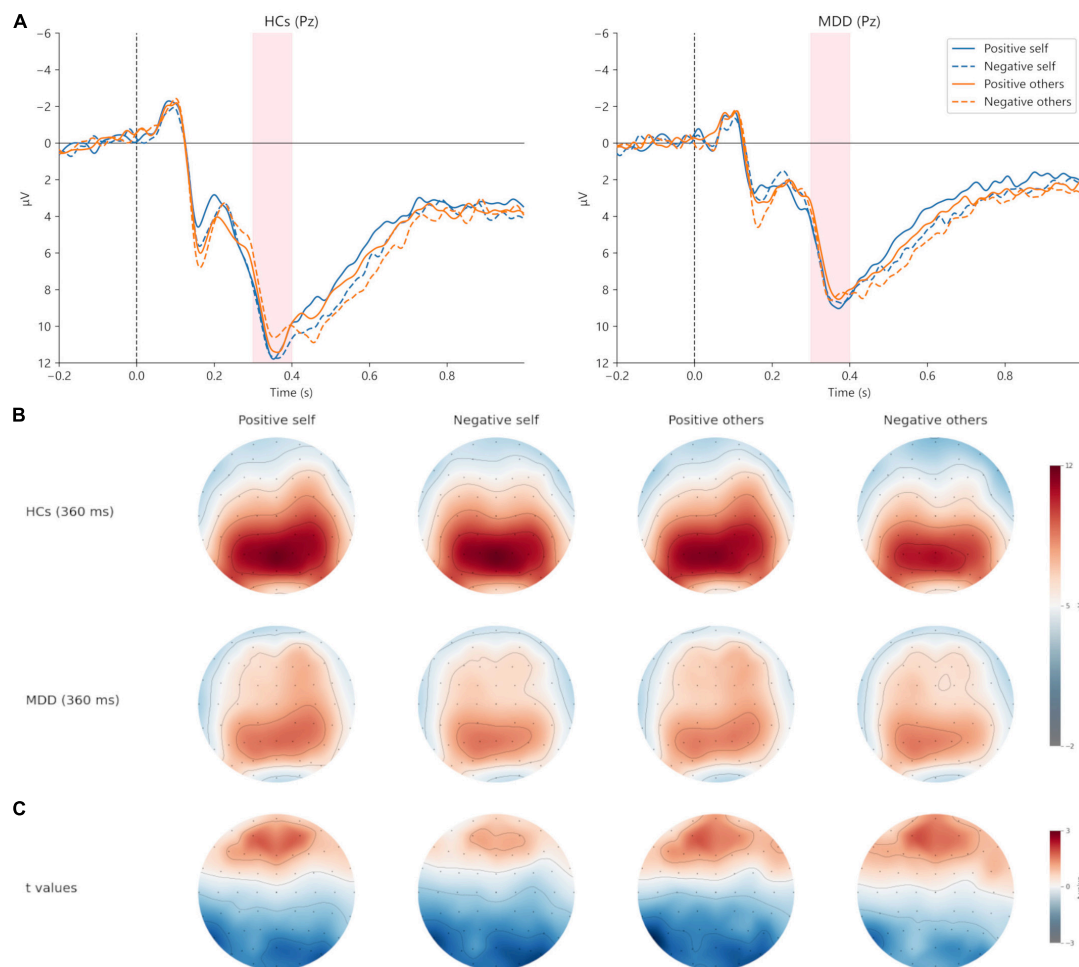


FIGURE 5

Grand averages (A) of P300 (300–400 ms) at Pz electrodes under positive self (blue solid lines), negative self (blue dashed lines), positive others (orange solid lines), and negative others (orange dashed lines) condition. Topographic maps of P300 at 360 ms (B) under four conditions. Topographic distribution of t values for P300 between MDD and HCs (C) under four conditions. MDD, major depressive disorder; HCs, healthy controls.

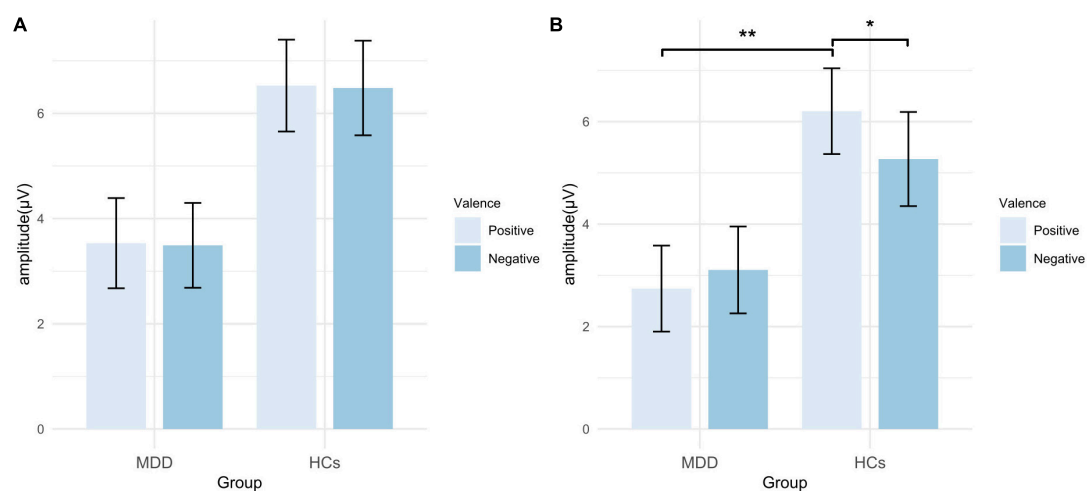


FIGURE 6

Peak amplitude of P300 in EAST. (A) Amplitudes of self-words; (B) amplitudes of other-words. MDD, major depressive disorder; HCs, healthy controls; EAST, External Affect Simon Task; error bars represent the standard error. * $p < 0.05$; ** $p < 0.01$.

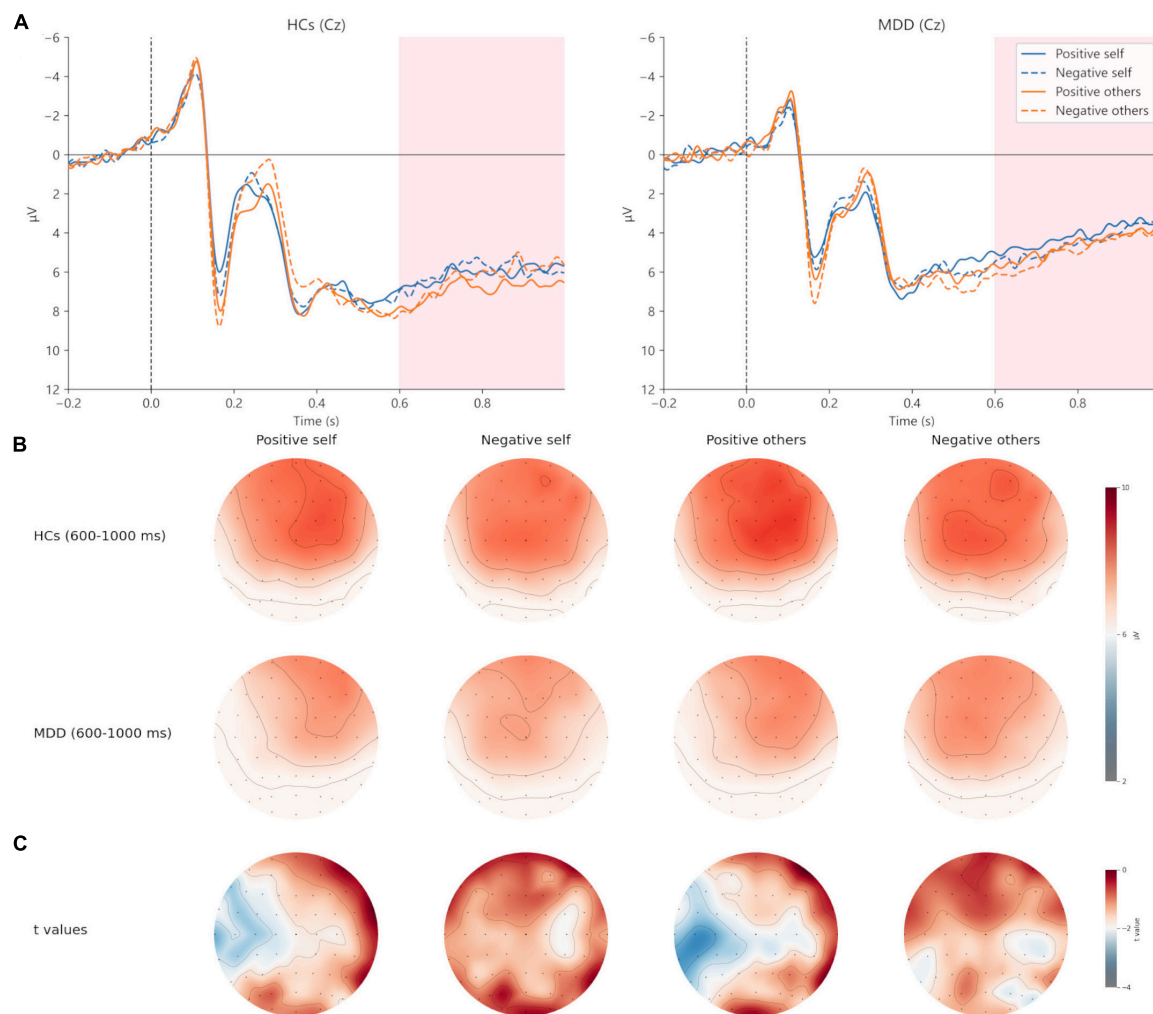


FIGURE 7

Grand averages (A) of LPP (600–1,000 ms) at Cz electrodes under positive self (blue solid lines), negative self (blue dashed lines), positive others (orange solid lines), and negative others (orange dashed lines) condition. Topographic distribution (B) of grand averaged LPP within a time window of 600–1,000 ms under four conditions. Topographic distribution of *t* values for LPP between MDD and HCs (C) under four conditions. MDD, major depressive disorder; HCs, healthy controls.

However, some other studies had different findings (6, 19, 25). The inconsistency may be caused by the characteristics of samples and the use of attribute words as the stimuli to induce ERP. Specifically, Allison et al. (22) recruited patients with MDD in remission and Auerbach et al. (6) only included female adolescents with MDD. Though the subjects in Dainer-Best et al.'s (25) study and Jiang et al.'s (19) study were adults with MDD who were currently in an episode, the paradigms they used were SRET and GNAT, respectively, in which positive or negative words were used to induce ERP. Given that MDD patients are characterized by emotion context insensitivity (ECI), referring to the phenomenon that the emotional reactivity of MDD patients is lower than that of HCs when faced with stimuli of different valence (positive adjectives or negative adjectives) (37). Thus, when attribute words are used to induce ERP, it is unclear whether the abnormality of ERP is originated from ECI or the abnormal implicit schemas (24, 38). Unlike IAT, GNAT, and SRET, words used to induce ERP in EAST are object words, which have been proven to activate the implicit attitudes effectively (20, 39–41). Therefore, the results of

the present study further clarified that the neural activities related to the implicit self-schema in MDD were mainly reflected in the late processing stage.

Regarding the neural activity patterns of other-schema, the findings were consistent with our hypotheses and behavioral results. For N200 and P300, the analyses showed that in HCs, the absolute value of N200 peak amplitude was greater and the P300 peak amplitude was smaller under the negative others condition. But no such effect was observed in MDD. Since N200 represents response inhibition, error monitoring and mismatch (18), the above results suggested that positive other-words were more consistent with HCs' implicit attitudes than negative other-words. This indicated that HCs had a positive other-schema, whereas MDD patients lacked it. Since P300 represents the allocation of cognitive and attentional resources (19), the above results showed that HCs allocated more cognitive and attentional resources to positive other-words, while MDD patients did not. Moreover, the absolute value of N200 peak amplitude in the negative others condition and the P300 peak amplitude in the

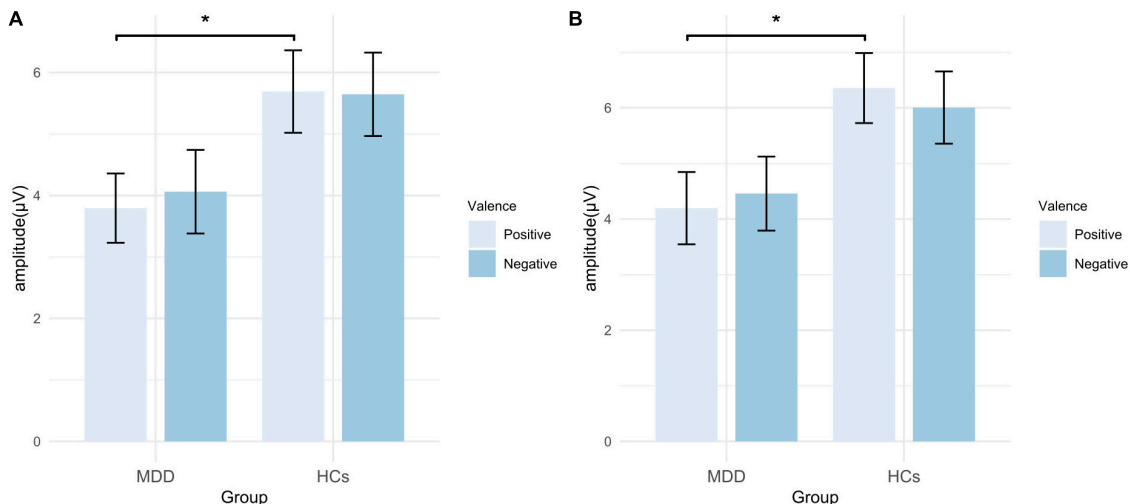


FIGURE 8

Mean amplitude of LPP in EAST. (A) Amplitudes of self-words; (B) amplitudes of other-words. MDD, major depressive disorder; HCs, healthy controls; EAST, External Affect Simon Task; error bars represent the standard error. * $p < 0.05$.

condition of the positive other in HCs were greater than that in MDD, respectively. Thus, in comparison to HCs, MDD participants had more negative implicit attitudes to other-representations and allocated fewer cognitive and attentional resources to positive other-words. For LPP amplitudes, the exploratory analyses revealed that MDD participants had smaller amplitudes than HCs in the positive others condition, suggesting that HCs processed positive other-words more elaborately than MDD patients. These findings provide evidence for theories that emphasize the importance of other-schema, such as cognitive theory, attachment theory and dyadic partner-schema model. Dyadic partner-schema model is proposed by Wilde and Dozois recently, and it demonstrates that the representations of self and others are highly similar, and that negative self-schema and other-schema will reinforce each other in MDD (29). Overall, the above results expand the previous understanding of the neural activity features related to the implicit other-schema in MDD.

Notably, HCs showed larger N200 latency in the positive self condition than the negative self condition, while no such effect was observed in MDD. Also, MDD participants showed greater N200 latency in the negative self condition than HCs. Another study on HCs also suggested that the positive implicit self-schema was associated with the greater N200 latency (21). But other studies did not find similar results. Existing evidence indicates that the N200 latency is influenced by factors such as memory (42) and stimuli evaluation speed (43). Thus, further investigation is necessary to clarify the role of these factors in the current findings. Furthermore, significant group main effects were found in all three ERP components, which may reflect the overall cognitive impairment in MDD (44, 45).

There are some limitations in our study. First, the majority of MDD patients in this study were moderately depressed, and the lack of mild and severe depressed patients might impact the results. Therefore, it is important to include MDD patients with varying degrees of depression to confirm our findings. Second, the relationship between self-schema and other-schema was not the

investigated in the current study. Exploring this relationship in future studies may provide further insights into the mechanisms underlying MDD. Third, compared with fMRI, ERP has a higher temporal resolution but a lower spatial resolution. Thus, future studies can use fMRI to comprehensively explore the brain regions or networks involved in implicit schemas of MDD patients. Fourth, although the MDD patients in the current study were not diagnosed with anxiety disorder, they still had mild anxiety symptoms. It is possible that these anxiety symptoms may have influenced our results. Comparing implicit schemas in MDD patients with and without comorbid anxiety disorders in future studies may help to clarify the impact of anxiety on implicit schemas in MDD. Finally, as far as we know, there is currently no study exploring the changes of implicit schemas in MDD following different interventions and their relationships with improvement in depressive symptoms. Investigating these issues may further elucidate the role of implicit schemas in etiology and treatment of MDD.

5. Conclusion

Our study explored the neural activity patterns of implicit self-schema and other-schema in MDD by combining ERP and EAST. Both behavioral and ERP indexes showed that MDD participants lacked positive self-schema and positive other-schema. Moreover, implicit other-schema might be related to abnormalities in the early automatic processing stage (i.e., N200 and P300) and the late elaborative processing stage (i.e., LPP), while implicit self-schema might be associated only with abnormalities in the late elaborative processing stage.

Data availability statement

The datasets presented in this article are not readily available because the research is still ongoing and the raw data of the current

article will be used for further analysis. Requests to access the datasets should be directed to the corresponding author.

Ethics statement

The studies involving human participants were reviewed and approved by the Ethics Committee of Shanghai Mental Health Center. The patients/participants provided their written informed consent to participate in this study.

Author contributions

J-YY analyzed the data and drafted the manuscript. J-YY and Z-WZ collected the data. YZ modified the manuscript. S-SS, Y-RW, JT, Y-HP, YW, and W-HJ contributed to the study design. J-YQ was the guarantor, supervised the data collection, statistical analysis, and modified the manuscript. All authors approved the final version of the manuscript.

Funding

This study was funded by the SMHC Clinical Research Center (No. CRC2017YB01), the Science and Technology Commission

of Shanghai Municipality (No. 21Y11905400), and the Shanghai Hospital Development Center (No. SHDC2020CR1027B).

Conflict of interest

The authors declare that the research was conducted in the absence of any commercial or financial relationships that could be construed as a potential conflict of interest.

Publisher's note

All claims expressed in this article are solely those of the authors and do not necessarily represent those of their affiliated organizations, or those of the publisher, the editors and the reviewers. Any product that may be evaluated in this article, or claim that may be made by its manufacturer, is not guaranteed or endorsed by the publisher.

Supplementary material

The Supplementary Material for this article can be found online at: <https://www.frontiersin.org/articles/10.3389/fpsy.2023.1131275/full#supplementary-material>

References

- Marcus M, Yasamy MT, van Ommeren M, Chisholm D, Saxena S. *Depression: A Global Public Health Concern*. Geneva: World Health Organization (2012).
- Fried EI, Flake JK, Robinaugh DJ. Revisiting the theoretical and methodological foundations of depression measurement. *Nat Rev Psychol*. (2022) 1:358–68. doi: 10.1038/s44159-022-00050-2
- Phillips WJ, Hine DW, Thorsteinsson EB. Implicit cognition and depression: a meta-analysis. *Clin Psychol Rev*. (2010) 30:691–709. doi: 10.1016/j.cpr.2010.05.002
- Beck AT. *Cognitive Therapy and the Emotional Disorders*. Oxford: International Universities Press (1976).
- Bretherton I. The origins of attachment theory: John Bowlby and Mary Ainsworth. *Dev Psychol*. (1992) 28:759–75. doi: 10.1037/0012-1649.28.5.759
- Auerbach RP, Stanton CH, Proudfoot GH, Pizzagalli DA. Self-referential processing in depressed adolescents: a high-density event-related potential study. *J Abnorm Psychol*. (2015) 124:233–45. doi: 10.1037/abn0000023
- Kiang M, Farzan F, Blumberger DM, Kutas M, McKinnon MC, Kansal V, et al. Abnormal self-schema in semantic memory in major depressive disorder: evidence from event-related brain potentials. *Biol Psychol*. (2017) 126:41–7. doi: 10.1016/j.biopsycho.2017.04.003
- Shestiyuk AY, Deldin PJ. Automatic and strategic representation of the self in major depression: trait and state abnormalities. *Am J Psychiatry*. (2010) 167:536–44. doi: 10.1176/appi.ajp.2009.06091444
- Monsonet M, Ballester S, Sheinbaum T, Valiente C, Espinosa R, Kwapiel TR, et al. Self-schemas and self-esteem discrepancies in subclinical paranoia: the essential role of depressive symptoms. *Front Psychiatry*. (2021) 12:623755. doi: 10.3389/fpsy.2021.623755
- Risch AK, Buba A, Birk U, Morina N, Steffens MC, Stangier U. Implicit self-esteem in recurrently depressed patients. *J Behav Ther Exp Psychiatry*. (2010) 41:199–206. doi: 10.1016/j.jbtep.2010.01.003
- Romero N, Sanchez A, Vázquez C, Valiente C. Explicit self-esteem mediates the relationship between implicit self-esteem and memory biases in major depression. *Psychiatry Res*. (2016) 242:336–44. doi: 10.1016/j.psychres.2016.06.003
- Franck E, De Raedt R, De Houwer J. Activation of latent self-schemas as a cognitive vulnerability factor for depression: the potential role of implicit self-esteem. *Cogn Emot*. (2008) 22:1588–99. doi: 10.1080/02699930801921271
- Kesting M-L, Mehl S, Rief W, Lindenmeyer J, Lincoln TM. When paranoia fails to enhance self-esteem: explicit and implicit self-esteem and its discrepancy in patients with persecutory delusions compared to depressed and healthy controls. *Psychiatry Res*. (2011) 186:197–202. doi: 10.1016/j.psychres.2010.08.036
- Lemmens LHJM, Roefs A, Arntz A, van Teeseling HC, Peeters F, Huibers MJH. The value of an implicit self-associative measure specific to core beliefs of depression. *J Behav Ther Exp Psychiatry*. (2014) 45:196–202. doi: 10.1016/j.jbtep.2013.10.006
- Lou Y, Lei Y, Astikainen P, Peng W, Otieno S, Leppänen PHT. Brain responses of dysphoric and control participants during a self-esteem implicit association test. *Psychophysiology*. (2021) 58:e13768. doi: 10.1111/psyp.13768
- Yao J, Lin Q, Zheng Z, Chen S, Wang Y, Jiang W, et al. Characteristics of implicit schemas in patients with major depressive disorder. *Gen Psychiatry*. (2022) 35:e100794. doi: 10.1136/gpsych-2022-100794
- De Houwer J. The extrinsic affective Simon task. *Exp Psychol*. (2003) 50:77–85. doi: 10.1026//1618-3169.50.2.77
- Folstein JR, Van Petten C. Influence of cognitive control and mismatch on the N2 component of the ERP: a review. *Psychophysiology*. (2008) 45:152–70. doi: 10.1111/j.1469-8986.2007.00602.x
- Jiang C, Lu H, Zhang J, Gao X, Wang J, Zhou Z. The neural correlates of the abnormal implicit self-esteem in major depressive disorder: an event-related potential study. *Front Psychiatry*. (2022) 13:822677. doi: 10.3389/fpsy.2022.822677
- Wu L, Gu R, Cai H, Zhang J. Electrophysiological evidence for executive control and efficient categorization involved in implicit self-evaluation. *Soc Neurosci*. (2016) 11:153–63. doi: 10.1080/17470919.2015.1044673
- Wu L, Cai H, Gu R, Luo YLL, Zhang J, Yang J, et al. Neural manifestations of implicit self-esteem: an ERP study. *PLoS One*. (2014) 9:e101837. doi: 10.1371/journal.pone.0101837

22. Allison GO, Kamath RA, Carrillo V, Alqueza KL, Pagliaccio D, Slavich GM, et al. Self-referential processing in remitted depression: an event-related potential study. *Biol Psychiatry Glob Open Sci.* (2021) 3:119–29. doi: 10.1016/j.bpsgos.2021.12.005
23. Hudson A, Wilson MJG, Green ES, Itier RJ, Henderson HA. Are you as important as me? Self-other discrimination within trait-adjective processing. *Brain Cogn.* (2020) 142:105569. doi: 10.1016/j.bandc.2020.105569
24. Benau EM, Hill KE, Atchley RA, O'Hare AJ, Gibson LJ, Hajcak G, et al. Increased neural sensitivity to self-relevant stimuli in major depressive disorder. *Psychophysiology.* (2019) 56:e13345. doi: 10.1111/psyp.13345
25. Dainer-Best J, Trujillo LT, Schnyer DM, Beevers CG. Sustained engagement of attention is associated with increased negative self-referent processing in major depressive disorder. *Biol Psychol.* (2017) 129:231–41. doi: 10.1016/j.biopsycho.2017.09.005
26. Grundy JG, Benarroch MFF, Lebar AN, Shedden JM. Electrophysiological correlates of implicit valenced self-processing in high vs. low self-esteem individuals. *Soc Neurosci.* (2015) 10:100–12. doi: 10.1080/17470919.2014.965339
27. Chen Y, Zhong Y, Zhou H, Zhang S, Tan Q, Fan W. Evidence for implicit self-positivity bias: an event-related brain potential study. *Exp Brain Res.* (2014) 232:985–94. doi: 10.1007/s00221-013-3810-z
28. Clayton PE, Carbine KA, Baldwin SA, Larson MJ. Methodological reporting behavior, sample sizes, and statistical power in studies of event-related potentials: barriers to reproducibility and replicability. *Psychophysiology.* (2019) 56:e13437. doi: 10.1111/psyp.13437
29. Wilde JL, Dozois DJA. A dyadic partner-schema model of relationship distress and depression: conceptual integration of interpersonal theory and cognitive-behavioral models. *Clin Psychol Rev.* (2019) 70:13–25. doi: 10.1016/j.cpr.2019.03.003
30. Chatav Y, Whisman MA. Partner schemas and relationship functioning: a states of mind analysis. *Behav Ther.* (2009) 40:50–6. doi: 10.1016/j.beth.2007.12.005
31. Wilde JL, Dozois DJA. It's not me, it's you: self- and partner-schemas, depressive symptoms, and relationship quality. *J Soc Clin Psychol.* (2018) 37:356–80. doi: 10.1521/jscp.2018.37.5.356
32. Röhner J, Schröder-Abé M, Schütz A. Exaggeration is harder than understatement, but practice makes perfect! *Exp Psychol.* (2011) 58:464–72. doi: 10.1027/1618-3169/a000114
33. McLean MA, Van den Bergh BRH, Baart M, Vroomen J, van den Heuvel MI. The late positive potential (LPP): a neural marker of internalizing problems in early childhood. *Int J Psychophysiol.* (2020) 155:78–86. doi: 10.1016/j.ijpsycho.2020.06.005
34. Hudson A, Green ES, Wilson MJG, Itier RJ, Henderson HA. The prominence of self-referential processing across ERP and memory consolidation in children. *Dev Neuropsychol.* (2021) 46:598–615. doi: 10.1080/87565641.2021.1991354
35. Li Y, Li M, Wei D, Kong X, Du X, Hou X, et al. Self-referential processing in unipolar depression: distinct roles of subregions of the medial prefrontal cortex. *Psychiatry Res Neuroimaging.* (2017) 263:8–14. doi: 10.1016/j.pscychres.2017.02.008
36. Yoshimura S, Okamoto Y, Onoda K, Matsunaga M, Ueda K, Suzuki S, et al. Rostral anterior cingulate cortex activity mediates the relationship between the depressive symptoms and the medial prefrontal cortex activity. *J Affect Disord.* (2010) 122:76–85. doi: 10.1016/j.jad.2009.06.017
37. Rottenberg J, Gross JJ, Gotlib IH. Emotion context insensitivity in major depressive disorder. *J Abnorm Psychol.* (2005) 114:627–39. doi: 10.1037/0021-843X.114.4.627
38. McIvor L, Sui J, Malhotra T, Drury D, Kumar S. Self-referential processing and emotion context insensitivity in major depressive disorder. *Eur J Neurosci.* (2021) 53:311–29. doi: 10.1111/ejn.14782
39. Banfield JF, van der Lugt AH, Münte TF. Juicy fruit and creepy crawlies: an electrophysiological study of the implicit Go/NoGo association task. *NeuroImage.* (2006) 31:1841–9. doi: 10.1016/j.neuroimage.2006.02.017
40. Bosson JK, Swann WB, Pennebaker JW. Stalking the perfect measure of implicit self-esteem: the blind men and the elephant revisited? *J Pers Soc Psychol.* (2000) 79:631–43. doi: 10.1037//0022-3514.79.4.631
41. van der Lugt AH, Banfield JF, Osinsky R, Münte TF. Brain potentials show rapid activation of implicit attitudes towards young and old people. *Brain Res.* (2012) 1429:98–105. doi: 10.1016/j.brainres.2011.10.032
42. Papaliagkas V, Kimiskidis V, Tsolaki M, Anogianakis G. Usefulness of event-related potentials in the assessment of mild cognitive impairment. *BMC Neurosci.* (2008) 9:107. doi: 10.1186/1471-2202-9-107
43. Azizian A, Freitas AL, Parvaz MA, Squires NK. Beware misleading cues: perceptual similarity modulates the N2/P3 complex. *Psychophysiology.* (2006) 43:253–60. doi: 10.1111/j.1469-8986.2006.00409.x
44. el Massioui F, Everett J, Martin MT, Jouvent R, Widlöcher D. Attention deficits in depression: an electrophysiological marker. *Neuroreport.* (1996) 7:2483–6. doi: 10.1097/00001756-199611040-00016
45. Klawohn J, Santopetro NJ, Meyer A, Hajcak G. Reduced P300 in depression: evidence from a flanker task and impact on ERN, CRN, and Pe. *Psychophysiology.* (2020) 57:e13520. doi: 10.1111/psyp.13520



OPEN ACCESS

EDITED BY

Jigar Jogia,
Zayed University, United Arab Emirates

REVIEWED BY

Song Wang,
Sichuan University, China
Xiufeng Xu,
The First Affiliated Hospital of Kunming Medical
University, China

*CORRESPONDENCE

Ling Xiao
✉ lingxiaoxiao@whu.edu.cn
Gaohua Wang
✉ wgh6402@whu.edu.cn

SPECIALTY SECTION

This article was submitted to
Mood Disorders,
a section of the journal
Frontiers in Psychiatry

RECEIVED 05 February 2023

ACCEPTED 15 March 2023

PUBLISHED 17 April 2023

CITATION

Rong B, Gao G, Sun L, Zhou M, Zhao H,
Huang J, Wang H, Xiao L and Wang G (2023)
Preliminary findings on the effect of childhood
trauma on the functional connectivity of the
anterior cingulate cortex subregions in major
depressive disorder.
Front. Psychiatry 14:1159175.
doi: 10.3389/fpsy.2023.1159175

COPYRIGHT

© 2023 Rong, Gao, Sun, Zhou, Zhao, Huang,
Wang, Xiao and Wang. This is an open-access
article distributed under the terms of the
[Creative Commons Attribution License
\(CC BY\)](https://creativecommons.org/licenses/by/4.0/). The use, distribution or reproduction
in other forums is permitted, provided the
original author(s) and the copyright owner(s)
are credited and that the original publication in
this journal is cited, in accordance with
accepted academic practice. No use,
distribution or reproduction is permitted which
does not comply with these terms.

Preliminary findings on the effect of childhood trauma on the functional connectivity of the anterior cingulate cortex subregions in major depressive disorder

Bei Rong^{1,2}, Guoqing Gao¹, Limin Sun^{1,2}, Mingzhe Zhou¹,
Haomian Zhao¹, Junhua Huang¹, Hanling Wang³, Ling Xiao^{1,2*}
and Gaohua Wang^{1,2,4*}

¹Department of Psychiatry, Renmin Hospital of Wuhan University, Wuhan, Hubei, China, ²Institute of Neuropsychiatry, Renmin Hospital of Wuhan University, Wuhan, Hubei, China, ³Xi'an Jiaotong-Liverpool University, Suzhou, Jiangsu, China, ⁴Taikang Center for Life and Medical Sciences, Wuhan University, Wuhan, Hubei, China

Objectives: Childhood trauma (CT) is a known risk factor for major depressive disorder (MDD), but the mechanisms linking CT and MDD remain unknown. The purpose of this study was to examine the influence of CT and depression diagnosis on the subregions of the anterior cingulate cortex (ACC) in MDD patients.

Methods: The functional connectivity (FC) of ACC subregions was evaluated in 60 first-episode, drug-naïve MDD patients (40 with moderate-to-severe and 20 with no or low CT), and 78 healthy controls (HC) (19 with moderate-to-severe and 59 with no or low CT). The correlations between the anomalous FC of ACC subregions and the severity of depressive symptoms and CT were investigated.

Results: Individuals with moderate-to-severe CT exhibited increased FC between the caudal ACC and the middle frontal gyrus (MFG) than individuals with no or low CT, regardless of MDD diagnosis. MDD patients showed lower FC between the dorsal ACC and the superior frontal gyrus (SFG) and MFG. They also showed lower FC between the subgenual/perigenual ACC and the middle temporal gyrus (MTG) and angular gyrus (ANG) than the HCs, regardless of CT severity. The FC between the left caudal ACC and the left MFG mediated the correlation between the Childhood Trauma Questionnaire (CTQ) total score and HAMD-cognitive factor score in MDD patients.

Conclusion: Functional changes of caudal ACC mediated the correlation between CT and MDD. These findings contribute to our understanding of the neuroimaging mechanisms of CT in MDD.

KEYWORDS

major depressive disorder, childhood trauma, resting state, functional connectivity, anterior cingulate cortex

Introduction

Major depressive disorder (MDD) is a prevalent psychiatric disease affecting approximately 15–18% of the general population around the world (1). Globally, depression was the leading contributor to disability in 2017 according to the World Health Organization, and its prevalence continues to increase (2). To date, the neurobiological mechanisms underlying depression remain incompletely characterized. Consequently, it is imperative to understand the neurobiological mechanisms of MDD and identify effective therapies for depression.

Neuroimaging studies point to the anterior cingulate cortex (ACC), a region involved in emotions, information processing, and regulation, which serves a vital role in the pathophysiology of depression (3, 4). Previously published studies ubiquitously found that abnormalities of gray matter volume (5–11), white matter volume (12, 13), and functional activity (14–17) of the ACC could be responsible for depression in MDD patients. In addition, accumulating evidence from previous studies indicated that the alterations in the structural and functional activity of ACC have emerged as a promising predictor of the effectiveness of depression treatment. For instance, the increased volume ratio of ACC was correlated to the improvement of depressive symptoms after ECT (18). After Cognitive Behavioral Therapy (CBT), the reduction in depressive symptoms was positively related to an increase in ACC volume (19). Additionally, changes in baseline metabolic activity in the ACC can also predict the effectiveness of antidepressant treatment (20). Evidence suggests that deep brain stimulation treatment targeted at white matter tracts adjacent to the subgenual ACC can relieve depression symptoms (21, 22). Thus, the structural and functional activity of ACC is crucial to the diagnosis, prognosis, and therapy of MDD.

There is wide recognition that childhood trauma (CT) contributes to MDD risk. Patients with depression who suffer maltreatment are more likely to develop chronic diseases and have worse treatment outcomes (23). In previous studies, the volume of ACC has been shown to be reduced in people with CT (24–28). These changes in the volume of ACC in CT are consistent with the findings reported in MDD studies (29), indicating that CT and MDD may be linked by the ACC. In spite of this, it remains unclear how CT affects MDD physiologically. Recently, there has been an increased focus on brain connectivity and how it relates to psychopathology as well as changes in gray matter structure and function (30, 31). By using functional magnetic resonance imaging (fMRI), we can detect the temporal organization of the functional brain circuits on a large scale organization of neural functional brain circuits by detecting temporally correlated, spontaneous variations in blood oxygen levels; this is also termed resting-state functional connectivity (rsFC) (32).

Previous evidence based on FC has suggested that MDD patients have extensively aberrant FC between the ACC and multiple areas of the brain (9, 14, 17). The structure and function of the ACC, however, are considered to be heterogeneous and can generally be divided into five subregions associated with distinct functions (33–35). Recent studies have investigated changes in ACC subregions in MDD (36–40). A previous study showed that the subregions of ACC (including subgenual, perigenual, and caudal ACC) exhibited a reduction in FC with the key hubs in

the default mode network (DMN), and a decreased FC of the caudal ACC to the precuneus has a negative link to depression symptoms (37). Additionally, a reduced FC of subgenual ACC to the middle frontal gyri (MFG) and inferior frontal gyri (IFG) has been related to rumination in medication-naïve, first-episode MDD adolescents (36). One study demonstrated that the FC of perigenual ACC-superior frontal gyrus (SFG) mediates the association between anhedonia and sleep quality in MDD patients (41). As a result, MDD may be characterized by the alteration of functional integration in subregions of the ACC. As with depression research, reduced subregions of ACC FC have been observed in individuals with CT, both clinically and non-clinically. Research on 64 late adolescents found that a higher level of CT was correlated to a lower FC of the subgenual ACC to the amygdala (42). However, a study of healthy adolescents found that adolescents with CT exhibited the reduced FC between the subgenual ACC and the fronto-parietal network (FPN) (including the dorsolateral prefrontal cortex (DLPFC), supramarginal gyrus (SMG), and cuneus) (43). In other studies, CT has been shown to be negatively associated with the FC of the rostral ACC to the amygdala and hippocampus (44, 45). These studies suggest that the alterations in the FC of ACC subregions were also related to the history of CT. To our knowledge, no studies have examined the alteration in the FC of ACC subregions in MDD patients with moderate-to-severe CT and with no or low CT.

This study aimed to investigate whether and how CT, current depression, and both affect FC patterns of ACC subregions in the first-episode, drug-naïve MDD patients compared with healthy controls (HCs). In addition, we also examined the association between the aberration in FC of ACC subregions and the severity of depressive symptoms. Finally, we explored the possible effect of ACC subregions FC in the associations between CT and depressive symptoms using a mediation analysis model.

Materials and methods

Participants

Sixty first-episode, drug-naïve MDD patients and 78 gender- and age-matched HC were included in the present study. All individuals with MDD were recruited from the department of psychiatry, Renmin Hospital of Wuhan University from April 2021 to July 2022. The recruitment of matched healthy control subjects was accomplished through advertisements. Patients were diagnosed using the Structured Clinical Interview for the Diagnostic and Statistical Manual of Mental Disorders (DSM-IV) (SCID). The 17-item Hamilton Depression Scale (HAMD-17) and 14-item Hamilton Anxiety Scale (HAMA) were used to measure the depression and anxiety levels of all participants. The inclusion criteria for MDD patients included: (1) meeting the DSM-IV diagnostic criteria for MDD, (2) having first-episode MDD with no history of treatment, including psychoactive drugs, psychotherapy, and so on, (3) being between the age of 18 and 65 years, (4) being right-handed, and (5) having a total score of HAMD-17 > 17. HCs were admitted to this study if they met the following criteria: (1) were without any major psychiatric illness and had no family history of major psychiatric illnesses, (2) were between the age of 18

and 65 years, and (3) were right-handed. Any participant who met any of the following criteria was excluded: (1) they were under the age of 18 or over 65 years old, (2) had a history of another DSM-IV Axis I psychiatric disorder, (3) had any neurological disorders or head injury, (4) had a substance abuse or dependency history, or (5) had other contraindications for imaging scanning. The five subscales of the HAMD-17 were scored as anxiety/somatization, weight, cognitive disturbance, retardation, and sleep disruption (46). The Chinese version of the Childhood Trauma Questionnaire (CTQ) was utilized to assess CT (47). It is a 28-item self-reported questionnaire that evaluates five aspects of childhood trauma, including emotional neglect (EN), physical neglect (PN), emotional abuse (EA), physical abuse (PA), and sexual abuse (SA). The cut-off scores of each subscale for moderate-to-severe trauma are: PN ≥ 10 , PA ≥ 10 , EN ≥ 15 , EA ≥ 13 , and SA ≥ 8 . In this study, individuals scoring above the subscale threshold (moderate-to-severe) were considered to have been exposed to corresponding CT (48). All participants provided informed consent for this study and were recruited. This current study received approval from the Ethics Committee of Renmin Hospital of Wuhan University.

MRI acquisition

All participants' imaging data were acquired on a 3.0T GE Signa HDx MRI scanner at Renmin Hospital of Wuhan University. In order to maintain motionlessness, participants were informed to keep their eyes closed and keep thinking of nothing special. High-resolution T1-weighted structural images were obtained by gradient-echo sequence: repetition time (TR) = 8.5 ms; echo time (TE) = 3.2 ms; flip angle = 12°; slice thickness = 1.0 mm; gap = 0.0 mm; field of view (FOV) = 256 mm \times 256 mm; matrix = 256 \times 256; voxel size = 1.0 mm \times 1.0 mm \times 1.0 mm; 176 slices. An echo planar imaging (EPI) sequence was used to acquire resting-state functional MRI data: TR = 2,000; TE = 30 ms; flip angle = 90°; voxel size = 3.4 mm \times 3.4 mm \times 4.0 mm; slice thickness = 4.0 mm; gap = 0 mm; FOV = 220 mm \times 220 mm; matrix = 64 \times 64; 36 slices; resulting in a total of 240 volumes acquired.

MRI data preprocessing

Preprocessing was carried out with Statistical Parametric Mapping (SPM12)¹ and Data Processing Assistant for Resting-State fMRI (DPARSF V5.2) (49). To ensure magnetization stability, the first 10 volumes of each participant were removed. Slice timing correction was conducted to account for interleaved acquisition. Functional images were realigned to correct the head motion. A participant with a maximum displacement over 3 mm or rotation over 3° was excluded from the analysis. Subject-wise 3D T1-weighted structural images were co-registered with the mean functional images. Subsequently, each participant's functional images were normalized to the standard Montreal Neurological Institute (MNI) space by using the transformation co-registered T1

to MNI space and resampled to 3.0 mm \times 3.0 mm \times 3.0 mm voxels. Spatial smoothing was performed using a 6 mm full-width half-maximum (FWHM) isotropic Gaussian kernel. Linear detrending was applied to remove low-frequency drift. Several confounding factors including WM signal, CSF signal, and Friston-24 head motion parameters were regressed to allow for minimal effects of possible motion-related confounds. A temporal bandpass filter at 0.01–0.1 Hz was applied to control physiological high-frequency noise. There were no subjects excluded for excessive head motion > 3 mm displacement or $> 3^\circ$.

Functional connectivity measurement

Using the DPABI toolbox, images were processed and then imported for seed-to-voxel FC analysis. In the present study, a total of 10 spherical regions of interest (ROIs) of 5 mm radius were identified for bilateral ACC, and bilateral caudal ACC (± 5 , -10 , 37), dorsal ACC (± 5 , 10, 33), rostral ACC (± 5 , 27, 21), perigenual ACC (± 5 , 47, 11), and subgenual ACC (± 5 , 34, -4) were created to examine the seed-based, whole-brain, voxel-wise functional connectivity patterns of each subregion of the ACC (34, 35). The map of the 10 ROIs is displayed in Figure 1. For each subject, the time series of all voxels within each ROI was extracted and subsequently averaged to calculate Pearson's correlation with the time series of all other voxels in the whole brain. Then Fisher's r -to- z transformation was utilized to ensure the normality of FC. Thus, each FC map of ROIs was obtained. Then two-sample t -test was utilized to compare the differences in the FC map of ROIs between the MDD and HC groups after controlling for confounders of gender, age, education, and head motion. The threshold $p < 0.001$ at the voxel level and $p < 0.05$ at the cluster level (two-tailed), with Gaussian random field (GRF) theory, was taken to indicate the statistical significance.

Statistical analysis

The Shapiro-Wilkes normality test and Levene's test were applied to evaluate variance distribution and homogeneity, respectively. Independent samples t -test or Mann-Whitney U test (for non-Gaussian distributions) were used to compare the demographic and behavioral variables between the two groups. One-way ANOVA test with Bonferroni-test or Welch-ANOVA with Games-Howell post-test (the variances were not equal) was used to evaluate demographic and behavioral variables comparisons among the four groups. The Chi-square test was applied to assess the gender differences. All the numerical data are expressed as the mean [standard deviation (SD)]. The significance level was set at $P < 0.05$ (SPSS 23.0; SPSS Inc., Chicago, IL, USA).

To separately test the main effect of diagnosis and CT level and the interaction between diagnosis and CT level on depression and anxiety level, 2 (diagnosis: MDD and HC) \times 2 (CT level: moderate-to-severe and no or low) two-way ANCOVAs were conducted, controlling for mean framewise displacement (FD). Demographic differences among the four groups were not significant.

¹ <http://www.fil.ion.ucl.ac.uk/spm>

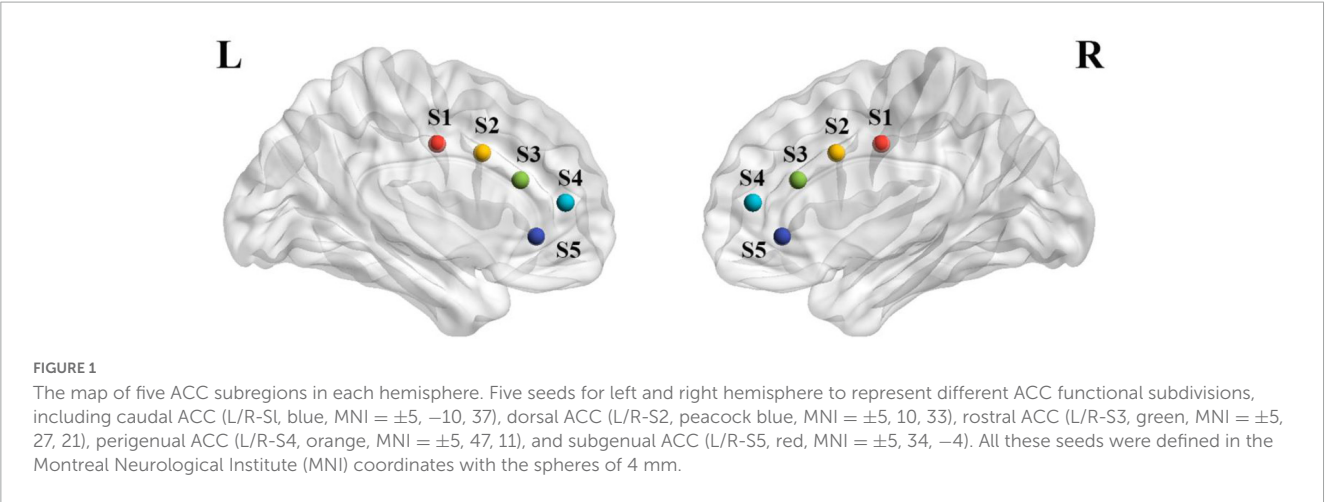


TABLE 1 Demographic and neuropsychiatric characteristics among four groups.

	MDD		HC			
	Moderate-to-severe CT (N = 40)	No or low CT (N = 20)	Moderate-to-severe CT (N = 19)	No or low CT (N = 59)	F/t/ χ^2	P
Demographic characteristics						
Age (years)	26.40 (5.38)	26.75 (8.81)	26.95 (7.83)	29.20 (8.94)	1.23 ^a	0.302
Gender (Male/female)	32 (80%)	16 (80%)	11 (57.89%)	42 (71.19%)	3.80 ^a	0.283
Education (years)	15.38 (1.73)	15.25 (2.97)	16.90 (2.18)	15.80 (2.30)	2.35 ^a	0.076
Mean FD (mm)	0.06 (0.04)	0.06 (0.03)	0.06 ± 0.03	0.06 (0.03)	0.02 ^a	0.997
Disease duration (month)	6.48 (4.12)	7.05 (4.27)	–	–	0.00	0.617
Clinical characteristics						
HAMD-17	26.55 (4.62)	24.90 (6.28)	1.68 (1.42)	0.90 (1.21)	706.55	<0.0011
HAMA	17.23 (2.87)	16.15 (2.52)	1.58 (2.12)	1.59 (1.78)	287.98	<0.0011
CTQ-EA	11.05 (4.38)	7.75 (2.17)	7.90 (3.07)	5.95 (1.41)	24.66	<0.0011
CTQ-PA	7.33 (2.77)	5.45 (0.76)	6.42 (3.11)	5.37 (0.61)	9.41	<0.00101
CTQ-SA	6.10 (2.57)	5.15 (0.67)	5.84 ± 2.85	5.15 (0.58)	3.26	0.032
CTQ-EN	16.38 (3.71)	9.85 (2.46)	11.05 (4.08)	8.14 (2.49)	66.35	<0.001
CTQ-PN	11.38 (3.59)	6.95 (1.85)	10.00 (2.67)	5.78 (1.25)	49.32	<0.001
CTQ-Total	52.26 (11.14)	35.15 (4.88)	41.21 ± 8.05	30.39 (4.18)	92.42	<0.001

Means with standard deviations in parentheses. F/t/ χ^2 : Variables of age, years of education, mean FD, HAMD-17, HAMA-14, and CTQ assessments were tested by one-way ANOVA or Welch-ANOVA as indicated by F; ^aanalysis by one-way ANOVA; gender was calculated using chi-square test as indicated by χ^2 ; disease duration was tested by two-sample *t*-test as indicated by *t*. Significant *post-hoc* tests (*p* < 0.05, Bonferroni corrected or Games–Howell corrected): HAMD-17: MDD_moderate-to-severe CT = MDD_no or low CT > HC_moderate-to-severe CT = HC_no or low CT; HAMA: MDD_moderate-to-severe CT = MDD_no or low CT > HC_moderate-to-severe CT = HC_no or low CT; CTQ-EA: MDD_moderate-to-severe CT > MDD_no or low CT = HC_moderate-to-severe CT > HC_no or low CT; CTQ-PA: MDD_moderate-to-severe CT = MDD_no or low CT = HC_moderate-to-severe CT = HC_no or low CT; CTQ-SA: MDD_moderate-to-severe CT > MDD_no or low CT = MDD_moderate-to-severe CT = HC_no or low CT; CTQ-EN: MDD_moderate-to-severe CT > MDD_no or low CT > HC_moderate-to-severe CT > HC_no or low CT; CTQ-PN: MDD_moderate-to-severe CT = HC_moderate-to-severe CT > MDD_no or low CT > HC_no or low CT; CTQ-Total: MDD_moderate-to-severe CT > HC_moderate-to-severe CT > MDD_no or low CT > HC_no or low CT. MDD, major depressive disorder; HC, healthy control; FD, frame displacement; HAMD-17, 17-items Hamilton Depression Scale; HAMA, Hamilton Anxiety Scale; CTQ-EA, Childhood Trauma Questionnaire-emotional abuse; CTQ-PA, Childhood Trauma Questionnaire-physical abuse; CTQ-SA, Childhood Trauma Questionnaire-sexual abuse; CTQ-EN, Childhood Trauma Questionnaire-emotional neglect; CTQ-PN, Childhood Trauma Questionnaire-physical neglect; CTQ-Total, Childhood Trauma Questionnaire total score.

Similarly, significant differences in the seed-to-voxel FC maps created by each seed among the four groups were investigated using 2 (diagnosis: MDD and HC) × 2 (CT level: moderate-to-severe, no or low) ANCOVAs, and gender, age, education level, and mean FD were included as covariates. Significant clusters for all maps comparisons were identified with a Gaussian random field (GRF) theory with a cluster level at *P* < 0.05 and a voxel-level threshold of *P* < 0.001 for multiple comparisons.

Partial correlations analysis was used to assess whether FCs were the main effect of CT level and were correlated with depressive levels, CTQ total score, and subscales score after controlling for age, gender, years of education, mean FD, and duration of illness (only in the MDD group). Multiple comparisons were performed using a False discovery rate (FDR) < 0.05. Then, mediation analysis was utilized by using Haye’s bootstrapping method (PROCESS macro based on SPSS model 4, utilizing 5000 bootstrap samples to estimate

the 95% confidence interval) (50) to test the influence of FC alterations in the subregions of ACC on the relationship between CT and depressive symptoms in the MDD group, controlling for gender, age, education level, and mean FD.

Results

Demographic and clinical characteristics

The demographic and clinical characteristics of the four groups are summarized in Table 1. No significant differences were found in age, gender, mean FD, and years of education among the four groups after Bonferroni correction ($p < 0.05/6 = 0.0083$) in this study. The disease duration has no difference between the MDD_moderate-to-severe CT group and MDD_no or low CT group.

Diagnosis and CT level effects on clinical variables

There was a significant main effect of diagnosis on all depressive and anxiety levels, with MDD patients exhibiting severe depressive and anxiety symptoms compared to the HCs. The main effect of CT was identified on the HAMD-17 total score, and the HAMD-cognitive disturbance factor indicated that the subjects with moderate-to-severe CT displayed higher levels of depressive and cognitive disturbance symptoms than those with no or low CT. The significant main effect of diagnosis and the interaction effect of diagnosis \times CT on HAMD total score was demonstrated only in the HC group; the individuals with moderate-to-severe CT exhibited higher levels of depressive symptoms than individuals with no or low CT. No significant main effect of CT or the interaction effect of diagnosis by CT on the HAMD-anxiety factor, HAMD-weight factor, HAMD-retardation factor, HAMD-sleep disorder factor, and HAMA were identified (Table 2).

Diagnosis and CT level effects on FC

For FCs from the bilateral caudate ACC, there was a significant main effect of CT. Individuals with moderate-to-severe CT independent of MDD diagnosis showed increased FC between bilateral caudate ACC and left middle frontal gyrus (MFG) (GRF correction with cluster-level at $P < 0.05$ and a voxel-level threshold of $P < 0.001$) (Figure 2). The main effect of diagnosis was significant (Figure 3). Patients with MDD exhibited decreased FC between the left caudal ACC and left MFG, right SFG, right supramarginal gyrus (SMG) and anterior cingulate cortex, supracallosal (ACCsup) (Figure 3A); between the right caudal ACC and right SFG, right SMG and left ACCsup (Figure 3B); between left dorsal ACC and left MFG, left ACCsup, right SFG and right SMG (Figure 3C); between right dorsal ACC and left MFG, right SFG and right SMG (Figure 3D); between left rostral ACC and left middle cingulate & paracingulate gyri (MCC) and left superior temporal gyrus (STG) (Figure 3E); between right rostral ACC and

TABLE 2 Diagnosis and childhood trauma effect on 17-items Hamilton Depression Scale (HAMD-17) and subscales.

Characteristics	MDD		HC		ANOVA					
	Moderate-to-severe CT	No or low CT	Moderate-to-severe CT	No or low CT	Effect of diagnosis			Effect of CT		
					F	P	Eta ²	F	P	Eta ²
HAMD-17	N = 40 26.55 (4.62)	N = 20 24.90 (4.50)	N = 19 2.05 (1.22)	N = 59 0.95 (1.20)	1237.50	<0.001	0.91	14.91	<0.001	0.10
HAMD-anxiety	6.85 (1.79)	6.70 (1.42)	0.79 (0.71)	0.46 (0.68)	467.93	<0.001	0.78	3.45	0.065	0.03
HAMD-weight	2.70 (1.57)	2.35 (1.66)	0.0 (0.00)	0.0 (0.00)	174.46	<0.001	0.57	0.84	0.362	0.01
HAMD-cognitive	5.20 (1.88)	4.85 (1.95)	0.47 (0.51)	0.10 (0.31)	520.92	<0.001	0.80	7.94	0.006	0.06
HAMD-retardation	7.60 (1.91)	7.30 (1.53)	0.31 (0.67)	0.10 (0.36)	1322.17	<0.001	0.91	3.72	0.056	0.03
HAMD-sleep	4.20 (1.49)	3.70 (1.69)	0.42 (0.69)	0.65 (0.08)	278.05	<0.001	0.68	2.50	0.12	0.02
HAMA	17.23 (2.87)	16.15 (2.52)	0.37 (0.68)	1.59 (1.78)	608.48	<0.001	0.82	0.31	0.58	0.00

Means with standard deviations in parentheses. HAMD-17, 17-items Hamilton Depression Scale; HAMD-anxiety, Hamilton Depression Scale-anxiety/somatization factor, a sum of item 10, 11, 12, 15 and 17 in HAMD-17; HAMD-weight, Hamilton Depression Scale-loss of the weight factor, item 16 in HAMD-17; HAMD-cognitive, Hamilton Depression Scale-cognitive disturbance factor, a sum of item 2, 3 and 9 in HAMD-17; HAMD-retardation, Hamilton Depression Scale-retardation factor, a sum of item 1, 7, 8 and 14 in HAMD-17; HAMD-sleep, Hamilton Depression Scale-sleep disorder factor, a sum of item 4, 5, and 6 in HAMD-17; HAMA, Hamilton Anxiety Scale; CT, childhood trauma; MDD, major depressive disorder patients; HC, healthy controls. *Further simple effects analysis suggested that only in the HC group, individuals with moderate-to-severe CT exhibited a higher level of depressive symptoms than individuals with no or low CT (HC_moderate-to-severe CT vs. HC_no or low CT; $p < 0.001$; MDD_moderate-to-severe CT vs. MDD_no or low CT; $p = 0.311$).

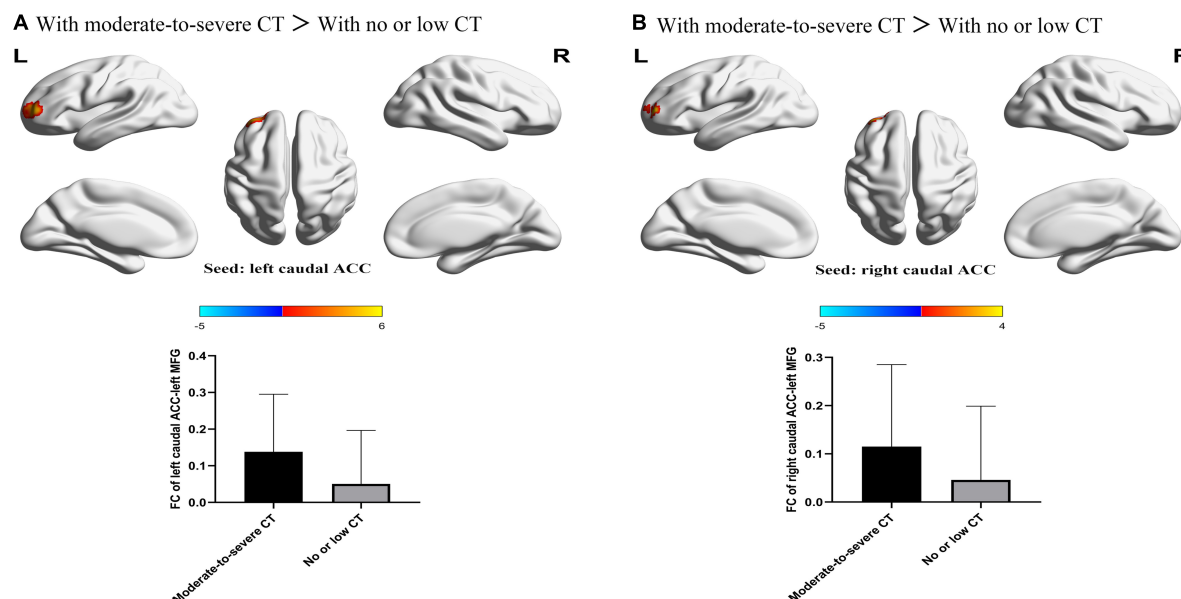


FIGURE 2

The significant main effect of CT level on FC between bilateral caudal ACC and the left MFG. (A) Individuals with a history of moderate-to-severe CT exhibited increased FC between the left caudal ACC seed and left MFG compared to individuals with no or low CT. (B) Individuals with a history of moderate-to-severe CT exhibited increased FC between the right caudal ACC and the left MFG compared to individuals with no or low CT. L, left; R, right; MDD, major depressive disorder; FC, functional connectivity; ACC, anterior cingulate cortex; MFG, middle frontal gyrus.

left MFG (Figure 3F); between left perigenual ACC and left middle temporal gyrus (MTG) and right angular gyrus (ANG) (Figure 3G); between left subgenual ACC and left MTG (Figure 3H). No other significant main effect or interactions of diagnosis-by-CT on FC could be identified (Table 3).

Correlation and mediation analysis in the MDD group

Given that the main effect of CT on HAMD-17 total score and HAMD-cognitive disturbance factor was detected, partial correlation and mediation analyses were performed to investigate the correlation between the altered FCs and the main effect of CT on the HAMD-17 total score and CTQ total score and subscales scores in MDD groups with age, gender, years of education, duration of illness, and mean FD included as covariates.

The FC between the left caudal ACC and the left MFG was positively correlated with CTQ-physical neglect score ($r = 0.400$, $p = 0.002$) (Figure 4A) and CTQ total score ($r = 0.352$, $p = 0.008$) (Figure 4B). The FC between the right caudal ACC and the left MFG was also positively correlated with CTQ-physical neglect score ($r = 0.444$, $p < 0.001$) (Figure 4C). The HAMD-cognitive score was positively correlated with CTQ total score ($r = 0.426$, $p < 0.001$) (Figure 4D). In the mediation analysis, the FC of left caudal ACC to left MFG partially mediates the relationship between CTQ total score and HAMD-cognitive disturbance factor in MDD patients (indirect effect: $\beta = -0.107$, bootstrapped 95% CI = -0.2155 to -0.0141 ; direct effect: $\beta = 0.493$, bootstrapped 95% CI = 0.2468 – 0.7448) with covariates of gender, age, education level, mean FD, and duration of illness; the FC of right caudal ACC to left MFG partially mediates the relationship between CTQ total

score and HAMD-cognitive disturbance factor in MDD patients (indirect effect: $\beta = -0.019$, bootstrapped 95% CI = -0.0407 to -0.002 ; direct effect: $\beta = 0.484$, bootstrapped 95% CI = 0.0429 – 0.1417) with covariates of gender, age, education level, mean FD, and duration of illness (Figure 5). The complete list of partial correlation and mediation analyses is presented in the [Supplementary material](#).

Discussion

This present study investigated the effects of CT severity and MDD on seed-to-voxel FC patterns of ACC subregions and the association among childhood trauma, altered FCs, and depressive symptoms. Our preliminary findings showed that there was a significant main effect of diagnosis and CT severity level, but no interaction effect between MDD and CT severity level on the FC of ACC subregions. Specifically, regardless of the diagnosis of MDD, individuals with moderate-to-severe CT exhibited increased FC between bilateral caudal ACC and left MFG relative to individuals with no or low CT. FC of the caudal ACC to MFG mediated the association between CTQ and the cognitive disturbance symptoms of MDD. In terms of the main effect of MDD diagnosis compared to the HC, the caudal ACC and dorsal ACC exhibited a reduction in FC within the regions of the cognitive control network (CCN), including the SFG, MFG, and SMG in MDD patients. In addition, the subgenual and perigenual ACC exhibited attenuated FC the ANG and MTG, which are the key regions of the DMN.

An important finding was that individuals with moderate to severe CT showed a significantly increased FC between the bilateral caudal ACC and MFG compared to the individuals with no or low CT. Caudal ACC plays a crucial role in conflict

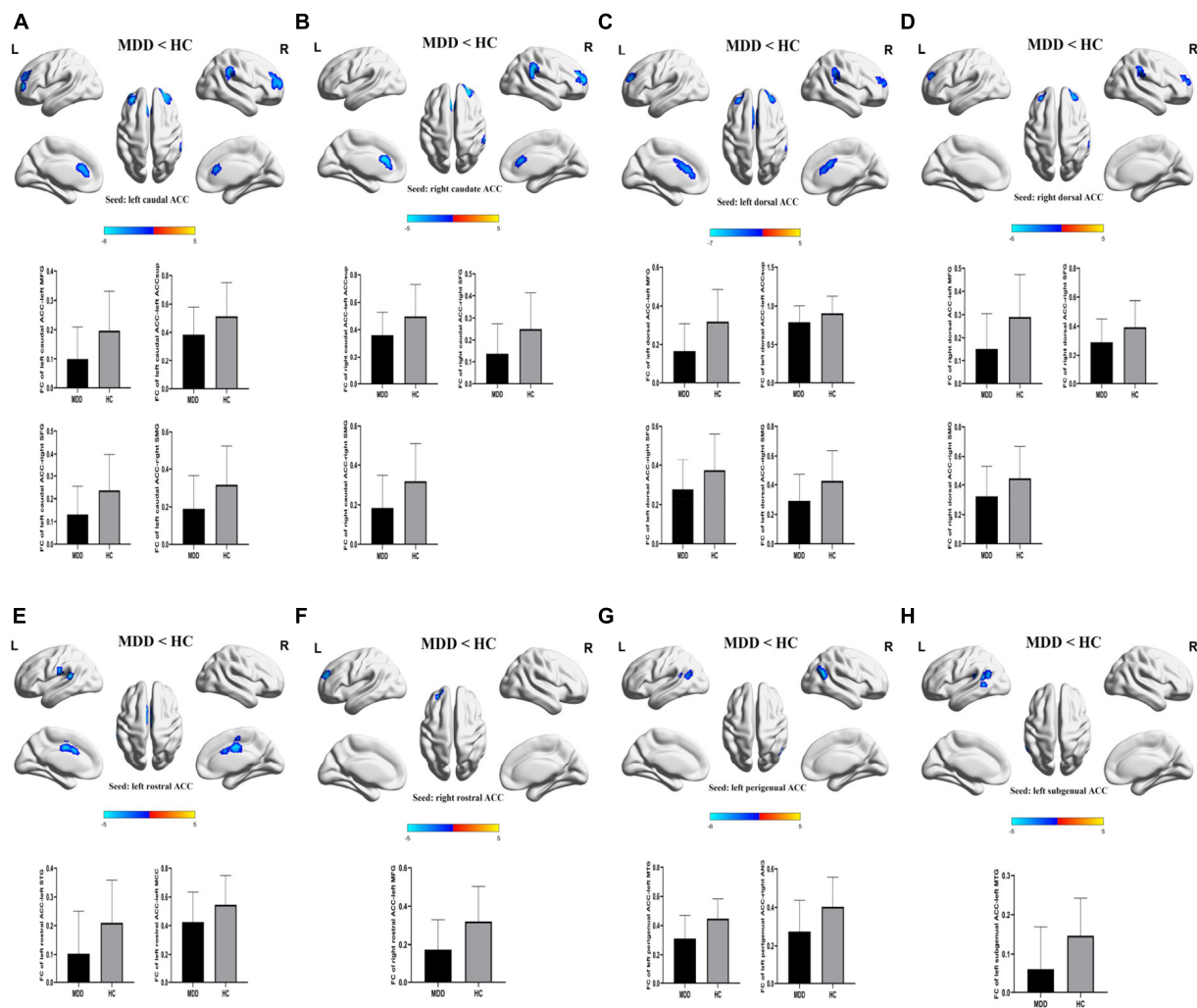


FIGURE 3

The significant main effect of diagnosis on FCs of ACC subregions. (A–H) MDD patients had decreased rsFCs of bilateral caudal ACC, bilateral dorsal ACC, bilateral rostral ACC, left perigenual ACC and left subgenual ACC compared to HC. Significance threshold was set at $p < 0.001$ at voxel level uncorrected, $p < 0.05$ at cluster level, with Gaussian random field correction (GRF). L, left; R, right; MDD, major depressive disorder; HC, healthy controls; FC, functional connectivity; CT, childhood trauma; ACC, anterior cingulate cortex; MFG, middle frontal gyrus; SFG, superior frontal gyrus; SMG, supra marginal gyrus; STG, superior temporal gyrus; MTG, middle temporal gyrus; ANG, angular gyrus. ACCsup, anterior cingulate cortex, supracallosal; MCC, middle cingulate & paracingulate gyri.

monitoring (51–53). MFG, which is part of the dorsolateral prefrontal cortex, is mainly involved in higher-order cognitive functions such as working memory and executive control (54). An influential theoretical framework proposed that the ACC detects potential conflicts and subsequently relays them to the DLPFC to implement execution control processes (55, 56). Stress and emotion-processing brain regions may be permanently altered as a result of traumatic experiences in childhood, resulting in greater sensitivity to stressful situations in adulthood (57). Higher FC between the caudal ACC and DLPFC may represent high demands of executive control function (decreased neural efficiency/greater effort) in individuals with moderate and severe CT. This finding indicated that individuals exposed to a higher level of CT often require a greater level of behavioral flexibility to adapt to changing environments and come up with alternate solutions to problems. The findings of this study are in agreement with those of several previous studies. Mueller et al. (58) reported that adolescents with

early-life stress exhibited increased activity in brain regions related to executive control. Moreover, we found there is no alteration of FC in other ACC subdivisions in individuals with CT, suggesting that CCN might be a potential biomarker for CT.

In contrast to the increased FC of the left caudal ACC to the left MFG, our results demonstrated decreased FC of the left caudal ACC to the left MFG. Having minimal executive control is associated with emotional regulation difficulties, ruminating, and a reduction in social skills, which are all predictive of psychopathology (59). Thus, the caudal ACC and MFG connectivity disruptions may impair executive control function and lead to rumination in MDD patients. Combining the above findings, the difference in FC patterns between the caudal ACC and MFG may hint at maltreatment-related changes in executive control networks and not just an epiphenomenon of concurrent MDD (60). Moreover, we also found that the FC between the caudal ACC and DLPFC partially mediated the

TABLE 3 Diagnosis and childhood trauma effects on functional connectivity of anterior cingulate cortex (ACC) subregions.

Seeds	Regions	BA	Cluster size	Peak MNI coordinates			Peak T-value
				X	Y	Z	
CT main effect							
With moderate-to-severe CT > with no or low CT							
L-caudal ACC	L-MFG	10	190	−42	57	9	5.3987
R-caudal ACC	L-MFG	10	81	−42	57	12	3.744
Diagnosis main effect							
MDD HC							
L-caudal ACC	L-MFG	10	245	−33	51	33	−5.6905
	R-SFG	10	287	30	48	12	−5.0098
	R-SMG	40	137	63	−36	30	−4.6357
	L-ACCsup	24	103	0	27	18	−4.3193
R-caudal ACC	R-SFG	10	200	30	57	15	−4.7783
	R-SMG	40	194	63	−36	33	−4.4833
	L-ACCsup	24	110	−3	24	18	−4.4963
L-dorsal ACC	L-MFG	10	126	−33	51	33	−6.331
	L-ACCsup	24	146	0	9	33	−4.7657
	R-SFG	10	108	33	45	21	−4.3784
	R-SMG	40	132	63	−33	27	−3.9664
R-dorsal ACC	L-MFG	10	79	−33	51	33	−5.5866
	R-SFG	10	91	30	48	21	−4.3912
	R-SMG	40	88	63	−33	36	−3.8902
L-rostral ACC	L-MCC	24	250	3	−9	39	−4.3242
	L-STG	22	116	−60	−39	15	−4.1172
R-rostral ACC	L-MFG	10	105	−33	51	33	−4.706
L-perigenual	R-ANG	39	149	57	−63	24	−5.5247
	L-MTG	21	109	−63	−57	21	−4.3724
L-subgenual	L-MTG	39	124	−48	−39	18	−4.2393

MDD, major depressive disorder; HC, healthy control; L, left; R, right; ACC, anterior cingulate cortex; SFG, superior frontal gyrus; MFG, middle frontal gyrus; SMG, supramarginal gyrus; STG, superior temporal gyrus; MTG, middle temporal gyrus; ANG, angular gyrus; ACCsup, anterior cingulate cortex supracallosal; MCC, middle cingulate & paracingulate gyri.

CTQ total score and HAMD-cognitive disturbance factor. This mediation analysis indicated that the impairment of executive control function caused by childhood trauma may embed latent vulnerability to MDD.

In our current study, compared with HCs, MDD patients showed a reduction in FC between the bilateral dorsal ACC and left MFG, right SFG and right SMG. Dorsal ACC is responsible for coordinating and integrating information to guide behavior. The SFG and MFG are located within the DLPFC that is involved in planning complex cognitive behavior, making decisions, and regulating emotions (61). The SMG is a part of the inferior parietal lobule (IPL). The CCN, which is mainly responsible for aspects of cognitive processing such as working memory, decision-making, and attentional allocation, is composed of the dorsal ACC, DLPFC, and IPL (62–65). The reduction in FC between the dorsal ACC and left MFG, right SFG and right SMG indicates a functional disruption within the CCN in MDD patients, which may contribute to MDD patients' difficulty in ignoring negative valence and stimuli from entering

and remaining in the working memory, leading to rumination, which is a core feature of MDD (31). These findings are consistent with prior studies (16, 66, 67). Furthermore, previous studies have observed that the increased metabolic CCN is responsible for the remission of depression (66, 68, 69). This suggested that the important role of dACC activity in depression physiopathology.

This present study demonstrated that both attenuated FC between the perigenual/subgenual ACC and MTG and reduction in FC between the perigenual ACC and ANG were found in MDD patients relative to HCs. The perigenual and subgenual ACC belong to the affective division of the ACC, which is an essential component of the affective network (AN) (70). The AN is presumed to be involved in emotional processing including fear, vigilance, and autonomic and visceral regulation (71, 72). The MTG and ANG are key hubs of the DMN which is responsible for emotion regulation, future planning, and self-observation (73). In MDD, the decreased FC between the subgenual/perigenual ACC and MTG can disrupt the communication of the AN to the DMN and result in emotional

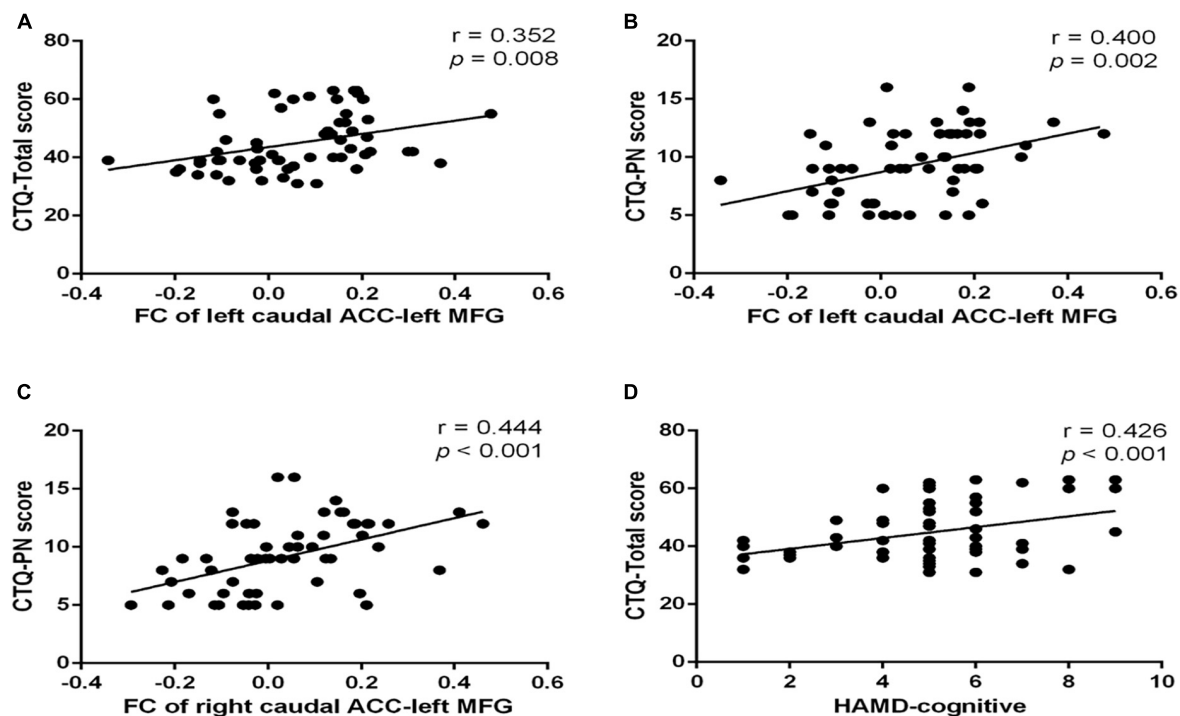


FIGURE 4

Scatter plots of partial correlation between significant FC and the target scales in MDD group. (A) Positive partial correlation between FC of left caudal ACC to left MFG and CTQ total score. (B) Positive partial correlation between FC of left caudal ACC to left MFG and CTQ-Physical neglect score. (C) Positive partial correlation between FC of right caudal ACC to left MFG and CTQ-Physical neglect score. (D) Positive partial correlation between HAMD-cognitive and CTQ-Total score. All correlations showed in this figure were constructed after controlling gender, age, years of education, duration of illness, and mean frame displacement value. MDD, major depressive disorder; FC, functional connectivity; CTQ, Childhood Trauma Questionnaire; CTQ-EN, emotional neglect subscale of childhood trauma questionnaire; CTQ-PN, physical neglect subscale of childhood trauma questionnaire; ACC, anterior cingulate cortex; MFG, middle frontal gyrus.

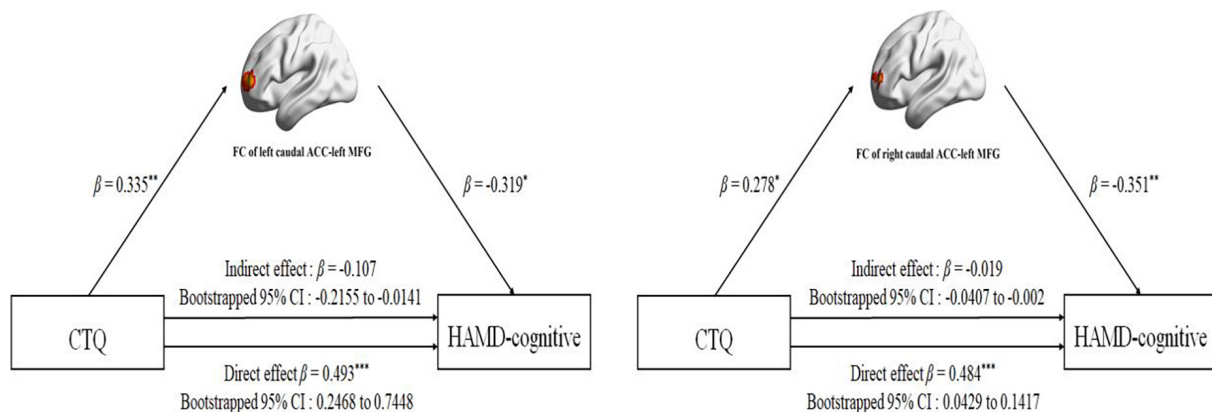


FIGURE 5

Mediation analysis for effect of the FC between bilateral caudal ACC and left MFG on the relationship between childhood traumatic (CTQ total score) and HAMD-cognitive disturbance factor (HAMD-cognitive score) in MDD group. For the path coefficient: * $p < 0.05$; ** $p < 0.01$; *** $p < 0.001$. CTQ, Childhood Trauma Questionnaire; HAMD-cognitive, Hamilton Depression Scale-cognitive disturbance factor; FC, functional connectivity; ACC, anterior cingulate cortex; MFG, middle frontal gyrus; β , standardized regression coefficient; CI, confidence interval.

regulation deficits. Several previous studies have supported these observations. One researcher found that MDD patients showed decreased subgenual ACC FC with the MTG; angular gyrus and posterior cingulate cortex (PCC) were related to higher depressive symptoms (74). Peng et al. (37) found a reduction in FC between the perigenual ACC and the DMN.

Currently, this is the first study examining the effect of MDD and CT on the FC of ACC subregions in MDD patients and HCs (with moderate-to-severe and with no or low CT). We used this study design to investigate separately as well as jointly the effects of MDD and CT on the FC of ACC subregions. Moreover, all MDD patients were medication-naïve,

removing the possibility of medication effects confounding the results. However, this study has several limitations. The severity of trauma was primarily determined by self-reported CTQ score, which may be influenced by recall bias; however, recent studies have demonstrated that subjective self-reported maltreatment is a reliable predictor of psychopathology (75). Since the results presented in the current study are based on the ROI-based FC, we may overlook potential findings. Other ROI-free FC analysis methods [e.g., functional connectivity density (FCD) (76)] should be considered in future studies. Neuroticism is an important risk factor for the development of MDD. A recent meta-analysis demonstrated that neuroticism was positively correlated with the activity of the subgenual ACC (77). Future studies should assess CT and the level of neuroticism in MDD patients, and then clarify more clearly the effect of CT on ACC functional activities in MDD without the influence of neuroticism. These findings should be interpreted with caution due to the relatively small samples of subjects in the MDD patients with low or no CT and HCs with moderate-to-severe CT groups; thus, it is recommended that more patients be included in future studies. Moreover, a high level of anxiety symptoms in MDD patients might have possibly affected these results in the current study; however, there was no significant correlation between the HAMA scores and the ACC subregions FC. Patients with depression without anxiety symptoms should be recruited to validate the findings of the current study in the future. Finally, this study is cross-sectional, which makes causality determination difficult; a longitudinal design would be particularly helpful in future research to clarify the way CT affects depression onset.

Conclusion

In summary, this study investigated the FC of ACC subdivisions in first-episode, drug-naïve MDD patients with moderate-to-severe and with no or low CT. Compared to the HCs, MDD patients showed decreased FC of the caudal ACC/dorsal ACC and the regions of the CCN (SFG, MFG, and SMG), and reduction in FC between the subgenual/perigenual ACC and the key regions of the DMN (ANG and MTG) indicated that depression might be caused by abnormal functional interactions between the brain areas in both the DMN and CCN. Individuals with moderate-to-severe CT demonstrated an increased FC of caudal ACC-MFG, indicating that the disrupted functional integration of caudal ACC may be characteristic of CT. Furthermore, enhanced FC of caudal ACC-MFG mediated the association between CT and depression, suggesting that the aberrant functional integration between caudal ACC and MFG is pivotal in understanding the link between depression and CT. In light of these findings, it may be possible to develop a better understanding of the roles of specific ACC subregions in MDD pathophysiology and the neurophysiological basis of the association between CT and MDD.

Data availability statement

The original contributions presented in this study are included in the article/**Supplementary material**, further inquiries can be directed to the corresponding authors.

Ethics statement

The studies involving human participants were reviewed and approved by the Ethics Committee of the Renmin Hospital of Wuhan University (WDRY2020-K236). The patients/participants provided their written informed consent to participate in this study.

Author contributions

GW and LX designed the current study. BR drafted the manuscript. BR, GG, LS, MZ, HZ, and JH performed the experiments. BR and HW analyzed the data. BR, GG, LX, and GW revised the manuscript. All authors read and approved the final manuscript.

Funding

This study was supported by the National Natural Science Foundation of China (Nos. 81871072 and 82071523), the Medical Science Advancement Program of Wuhan University (No. TFLC2018001), and the Key Research and Development Program of Hubei Province (2020BCA064).

Acknowledgments

The authors gratefully acknowledge Ning Tu in PET-CT/MRI Center, Renmin Hospital of Wuhan University for extensive time and effort in data acquisition.

Conflict of interest

The authors declare that the research was conducted in the absence of any commercial or financial relationships that could be construed as a potential conflict of interest.

Publisher's note

All claims expressed in this article are solely those of the authors and do not necessarily represent those of their affiliated organizations, or those of the publisher, the editors and the reviewers. Any product that may be evaluated in this article, or claim that may be made by its manufacturer, is not guaranteed or endorsed by the publisher.

Supplementary material

The Supplementary Material for this article can be found online at: <https://www.frontiersin.org/articles/10.3389/fpsyt.2023.1159175/full#supplementary-material>

References

- Kessler R, Bromet E. The epidemiology of depression across cultures. *Annu Rev Public Health*. (2013) 34:119–38. doi: 10.1146/annurev-publhealth-031912-114409
- WHO. *Depression and Other Common Mental Disorders: Global Health Estimates*. Geneva: World Health Organization (2017).
- Botvinick M, Cohen J, Carter C. Conflict monitoring and anterior cingulate cortex: an update. *Trends Cogn Sci*. (2004) 8:539–46. doi: 10.1016/j.tics.2004.10.003
- Pizzagalli D. Frontocingulate dysfunction in depression: toward biomarkers of treatment response. *Neuropsychopharmacology*. (2011) 36:183–206. doi: 10.1038/npp.2010.166
- Arnone D, McIntosh A, Ebmeier K, Munafo M, Anderson I. Magnetic resonance imaging studies in unipolar depression: systematic review and meta-regression analyses. *Eur Neuropsychopharmacol*. (2012) 22:1–16. doi: 10.1016/j.euroneuro.2011.05.003
- Belleau E, Treadway M, Pizzagalli D. The impact of stress and major depressive disorder on hippocampal and medial prefrontal cortex morphology. *Biol Psychiatry*. (2019) 85:443–53. doi: 10.1016/j.biopsych.2018.09.031
- Riva-Posse P, Holtzheimer P, Mayberg H. Cingulate-mediated depressive symptoms in neurologic disease and therapeutics. *Handb Clin Neurol*. (2019) 166:371–9. doi: 10.1016/B978-0-444-64196-0.00021-2
- Caetano S, Kaur S, Brambilla P, Nicoletti M, Hatch J, Sassi R, et al. Smaller cingulate volumes in unipolar depressed patients. *Biol Psychiatry*. (2006) 59:702–6. doi: 10.1016/j.biopsych.2005.10.011
- Schmaal L, Hibar D, Sämann P, Hall G, Baune B, Jahanshad N, et al. Cortical abnormalities in adults and adolescents with major depression based on brain scans from 20 cohorts worldwide in the ENIGMA major depressive disorder working group. *Mol Psychiatry*. (2017) 22:900–9. doi: 10.1038/mp.2016.60
- Yucel K, McKinnon M, Chahal R, Taylor V, Macdonald K, Joffe R, et al. Anterior cingulate volumes in never-treated patients with major depressive disorder. *Neuropsychopharmacology*. (2008) 33:157–63. doi: 10.1038/npp.2008.40
- Ibrahim H, Kulikova A, Ly H, Rush A, Sherwood Brown E. Anterior cingulate cortex in individuals with depressive symptoms: a structural MRI study. *Psychiatry Res*. (2022) 319:111420. doi: 10.1016/j.psychres.2021.111420
- Ballmaier M, Toga A, Blanton R, Sowell E, Lavretsky H, Peterson J, et al. Anterior cingulate, gyrus rectus, and orbitofrontal abnormalities in elderly depressed patients: an MRI-based parcellation of the prefrontal cortex. *Am J Psychiatry*. (2004) 161:99–108. doi: 10.1176/appi.ajp.161.1.99
- Olvet D, Delaparte L, Yeh F, DeLorenzo C, McGrath P, Weissman M, et al. A comprehensive examination of white matter tracts and connectometry in major depressive disorder. *Depress Anxiety*. (2016) 33:56–65. doi: 10.1002/da.22445
- Zhu X, Wang X, Xiao J, Liao J, Zhong M, Wang W, et al. Evidence of a dissociation pattern in resting-state default mode network connectivity in first-episode, treatment-naïve major depression patients. *Biol Psychiatry*. (2012) 71:611–7. doi: 10.1016/j.biopsych.2011.10.035
- Ye T, Peng J, Nie B, Gao J, Liu J, Li Y, et al. Altered functional connectivity of the dorsolateral prefrontal cortex in first-episode patients with major depressive disorder. *Eur J Radiol*. (2012) 81:4035–40. doi: 10.1016/j.ejrad.2011.04.058
- Wu X, Lin P, Yang J, Song H, Yang R, Yang J. Dysfunction of the cingulo-opercular network in first-episode medication-naïve patients with major depressive disorder. *J Affect Disord*. (2016) 200:275–83. doi: 10.1016/j.jad.2016.04.046
- Rolls E, Cheng W, Gong W, Qiu J, Zhou C, Zhang J, et al. Functional connectivity of the anterior cingulate cortex in depression and in health. *Cereb Cortex*. (2019) 29:3617–30. doi: 10.1093/cercor/bhy236
- Ota M, Noda T, Sato N, Okazaki M, Ishikawa M, Hattori K, et al. Effect of electroconvulsive therapy on gray matter volume in major depressive disorder. *J Affect Disord*. (2015) 186:186–91. doi: 10.1016/j.jad.2015.06.051
- Fujino J, Yamasaki N, Miyata J, Sasaki H, Matsukawa N, Takemura A, et al. Anterior cingulate volume predicts response to cognitive behavioral therapy in major depressive disorder. *J Affect Disord*. (2015) 174:397–9. doi: 10.1016/j.jad.2014.12.009
- Arnone D. Functional MRI findings, pharmacological treatment in major depression and clinical response. *Prog Neuropsychopharmacol Biol Psychiatry*. (2019) 91:28–37. doi: 10.1016/j.pnpbp.2018.08.004
- Riva-Posse P, Choi K, Holtzheimer P, Crowell A, Garlow S, Rajendra J, et al. A connectomic approach for subcallosal cingulate deep brain stimulation surgery: prospective targeting in treatment-resistant depression. *Mol Psychiatry*. (2018) 23:843–9. doi: 10.1038/mp.2017.59
- Mayberg H, Riva-Posse P, Crowell A. Deep brain stimulation for depression: keeping an eye on a moving target. *JAMA Psychiatry*. (2016) 73:439–40. doi: 10.1001/jamapsychiatry.2016.0173
- Wiersma J, Hovens J, Van Oppen P, Giltay E, Van Schaik D, Beekman A, et al. The importance of childhood trauma and childhood life events for chronicity of depression in adults. *J Clin Psychiatry*. (2009) 70:983–9. doi: 10.4088/JCP.08m04521
- Cohen R, Grieve S, Hoth K, Paul R, Sweet L, Tate D, et al. Early life stress and morphometry of the adult anterior cingulate cortex and caudate nuclei. *Biol Psychiatry*. (2006) 59:975–82. doi: 10.1016/j.biopsych.2005.12.016
- Dannlowski U, Stuhrmann A, Beutelmann V, Zwanzger P, Lenzen T, Grotegerd D, et al. Limbic scars: long-term consequences of childhood maltreatment revealed by functional and structural magnetic resonance imaging. *Biol Psychiatry*. (2012) 71:286–93. doi: 10.1016/j.biopsych.2011.10.021
- Wang L, Dai Z, Peng H, Tan L, Ding Y, He Z, et al. Overlapping and segregated resting-state functional connectivity in patients with major depressive disorder with and without childhood neglect. *Hum Brain Mapp*. (2014) 35:1154–66. doi: 10.1002/hbm.22241
- Teicher M, Samson J. Annual research review: enduring neurobiological effects of childhood abuse and neglect. *J Child Psychol Psychiatry*. (2016) 57:241–66. doi: 10.1111/jcpp.12507
- Kelly P, Viding E, Wallace G, Schaer M, De Brito S, Robustelli B, et al. Cortical thickness, surface area, and gyrification abnormalities in children exposed to maltreatment: neural markers of vulnerability? *Biol Psychiatry*. (2013) 74:845–52. doi: 10.1016/j.biopsych.2013.06.020
- Koolschijn P, van Haren N, Lensvelt-Mulders G, Hulshoff Pol H, Kahn R. Brain volume abnormalities in major depressive disorder: a meta-analysis of magnetic resonance imaging studies. *Hum Brain Mapp*. (2009) 30:3719–35. doi: 10.1002/hbm.20801
- Krug S, Müller T, Kayali Ö, Leichter E, Peschel S, Jahn N, et al. Altered functional connectivity in common resting-state networks in patients with major depressive disorder: a resting-state functional connectivity study. *J Psychiatr Res*. (2022) 155:33–41. doi: 10.1016/j.jpsychires.2022.07.040
- Kaiser R, Andrews-Hanna J, Wager T, Pizzagalli D. Large-scale network dysfunction in major depressive disorder: meta-analysis of resting-state functional connectivity. *JAMA Psychiatry*. (2015) 72:603–11. doi: 10.1001/jamapsychiatry.2015.0071
- Power J, Schlaggar B, Petersen S. Recent progress and outstanding issues in motion correction in resting state fMRI. *Neuroimage*. (2015) 105:536–51. doi: 10.1016/j.neuroimage.2014.10.044
- Öngür D, Ferry A, Price J. Architectonic subdivision of the human orbital and medial prefrontal cortex. *J Comp Neurol*. (2003) 460:425–49. doi: 10.1002/cne.10609
- Kelly A, Di Martino A, Uddin L, Shehzad Z, Gee D, Reiss P, et al. Development of anterior cingulate functional connectivity from late childhood to early adulthood. *Cereb Cortex*. (2009) 19:640–57. doi: 10.1093/cercor/bhn117
- Margulies D, Kelly A, Uddin L, Biswal B, Castellanos F, Milham M. Mapping the functional connectivity of anterior cingulate cortex. *Neuroimage*. (2007) 37:579–88. doi: 10.1016/j.neuroimage.2007.05.019
- Connolly C, Wu J, Ho T, Hoeft F, Wolkowitz O, Eisendrath S, et al. Resting-state functional connectivity of subgenual anterior cingulate cortex in depressed adolescents. *Biol Psychiatry*. (2013) 74:898–907. doi: 10.1016/j.biopsych.2013.05.036
- Peng X, Wu X, Gong R, Yang R, Wang X, Zhu W, et al. Sub-regional anterior cingulate cortex functional connectivity revealed default network subsystem dysfunction in patients with major depressive disorder. *Psychol Med*. (2021) 51:1687–95. doi: 10.1017/S0033291720000434
- Reynolds S, Carrey N, Jaworska N, Langevin L, Yang X, Macmaster F. Cortical thickness in youth with major depressive disorder. *BMC Psychiatry*. (2014) 14:83. doi: 10.1186/1471-244X-14-83
- Wu Z, Wang C, Ma Z, Pang M, Wu Y, Zhang N, et al. Abnormal functional connectivity of habenula in untreated patients with first-episode major depressive disorder. *Psychiatry Res*. (2020) 285:112837. doi: 10.1016/j.psychres.2020.112837
- Zhou Y, Shi L, Cui X, Wang S, Luo X. Functional connectivity of the caudal anterior cingulate cortex is decreased in autism. *PLoS One*. (2016) 11:e0151879. doi: 10.1371/journal.pone.0151879
- Wu Z, Fang X, Yu L, Wang D, Liu R, Teng X, et al. Abnormal functional connectivity of the anterior cingulate cortex subregions mediates the association between anhedonia and sleep quality in major depressive disorder. *J Affect Disord*. (2022) 296:400–7. doi: 10.1016/j.jad.2021.09.104
- Herrington R, Birn R, Ruttle P, Burghy C, Stodola D, Davidson R, et al. Childhood maltreatment is associated with altered fear circuitry and increased internalizing symptoms by late adolescence. *Proc Natl Acad Sci USA*. (2013) 110:19119–24. doi: 10.1073/pnas.1310766110
- Hoffmann E, Viding E, Puetz V, Gerin M, Sethi A, Rankin G, et al. Evidence for depressogenic spontaneous thoughts and altered resting-state connectivity in adolescents with a maltreatment history. *J Am Acad Child Adolesc Psychiatry*. (2018) 57:687–95.e4. doi: 10.1016/j.jaac.2018.05.020
- Birn R, Patriat R, Phillips M, Germain A, Herrington R. Childhood maltreatment and combat posttraumatic stress differentially predict fear-related fronto-subcortical connectivity. *Depress Anxiety*. (2014) 31:880–92. doi: 10.1002/da.22291

45. Kaiser R, Clegg R, Goer F, Pechtel P, Beltzer M, Vitaliano G, et al. Childhood stress, grown-up brain networks: corticolimbic correlates of threat-related early life stress and adult stress response. *Psychol Med.* (2018) 48:1157–66. doi: 10.1017/S0033291717002628
46. Maier W, Philipp M, Gerken A. [Dimensions of the Hamilton depression scale. Factor analysis studies]. *Eur Arch Psychiatry Neurol Sci.* (1985) 234:417–22. doi: 10.1007/BF00386061
47. Zhao X, Zhang Y, Li L, Zhou Y, Li H, Yang S. Reliability and validity of the Chinese version of childhood trauma questionnaire. *Chin J Clin Rehabil.* (2005) 9:105–7.
48. Fink L, Bernstein D. *Childhood Trauma Questionnaire: A Retrospective Self-Report Manual.* San Antonio, TX: The Psychological Corporation (1998).
49. Chao-Gan Y, Yu-Feng Z. DPARSF: a MATLAB toolbox for “pipeline” data analysis of resting-state fMRI. *Front Syst Neurosci.* (2010) 4:13. doi: 10.3389/fnsys.2010.00013
50. Hayes A, Rockwood N. Regression-based statistical mediation and moderation analysis in clinical research: observations, recommendations, and implementation. *Behav Res Ther.* (2017) 98:39–57. doi: 10.1016/j.brat.2016.11.001
51. Fan J, Hof P, Guise K, Fossella J, Posner M. The functional integration of the anterior cingulate cortex during conflict processing. *Cereb Cortex.* (2008) 18:796–805. doi: 10.1093/cercor/bhm125
52. Haas B, Omura K, Constable R, Canli T. Interference produced by emotional conflict associated with anterior cingulate activation. *Cogn Affect Behav Neurosci.* (2006) 6:152–6. doi: 10.3758/cabn.6.2.152
53. Mansouri F, Tanaka K, Buckley M. Conflict-induced behavioural adjustment: a clue to the executive functions of the prefrontal cortex. *Nat Rev Neurosci.* (2009) 10:141–52. doi: 10.1038/nrn2538
54. Arnsten A. Stress weakens prefrontal networks: molecular insults to higher cognition. *Nat Neurosci.* (2015) 18:1376–85. doi: 10.1038/nn.4087
55. Botvinick M, Braver T, Barch D, Carter C, Cohen J. Conflict monitoring and cognitive control. *Psychol Rev.* (2001) 108:624–52. doi: 10.1037/0033-295x.108.3.624
56. Kerns J, Cohen J, MacDonald A, Cho R, Stenger V, Carter C. Anterior cingulate conflict monitoring and adjustments in control. *Science.* (2004) 303:1023–6. doi: 10.1126/science.1089910
57. Zhai Z, Yip S, Lacadie C, Sinha R, Mayes L, Potenza M. Childhood trauma moderates inhibitory control and anterior cingulate cortex activation during stress. *Neuroimage.* (2019) 185:111–8. doi: 10.1016/j.neuroimage.2018.10.049
58. Mueller S, Maheu F, Dozier M, Peloso E, Mandell D, Leibenluft E, et al. Early-life stress is associated with impairment in cognitive control in adolescence: an fMRI study. *Neuropsychologia.* (2010) 48:3037–44. doi: 10.1016/j.neuropsychologia.2010.06.013
59. Snyder H, Miyake A, Hankin B. Advancing understanding of executive function impairments and psychopathology: bridging the gap between clinical and cognitive approaches. *Front Psychol.* (2015) 6:328. doi: 10.3389/fpsyg.2015.00328
60. McCrory E, Gerin M, Viding E. Annual research review: childhood maltreatment, latent vulnerability and the shift to preventative psychiatry—the contribution of functional brain imaging. *J Child Psychol Psychiatry.* (2017) 58:338–57. doi: 10.1111/jcpp.12713
61. John J, Wang L, Moffitt A, Singh H, Gado M, Csernansky J. Inter-rater reliability of manual segmentation of the superior, inferior and middle frontal gyri. *Psychiatry Res.* (2006) 148:151–63. doi: 10.1016/j.psychres.2006.05.006
62. Carter C, van Veen V. Anterior cingulate cortex and conflict detection: an update of theory and data. *Cogn Affect Behav Neurosci.* (2007) 7:367–79. doi: 10.3758/cabn.7.4.367
63. Dutta A, McKie S, Deakin J. Resting state networks in major depressive disorder. *Psychiatry Res.* (2014) 224:139–51. doi: 10.1016/j.psychres.2014.10.003
64. Miller E. The prefrontal cortex and cognitive control. *Nat Rev Neurosci.* (2000) 1:59–65. doi: 10.1038/35036228
65. Vincent J, Kahn I, Snyder A, Raichle M, Buckner R. Evidence for a frontoparietal control system revealed by intrinsic functional connectivity. *J Neurophysiol.* (2008) 100:3328–42. doi: 10.1152/jn.90355.2008
66. Alexopoulos G, Hoptman M, Kanellopoulos D, Murphy C, Lim K, Gunning F. Functional connectivity in the cognitive control network and the default mode network in late-life depression. *J Affect Disord.* (2012) 139:56–65. doi: 10.1016/j.jad.2011.12.002
67. Joermann J. Cognitive inhibition and emotion regulation in depression. *Curr Dir Psychol Sci.* (2010) 19:161–6. doi: 10.1177/0963721410370293
68. Drevets W. Neuroimaging studies of mood disorders. *Biol Psychiatry.* (2000) 48:813–29. doi: 10.1016/s0006-3223(00)01020-9
69. Fitzgerald P, Oxley T, Laird A, Kulkarni J, Egan G, Daskalakis Z. An analysis of functional neuroimaging studies of dorsolateral prefrontal cortical activity in depression. *Psychiatry Res.* (2006) 148:33–45. doi: 10.1016/j.psychres.2006.04.006
70. Bush G, Luu P, Posner M. Cognitive and emotional influences in anterior cingulate cortex. *Trends Cogn Sci.* (2000) 4:215–22. doi: 10.1016/S1364-6613(00)01483-2
71. Johansen-Berg H, Gutman D, Behrens T, Matthews P, Rushworth M, Katz E, et al. Anatomical connectivity of the subgenual cingulate region targeted with deep brain stimulation for treatment-resistant depression. *Cereb Cortex.* (2008) 18:1374–83. doi: 10.1093/cercor/bhm167
72. Mayberg H, Liotti M, Brannan S, McGinnis S, Mahurin R, Jerabek P, et al. Reciprocal limbic-cortical function and negative mood: converging PET findings in depression and normal sadness. *Am J Psychiatry.* (1999) 156:675–82. doi: 10.1176/ajp.156.5.675
73. Raichle M. The brain’s default mode network. *Annu Rev Neurosci.* (2015) 38:433–47. doi: 10.1146/annurev-neuro-071013-014030
74. Strikwerda-Brown C, Davey C, Whittle S, Allen N, Byrne M, Schwartz O, et al. Mapping the relationship between subgenual cingulate cortex functional connectivity and depressive symptoms across adolescence. *Soc Cogn Affect Neurosci.* (2015) 10:961–8. doi: 10.1093/scan/nsu143
75. Danese A, Widom C. Objective and subjective experiences of child maltreatment and their relationships with psychopathology. *Nat Hum Behav.* (2020) 4:811–8. doi: 10.1038/s41562-020-0880-3
76. Wang S, Zhao Y, Li J. True grit and brain: trait grit mediates the connection of DLPFC functional connectivity density to posttraumatic growth following COVID-19. *J Affect Disord.* (2023) 325:313–20. doi: 10.1016/j.jad.2023.01.022
77. Lin J, Li L, Pan N, Liu X, Zhang X, Suo X, et al. Neural correlates of neuroticism: a coordinate-based meta-analysis of resting-state functional brain imaging studies. *Neurosci Biobehav Rev.* (2023) 146:105055. doi: 10.1016/j.neubiorev.2023.105055



OPEN ACCESS

EDITED BY

Liang Gong,
Chengdu Second People's Hospital, China

REVIEWED BY

Igor D. Bandeira,
Stanford University, United States
Masaru Tanaka,
University of Szeged (ELKH-SZTE), Hungary

*CORRESPONDENCE

Jianqiao Fang
✉ fangjianqiao7532@163.com
Xiaomei Shao
✉ 13185097375@163.com;
✉ shaoxiaomei@zcmu.edu.cn

[†]These authors have contributed equally to this work and share the first authorship

RECEIVED 08 March 2023

ACCEPTED 27 April 2023

PUBLISHED 15 May 2023

CITATION

Wu X, Tu M, Chen N, Yang J, Jin J, Qu S, Xiong S, Cao Z, Xu M, Pei S, Hu H, Ge Y, Fang J and Shao X (2023) The efficacy and cerebral mechanism of intradermal acupuncture for major depressive disorder: a study protocol for a randomized controlled trial.
Front. Psychiatry 14:1181947.
doi: 10.3389/fpsyt.2023.1181947

COPYRIGHT

© 2023 Wu, Tu, Chen, Yang, Jin, Qu, Xiong, Cao, Xu, Pei, Hu, Ge, Fang and Shao. This is an open-access article distributed under the terms of the [Creative Commons Attribution License \(CC BY\)](https://creativecommons.org/licenses/by/4.0/). The use, distribution or reproduction in other forums is permitted, provided the original author(s) and the copyright owner(s) are credited and that the original publication in this journal is cited, in accordance with accepted academic practice. No use, distribution or reproduction is permitted which does not comply with these terms.

The efficacy and cerebral mechanism of intradermal acupuncture for major depressive disorder: a study protocol for a randomized controlled trial

Xiaoting Wu^{1,2†}, Mingqi Tu^{1,2†}, Nisang Chen^{1,2}, Jiajia Yang³, Junyan Jin^{1,2}, Siying Qu^{1,2}, Sangsang Xiong^{1,2}, Zhijian Cao³, Maosheng Xu³, Shuangyi Pei², Hantong Hu², Yinyan Ge², Jianqiao Fang^{2*} and Xiaomei Shao^{1,2*}

¹Key Laboratory for Research of Acupuncture Treatment and Transformation of Emotional Diseases, The Third Clinical Medical College, Zhejiang Chinese Medical University, Hangzhou, China, ²The Third Affiliated Hospital of Zhejiang Chinese Medical University, Hangzhou, China, ³The First Affiliated Hospital of Zhejiang Chinese Medical University, Hangzhou, China

Background: Major depressive disorder (MDD) has emerged as the fifth leading cause of years lived with disability, with a high prevalent, affecting nearly 4% of the global population. While available evidence suggests that intradermal acupuncture may enhance the effectiveness of antidepressants, whether its efficacy is a specific therapeutic effect or a placebo effect has not been reported. Moreover, the cerebral mechanism of intradermal acupuncture as a superficial acupuncture (usually subcutaneous needling to a depth of 1–2mm) for MDD remains unclear.

Methods: A total of 120 participants with MDD will be enrolled and randomized to the waiting list group, sham intradermal acupuncture group and active intradermal acupuncture group. All 3 groups will receive a 6-week intervention and a 4-week follow-up. The primary outcome will be measured by the Hamilton Depression Rating Scale-17 and the secondary outcome measures will be the Self-Rating depression scale and Pittsburgh sleep quality index. Assessments will be conducted at baseline, 3weeks, 6weeks, and during the follow-up period. In addition, 20 eligible participants in each group will be randomly selected to undergo head magnetic resonance imaging before and after the intervention to explore the effects of intradermal acupuncture on brain activity in MDD patients.

Discussion: If the intradermal acupuncture is beneficial, it is promising to be included in the routine treatment of MDD.

Clinical Trial Registration: [Clinicaltrials.gov](https://clinicaltrials.gov), NCT05720637.

KEYWORDS

major depressive disorder, intradermal acupuncture, cerebral mechanism, magnetic resonance imaging, magnetic resonance spectroscopy, selective serotonin reuptake inhibitors

Background

Major depressive disorder (MDD) is a mental disorder characterized by behavioral, cognitive, and emotional changes. It has emerged as the fifth leading cause of years lived with disability (GBD 2016 Disease and Injury Incidence and Prevalence Collaborators, 2017), affecting nearly 4% of the global population with an annual incidence of approximately 290 million cases (1). Symptoms of MDD include low self-esteem, loss of interest or pleasure, social withdrawal, poor concentration, insomnia, poor appetite or overeating, and in severe cases, self-harm and suicide (2, 3). Given its chronicity and high relapse rate, MDD is difficult to treat and has a serious long-term impact on the quality of life of patients. It has been regarded as a major public health concern.

Given the complexity of genetic and environmental factors, several hypotheses for the pathogenesis of MDD have been derived. Available evidence suggests that genetic mutations, oxidative stress, chronic inflammation, peripheral hormone-type factors dysregulation, and neurotransmitter dysfunction (e.g., serotonin 5-HT) may drive the development of MDD (4–6). For example, in a chronic mild stress model of MDD, structural damage in the hippocampus, hypothalamus and cortex could be observed, which may have contributed to the depression-like behavior (7–9). The prefrontal cortex (PFC) plays a critical role in the interaction between the central and the autonomic nervous system (10, 11). Dysfunction of the PFC results in impairment of emotional memory circuits and aversive learning, followed by chemical dysregulation, ultimately leading to cognitive changes and disturbed behavioral responses in MDD (12, 13). What is more, the monoamine hypothesis is widely regarded as the prevailing theory in the pathogenesis of MDD, with particular emphasis on the 5-HT hypothesis (14, 15). This point that reduced 5-HT levels increase the risk of developing MDD, which provides the underlying rationale for selective serotonin reuptake inhibitor (SSRI) as the frontline antidepressant (4, 16). Nevertheless, a recent systematic review has cast doubt on the consistency of evidence suggesting that MDD is linked to or caused by decreased 5-HT activity (17). Notably, long-term antidepressant administration may even lead to a decrease in plasma 5-HT, adding to the confusion surrounding the actual relationship between MDD and 5-HT (18–20).

When it comes to the treatment of MDD, it is based on symptom control and devoted to restoring the patient's psychological and physical function to baseline levels (21). Clinical evidence-based treatments for MDD consist of antidepressants such as selective serotonin reuptake inhibitors (SSRIs), as well as psychological interventions such as counseling, behavioral activation, cognitive behavioral therapy, and interpersonal therapy (22, 23). Generally, SSRIs are the frontline antidepressant for MDD with overall effectiveness, but they have some limitations, including delayed onset,

inadequate response, side effects, drug resistance, or withdrawal syndromes in long-term use, which negatively impact treatment outcomes (24, 25). Or worse, instead of achieving remission, some patients exacerbate emotional or somatic symptoms, increasing the risk of comorbidities (26, 27). While newer antidepressants, such as Vilazodone and Vortioxetine, may improve the tolerability and efficacy with a lower risk of adverse effects, they are often prohibitively expensive and not available in generic formulations, making it challenging to meet the daily needs of MDD patients (2, 28). Hence, given the limitations of current antidepressants, there is a pressing need for new (combination) treatments that can improve efficacy and safety.

One such treatment option is acupuncture, a component of Traditional Chinese Medicine that has been used internationally for the treatment of MDD (29, 30). Treatment with acupuncture alone or in combination with appropriate adjuncts has been reported to be significantly effective in reducing the severity of MDD, relieving patients' somatic symptoms, and improving sleep (31, 32). Compared to SSRIs-only, acupuncture combined with SSRIs for MDD has a faster onset of effect and fewer side effects (33). Despite these promising findings, the quality of these studies was poor. As noted by the Cochrane review, there was no evidence of differences in adverse effects between acupuncture and control acupuncture/usual treatment in most studies (29). Moreover, effect expectations and placebo effects have not been clearly elucidated, and these might lead to an overestimation of the actual therapeutic effects of acupuncture. In this way, it is essential to evaluate the effect expectations, integrity of blinding, incidence of adverse events rate, and treatment adherence in both the acupuncture and controls to improve the quality of the study.

Among the various acupuncture methods, intradermal acupuncture (IA) is a treatment method that uses short indwelling needles retained under the skin to produce continuous stimulation for long-lasting efficacy (34). This method is characterized by its ease of operation, painlessness, convenience, and negligible interference with the patient's daily activities. It can facilitate patient compliance and treatment effectiveness, making it an ideal choice for treating chronic diseases such as insomnia and MDD (34, 35). Evidence from studies supported that IA can significantly reduce the Pittsburgh sleep quality index (PSQI) scale scores and effectively improve insomnia symptoms (35, 36). Insomnia is one of the key risk factors for MDD, and while IA has been studied for its efficacy in alleviating insomnia, there is limited research on its therapeutic effects and mechanisms on MDD (37, 38). One preliminary clinical study revealed that IA could improve Beck Depression Inventory scores in patients with MDD (37), and another demonstrated that at 2 weeks after the intervention, patients in the AIA combined with SSRIs group showed a significant decrease in the Hamilton Depression Rating Scale-17 (HAMD-17) and the Self-Rating Depression Scale (SDS) scores compared to the SIA combined with SSRIs group, indicating that IA enhanced the antidepressant efficacy of SSRIs (38). However, both studies had limitations such as small sample sizes, short observation periods, and no investigation of medication side effects. Thus, high-quality clinical studies on the efficacy of IA for MDD are still lacking.

Functional magnetic resonance imaging (fMRI) is a common neuroimaging method with characteristics of non-invasive, non-radiation exposure and high spatial resolution for observing

Abbreviations: MDD, Major depressive disorder; IA, Intradermal acupuncture; AIA, Active intradermal acupuncture; SIA, Sham intradermal acupuncture; SSRIs, Selective serotonin reuptake inhibitors; RCT, Randomized controlled trial; MRI, Magnetic resonance imaging; rs-fMRI, Resting state-functional MRI; MRS, Magnetic resonance spectroscopy; HAMD-17, Hamilton depression rating scale-17; SDS, Self-Rating depression scale; PSQI, Pittsburgh sleep quality index; ACC, Anterior cingulate cortex; PFC, Prefrontal cortex.

brain activity in human (39). There are 3 methods to analyze fMRI data to present the homogeneity and spontaneous activity of the brain: functional connectivity (FC) describes the synchronicity between different regions, while regional homogeneity (ReHo) and amplitude of low frequency fluctuation (ALFF) describe the homogeneity and intensity of regional activity, respectively (40). In MDD, emotion-related brain regions mainly include the PFC, anterior cingulate cortex (ACC), amygdala, hippocampus, and hypothalamus. Compared to healthy controls, MDD patients showed abnormalities in these regions in ALFF, ReHo, and FC, which may be related to the development and severity of MDD (41–44). These findings suggest that impaired function of specific brain regions may be associated with the development and severity of MDD. In addition, abnormal levels of γ -aminobutyric acid (GABA) and glutamate acid (Glu) have been found in the ventral PFC/ACC of MDD patients based on magnetic resonance spectroscopy (MRS), an fMRI-based technique commonly used to detect levels of multiple neurotransmitters or metabolites in the brain (45, 46).

However, there were few studies on the therapeutic mechanisms of IA and no neuroimaging evidence. As previously mentioned, fMRI has been used not only to observe activity in specific brain regions in MDD patients, but also to quantify the brain response induced by acupuncture for MDD in an attempt to illuminate the cerebral mechanism (47). Importantly, the activity in brain regions such as the ACC, hypothalamus, amygdala and dorsolateral PFC, was found to be positively correlated with the efficacy of acupuncture for MDD, suggesting that acupuncture can improve depressive symptoms by modulating brain networks (47–49). What this evidence focused on, however, was the cerebral mechanism of manual and electroacupuncture for MDD, and not IA. To date, there has been no report on whether the cerebral mechanisms of IA as superficial acupuncture (usually needling to a depth of 1–2 mm subcutaneously) for MDD are consistent with those of deep acupuncture. Previous studies have revealed that the effects of acupuncture are strongly influenced by the depth of needling, as the cutaneous and deep tissues innervated by the somatosensory system show different densities of innervation (50, 51). Additionally, Feng et al. analyzed the brain network connectivity in patients with mild cognitive impairment who received deep or superficial stimulation using fMRI, and found significant differences in correlations between specific brain regions (52). These studies have provided insight into the differing mechanisms of treatment with deep and superficial acupuncture. As such, the antidepressant mechanism of IA needs to be further explored.

Together, we design a randomized controlled trial (RCT) with two aims. First, the clinical efficacy and safety of AIA for MDD will be evaluated by comparing with the SIA/waiting list. Second, the effects of AIA on brain activity of MDD patients will be detected by fMRI and MRS, and the correlation between the effects and clinical variables will be analyzed to initially explore the cerebral mechanisms of AIA on MDD.

Methods

This study is a 10-week trial with a randomized block method in which patients with MDD will be allocated in a balanced ratio (1:1:1). This study protocol is reported based on the Standard Protocol Items:

Recommendations for Intervention Trials (SPIRIT) statement. More, this study has been approved by the Medical Ethics Committee of the Third Affiliated Hospital of Zhejiang Chinese Medical University (approval number: ZSLL-KY-2022-001-01-01), and is registered within the [ClinicalTrials.gov](https://clinicaltrials.gov) Identifier: NCT05720637.

Study design

This study is a double-blind, randomized controlled trial. Participants will be randomized into waiting list group (patients in this group will be treated with SSRIs only), sham intradermal acupuncture combined with SSRIs (SIA) group and active intradermal acupuncture combined with SSRIs (AIA) group in a 1:1:1 allocation ratio. The flow chart shown in [Figure 1](#) illustrates the trial in more detail.

Setting

The trial will be conducted at the Third Affiliated Hospital of Zhejiang Chinese Medical University, Tongde Hospital of Zhejiang Province and Hangzhou First People's Hospital.

Participant recruitment

A total of 120 eligible participants will be recruited from three centers. The recruitment will be advertised online or offline and participants can contact the researcher via WeChat or telephone. Eligible volunteers will be invited to participate in the study. After confirming the details of the study process, they will sign an informed consent form and undergo a baseline assessment.

Sample size

Combining the relevant literature with our preliminary pre-experiment, it was predicted that the mean reduction in HAMD for each group at the end of the intervention would be 12.1, 9.7, and 9.5 with standard deviations of 2.7, 3.7, and 3.2, respectively. When $\alpha = 0.05$, $1 - \beta = 0.9$ and the sample sizes of the 3 groups are equal, a sample size of 32 per group is calculated using the PASS 15 software. Allowing for the possibility of loss and attrition (20%), 40 subjects per group, for a total of 120, is reasonable.

In addition, relatively stable results could be obtained in neuroimaging studies with 20 subjects per group (53, 54). Therefore, 20 eligible subjects from each group will be randomly selected and undergo head MRI scans before and after the intervention.

Eligibility criteria

Inclusion criteria

Participants with all of the following criteria will be included:

- (1) Patients diagnosed with MDD according to the International Classification of Disease-10 (ICD-10); HAMD-17 ≥ 17 ;

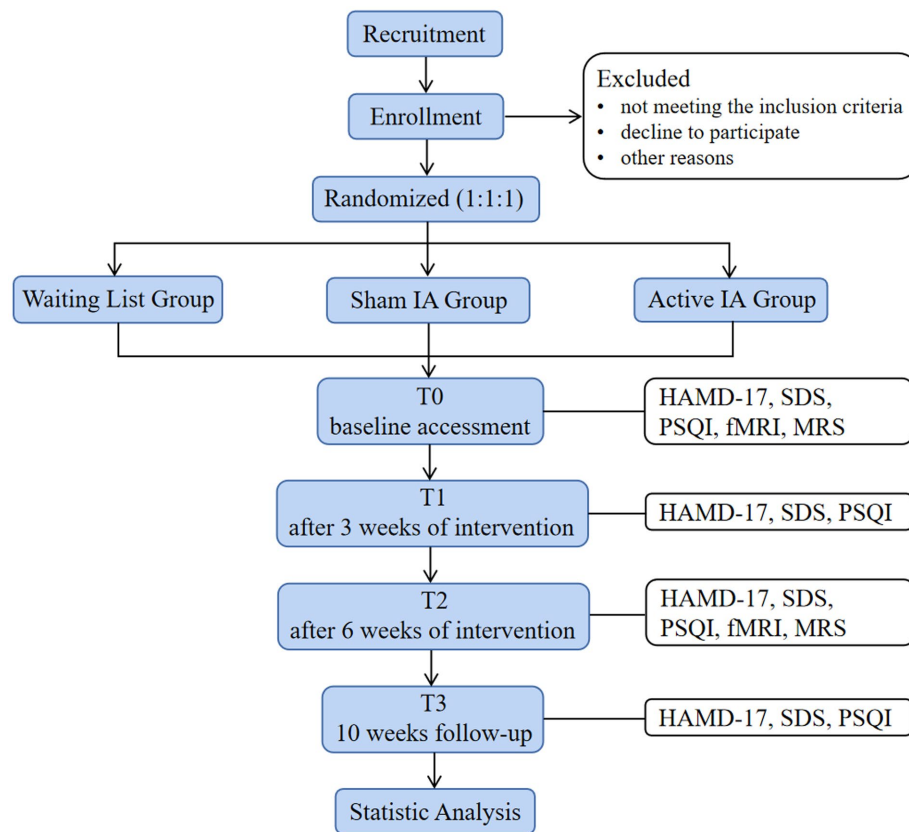


FIGURE 1
Flowchart of this study.

- (2) Aged between 18 and 60 years (no limitation on gender);
- (3) Administration of SSRIs at least 6 weeks;
- (4) Patients undergoing MRI and MRS should be right-handed and free of traumatic brain injury, claustrophobia or metal implants;
- (5) Written informed consent is obtained by the person.

Exclusion criteria

Participants with any of the following criteria will be excluded:

- (1) ICD-10 diagnoses: schizophrenia, bipolar disorder, manic episode or other psychotic disorders; alcohol and drug addiction; a current substance use disorder and lifetime history of substance abuse;
- (2) Significant skin lesions, severe allergic diseases, tumors, and severe or unstable internal diseases involving the cardiovascular, digestive, endocrine, or hematological system;
- (3) Positive suicidal tendency (suicidal intent and recent suicidal behavior) is determined by any affirmative response to items 5 or 6b or 7b of the Columbia-suicide severity rating scale;
- (4) Allergy to adhesive tape, fear of intradermal acupuncture;
- (5) Pregnancy and lactation;
- (6) Mental retardation and difficulty cooperating with doctors;
- (7) Previously treated with intradermal acupuncture or participating in other clinical trials.

Withdrawal criteria and management

Withdrawal or dropout criteria

- (1) Serious adverse reactions or other unexpected events that make continued participation in the study inappropriate.
- (2) Difficulty in cooperation and poor compliance.
- (3) Participants use a treatment that is prohibited in this study or does not follow medical advice to change the dose of medication.
- (4) Participants have a serious adverse reaction related to acupuncture treatment.
- (5) Participants voluntarily withdraw from the study, but those receiving more than 1/2 session should be counted in the efficacy statistics.

Withdrawal management

Details of all withdrawn participants should be recorded on the case report files (CRF) to ensure credibility and transparency. For participants who withdraw due to adverse reactions or unexpected events, the researcher should make a detailed record on the CRF and the psychiatrist should take appropriate measures according to the participant's actual condition. Once participants are enrolled in the trial in order, those receiving more than 1/2 sessions should be counted in the efficacy statistics. An intentionality analysis will be conducted on all eliminated and withdrawn participants.

Randomization and allocation concealment

Eligible participants will be assigned to the waiting list group, SIA group and AIA group with a random block scheme using SPSS 25 (SPSS Inc., Chicago, IL, United States) software, which will be stratified by the sex and age. The block size will adopt 6. Then, the random numbers will be placed in sealed envelopes by an independent assistant, and provided to the participants after the baseline assessment.

Blinding

Participants, outcome assessors and statisticians will be blinded to the group allocation. Due to the proprietary treatment modalities of acupuncture, it is not possible to blind acupuncturists, and therefore they will be instructed not to communicate with participants about the treatment allocation. Acupuncture will be performed in an isolatable room to avoid communication between participants, thus ensuring a good implementation of the blinding method.

Intervention

Medication administration and acupuncture will be performed by certified psychiatrists and acupuncturists, respectively. Acupuncturists will receive specific training to fully understand the standardized operation, including acupoints selection and positioning, acupuncture manipulation and frequency.

Antidepressant medication

All eligible participants will be treated with oral SSRIs. Before being included, participants should have been taking SSRIs for at least 6 weeks to achieve stable antidepressant treatment, and those who do not respond well to SSRIs will be excluded. For participants not taking SSRIs before this trial, the medication dose will be increased to the recommended level (20 mg/d for fluoxetine, paroxetine and citalopram, 10 mg/d for escitalopram, 50 mg/d for sertraline and 100 mg/d for fluvoxamine) (55). This dosing regimen has been widely used in China. If the participant tolerates the initial SSRI medication poorly, the psychiatrist will switch the prescription to another SSRI according to the medication protocol, and they should be in an antidepressant regimen stable before enrollment. Moreover, the researcher should not change the antidepressant regimen during the trial. Although temporary administration of Valium is allowed, it should be approved by a psychiatrist and recorded in detail on the CRFs. Participants will be instructed to keep a medication diary for the psychiatrist to assess compliance with treatment.

Waiting list

Participants randomly assigned to the waiting list group will be treated with SSRIs only for 6 weeks, they could choose 6 weeks' intradermal acupuncture treatments free of charge after the clinical trial.

Active intradermal acupuncture

Participants randomly assigned to the AIA group will receive an acupuncture intervention for approximately 6 weeks, once every 4 days, for a total of 10 times. In Traditional Chinese Medicine (TCM) theory, the principles of treatment for MDD are dispersing stagnated hepatoqi and tranquilize the mind. Therefore, 4 commonly used acupoints (all taken bilaterally) with such effects will be selected as targets in this trial, namely Shenmen (HT7), Neiguan (PC6), Sanyinjiao (SP6) and Taichong (LR3); (Figure 2). Depending on the location of the acupoint, a $\phi 0.20 \times 1.5$ mm or $\phi 0.20 \times 1.2$ mm AIA (SEIRIN Co., Japan) will puncture perpendicularly and retained in the skin. It will be retained for 72 h and removed and rested for 1 day. During the retention period, participants will be asked to apply pressure 3–4 times a day for approximately 1 min at 4-h intervals, stimulating as much as tolerated (Table 1).

Sham intradermal acupuncture

The SIA (SEIRIN Co., Japan) has the same size, color and material as the AIA, but with a thin silicone pad in the middle instead of a needle body (Figure 3). SIA will also be attached to the acupoints and retained for 72 h, then removed for a day's rest (Table 1). A total of 10 treatments will be administered over 6 weeks.

Outcomes

Table 2 shows details of assessments at enrollment, allocation, treatment, and follow-up periods.

Primary outcome

Changes in the Hamilton Depression Rating Scale-17 (HAMD-17) Scores.

In this trial, changes in HAMD-17 scores measured between baseline and 6 weeks of treatment will be defined as the primary outcome. The HAMD-17 is used to assess the severity of clinical depressive symptoms and the effectiveness of treatment before and after clinical trials (56, 57). It includes anxiety/somatization, cognitive impairment, retardation, sleep disorder and weight changes. A higher HAMD-17 score indicates a greater severity of MDD symptoms, which are classified into the following four levels: 0–7 is normal, 8–16 is mild, 17–23 is moderate and 24 or more is severe (58).

Secondary outcome

Secondary outcomes are MDD symptoms, sleep quality and adverse events during the intervention. They include the changes in SDS (week 3, 6 and 10) and PSQI (week 3, 6 and 10) compared to the baseline period. Also, changes from baseline in HAMD-17 scores at weeks 3 and 10 will be measured.

The SDS items are chosen based on depression symptom factor analytic investigations (59). The standard score is the total of all scores multiplied by 1.25 to the nearest whole number on this scale, which has 20 questions. The SDS is designed in such a way that the less depressed patients' chief complaint scores are lower, while the more depressed patients' chief complaint scores are higher. A standard score below 50 is normal; 50–59 is mild; 60–69 is moderate;

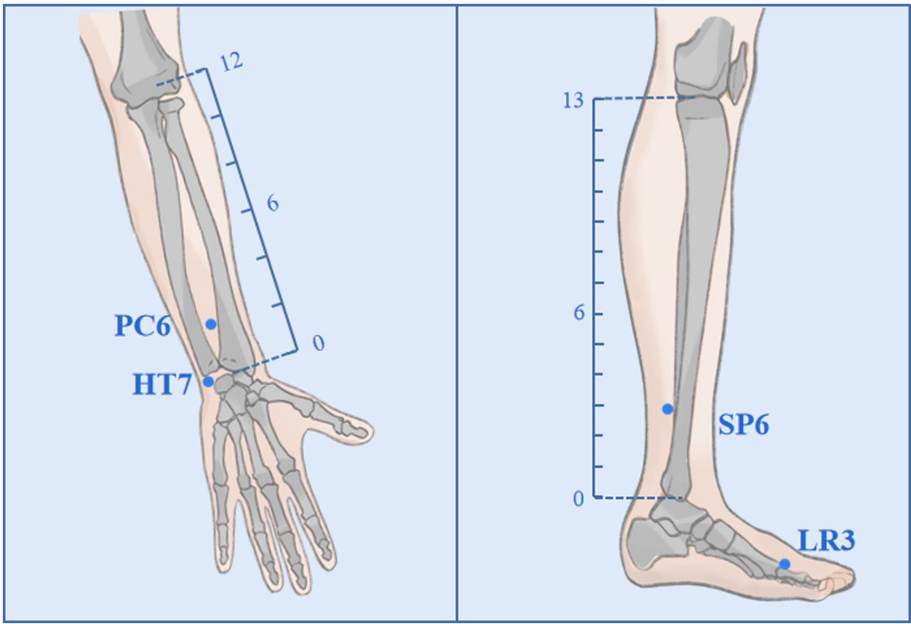


FIGURE 2
Acupoints and locations. The locations of Neiguan (PC6), Shenmen (HT7), Sanyinjiao (SP6), and Taichong (LR3).

TABLE 1 Details on active IA and sham IA.

No. Acupoint		Active intradermal acupuncture			Sham intradermal acupuncture		
		Method	Frequency	Needle sizes	Method	Frequency	Needle sizes
1	Taichong (LR3)	Punctured perpendicularly and retained in the skin, applying pressure 4 times a day.	Retained for 72 h each time,10 times in total.	φ0.20*1.5 mm	Attached to the skin surface without applying pressure.	Retained for 72 h each time,10 times in total.	—
2	Neiguan (PC6)			φ0.20*1.2 mm			
3	Sanyinjiao (SP6)			φ0.20*1.5 mm			
4	Shenmen (HT7)			φ0.20*1.2 mm			

70 or more is severe (60). The SDS is frequently used in the assessment of clinical MDD due to its high sensitivity and good internal consistency (61).

The PSQI is a self-assessment questionnaire developed by psychiatrist Dr. Buysse in 1989 and is commonly used to assess the quality of sleep during the preceding month (62). It has 19 items covering 7 factors, namely subjective sleep quality, latency, duration, efficiency, disorders, medication use, and daytime dysfunction, with a total score of 21. Higher scores on the PSQI indicate poorer quality of sleep, with a threshold score of 7.

MRI and MRS data acquisition

For getting high-quality MRI scans, not only will the radiologist receive standardized training, but the participants will also be given uniform instructions. Specifically, during the MRI and MRS test, patients will be instructed to lie flat and relaxed, as well as the radiologist will stabilize the patient’s head with a head mask and sponge, and put earplugs in their ears to reduce noise stimulation from the device. Patients are scanned before and after the treatment session (week 0 and week 6, respectively).

All scans will be performed with a 3.0 Tesla MR scanner (GE Discovery MR750, GE Healthcare, Chicago, IL, United States). The 8-channel head coil is used for signal reception to obtain the T1-weighted structural image and echo-planar T2*-weighted image (EPI). MRI and MRS data acquisition will be performed in the absence of definite intracranial abnormalities after routine serial axial scans have ruled out intracerebral organic lesions or pseudo-images.

Structural images will be acquired by 3D T1BRAVO sequence: time of repetition (TR)=8.2 ms, time of echo (TE)=3.2 ms, flip angle=12, field of view (FOV)=256 mm×256 mm, matrix=512×512, and slice thickness=1 mm. Resting state functional data will be obtained via EPI for 240 time points in the sequence: TR=2000 ms, TE=35 ms, flip angle=90, slice thickness=5 mm, slice gap=1 mm, FOV=256 mm×256 mm, and matrix=64×64. ¹H-MRS will be performed using point-resolved echo spin spectroscopy (PRESS) with single voxel multiple acquisitions, the region of interest (ROI) is proposed to be the hypothalamus, and scan parameters of TR=2,200 ms, TE=35 ms, voxel size=13 mm×12 mm×10 mm, total number of scans=64, number of excitations (NEX)=8, automatic machine homogenization, water suppression. Pre-scan auto-leveling will require full width half height (FWHM) <13 Hz and water suppression >95%. The functional images will be pre-processed using



FIGURE 3

Active intradermal acupuncture (AIA) and sham intradermal acupuncture (SIA). (A) shows the AIA with an intradermal needle, while (B) shows the SIA with a thin silicone pad.

the software DPARSE, and the metabolite spectra will be processed and analyzed through the LCModel.

In addition, with the increased accessibility of brain MRI techniques in scientific research, incidental findings such as anatomic variants, white matter changes, intracranial tumors or cystic lesions have become common (63). The percentage of reported incidental findings ranged from 2 to 32%, and it is closely related to the field strength, sequence and the subject cohort (64, 65). This trial is the first study on the cerebral mechanisms of IA for MDD based on fMRI and MRS. Before and after the intervention, changes in brain activity will be analyzed to initially explore the effects of IA on the brain regions of MDD patients. Unlike clinical practice, the number of structural sequences in mechanistic studies is limited. This makes it hard to change the protocol when incidental findings are encountered during the study, therefore incidental findings will be managed by classification (64, 66). For normal variations (Category I) without clear diagnostic consequences, no reports will be made. For additional medical clarification (Category II) and emergency clarification (Category III), additional MR sequences or other methods will be performed by radiologists to confirm these incidental findings, and inform the participant of the results (64, 66). At the same time, these data that affect the analysis will be excluded.

Evaluation of acupuncture expectation and compliance

A six-point method (0–5 point) will be used to assess acupuncture expectations before the first acupuncture intervention. The higher the score, the higher expectation of efficacy, and those who cannot believe acupuncture at all will write down why. At the end of the acupuncture intervention (end of week 6), compliance will be evaluated with the

formula: Compliance Rate = (actual treatment times/total treatment times) * 100%.

Blind success rate evaluation

At the end of the last treatment, the percentage of patients in the SIA and AIA groups who consider themselves to have been treated with acupuncture will be compared.




Adverse events

The details of all adverse events in this study will be recorded on CRFs, and the patients will be properly and timely managed. Adverse events such as bleeding, hematoma, or unbearable pain caused by the needle, as well as drug-induced nausea, vomiting or dizziness, will all be recorded. Serious adverse events will be reported to the ethics committee.

Quality control and data management

Before the conduct of the formal trial, professional clinical training will be provided to familiarize researchers with the process and focus on implementation details. They will sign a standard operating procedures document and relevant confidentiality commitment. The quality of the data for all enrolled participants will be checked regularly. The researcher will submit CRFs to the data management center, where the clinical research associate (CRA) will check for accuracy and issue queries on inconsistent data, which will then need to be clarified by the researcher.

TABLE 2 Assessment during enrollment, allocation, treatment, and follow-up.

	Screening and baseline	Treatment		Follow-up
Timepoint	Week 0	Week 3	Week 6	Week 10
Eligibility Criteria	×			
Consent	×			
Allocation	×			
Interventions:				
Active IA				
Sham IA				
Waiting list				
Assessments:				
HAMD-17	×	×	×	×
SDS	×	×	×	×
PSQI	×	×	×	×
MRI	×		×	
MRS	×		×	
Acupuncture expectation	×			
Acupuncture compliance			×	
Blind success rate evaluation			×	
Adverse events		×	×	×
Medication record		×	×	×

To ensure the authenticity, completeness and accuracy of the trial data, researchers will be instructed to record participants' data on the original paper CRFs following the protocol.

Statistical analyses

All analyses will be performed by blinded statisticians using the IBM SPSS 25.0 software. MRI data are pre-processed using DPARSF software for functional connectivity images, while MRS data are pre-calibrated using LCModel software. Normally distributed continuous variables will be presented as the mean \pm SD, and non-normal variables as the median and interquartile range. Generally, the Kruskal-Wallis test will be used to compare the inter-group changes among all three groups, the Chi-square (χ^2) test will be used for the categorical variables, and the generalized (logit) mixed modeling for the repeatedly measured data. Statistical significance will be defined as a value of $p < 0.05$.

Discussion

MDD is characterized by a high incidence, low cure rate and high recurrence rate. It lacks effective and safe treatment options. Although

numerous studies have shown acupuncture is effective in attenuating antidepressant side effects and alleviating depressive symptoms, its treatment specificity is often questioned owing to poor trial design and management, making it difficult to provide robust conclusions. Consequently, there is an urgent need for a high-quality RCT to be conducted.

The aim of this study is to evaluate the efficacy and safety of IA for MDD. To minimize potential sources of bias and imprecision that could affect clinical outcomes, several measures will be implemented. Firstly, participants will be recruited from multiple centers and randomly assigned to the AIA, SIA, and waiting groups in a 1:1:1 ratio, thus reducing selection bias. Secondly, to ensure blinding and reduce performance bias, sham intradermal needles that are indistinguishable in appearance from the active will be used, and only participants who have not previously received IA will be included in the study. Additionally, participants in the acupuncture group (both SIA and AIA groups) will be surveyed to confirm successful blinding at the end of the intervention. While acupuncturists cannot be blinded, they will be instructed not to reveal any information about group assignments to participants. Thirdly, another potential source of bias is the effects of patient expectations and compliances. Therefore, these factors will be quantified in the acupuncture group at the start and end of the intervention to mitigate their impact on the true therapeutic effects of IA. Finally, standardized outcome assessments will be used to reduce the risk of imprecision. For instance, both clinician-administered (HAMD-17) and self-reported (SDS) scales will be utilized to assess the improvement of MDD symptoms, reducing the potential for measurement error on a single scale. Outcome assessors will receive uniform training prior to the trial and will be blinded to group assignment, which may minimize inter-assessor variability. Overall, the measures described above in this study design will help reduce the risk of bias and imprecision, resulting in a more robust assessment of the efficacy of IA for MDD. However, it is worth noting that no study can be entirely free of bias, and the results of this study will be interpreted with caution and validated by future studies.

Furthermore, due to the portability and simplicity of IA, it is almost independent of the operating environment and can be widely applicable to MDD. IA can be self-administered at home under the guidance of acupuncturists, which will greatly promote patient compliance and may be a promising treatment option for the management of MDD. Indeed, availability and generalizability of IA may be limited by factors such as age differences, cultural differences, access to healthcare, and trained practitioners, which require further investigation.

Conclusion

To conclude, in this trial, our focus will be on comparing the therapeutic differences among the AIA group, SIA group and wait list group to investigate whether AIA positively affects MDD, as well as the enhanced effects and safety when combined with SSRIs, ultimately clarifies whether the effect of IA is specific or placebo. Furthermore, we will explore the effects of IA on emotion-related brain networks based on MRI in an attempt to explain the therapeutic mechanisms of IA. By this way, this study will provide high-quality clinical evidence for IA for MDD, identify the actual efficacy of IA and promote its clinical application.

Limitations and future directions

This trial has the following limitations. First, patients will be recruited in only one region, Hangzhou (the provincial capital city of China), which may introduce regional bias as an influencing factor. Second, the sample size is relatively small and a larger sample size will be needed to improve the study's power. Third, a detailed subgroup analysis of MDD patients is not performed, and the degree of MDD as well as role of comorbid personality disorders will be studied as influencing factors in the future. Fourth, the exploration of the cerebral mechanisms of IA for MDD in this study is only preliminary. Due to the limitation of scanning time, the region of interest for performing MRS will be hypothalamus only. It will be extended to more emotion-related regions in future studies. Fifth, given the characteristics of MDD and to avoid patient questionnaire fatigue, only the HAM-D-17, SDS, and PSQI scales will be used. Future research will employ additional measures, such as the Beck Depression Inventory and Quality-of-Life assessments, to assess MDD symptoms.

Ethics statement

The studies involving human participants were reviewed and approved by Ethics Committee of the Third Affiliated Hospital of Zhejiang University of Traditional Chinese Medicine, the main center (ZSLL-KY-2022-001-01-01). The participants provided their written informed consent to participate in this study.

Author contributions

All authors contributed to this trial concept and design. JF and XS designed the trial protocol. XW and MT wrote the first

draft of the manuscript. MX, ZC, SP, HH, and YG critically revised the article, NC, JY, JJ, SQ, and SX took part in the recruiting process. All authors read and approved the final manuscript.

Funding

The trial was supported by the Zhejiang Provincial TCM Science and Technology Program–Zhejiang Provincial TCM Modernization Special Project (2022ZX010).

Acknowledgments

The authors would like to thank all participants for their collaboration.

Conflict of interest

The authors declare that the research was conducted in the absence of any commercial or financial relationships that could be construed as a potential conflict of interest.

Publisher's note

All claims expressed in this article are solely those of the authors and do not necessarily represent those of their affiliated organizations, or those of the publisher, the editors and the reviewers. Any product that may be evaluated in this article, or claim that may be made by its manufacturer, is not guaranteed or endorsed by the publisher.

References

- García-Montero C, Ortega MA, Alvarez-Mon MA, Fraile-Martínez O, Romero-Bazán A, Lahera G, et al. The problem of malnutrition associated with major depressive disorder from a sex-gender perspective. *Nutrients*. (2022) 14:1107. doi: 10.3390/nu14051107
- McCarron RM, Shapiro B, Rawles J, Luo J. Depression. *Ann Intern Med*. (2021) 174:Itc65–itc80. doi: 10.7326/AITC202105180
- Otte C, Gold SM, Penninx BW, Pariante CM, Etkin A, Fava M, et al. Major depressive disorder. *Nat Rev Dis Primers*. (2016) 2:16065. doi: 10.1038/nrdp.2016.65
- Borotto-Escuela DO, Ambrogini P, Chruścicka B, Lindskog M, Crespo-Ramirez M, Hernández-Mondragón JC, et al. The role of central serotonin neurons and 5-HT Heteroreceptor complexes in the pathophysiology of depression: a historical perspective and future prospects. *Int J Mol Sci*. (2021) 22:1927. doi: 10.3390/ijms22041927
- Fakhoury M. Revisiting the serotonin hypothesis: implications for major depressive disorders. *Mol Neurobiol*. (2016) 53:2778–86. doi: 10.1007/s12035-015-9152-z
- Kupfer DJ, Frank E, Phillips ML. Major depressive disorder: new clinical, neurobiological, and treatment perspectives. *Lancet*. (2012) 379:1045–55. doi: 10.1016/S0140-6736(11)60602-8
- Gong Y, Chai Y, Ding JH, Sun XL, Hu G. Chronic mild stress damages mitochondrial ultrastructure and function in mouse brain. *Neurosci Lett*. (2011) 488:76–80. doi: 10.1016/j.neulet.2010.11.006
- Becker LJ, Fillinger C, Waegaert R, Journée SH, Hener P, Ayazgok B, et al. The basolateral amygdala-anterior cingulate pathway contributes to depression-like behaviors and comorbidity with chronic pain behaviors in male mice. *Nat Commun*. (2023) 14:2198. doi: 10.1038/s41467-023-37878-y
- Tanaka M, Szabó Á, Spekter E, Polyák H, Tóth F, Vécsei L. Mitochondrial impairment: a common motif in neuropsychiatric presentation? The link to the tryptophan-Kynurenine metabolic system. *Cells*. (2022) 11:2607. doi: 10.3390/cells11162607
- Belleau EL, Treadway MT, Pizzagalli DA. The impact of stress and major depressive disorder on hippocampal and medial prefrontal cortex morphology. *Biol Psychiatry*. (2019) 85:443–3. doi: 10.1016/j.biopsych.2018.09.031
- Battaglia S, Thayer JF. Functional interplay between central and autonomic nervous systems in human fear conditioning. *Trends Neurosci*. (2022) 45:504–6. doi: 10.1016/j.tins.2022.04.003
- Tanaka M, Szabó Á, Vécsei L. Integrating armchair, bench, and bedside research for behavioral neurology and neuropsychiatry: editorial. *Biomedicine*. (2022) 10:2999. doi: 10.3390/biomedicines10122999
- Battaglia S, Di Fazio C, Vicario CM, Avenanti A. Neuropharmacological modulation of N-methyl-D-aspartate, noradrenaline and Endocannabinoid receptors in fear extinction learning: synaptic transmission and plasticity. *Int J Mol Sci*. (2023) 24:5926. doi: 10.3390/ijms24065926
- Rm H. History and evolution of the monoamine hypothesis of depression. *J Clin Psychiatry*. (2000) 61:4–6.
- Tartt AN, Mariani MB, Hen R, Mann JJ, Boldrini M. Dysregulation of adult hippocampal neuroplasticity in major depression: pathogenesis and therapeutic implications. *Mol Psychiatry*. (2022) 27:2689–99. doi: 10.1038/s41380-022-01520-y
- Yohn CN, Gergues MM, Samuels BA. The role of 5-HT receptors in depression. *Mol Brain*. (2017) 10:28. doi: 10.1186/s13041-017-0306-y
- Moncrieff J, Cooper RE, Stockmann T, Amendola S, Hengartner MP, Horowitz MA. The serotonin theory of depression: a systematic umbrella review of the evidence. *Mol Psychiatry*. (2022). doi: 10.1038/s41380-022-01661-0

18. Pech J, Forman J, Kessing LV, Knorr U. Poor evidence for putative abnormalities in cerebrospinal fluid neurotransmitters in patients with depression versus healthy non-psychiatric individuals: a systematic review and meta-analyses of 23 studies. *J Affect Disord.* (2018) 240:6–16. doi: 10.1016/j.jad.2018.07.031
19. Fava GA. May antidepressant drugs worsen the conditions they are supposed to treat? The clinical foundations of the oppositional model of tolerance. *Ther Adv Psychopharmacol.* (2020) 10:970325. doi: 10.1177/2045125320970325
20. Bosker FJ, Tanke MAC, Jongsma ME, Cremers TIFH, Jagtman E, Pietersen CY, et al. Biochemical and behavioral effects of long-term citalopram administration and discontinuation in rats: role of serotonin synthesis. *Neurochem Int.* (2010) 57:948–7. doi: 10.1016/j.neuint.2010.10.001
21. Cuijpers P, Quero S, Dowrick C, Arroll B. Psychological treatment of depression in primary care: recent developments. *Curr Psychiatry Rep.* (2019) 21:129. doi: 10.1007/s11920-019-1117-x
22. Gelenberg AJ. Using assessment tools to screen for, diagnose, and treat major depressive disorder in clinical practice. *J Clin Psychiatry.* (2010) 71:e01. doi: 10.4088/JCP.9058se1c.01gry
23. Monroe SM, Harkness KL. Major depression and its recurrences: life course matters. *Annu Rev Clin Psychol.* (2022) 18:329–7. doi: 10.1146/annurev-clinpsy-072220-021440
24. Horowitz MA, Taylor D. Tapering of SSRI treatment to mitigate withdrawal symptoms. *Lancet Psychiatry.* (2019) 6:538–6. doi: 10.1016/S2215-0366(19)30032-X
25. Schuch FB, Vancampfort D, Richards J, Rosenbaum S, Ward PB, Stubbs B. Exercise as a treatment for depression: a meta-analysis adjusting for publication bias. *J Psychiatr Res.* (2016) 77:42–51. doi: 10.1016/j.jpsychires.2016.02.023
26. Chung KF, Yu YM, Yeung WF. Correlates of residual fatigue in patients with major depressive disorder: the role of psychotropic medication. *J Affect Disord.* (2015) 186:192–7. doi: 10.1016/j.jad.2015.07.026
27. Romera I, Pérez V, Quail D, Berggren L, Lenox-Smith A, Gilaberte I. Individual residual symptoms and functional impairment in patients with depression. *Psychiatry Res.* (2014) 220:258–2. doi: 10.1016/j.psychres.2014.07.042
28. Carvalho AF, Sharma MS, Brunoni AR, Vieta E, Fava GA. The safety, tolerability and risks associated with the use of newer generation antidepressant drugs: a critical review of the literature. *Psychother Psychosom.* (2016) 85:270–8. doi: 10.1159/000447034
29. Smith CA, Armour M, Lee MS, Wang LQ, Hay PJ. Acupuncture for depression. *Cochrane Database Syst Rev.* (2018) 2018:CD004046. doi: 10.1002/14651858.CD004046.pub4
30. Armour M, Smith CA, Wang LQ, Naidoo D, Yang GY, MacPherson H, et al. Acupuncture for depression: a systematic review and meta-analysis. *J Clin Med.* (2019) 8:E1140. doi: 10.3390/jcm8081140
31. Zhao B, Li Z, Wang Y, Ma X, Wang X, Wang X, et al. Can acupuncture combined with SSRIs improve clinical symptoms and quality of life in patients with depression? Secondary outcomes of a pragmatic randomized controlled trial. *Complement Ther Med.* (2019) 45:295–2. doi: 10.1016/j.ctim.2019.03.015
32. Yang NN, Lin LL, Li YJ, Li HP, Cao Y, Tan CX, et al. Potential mechanisms and clinical effectiveness of acupuncture in depression. *Curr Neuropharmacol.* (2022) 20:738–0. doi: 10.2174/1570159X19666210609162809
33. Yi L, Hui F, Yali M, Jingfang C, Hongjing M, Mingfen S, et al. Effect of soothing-liver and nourishing-heart acupuncture on early selective serotonin reuptake inhibitor treatment onset for depressive disorder and related indicators of neuroimmunology: a randomized controlled clinical trial. *J Tradit Chin Med.* (2015) 35:507–3. doi: 10.1016/s0254-6272(15)30132-1
34. Chen L, Li M, Fan L, Zhu X, Liu J, Li H, et al. Optimized acupuncture treatment (acupuncture and intradermal needling) for cervical spondylosis-related neck pain: a multicenter randomized controlled trial. *Pain.* (2021) 162:728–9. doi: 10.1097/j.pain.0000000000002071
35. Jing R, Feng K. Efficacy of intradermal acupuncture for insomnia: a meta-analysis. *Sleep Med.* (2021) 85:66–74. doi: 10.1016/j.sleep.2021.06.034
36. Lee SY, Baek YH, Park SU, Moon SK, Park JM, Kim YS, et al. Intradermal acupuncture on shen-men and nei-kuan acupoints improves insomnia in stroke patients by reducing the sympathetic nervous activity: a randomized clinical trial. *Am J Chin Med.* (2009) 37:1013–21. doi: 10.1142/S0192415X09007624
37. Noda Y, Izuno T, Tsuchiya Y, Hayasaka S, Matsumoto K, Murakami H, et al. Acupuncture-induced changes of vagal function in patients with depression: a preliminary sham-controlled study with press needles. *Complement Ther Clin Pract.* (2015) 21:193–0. doi: 10.1016/j.ctcp.2015.07.002
38. Wang H, Liu XR, Wu XJ, He TZ, Miao D, Jiang JF, et al. Additional value of auricular intradermal acupuncture alongside selective serotonin reuptake inhibitors: a single-blinded, randomized, sham-controlled preliminary clinical study. *Acupunct Med.* (2021) 39:596–2. doi: 10.1177/0964528421997155
39. Aruldass AR, Kitzbichler MG, Morgan SE, Lim S, Lynall ME, Turner L, et al. Dysconnectivity of a brain functional network was associated with blood inflammatory markers in depression. *Brain Behav Immun.* (2021) 98:299–9. doi: 10.1016/j.bbi.2021.08.226
40. Song Y, Xu W, Chen S, Hu G, Ge H, Xue CY, et al. Functional MRI-specific alterations in salience network in mild cognitive impairment: an ALE Meta-analysis. *Front Aging Neurosci.* (2021) 13:695210. doi: 10.3389/fnagi.2021.695210
41. Han KM, De Berardis D, Fornaro M, Kim YK. Differentiating between bipolar and unipolar depression in functional and structural MRI studies. *Prog Neuro-Psychopharmacol Biol Psychiatry.* (2019) 91:20–7. doi: 10.1016/j.pnpbp.2018.03.022
42. Kang SG, Cho SE. Neuroimaging biomarkers for predicting treatment response and recurrence of major depressive disorder. *Int J Mol Sci.* (2020) 21:E2148. doi: 10.3390/ijms21062148
43. Pizzagalli DA, Roberts AC. Prefrontal cortex and depression. *Neuropsychopharmacology.* (2022) 47:225–6. doi: 10.1038/s41386-021-01101-7
44. Lai CH. The alterations in regional homogeneity of parieto-cingulate and temporocerebellum regions of first-episode medication-naïve depression patients. *Brain Imaging Behav.* (2016) 10:187–4. doi: 10.1007/s11682-015-9381-9
45. Kantrowitz JT, Dong Z, Milak MS, Rashid R, Kegeles LS, Javitt DC, et al. Ventromedial prefrontal cortex/anterior cingulate cortex Glx, glutamate, and GABA levels in medication-free major depressive disorder. *Transl Psychiatry.* (2021) 11:419. doi: 10.1038/s41398-021-01541-1
46. Moriguchi S, Takamiya A, Noda Y, Horita N, Wada M, Tsugawa S, et al. Glutamatergic neurometabolite levels in major depressive disorder: a systematic review and meta-analysis of proton magnetic resonance spectroscopy studies. *Mol Psychiatry.* (2019) 24:952–4. doi: 10.1038/s41380-018-0252-9
47. Zhang J, Wu X, Nie D, Zhuo Y, Li J, Hu Q, et al. Magnetic resonance imaging studies on acupuncture therapy in depression: a systematic review. *Front Psych.* (2021) 12:670739. doi: 10.3389/fpsy.2021.670739
48. Yang M, Zhou Y, Wu Y, Ge X, Wu Q. Clinical observation of electroacupuncture for depression and its brain response monitored by fMRI. *Sichuan Mental Health.* (2016) 29:132–6. doi: 10.11886/j.issn.1007-3256.2016.02.008
49. Li K, Guo J, Chen Y. Efficacy of electro-acupuncture combined with antidepressant medicine in the treatment of primary depression with Rs-fMRI technique. *J Clin Acupunct Moxibustion.* (2017) 33:26–9. doi: 10.3969/j.issn.1005-0779.2017.12.008
50. Goh YL, Ho CE, Zhao B. Acupuncture and depth: future direction for acupuncture research. *Evid Based Complement Alternat Med.* (2014) 2014:871217. doi: 10.1155/2014/871217
51. Ma Q. Somatotopic organization of autonomic reflexes by acupuncture. *Curr Opin Neurobiol.* (2022) 76:102602. doi: 10.1016/j.conb.2022.102602
52. Feng Y, Bai L, Ren Y, Chen S, Wang H, Zhang W, et al. fMRI connectivity analysis of acupuncture effects on the whole brain network in mild cognitive impairment patients. *Magn Reson Imaging.* (2012) 30:672–82. doi: 10.1016/j.mri.2012.01.003
53. Hugenschmidt CE, Laurienti PJ. Power and sample size calculation for neuroimaging studies by non-central random field theory. *NeuroImage.* (2007) 37:721–30. doi: 10.1016/j.neuroimage.2007.06.009
54. Qiu K, Jing M, Sun R, Yang J, Liu X, He Z, et al. The status of the quality control in acupuncture-neuroimaging studies. *Evid Based Complement Alternat Med.* (2016) 2016:3685785–14. doi: 10.1155/2016/3685785
55. Furukawa TA, Cipriani A, Cowen PJ, Leucht S, Egger M, Salanti G. Optimal dose of selective serotonin reuptake inhibitors, venlafaxine, and mirtazapine in major depression: a systematic review and dose-response Meta-analysis. *Focus (Am Psychiatr Publ).* (2020) 18:211–9. doi: 10.1176/appi.focus.18204
56. Hamilton M. A rating scale for depression. *J Neurol Neurosurg Psychiatry.* (1960) 23:56–62. doi: 10.1136/jnnp.23.1.56
57. Hamilton M. Development of a rating scale for primary depressive illness. *Br J Soc Clin Psychol.* (1967) 6:278–96. doi: 10.1111/j.2044-8260.1967.tb00530.x
58. Zimmerman M, Martinez JH, Young D, Chelminski I, Dalrymple K. Severity classification on the Hamilton depression rating scale. *J Affect Disord.* (2013) 150:384–8. doi: 10.1016/j.jad.2013.04.028
59. Zung WKK. A self-rating depression scale. *Arch Gen Psychiatry.* (1965) 12:63–70. doi: 10.1001/archpsyc.1965.01720310065050
60. Zung WKK. From art to science: the diagnosis and treatment of depression. *Arch Gen Psychiatry.* (1973) 29:328–37. doi: 10.1001/archpsyc.1973.0420003002600
61. Dunstan DA, Scott N, Todd AK. Screening for anxiety and depression: reassessing the utility of the Zung scales. *BMC Psychiatry.* (2017) 17:329. doi: 10.1186/s12888-017-1489-6
62. Buysse DJ, Reynolds CF, Monk TH, Berman SR, Kupfer DJ. The Pittsburgh sleep quality index: a new instrument for psychiatric practice and research. *Psychiatry Res.* (1989) 28:193–3. doi: 10.1016/0165-1781(89)90047-4
63. Langner S, Buelow R, Fleck S, Angermaier A, Kirsch M. Management of Intracranial Incidental Findings on brain MRI. *Rofo.* (2016) 188:1123–33. doi: 10.1055/s-0042-111075
64. Hegenscheid K, Seipel R, Schmidt CO, Völzke H, Kühn JP, Biffar R, et al. Potentially relevant incidental findings on research whole-body MRI in the general adult population: frequencies and management. *Eur Radiol.* (2013) 23:816–6. doi: 10.1007/s00330-012-2636-6
65. Orme NM, Fletcher JG, Siddiki HA, Harmsen WS, O'Byrne MM, Port JD, et al. Incidental findings in imaging research. *Arch Intern Med.* (2010) 170:1525–32. doi: 10.1001/archinternmed.2010.317
66. Bamberg F, Kauczor HU, Weckbach S, Schlett CL, Forsting M, Ladd SC, et al. Whole-body MR imaging in the German National Cohort: rationale, design, and technical background. *Radiology.* (2015) 277:206–0. doi: 10.1148/radiol.2015142272



OPEN ACCESS

EDITED BY

Chien-Han Lai,
National Yang-Ming University, Taiwan

REVIEWED BY

Feng Liu,
Tianjin Medical University General Hospital,
China
Linling Li,
Shenzhen University, China

*CORRESPONDENCE

Laichang He
✉ laichang_he@163.com

[†]These authors have contributed equally to this work

RECEIVED 19 February 2023

ACCEPTED 12 June 2023

PUBLISHED 28 June 2023

CITATION

Hu Z, Zhou C and He L (2023) Abnormal dynamic functional network connectivity in patients with early-onset bipolar disorder. *Front. Psychiatry* 14:1169488. doi: 10.3389/fpsy.2023.1169488

COPYRIGHT

© 2023 Hu, Zhou and He. This is an open-access article distributed under the terms of the [Creative Commons Attribution License \(CC BY\)](https://creativecommons.org/licenses/by/4.0/). The use, distribution or reproduction in other forums is permitted, provided the original author(s) and the copyright owner(s) are credited and that the original publication in this journal is cited, in accordance with accepted academic practice. No use, distribution or reproduction is permitted which does not comply with these terms.

Abnormal dynamic functional network connectivity in patients with early-onset bipolar disorder

Ziyi Hu[†], Chun Zhou[†] and Laichang He^{*}

Department of Radiology, First Affiliated Hospital of Nanchang University, Nanchang, China

Objective: To explore the changes in dynamic functional brain network connectivity (dFNC) in patients with early-onset bipolar disorder (BD).

Methods: Resting-state functional magnetic resonance imaging (rs-fMRI) data were collected from 39 patients with early-onset BD and 22 healthy controls (HCs). Four repeated and stable dFNC states were characterised by independent component analysis (ICA), sliding time windows and k-means clustering, and three dFNC temporal metrics (fraction of time, mean dwell time and number of transitions) were obtained. The dFNC temporal metrics and the differences in dFNC between the two groups in different states were evaluated, and the correlations between the differential dFNC metrics and neuropsychological scores were analysed.

Results: The dFNC analysis showed four connected patterns in all subjects. Compared with the HCs, the dFNC patterns of early-onset BD were significantly altered in all four states, mainly involving impaired cognitive and perceptual networks. In addition, early-onset BD patients had a decreased fraction of time and mean dwell time in state 2 and an increased mean dwell time in state 3 ($p < 0.05$). The mean dwell time in state 3 of BD showed a positive correlation trend with the HAMA score ($r = 0.4049$, $p = 0.0237 \times 3 > 0.05$ after Bonferroni correction).

Conclusion: Patients with early-onset BD had abnormal dynamic properties of brain functional network connectivity, suggesting that their dFNC was unstable, mainly manifesting as impaired coordination between cognitive and perceptual networks. This study provided a new imaging basis for the neuropathological study of emotional and cognitive deficits in early-onset BD.

KEYWORDS

early-onset bipolar disorder, magnetic resonance imaging, dynamic functional network connectivity, brain imaging, brain functional network

1. Introduction

Alternating depressive and manic or hypomanic episodes occur along with asymptomatic periods of euthymia in patients with bipolar disorder (BD), which is a mood disease marked by fluctuations in the mood state causing acute dysfunction. The prevalence of BD has exceeded 1% worldwide, and it is one of the major causes of disability in young people. Moreover, the risk of suicide in patients with BD is 20 times higher than that in the general population, and BD can lead to serious cognitive dysfunction (1, 2). The incidence of BD shows a bimodal distribution with age, with peaks at 15–24 years and 45–54 years (3). The onset of BD is before the age of 14 years in approximately 31% of patients and before the age of 20 years in

approximately 59% of patients; these patients are considered to have early-onset BD (4). The presentation and clinical course of BD seem to be related to the age of onset. Patients with early-onset BD have a complex and variable condition and are prone to relapse. They tend to be more emotionally unstable, have more comorbidities, and more frequent suicide attempts and panic episodes, which eventually leads to a poor prognosis (5). Most cases of early-onset BD begin in childhood or adolescence, a period of greater biological vulnerability due to the anatomical and functional immaturity of the brain, particularly in the regions responsible for cognition, inhibition, emotion and reward (6, 7). Thus, studying the functional changes in the brains of people with early-onset BD may help improve the present understanding of the neurobiological features of BD.

Resting-state functional magnetic resonance imaging (rs-fMRI) is a neuroimaging technique that dynamically measures the blood oxygenation level-dependent (BOLD) signal in the brain, reflecting neural activity. Brain functional connectivity (FC), which is used to analyse the statistical correlation between BOLD signals from multiple brain regions at rest, has been widely used in clinical studies to observe BD features in adults (8). Anomalies in neuronal communication within certain brain networks and circuits, particularly the interactions between the default mode network (DMN) and brain regions involved in emotion processing, are the focus of research into the pathophysiological mechanisms underlying BD (9, 10). During manic and depressive episodes as well as during remission, BD patients were observed to have altered FC in the prefrontal cortex, inferior frontal cortex, cingulate cortex, thalamus, amygdala, and limbic system (11, 12). Rey et al. identified selective abnormalities in the connectivity between the amygdala and DMN regions, including reduced posterior cingulate cortex connectivity and increased medial prefrontal cortex connectivity (13). Paediatric BD patients had significantly disordered functional integration of the DMN and task-positive network/salience network, and this altered functional integration was associated with emotional and cognitive dysregulation (14). Damage across relevant networks may affect the effective cognitive and emotional activities of BD patients, who exhibit aberrant FC changes within or between certain brain networks. In fact, the human brain is never static, and the functional connections of the brain change even in a state of rest. The assumption that functional network connections remain unchanged during rs-fMRI scans does not adequately reflect the spontaneous activity of the human brain.

Dynamic functional network connectivity (dFNC) estimates time-varying FC on a temporal scale with good temporal resolution and generates high-dimensional datasets. Notably, dFNC actually captures changes in the brain's intrinsic FC during various physiological states and may be a more sensitive marker than static FC (15–18). Long et al. found greater variability in dFNC in BD patients, which was characterised by overconnectivity of the thalamic network and the sensorimotor network (SMN) (19). Wang et al. reported reduced dFNC variability between the posterior DMN and right central executive network in a triple network model of BD (20). Large-scale dynamic and holistic brain analysis at the network level can more comprehensively describe the variation in brain FC in BD patients. The majority of recent neuroimaging studies on BD focused on static FC or dynamic FC in local networks or certain specific seed regions (20–22). The brain is a vast and sophisticated network, and anomalies in specific pathways or localised activity do not yet completely account for functional alterations at the level of the entire neural network.

dFNC assists in the investigation of functional interactions between brain networks and the evaluation of their underlying network architecture without limiting the scope to a specified set of regional connections. There is a serious dearth of research on whole-brain dynamic network connection patterns in BD patients, particularly those with early-onset BD.

In this study, we compared the dFNC of 39 patients with early-onset BD with those of 22 healthy controls (HCs) matched for age, sex, and years of education. Data-driven independent component analysis (ICA) was first used to extract resting-state networks (RSNs), which exhibited spatially isolated distribution and temporally correlated functional activity in several brain regions. The time series data were then windowed, and a dFNC matrix was created using a sliding window technique. Subsequently, these matrices were clustered into different dynamic states using the k-means algorithm, and finally, a state analysis was performed to compare the dFNC and temporal metrics between the two groups. Our study aimed to determine whether dynamic patterns of organisation within the brain at the network level were altered in patients with early-onset BD and to assess the relevance of such altered network properties to clinical scores. This exploration helped to detect potentially altered functional network interactions in patients at the peak onset age and may provide some new insights to improve the present understanding of the neuropathological mechanisms of the disease.

2. Materials and methods

2.1. Participants

The study was approved by the Biomedical Ethics Committee of the First Affiliated Hospital of Nanchang University, and written informed consent was obtained from each subject or their guardians before the formal study took place. The Structured Clinical Interview-Patient Version as described in the DSM-IV-TR was used for diagnosis, and 39 patients diagnosed with early-onset BD were recruited. The severity of each patient's emotional symptoms was assessed using the 24-item Hamilton Depression Rating Scale (HAMD-24), the Hamilton Anxiety Rating Scale (HAMA) and the Young Mania Rating Scale (YMRS) within 24 h before or after the scan. Inclusion criteria for early-onset BD patients were being 12–20 years of age and meeting the DSM-IV-TR diagnostic criteria for BD, including at least one manic, depressive, or remitting episode. At the time of scanning, all patients were either medication-naïve or had been unmedicated for at least 6 months and were not receiving psychotherapy or electroconvulsive therapy. Exclusion criteria were as follows: organic brain lesions, severe physical or neurologic deficits, history of head trauma, drug or alcohol abuse, poor compliance with MRI examinations, contraindications to MRI, and substandard image quality. We also randomly recruited 22 HCs matched for age, sex, and years of education, excluding those with current or past neurological or psychiatric disorders or with any history of psychiatric disorders in first-degree relatives as determined through a Structured Clinical Interview-Nonpatient Version as described in the DSM-IV-TR. The remaining controls were subjected to the same exclusion criteria as the patient group. All subjects were right-handed according to the Edinburgh Habitual Handedness Scale criteria.

2.2. MRI data acquisition

All MRI data were collected in a Siemens Trio Tim 3.0 T imaging system equipped with a standard 8-channel head coil. Functional images were acquired using a single-shot gradient-echo EPI sequence with the following parameters: TR = 2000 ms, TE = 30 ms, number of slices = 30, slice thickness = 4 mm, gap = 1.2 mm, flip angle = 90°, field of view (FOV) = 200 × 200 mm², matrix = 64 × 64, voxel size = 3.0 × 3.0 × 4.0 mm³, and number of timepoints 240 (8 min 6 s total duration). During the scan, subjects were asked to relax, close their eyes, remain still, and think of nothing in particular so that images of high quality could be obtained. The 3D T1-weighted gradient-echo sequence parameters were as follows: TR = 1900 ms, TE = 2.26 ms, number of slices = 176, slice thickness = 1 mm, gap = 0.5 mm, flip angle = 9°, FOV = 256 × 256 mm², matrix = 256 × 256, and voxel size = 1.0 × 1.0 × 1.0 mm³.

2.3. Data preprocessing

The rs-fMRI data were preprocessed using GRETNA toolbox 2.0.0 in MATLAB 2014b. The preprocessing procedure included (1) discarding the first 10 time points of the images for MR signal equilibrium, (2) slice timing correction, (3) head motion correction, (4) space normalisation, registering functional data to the corresponding structural T1-weighted image and aligning the T1 images to Montreal Neurological Institute (MNI) space with resampling to a voxel size of 3 × 3 × 3 mm³, and (5) smoothing with an isotropic Gaussian kernel of 8 mm full width at half maximum to improve the signal-to-noise ratio.

2.4. Ica

The GIFT package¹ in MATLAB 2014b was used to separate blind sources from the preprocessed fMRI data and decompose them into independent spatial components and time series. The process of ICA mainly included component estimation, data downscaling, inverse reconstruction, component selection, and postprocessing. The specific steps were as follows: (1) Component estimation: The best component number was estimated from all subjects' fMRI data based on the minimum descriptive length (MDL) criterion, (2) Data downscaling: Principal component analysis (PCA) was used to compress and then downscale the data, and the Infomax algorithm was used for group ICA to decompose the data into independent components (ICs). The data downscaling step was repeated 100 times using the ICASSO algorithm to determine the ICs with the highest consistency and stability, (3) Inverse reconstruction: The temporal and spatial components of each subject at the individual level were reconstructed by the time-space dual regression method, and the intensity values corresponding to each voxel were Fisher-z transformed. The z-transformed data approximately obeyed a normal distribution, (4) Component selection: The Display GUI module in the GIFT software package displayed the obtained components, and ICs associated with

cerebrospinal fluid, motor or vascular evoked pseudoactivation were discarded. Maximum spatial overlap and visual examination based on the Stanford functional risk standard template resulted in seven RSNs, namely, the DMN, frontoparietal network (FPN), dorsal attention network (DAN), ventral attention network (VAN), SMN, visual network (VN) and auditory network (AUN). In addition, ICA was repeated on the data from each the BD and HCs group to verify the reproducibility and reliability of the components obtained for both groups, and (5) Postprocessing: To remove scanner drift and artefacts associated with respiration, heartbeat, and movement, the selected components were subjected to detrending, despiking, low-pass filtering (0.01 ~ 0.15 Hz) and regression of the realignment parameters.

2.5. dFNC analysis

The dFNC matrix was calculated using a sliding window method. Previous studies found that the dynamic state changes in the brain can be effectively obtained when the window width is between 30 and 60 s (23, 24). In this study, the window width was set to a TR of 30 (60 s), and the window was slid along the time axis in steps of 1 TR. The Pearson correlation coefficients between all pairs of BOLD signals in each window were calculated to construct a series of dynamic covariance matrices. Since the covariance estimates of short time series were affected by substantial noise, we used the L1 regularisation method (number of repetitions = 10) to improve the sparsity of the dFNC matrix of each window.

The dFNC matrices of all subjects were clustered using the k-means clustering algorithm to assess the frequency and structure of recurrent dFNC patterns. In this analysis, the Manhattan city distance was used to measure the similarity between different time windows. To increase the chance of the clustering algorithm escaping local minima, we set the maximum number of iterations to 500 and the number of repetitions to 150. The elbow rule was used to determine the optimal number of clusters, $k = 4$. The dFNC matrix of all subjects was clustered into four dFNC states, which were recurrent instantaneous FC patterns across different windows and subjects. The dFNC matrix at the centre of each cluster was called the cluster centroid.

Several temporal characteristics were calculated as follows: (i) the fraction of time was defined as the ratio of the number of time windows in a state to the total number of time windows, (ii) the mean dwell time was the average time in a particular state, and (iii) the number of transitions was the number of times the subject switched from one state to another during the scan time.

2.6. Statistical analysis

The differences in dFNC between the BD and HCs groups were analysed directly with the Stats module of the GIFT software package using two independent samples t tests with false discovery rate (FDR) correction, and $p < 0.05$ indicated a statistically significant difference. The rest of the data were statistically analysed using SPSS 25.0 software. The age, sex, years of education, clinical neuropsychological scores, and dFNC temporal characteristics of the participants in the two groups were tested for normality separately, and measures that met the criteria for a normal distribution were expressed as the

¹ <http://icatb.sourceforge.net/>

mean \pm SD. The difference between the groups was compared by two independent samples *t* tests. The chi-square test was used to compare the proportion of each sex in the groups. The samples of dFNC temporal characteristics from the two groups were independent of each other, but none conformed to a normal distribution, so a nonparametric test (Mann–Whitney *U* test) was used to assess the differences between the groups, and $p < 0.05$ indicated a statistically significant difference. Finally, the relationship between dFNC temporal characteristics and clinical variables (YMRS, HAMA, and HAMD scores) was explored using Spearman's partial correlation analysis with age, sex, and education as control variables, using Bonferroni correction, with statistically significant differences at $p \times n < 0.05$.

3. Results

3.1. Demographics and clinical characteristics

After data preprocessing, 39 patients with early-onset BD and 22 HCs were finally included in this study. Demographics and clinical characteristics of the two groups are presented in Table 1; there were no differences between groups in age, sex, or years of education (all $p > 0.05$). The YMRS, HAMA and HAMD scores of early-onset BD patients were significantly higher than those of HCs ($p < 0.0001$).

3.2. Cluster analysis

Using the *k*-means clustering algorithm, we identified four recurring patterns of transient FC, i.e., dFNC states: state 1 (33% of all time windows) had sparse connectivity and exhibited general weakening of whole-brain functional network connectivity; state 2 (29% of all time windows) had partial connectivity, exhibiting increased or weakened FC within and between some networks; state 3 (14% of all time windows) showed strong connectivity, exhibiting strong positive connectivity amongst large-scale functional networks; and state 4 (24% of all time windows) was characterised by modular connectivity, which manifested as negative connectivity with obvious modularity between the FPN, DMN, SMN and the AN and AUN

(Figure 1). It should be noted that not all subjects showed all four states, so the number of subjects with data demonstrating each state was not necessarily the same. The results of the dFNC matrix index of all subjects under all windows are shown in Figure 2. The data showed evidence of state 1 most frequently and had the longest mean dwell time, whilst state 3 appeared least frequently and had the shortest mean dwell time. The frequencies of transitioning from state 2 to state 1 and from state 4 to states 1 or 2 were highest amongst all subjects.

3.3. Comparison of dFNC temporal metrics between groups

Figure 3 shows that compared to HCs, BD patients had a significantly reduced fraction of time and mean dwell time in state 2 and a significantly increased mean dwell time in state 3 (Mann–Whitney *U* test, $p < 0.05$), but the number of transitions was not significantly different between HCs and BD patients. In the same way, the three dFNC temporal metrics (fraction of time, mean dwell time, and number of transitions) were not significantly different in state 1 and state 4.

3.4. Comparison of dFNC between groups

Two independent sample *t* tests were used to further compare the dFNC matrix of each state between groups, and it was found that the dFNC of early-onset BD patients was significantly different in states 1–4 compared to that of HCs (FDR corrected, $p < 0.05$) (Figure 4). The specific results were as follows: The brain network connections with increased dFNC in state 1 were the DMN–VN and DMN–AUN, with the highest connectivity strength between the DMN and AUN; the brain networks with decreased dFNC were the VN and VN–VAN. The brain network connections with increased dFNC in state 2 were the DAN–AUN; the brain network connections with decreased dFNC included the DMN–DAN, DMN–AUN, VAN–VN, and VAN–AUN, with the lowest connectivity strength between the DMN and AUN. The brain network connections with increased dFNC in states 3 and 4 were the DMN–VN and DMN–AUN, respectively.

3.5. Correlation analysis

The mean dwell time in state 3 of BD was correlated with the HAMA score ($r = 0.4049$, $p = 0.0237 \times 3 > 0.05$ after Bonferroni correction) in a trend manner (Figure 5). There was no significant correlation between the remaining dFNC temporal metrics and clinical neuropsychological scores.

4. Discussion

In this study, the differences in dFNC between patients with early-onset BD and HCs were investigated based on rs-fMRI with ICA, sliding time window and clustering analysis. The following were our key discoveries: (1) dFNC analysis showed four connected patterns: state 1 showing sparse connectivity, state 2 showing partial connectivity, state 3 showing strong connectivity, and state 4 showing

TABLE 1 Demographics and clinical characteristics of all subjects.

Clinical variables (Mean \pm SD)	Early-onset BD ($n = 39$)	HCs ($n = 22$)	<i>p</i> value
Age (years)	16.97 \pm 2.37	17.31 \pm 2.25	0.58
Sex (M/F)	19/20	11/11	0.76*
Handedness (R/L)	39/0	22/0	–
Educational level (years)	10.97 \pm 2.37	11.32 \pm 2.25	0.58
YMRS	21.56 \pm 4.81	2.64 \pm 2.90	<0.0001
HAMA	23.64 \pm 7.04	4.18 \pm 4.56	<0.0001
HAMD	32.38 \pm 6.47	3.77 \pm 4.81	<0.0001

*Represents the chi-square test *p* value for sex. M, male; F, female; R, right; L, left; SD, standard deviation.

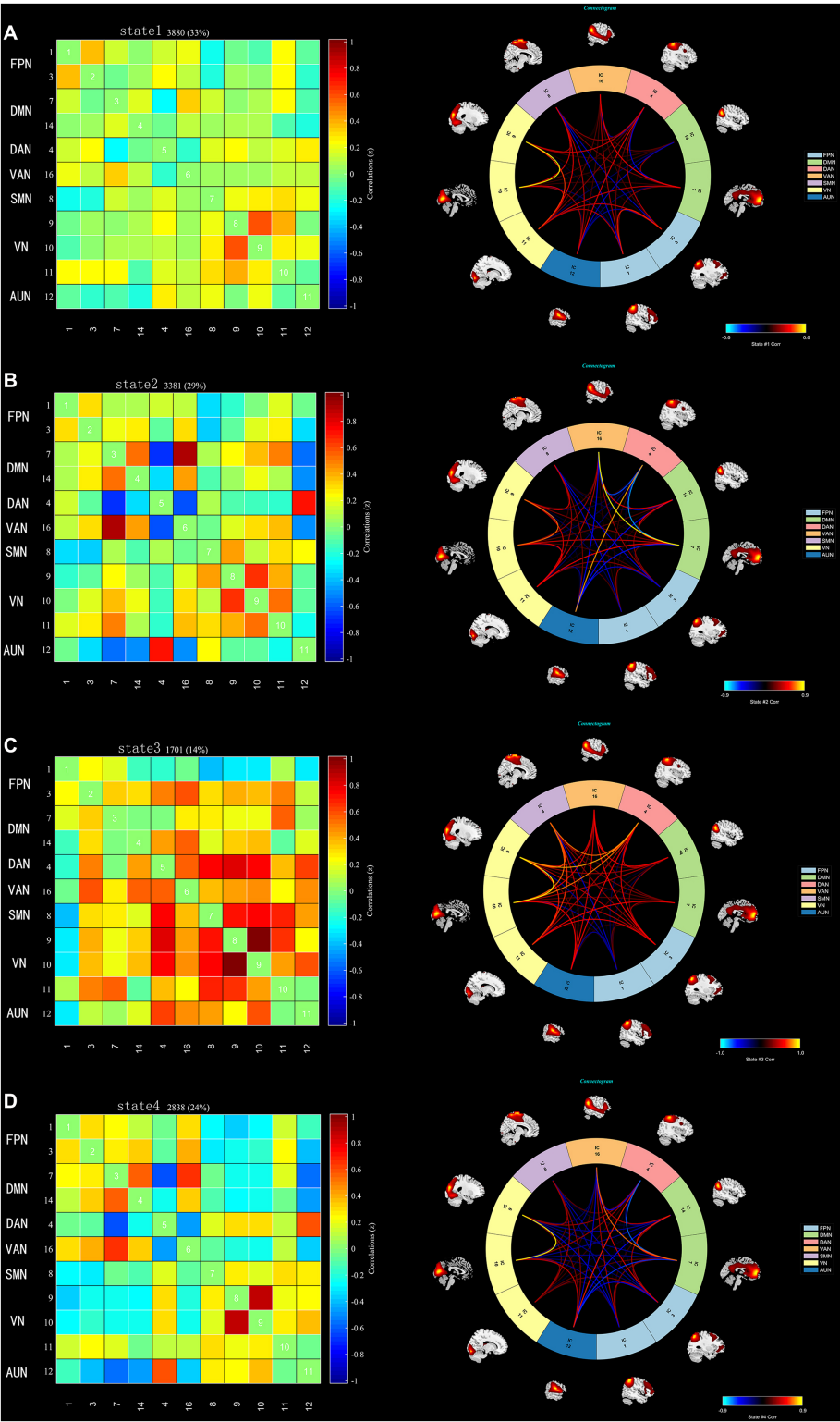


FIGURE 1
The dFNC matrices for states 1–4 and the dFNC diagrams for each state. The horizontal and vertical axes are the selected ICs and their functional networks are depicted. The colour bars indicate the z values of the dFNC. **(A)** State 1 with sparse connectivity, **(B)** State 2 with partial connectivity, **(C)** State 3 with strong connectivity, **(D)** State 4 with modular connectivity.

modular connectivity, (2) there were significant differences between the patient group and the HC group in two temporal metrics (fraction of time and mean dwell time), and (3) in patients with early-onset BD,

there was dynamic functional network reorganisation, which showed impaired coordination function between cognitive and perceptual networks.

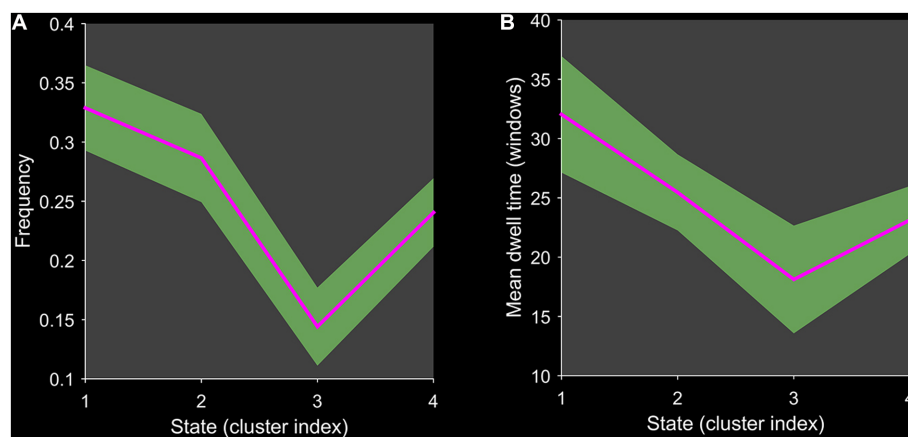


FIGURE 2

Line chart of the dFNC matrix index. Plots show (A) the frequency of each state and (B) the mean dwell time of each state.

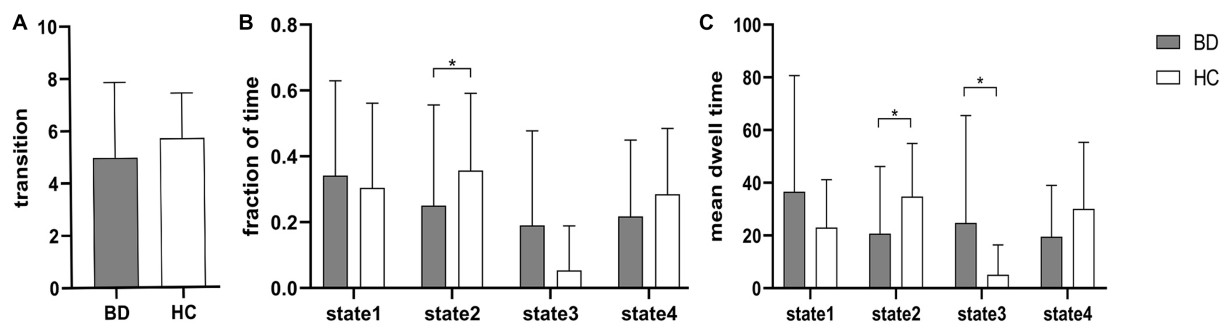


FIGURE 3

Between-group comparison of dFNC temporal metrics. Bar charts show (A) the number of transitions, (B) the fraction of time and (C) the mean dwell time. * above the bars indicates a significant difference between the two groups, $p < 0.05$.

We identified four stable and repetitive dFNC states in all subjects. The sparsely connected network in state 1 had the highest proportion of occurrence and the longest mean dwell time, possibly reflecting the average of other states that were not distinct or frequent enough to be separated and characterising the baseline activity of neurons in the resting brain (25). BD is a “disconnected disorder” in which emotional dysregulation results from the unstable neuronal dynamics of systemic circuits (26). The fraction of time and mean dwell time of state 2 were both reduced in individuals with early-onset BD compared with those of HCs, suggesting that early-onset BD patients were more likely to transition from state 2 to other states. This reduction in state 2 in patients with early-onset BD implies abnormal and more unstable information transfer within or between functional networks, ultimately suggesting abnormal local segregation and global integration of functional brain networks. State 3 was characterised by tight and strong connections. The increased mean dwell time in state 3 in early-onset BD patients suggests that there is more complex brain activity and increased abnormal information exchange and transmission within and between networks. Correlation analysis showed that the mean dwell time in state 3 in early-onset BD patients was positively correlated with the HAMA scores in a trend manner. The results must be interpreted with caution because less than half of patients with early-onset BD showed evidence of state 3 in the rs-fMRI

data. Studies have shown that patients with BD and generalised anxiety disorder have functional abnormalities in brain regions, such as the frontal lobe and limbic system that are related to the severity of anxiety (27, 28). Therefore, we believe that the longer the mean dwell time is in state 3 in early-onset BD patients, the more likely their HAMA score will be elevated. However, a larger sample size is needed to verify this inference.

In recent years, the study of the functional interactions between RSNs has shown considerable promise as a potential pathway for the diagnosis of neuropsychiatric disorders (29, 30). The RSNs of the brain can be roughly divided into two categories: higher cognitive networks (the DMN, FPN, DAN, and VAN) and lower sensory and perceptual networks (the SMN, VN, and AUN). Intranetwork and internetwork connectivity reflect the segregation and integration of brain information, respectively (31). Previous studies have shown that BD is associated with a wide range of FC deficits that are thought to be caused by abnormalities in the integration and segregation of brain networks (32). BD patients have more abnormal internetwork connectivity than intranetwork connectivity, suggesting the importance of cross-regional cooperation between brain regions in emotion regulation and cognitive function (33), which is similar to our findings. In our study, patients with early-onset BD showed reduced connectivity amongst many brain networks in state 2 compared to that of controls, especially between the

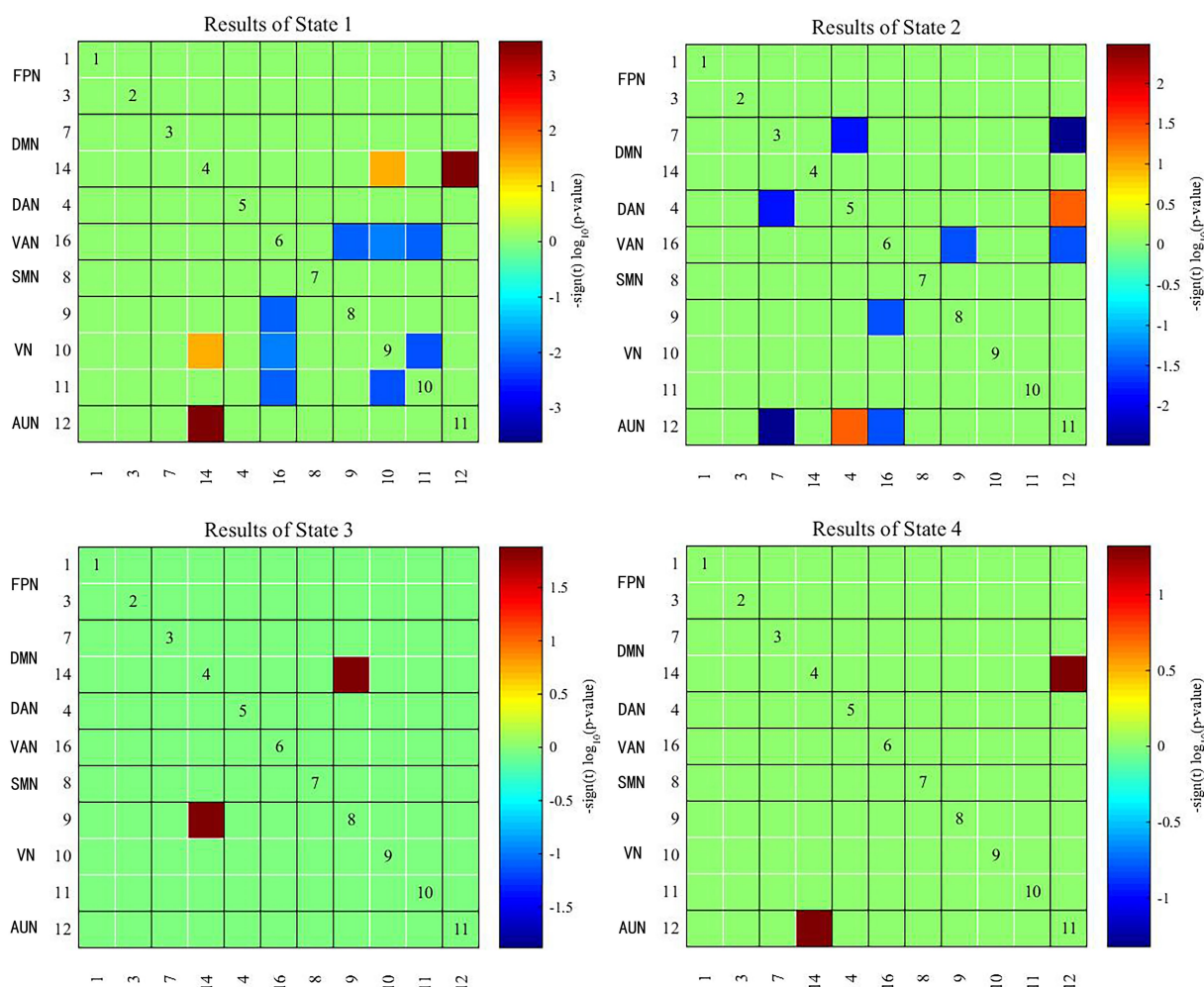


FIGURE 4

Significant differences in dFNC between early-onset BD patients and HCs. The horizontal and vertical axes represent the ICs and their functional networks. The coloured rectangles represent the dFNC between the two corresponding ICs, with warm colours indicating increased connectivity and cool colours indicating decreased connectivity.

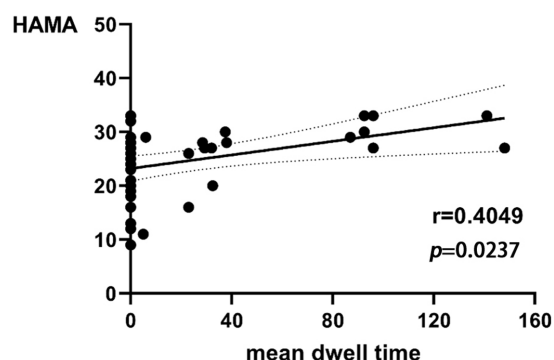


FIGURE 5

Relationship between HAMA scores and mean dwell time in state 3 of BD.

DMN and AUN. The DMN is considered a key component of the functional structure of the brain, involving self-referential and reflective activities that are preferentially activated in resting states and

inhibited in a wide range of cognitive tasks. In addition, the DMN acts as a “cohesion connector,” exhibiting high network cohesion and high internetwork integration and integrating information from primary functional and cognitive networks to support a wide range of brain functions (7, 34). It has been shown that the functional separation and integration of the DMN in BD patients is inefficient, which may imply impaired local processing and long-distance information transfer in the DMN (9, 35, 36). The AUN includes the primary auditory cortex and the secondary auditory cortex. The primary auditory cortex mainly encodes the properties of the auditory stimulus, whilst the secondary auditory cortex integrates and connects this information to produce a specific percept (37). The decreased FC between the DMN and AUN indicated that external perception ability and self-consciousness integration were impaired in early-onset BD patients. The DAN is primarily responsible for attentional orienting and visual and spatial perception, and it has the function of allocating of cognitive resources in response to stimuli (38, 39). The interaction between the internal cognitive processing network (DMN) and the external directed cognitive network (DAN) reflects the switch between the intrinsic and extrinsic focus of attention (40). The reduced FC between the two

networks in this study may explain the abnormal control of attention in early-onset BD patients. In addition, many abnormalities in the FC of other brain regions within the cognitive network, within the perceptual network, and between the two were also observed in patients with early-onset BD, which further demonstrated the existence of abnormal local segregation and global integration of functional brain networks in early-onset BD patients.

In the present study, the brain networks with increased dFNC in early-onset BD patients in state 1 were the DMN-VN and DMN-AUN. Notably, increased dFNC of the DMN-VN and DMN-AUN also occurred in state 3 and state 4. The dFNC enhancement between the DMN and VN and between the DMN and AUN in multiple states may be characteristic of brain network damage in early-onset BD patients. Previous studies by our group identified a possible developmental pattern of hyperconnectivity supporting switching between higher cognitive networks and primary perceptual networks in patients with early-onset BD, which generally occurs during childhood and adolescence. The VN and AUN are involved in the perceptual processing of information exchange with the external environment. The higher dFNC between these networks compared with the normal state may be related to patients' greater sensitivity to external visual or auditory stimuli and emotions (41). Different patterns of visual attention deficits in BD patients were associated with different external emotional stimuli, suggesting the interactive influence of cognitive and emotional functions (42). Biological activities, such as head or body movements, facial expressions, and auditory stimuli stimulate the brain to engage in a wide range of cognitive activities (43, 44), which may explain the cognitive deficits seen in BD patients. Thus, the abnormalities of neural circuits amongst the DMN, DAN, VN and AUN in early-onset BD patients may be responsible for the abnormal reception of external stimuli, psychological activity and cognitive performance compared with those of HCs. Abnormal dynamic brain network reorganisation may constitute a potential imaging biomarker for early-onset BD. Furthermore, we inferred that the enhanced integration of the DMN may represent an adaptive response to the diminished integration of the DMN observed in state 2. This interpretation is speculative and must be confirmed by further studies.

Although audiovisual dysfunction is not a typical clinical symptom of BD, studies have shown that neurophysiological deficits and poorer task performance in adolescent BD imply that visual and auditory pathways do not transfer sensory data well to the audiovisual cortex and that the frontal cortex does not integrate incoming signals well into unified and coherent perceptual actions (45). Our results showed abnormal connectivity between the VN and higher cognitive networks (i.e., the DMN, DAN, and VAN), the AUN and higher cognitive networks, and within the VN across multiple states in early-onset BD. This connectivity reflects the disrupted dynamic reconfiguration of sensory and perceptual systems and a failure of dynamic integration of higher-order processes, which may underlie the perceptual and cognitive deficits in early-onset BD. This study also further validated our group's previous findings that audiovisual integration relies on a brain network mechanism of feedback information flow between higher-order networks and the underlying perceptual cortex.

In this study, we found abnormal dynamic properties of whole-brain functional network connectivity in early-onset BD by measuring dFNC; these changes may imply abnormal separation and integration processes in the brain. Patients with early-onset BD had impaired coordination

between cognitive and perceptual networks, which specifically manifested as impaired coordination between internal introspection and external environmental detection, as well as perceptual dysfunction. In addition, the specific dFNC temporal metrics were altered in early-onset BD patients, which may provide a new imaging basis for clinical symptom prediction and assessment in these patients.

Our study had several limitations. First, the present study had a relatively small sample size, and we did not conduct a grouping study that considered the different subtypes of early-onset BD. There may be heterogeneity amongst different subtypes. The sample size should be expanded for a more precise grouping study in the future. In addition, correlation analysis required a larger sample size for validation. Second, the study protocol did not include collection of relevant cognitive test scores and behavioural measures, and these incomplete scales limited our interpretation of cognitive-related networks. Third, the choice of sliding window size may influence the assessment of dynamic brain connections. Future analyses should be performed using different window widths to verify the reliability and reproducibility of the results. Finally, our study was a cross-sectional study lacking longitudinal comparisons, so the findings may have certain limitations.

Data availability statement

The raw data supporting the conclusions of this article will be made available by the authors, without undue reservation.

Ethics statement

The studies involving human participants were reviewed and approved by Biomedical Ethics Committee of the First Affiliated Hospital of Nanchang University. Written informed consent to participate in this study was provided by the participants' legal guardian/next of kin.

Author contributions

ZH: writing - original draft, data curation, software, proof Checking. CZ: investigation, modified the language, revision, proof Checking. LH: supervision and writing - review and editing. All authors contributed to the article and approved the submitted version.

Funding

This study was funded by the National Natural Science Foundation of China (Grant/Award Number: "81460329") and the Natural Science Foundation of Jiangxi Province (Grant/Award Numbers: "20192ACBL20039," and "202310454/202310456").

Conflict of interest

The authors declare that the research was conducted in the absence of any commercial or financial relationships that could be construed as a potential conflict of interest.

Publisher's note

All claims expressed in this article are solely those of the authors and do not necessarily represent those of their affiliated

References

- Pompili M, Gonda X, Serafini G, Innamorati M, Sher L, Amore M, et al. Epidemiology of suicide in bipolar disorders: a systematic review of the literature. *Bipolar Disord.* (2013) 15:457–90. doi: 10.1111/bdi.12087
- Grande I, Berk M, Birmaher B, Vieta E. Bipolar disorder. *Lancet.* (2016) 387:1561–72. doi: 10.1016/S0140-6736(15)00241-X
- Rowland TA, Marwaha S. Epidemiology and risk factors for bipolar disorder. *Ther Adv Psychopharmacol.* (2018) 8:251–69. doi: 10.1177/2045125318769235
- Van Meter A, Moreira ALR, Youngstrom E. Updated meta-analysis of epidemiologic studies of Pediatric bipolar disorder. *J Clin Psychiatry.* (2019) 80:18r12180. doi: 10.4088/JCP.18r12180
- Miller JN, Black DW. Bipolar disorder and suicide: a review. *Curr Psychiatry Rep.* (2020) 22:6. doi: 10.1007/s11920-020-1130-0
- Araim M, Haque M, Johal L, Mathur P, Nel W, Rais A, et al. Maturation of the adolescent brain. *Neuropsychiatr Dis Treat.* (2013) 9:449–61. doi: 10.2147/NDT.S39776
- Gu S, Satterthwaite TD, Medaglia JD, Yang M, Gur RE, Gur RC, et al. Emergence of system roles in normative neurodevelopment. *Proc Natl Acad Sci U S A.* (2015) 112:13681–6. doi: 10.1073/pnas.1502829112
- Chen G, Zhao L, Jia Y, Zhong S, Chen F, Luo X, et al. Abnormal cerebellum-DMN regions connectivity in unmedicated bipolar II disorder. *J Affect Disord.* (2019) 243:441–7. doi: 10.1016/j.jad.2018.09.076
- Wang Y, Zhong S, Jia Y, Sun Y, Wang B, Liu T, et al. Disrupted resting-state functional connectivity in nonmedicated bipolar disorder. *Radiology.* (2016) 280:529–36. doi: 10.1148/radiol.2016151641
- Zovetti N, Rossetti MG, Perlini C, Maggioni E, Bontempi P, Bellani M, et al. Default mode network activity in bipolar disorder. *Epidemiol Psychiatr Sci.* (2020) 29:e166. doi: 10.1017/S2045796020000803
- Dutra SJ, Man V, Kober H, Cunningham WA, Gruber J. Disrupted cortico-limbic connectivity during reward processing in remitted bipolar I disorder. *Bipolar Disord.* (2017) 19:661–75. doi: 10.1111/bdi.12560
- Goya-Maldonado R, Brodmann K, Keil M, Trost S, Dechent P, Gruber O. Differentiating unipolar and bipolar depression by alterations in large-scale brain networks. *Hum Brain Mapp.* (2016) 37:808–18. doi: 10.1002/hbm.23070
- Rey G, Piguet C, Benders A, Favre S, Eickhoff SB, Aubry JM, et al. Resting-state functional connectivity of emotion regulation networks in euthymic and non-euthymic bipolar disorder patients. *Eur Psychiatry.* (2016) 34:56–63. doi: 10.1016/j.eurpsy.2015.12.005
- Cao W, Chen H, Jiao Q, Cui D, Guo Y, Gao W, et al. Altered functional integration in the salience and default mode networks in euthymic Pediatric bipolar disorder. *Neural Plast.* (2020) 2020:5853701. doi: 10.1155/2020/5853701
- Sanfratello L, Houck JM, Calhoun VD. Relationship between MEG global dynamic functional network connectivity measures and symptoms in schizophrenia. *Schizophr Res.* (2019) 209:129–34. doi: 10.1016/j.schres.2019.05.007
- Ma L, Yuan T, Li W, Guo L, Zhu D, Wang Z, et al. Dynamic functional connectivity alterations and their associated gene expression pattern in autism Spectrum disorders. *Front Neurosci.* (2021) 15:794151. doi: 10.3389/fnins.2021.794151
- Xue K, Liang S, Yang B, Zhu D, Xie Y, Qin W, et al. Local dynamic spontaneous brain activity changes in first-episode, treatment-naïve patients with major depressive disorder and their associated gene expression profiles. *Psychol Med.* (2022) 52:2052–61. doi: 10.1017/S0033291720003876
- Liu F, Wang Y, Li M, Wang W, Li R, Zhang Z, et al. Dynamic functional network connectivity in idiopathic generalized epilepsy with generalized tonic-clonic seizure. *Hum Brain Mapp.* (2017) 38:957–73. doi: 10.1002/hbm.23430
- Long Y, Liu Z, Chan CKY, Wu G, Xue Z, Pan Y, et al. Altered temporal variability of local and large-scale resting-state brain functional connectivity patterns in schizophrenia and bipolar disorder. *Front Psych.* (2020) 11:422. doi: 10.3389/fpsy.2020.00422
- Wang J, Wang Y, Huang H, Jia Y, Zheng S, Zhong S, et al. Abnormal dynamic functional network connectivity in unmedicated bipolar and major depressive disorders based on the triple-network model. *Psychol Med.* (2020) 50:465–74. doi: 10.1017/S003329171900028X
- Fateh AA, Cui Q, Duan X, Yang Y, Chen Y, Li D, et al. Disrupted dynamic functional connectivity in right amygdalar subregions differentiates bipolar disorder from major depressive disorder. *Psychiatry Res Neuroimaging.* (2020) 304:111149. doi: 10.1016/j.pscychres.2020.111149
- Yin Z, Chang M, Wei S, Jiang X, Zhou Y, Cui L, et al. Decreased functional connectivity in insular subregions in depressive episodes of bipolar disorder and major depressive disorder. *Front Neurosci.* (2018) 12:842. doi: 10.3389/fnins.2018.00842
- Faghiri A, Stephen JM, Wang YP, Wilson TW, Calhoun VD. Changing brain connectivity dynamics: from early childhood to adulthood. *Hum Brain Mapp.* (2018) 39:1108–17. doi: 10.1002/hbm.23896
- de Lacy N, Doherty D, King BH, Rachakonda S, Calhoun VD. Disruption to control network function correlates with altered dynamic connectivity in the wider autism spectrum. *Neuroimage Clin.* (2017) 15:513–24. doi: 10.1016/j.nicl.2017.05.024
- Allen EA, Damaraju E, Plis SM, Erhardt EB, Eichele T, Calhoun VD. Tracking whole-brain connectivity dynamics in the resting state. *Cereb Cortex.* (2014) 24:663–76. doi: 10.1093/cercor/bhs352
- Perry A, Roberts G, Mitchell PB, Breakspear M. Connectomics of bipolar disorder: a critical review, and evidence for dynamic instabilities within interoceptive networks. *Mol Psychiatry.* (2019) 24:1296–318. doi: 10.1038/s41380-018-0267-2
- Fonzo GA, Etkin A. Brain connectivity reflects mental and physical states in generalized anxiety disorder. *Biol Psychiatry.* (2016) 80:733–5. doi: 10.1016/j.biopsych.2016.08.026
- de Sa AS, Campos C, Rocha NB, Yuan TF, Paes F, Arias-Carrion O, et al. Neurobiology of bipolar disorder: abnormalities on cognitive and cortical functioning and biomarker levels. *CNS Neurol Disord Drug Targets.* (2016) 15:713–22. doi: 10.2174/1871527315666160321111359
- He H, Sui J, Du Y, Yu Q, Lin D, Drevets WC, et al. Co-altered functional networks and brain structure in unmedicated patients with bipolar and major depressive disorders. *Brain Struct Funct.* (2017) 222:4051–64. doi: 10.1007/s00429-017-1451-x
- Li Q, Cao W, Liao X, Chen Z, Yang T, Gong Q, et al. Altered resting state functional network connectivity in children absence epilepsy. *J Neurol Sci.* (2015) 354:79–85. doi: 10.1016/j.jns.2015.04.054
- Yang B, Wang M, Zhou W, Wang X, Chen S, Potenza MN, et al. Disrupted network integration and segregation involving the default mode network in autism spectrum disorder. *J Affect Disord.* (2023) 323:309–19. doi: 10.1016/j.jad.2022.11.083
- O'Donoghue S, Holleran L, Cannon DM, McDonald C. Anatomical dysconnectivity in bipolar disorder compared with schizophrenia: a selective review of structural network analyses using diffusion MRI. *J Affect Disord.* (2017) 209:217–28. doi: 10.1016/j.jad.2016.11.015
- Liu M, Wang Y, Zhang A, Yang C, Liu P, Wang J, et al. Altered dynamic functional connectivity across mood states in bipolar disorder. *Brain Res.* (2021) 1750:147143. doi: 10.1016/j.brainres.2020.147143
- Buckner RL, Andrews-Hanna JR, Schacter DL. The brain's default network: anatomy, function, and relevance to disease. *Ann N Y Acad Sci.* (2008) 1124:1–38. doi: 10.1196/annals.1440.011
- Wang Y, Wang J, Jia Y, Zhong S, Zhong M, Sun Y, et al. Topologically convergent and divergent functional connectivity patterns in unmedicated unipolar depression and bipolar disorder. *Transl Psychiatry.* (2017) 7:e1165. doi: 10.1038/tp.2017.117
- Wang Y, Wang J, Jia Y, Zhong S, Niu M, Sun Y, et al. Shared and specific intrinsic functional connectivity patterns in Unmedicated bipolar disorder and major depressive disorder. *Sci Rep.* (2017) 7:3570. doi: 10.1038/s41598-017-03777-8
- Gavrilescu M, Rossell S, Stuart GW, Shea TL, Innes-Brown H, Henshall K, et al. Reduced connectivity of the auditory cortex in patients with auditory hallucinations: a resting state functional magnetic resonance imaging study. *Psychol Med.* (2010) 40:1149–58. doi: 10.1017/S0033291709991632
- Maidan I, Jacob Y, Giladi N, Hausdorff JM, Mirelman A. Altered organization of the dorsal attention network is associated with freezing of gait in Parkinson's disease. *Parkinsonism Relat Disord.* (2019) 63:77–82. doi: 10.1016/j.parkreldis.2019.02.036
- Corbetta M, Patel G, Shulman GL. The reorienting system of the human brain: from environment to theory of mind. *Neuron.* (2008) 58:306–24. doi: 10.1016/j.neuron.2008.04.017
- Weissman DH, Roberts KC, Visscher KM, Woldorff MG. The neural bases of momentary lapses in attention. *Nat Neurosci.* (2006) 9:971–8. doi: 10.1038/nn1727
- Mitchell RL, Elliott R, Barry M, Cruttenden A, Woodruff PW. Neural response to emotional prosody in schizophrenia and in bipolar affective disorder. *Br J Psychiatry.* (2004) 184:223–30. doi: 10.1192/bjp.184.3.223
- Zhang B, Jia Y, Wang C, Shao X, Wang W. Visual event-related potentials in external emotional conditions in bipolar disorders I and II. *Neurophysiol Clin.* (2019) 49:359–69. doi: 10.1016/j.neucli.2019.09.002

43. Hoekert M, Bais L, Kahn RS, Aleman A. Time course of the involvement of the right anterior superior temporal gyrus and the right fronto-parietal operculum in emotional prosody perception. *PLoS One*. (2008) 3:e2244. doi: 10.1371/journal.pone.0002244
44. Sander D, Grandjean D, Pourtois G, Schwartz S, Seghier ML, Scherer KR, et al. Emotion and attention interactions in social cognition: brain regions involved in processing anger prosody. *NeuroImage*. (2005) 28:848–58. doi: 10.1016/j.neuroimage.2005.06.023
45. Xiao W, Manyi G, Khaleghi A. Deficits in auditory and visual steady-state responses in adolescents with bipolar disorder. *J Psychiatr Res*. (2022) 151:368–76. doi: 10.1016/j.jpsychires.2022.04.041



OPEN ACCESS

EDITED BY

Manpreet Kaur Singh,
Stanford University,
United States

REVIEWED BY

Julia Schröder,
University Hospital RWTH Aachen, Germany
Keita Watanabe,
Kyoto University, Japan

*CORRESPONDENCE

Erin A. Kaufman
✉ erin.anne.kaufman@gmail.com

[†]These authors have contributed equally to this work and share first authorship

RECEIVED 07 March 2023

ACCEPTED 11 September 2023

PUBLISHED 16 October 2023

CITATION

Reisch AA, Bessette KL, Jenkins LM, Skerrett KA, Gabriel LB, Kling LR, Stange JP, Ryan KA, Schreiner MW, Crowell SE, Kaufman EA and Langenecker SA (2023) Human emotion processing accuracy, negative biases, and fMRI activation are associated with childhood trauma.

Front. Psychiatry 14:1181785.
doi: 10.3389/fpsy.2023.1181785

COPYRIGHT

© 2023 Reisch, Bessette, Jenkins, Skerrett, Gabriel, Kling, Stange, Ryan, Schreiner, Crowell, Kaufman and Langenecker. This is an open-access article distributed under the terms of the [Creative Commons Attribution License \(CC BY\)](https://creativecommons.org/licenses/by/4.0/). The use, distribution or reproduction in other forums is permitted, provided the original author(s) and the copyright owner(s) are credited and that the original publication in this journal is cited, in accordance with accepted academic practice. No use, distribution or reproduction is permitted which does not comply with these terms.

Human emotion processing accuracy, negative biases, and fMRI activation are associated with childhood trauma

Alexis A. Reisch^{1†}, Katie L. Bessette^{1,2,3†}, Lisanne M. Jenkins¹, Kristy A. Skerrett¹, Laura B. Gabriel^{1,4}, Leah R. Kling¹, Jonathan P. Stange⁵, Kelly A. Ryan⁴, Mindy Westlund Schreiner², Sheila E. Crowell^{2,6,7}, Erin A. Kaufman^{2*} and Scott A. Langenecker^{1,3,4}

¹Cognitive Neuroscience Center, Department of Psychiatry, University of Illinois at Chicago, Chicago, IL, United States, ²Department of Psychiatry and Huntsman Mental Health Institute, University of Utah, Salt Lake City, UT, United States, ³Semel Institute for Neuroscience and Human Behavior, University of California, Los Angeles, Los Angeles, CA, United States, ⁴Department of Psychiatry, University of Michigan, Ann Arbor, MI, United States, ⁵Departments of Psychology and Psychiatry and the Behavioral Sciences, University of Southern California, Los Angeles, CA, United States, ⁶Department of Psychology, University of Utah, Salt Lake City, UT, United States, ⁷Department of Obstetrics and Gynecology, University of Utah, Salt Lake City, UT, United States

Introduction: Emerging literature suggests that childhood trauma may influence facial emotion perception (FEP), with the potential to negatively bias both emotion perception and reactions to emotion-related inputs. Negative emotion perception biases are associated with a range of psychiatric and behavioral problems, potentially due or as a result of difficult social interactions. Unfortunately, there is a poor understanding of whether observed negative biases are related to childhood trauma history, depression history, or processes common to (and potentially causative of) both experiences.

Methods: The present cross-sectional study examines the relation between FEP and neural activation during FEP with retrospectively reported childhood trauma in young adult participants with remitted major depressive disorder (rMDD, $n = 41$) and without psychiatric histories (healthy controls [HC], $n = 34$). Accuracy of emotion categorization and negative bias errors during FEP and brain activation were each measured during exposure to fearful, angry, happy, sad, and neutral faces. We examined participant behavioral and neural responses in relation to total reported severity of childhood abuse and neglect (assessed with the Childhood Trauma Questionnaire, CTQ).

Results: Results corrected for multiple comparisons indicate that higher trauma scores were associated with greater likelihood of miscategorizing happy faces as angry. Activation in the right middle frontal gyrus (MFG) positively correlated with trauma scores when participants viewed faces that they correctly categorized as angry, fearful, sad, and happy.

Discussion: Identifying the neural mechanisms by which childhood trauma and MDD may change facial emotion perception could inform targeted prevention efforts for MDD or related interpersonal difficulties.

KEYWORDS

major depressive disorder, childhood trauma, facial emotion perception, response bias, middle frontal gyrus, facial emotion perception test

Introduction

Depression and childhood trauma are each related to difficulties in emotion perception, biases, as well as differences in functional activation and morphometric measurements of distributed brain regions including corticostriatal and corticolimbic circuits. In addition, childhood trauma is associated with increased risk of and specific trajectories for affective disorders [e.g., (1, 2)]. While such pathways of increased risk are well replicated in the literature, it is not yet clear what cognitive performance and brain developmental changes might drive such increased risk. We and others have proposed that changes in cognitive control might underlie such risk (3), but there are other (and many) possible risk factors. For example, commonalities in functional activation patterns are frequently reported in prefrontal and limbic regions (e.g., hippocampus, amygdala, dorsolateral prefrontal cortex [DLPFC], and anterior cingulate) and occasionally striatal regions [e.g., nucleus accumbens; (4)] during tasks that involve working memory and emotional conflict (5–11). It is possible that these observed activation differences in depression and childhood trauma relate to dysfunctional emotion processing (12, 13). For example, elevations in childhood trauma are correlated with altered performance on facial emotion perception (FEP) tasks, such that there is increased sensitivity to negative emotions, including a bias toward misperceiving negative emotions (12, 14–16). Notably, commonly reported elevated bilateral amygdala reactivity to sad faces in individuals exposed to childhood adversity [e.g., (17, 18)] is *not* associated with behavioral differences in accurately categorizing emotions (19), hinting that increased amygdala reactivity in these individuals is unrelated to FEP. Moreover, commonalities across depression and child trauma may be due to different experiences leading to similar outcomes (e.g., equifinality); for instance, both childhood trauma and parental warmth and support (even in the context of healthy development) impact amygdalar activation to negative faces in youth (20).

FEP difficulties are also, often observed among persons in both active and remitted states of major depressive disorder [MDD; (21)], and among groups at elevated risk for developing MDD (22–24), potentially through a stress sensitization process (25). Moreover, a consistent gaze bias to attend to sad faces is observed among individuals with MDD, irrespective of phase of illness (26, 27). Individuals with active MDD exhibit enhanced memory for previously displayed negative facial expressions, allocate more visual attention to sad faces than neutral faces (although sometimes only display less attention to happy faces (28), and are more likely to interpret emotionally neutral faces as sad compared with healthy controls [HCs; (12, 29, 30)]. Notably, individuals with remitted MDD (rMDD), who are at 4–6 times higher risk for experiencing another depressive episode, display an array of FEP biases, including greater facial fear recognition (31). Indeed, bias toward negative faces has predicted MDD relapse (32). Atypical patterns of responding to emotional inputs are also observed among youth at elevated risk of MDD. For example, children and adolescents of depressed mothers demonstrated greater attentional avoidance (gaze) of sad faces (33), and are more likely to categorize neutral stimuli as negative emotions (34, 35). Taken together, extant research suggests that individuals with active MDD, rMDD, and those at high risk of MDD each experience disruptions in FEP and related processes.

Even though emotion processing difficulties are associated with both childhood trauma and MDD, integrated efforts to understand these relationships and any dissociations between them are just beginning to be elucidated. Despite well-established links with trauma preceding negative affective biases and MDD, it still remains unclear whether negative affective biases or poor FEP accuracy are *driven* by trauma history, depression history, or processes common to both experiences. It is also unclear whether individuals' histories are associated with unique neural patterns of responding during exposure to positive, negative, and neutral facial expressions. Of note, active symptoms of depression may obscure trait-based measurements of these cognitive processes [e.g., (36)]. For example, a bias to positive emotions (e.g., happy) could be present in remission, whereas a bias to negative emotions may be present during active high-symptom states. As the goal is to understand the effects of trauma rather than fluctuating symptom-related processes, this study recruited individuals in the remitted mood state. In fact, little is known about within-subject shifts in symptoms as they pertain to emotion processing biases.

The present study assesses FEP and negative biases via a forced-choice categorization paradigm of facial expressions among young adults with and without a history of MDD and varying levels of childhood trauma. It is designed to probe the effects of trauma history dimensionally among these two groups: individuals with and without MDD. In those with MDD, the potential confounding effects of active mood symptoms are reduced by examining individuals in the remitted phase. We hypothesized that (a) individuals with histories of more severe (retrospectively reported) childhood trauma would display a bias to categorize more faces incorrectly as fearful and angry, thus demonstrating a potentially adaptive response (a bias, but with lower accuracy overall) that may have been overgeneralized beyond the context of traumatic situations, and that (b) increased childhood trauma would have the greatest impact on the processing of fearful and angry faces in regions implicated in emotional reactivity and regulation (e.g., heightened amygdala activation and/or blunted DLPFC activation), which may be more pronounced among participants with rMDD.

Methods

Participants

Participants (ages 18 to 23) were young adults recruited with either no history of mental illness (healthy control, HC; $n=34$), or with a history of MDD, currently remitted (rMDD; $n=41$), as determined by qualified clinicians via clinical interview using diagnostic criteria from the DSM (Diagnostic Interview for Genetic Studies, or DIGS; (37)). A parent or guardian completed a phone interview modified Family Interview for Genetic Studies) or medical records were obtained to confirm participant diagnoses and eligibility. Participants were recruited as part of a larger IRB approved study investigating neurobiological intermediate phenotypes in MDD. Procedures took place at two study sites: the University of Michigan (UM, 2011–2013) and then the University of Illinois at Chicago (UIC, 2013–2016).

TABLE 1 Participant demographics.

	HC (<i>n</i> = 34)	rMDD (<i>n</i> = 41)
Mean age, years	20.67 (1.66)	21.39 (1.55)
Females, <i>n</i> (%)	21 (63.63)	26 (68.42)
Mean education, years (SD)	14.55 (1.42)	14.74 (1.35)
Mean IQ estimate (SD)*	106.00 (9.70)	107.10 (8.82)
Race, <i>n</i> (%)		
Black/African-American	1 (3%)	4 (10%)
Asian	5 (15%)	5 (12%)
Native American/Pacific Islander	0	0
Alaska Native	0	0
White	26 (76%)	28 (68%)
Multiracial/Mixed	0	2 (5%)
Hispanic, <i>n</i> (%)	4 (12%)	4 (10%)
Handedness (<i>n</i> right: <i>n</i> left) (% right)	31:3 (91%)	37:4 (90%)
Site, <i>n</i> (%)		
University of Michigan	11 (33%)	14 (37%)
University of Illinois at Chicago	22 (67%)	24 (63%)
Illness characteristics		
Past psychiatric medication, <i>n</i> [§]	NA	12 (31%)
History of co-morbid anxiety, <i>n</i> [§]	NA	13 (34%)
Number of MDEs (SD) [§]	NA	1.82 (1.20)
Age of first onset, years (SD)	NA	16.37 (3.35)
Age of last episode	NA	18.83 (3.86)
Current HDRS Recent Distress*	1.67 (1.12)	3.62 (1.72)
Beck anxiety inventory (SD)*	0.19 (1.02)	−0.20 (0.78)
Beck Depression Inventory (SD)*	1.90 (2.66)	4.40 (5.10)
FEPT accuracy	0.91 (1.53)	4.59 (6.20)
CTQ Total^*	81.10 (8.76)	80.56 (13.81)
Physical abuse	28.28 (4.15)	32.95 (9.01)
Emotional abuse*	5.53 (0.76)	5.78 (1.79)
Sexual abuse	6.00 (1.87)	8.03 (3.78)
Physical neglect	5.06 (0.25)	5.06 (0.35)
Emotional neglect	5.55 (1.05)	5.83 (1.50)
	6.40 (2.53)	7.92 (4.29)

CTQ, Childhood Trauma Questionnaire; HC, Healthy Controls; HDRS, Hamilton Depression Rating Score; IQ, Intelligence Quotient; MDE, Major Depressive Episodes; rMDD, remitted Major Depressive Disorder.

[§]Exclusionary criteria for HCs.

[^]Truncated 2 outliers.

*Group differences significant at $p < 0.05$.

Participants demographics are presented in Table 1. There were no exclusions based upon childhood trauma history. Exclusions were for active substance misuse; substance dependence (including alcohol and nicotine) within the past year; developmental disability (with the exception of attention-deficit/hyperactivity disorder); current active suicidal plan or intent; suicide attempt in the past six months; use of psychoactive medications within the past 30 days; symptoms of schizophrenia or psychosis; family history of schizophrenia or

psychosis; and incompatibilities with MRI. Those classified in the HC group reported no prior psychiatric problems including a history of depressive episodes. Individuals with rMDD had relatively few prior depressive episodes (mode = 1 prior depressive episode), and had been in remission on average 3 years.

Measures

Childhood trauma questionnaire

The CTQ is a 28-item valid and reliable retrospective assessment that asks respondents to report on five subscales of abuse and neglect as experienced in their childhood. The CTQ demonstrates (38) strong psychometric properties in diverse clinical and community samples (39), and has shown high inter-rater kappa reliability in validation studies (40). The current study used the total score, which can range from 25 to 125, with a total clinical cut-off score of 49 (41). In the current sample, the total score ranged from 25 to 63 and reliability was good, $\alpha = 0.84$.

Facial emotion perception test

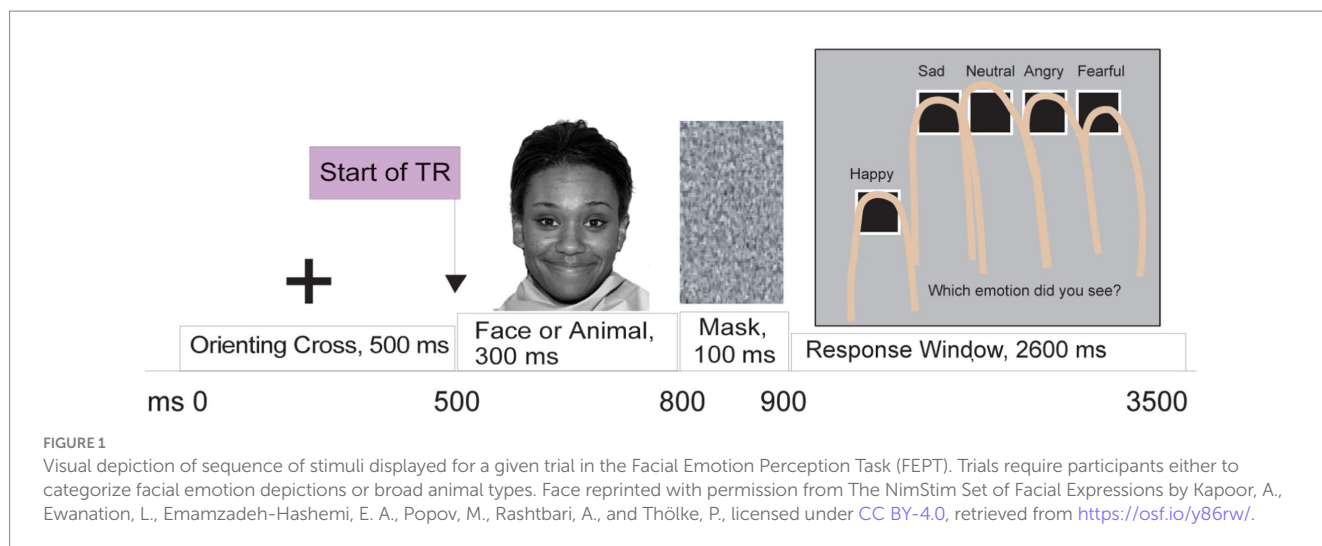
This task measures participants' accuracy in categorizing facial expressions (21, 22, 42–44), and can be used to detect biases in facial emotion perception. The task includes 5 runs of the FEPT while in the MRI, with each run lasting 260s and including 154 trials (see Figure 1). The FEPT has been described in detail elsewhere (21, 22) continues to use animals as a contrast, and uses the MacBrain Foundation Stimuli (45, 46).

Recent distress symptoms

A recent distress factor score was calculated (as a covariate of no interest) by performing a principal factor analysis (with regression factor) using the scores of the Beck Anxiety Inventory [BAI, (47) and the Beck Depression Inventory (BDI-II), (48, 49)]. These scales assess anxiety or depression symptoms in the past two weeks. These were combined because of a restriction of range due to selection criteria (i.e., in remission). Means for recent distress did not significantly differ between groups, as reported in Table 1.

Procedures

In their first visit, participants completed informed consent in accordance with the Declaration of Helsinki, as well as diagnostic interviews and questionnaires. MRI procedures were completed during a separate second visit. On the second visit, participants were given full instructions and completed a practice run of the task that uses the Ekman and Friesen face stimuli (50). While in the scanner, participants completed five runs of this task each lasting 4 min and 20s, for a total of 21 min and 20s. As described in detail elsewhere (22), the FEPT task requires participants to choose between five categorical choices regarding a facial emotion expression or animal groups. The current study focuses entirely on the facial emotion perception component. Briefly, participants are shown a cross for 500 ms before a face appears for 300 ms displaying one of five emotions (happy, sad, angry, fearful, or neutral), quickly followed by a resampled grayscale mask for 100 ms. Participants are then given 2,600 ms to



report which emotion was displayed, and are shown a screen indicating which finger corresponds to which emotion. The same button consistently represents the same emotion across all trials for each participant, but buttons are counterbalanced across participants. Participants are not given feedback post-response. The primary variables of interest for this study were the proportion of correctly identified emotional expressions for each emotion category. All participants received monetary compensation for their participation.

Neuroimaging

Neuroimaging data were collected in a 3 Tesla scanner (Signa at UM or Discover at UIC, General Electric, Milwaukee, WI). For each run of the FEPT, blood-oxygen level dependent (BOLD) images were collected at UM in 29 interleaved 4 mm slices with a TR of 2 s, resulting in a total of 126 volumes collected per run, and at UIC in 44 interleaved 3 mm slices with a TR of 2 s. The task was presented using E-Prime 2.0 displayed on a monitor outside the scanner, and participants responded to the task using a five-button response 'claw' (51). Please see [Appendix](#) for additional details.

Processing of neuroimaging data

MRI data were preprocessed using SPM8 (<https://www.fil.ion.ucl.ac.uk/spm/doc/>) and AFNI (52). fMRI data were slice-time corrected and realigned to the 10th volume in FSL (<http://fsl.fmrib.ox.ac.uk/fsl/fslwiki/>) using MCFLIRT (53). Next, FSL's Brain Extraction Tool was used to extract anatomical images, then SPM8 was used to co-register to functional images and normalize to Montreal Neurological Institute (MNI152) space. Smoothing was completed with a full width at half maximum kernel of 5 mm. First-level event-related models for each condition (fearful, angry, sad, happy, neutral correct responses) included deviations in translation and rotations along with first temporal derivative and square of parameters to estimate hemodynamic changes for each accurately categorized emotion aggregated over the multiple exposures (24–30 events for each emotion, only for correct responses).

Second-level brain activation models were created in SPM8 using a multiple regression model for each facial emotion category, with

total CTQ score as the predictor of interest. To control for the potential effects of diagnosis and concurrent symptoms on both neurobiology and trauma recall, diagnosis, recent distress, and the number of days between clinical symptom measurement and MRI were included as covariates of no interest. In addition, sex, site, and average x, y, and z movement deviation in the scanner were added to the second-level model as covariates of no interest. A restricted space was also applied to the model using a dilated gray matter mask, so that only gray matter structures would be considered. Results are displayed on the average brain from the first 55 participants enrolled in the study. Whole brain analyses indicated a significant effect of activation for the relation of CTQ and all five facial emotions in right middle frontal gyrus (MFG).

Post-hoc ROI analyses

To follow-up this effect in right MFG, we examined associations with all emotions and during rest, using one 8 mm radius spherical ROI center (MNI coordinates x, y, z = +40, +41, +32) in the right middle frontal gyrus (MFG), extracted with MarsBaR. A partial correlation to compare the associations was then performed on the extracted values for rMFG and each emotion and resting blocks.

Statistical analyses

Behavioral performance, demographic, and clinical data were analyzed using SPSS v26. There were two CTQ scores greater than three standard deviations from the mean, and these were truncated to three standard deviations from the mean (54). All FEPT variables demonstrated normality for skewness (± 2) and kurtosis (± 7), and all normality assumptions held. Pearson correlations were computed between accuracy of specific emotions and CTQ total score.

We also performed a partial correlation between CTQ total and the number of emotional face stimuli categorized in a certain way (e.g., number of neutral faces categorized as angry) while controlling for diagnosis (rMDD vs. HC), sex, site, and recent distress scores. Correlations were also run separately by diagnosis (HC and rMDD) to investigate specific effects of biases and childhood trauma within subgroups that might be distorted by known differences in emotion perception accuracy. Correlations that would survive false discovery

rate (FDR) adjustment (55) for multiple comparisons ($q=0.25$) are so noted.

Results

Performance and trauma results

The HC group demonstrated a significant inverse relation between CTQ scores and accurate identification of happy facial expressions ($r=-0.54$, $p=0.003$), in addition to a positive relation between CTQ and no response to happy faces ($r=0.38$, $p=0.04$, Table 2). This effect was not present in the rMDD group. CTQ scores were not significantly related to FEP accuracy across groups for any of the other four emotion categories. In regards to errors, across the whole sample there was a positive association between CTQ total scores and a negative affective bias for categorizing happy faces as angry (whole sample: $r=0.40$, $p=0.001$; HC: $r=0.50$, $p=0.006$; rMDD: $r=0.32$, $p=0.06$). Among the HC group only, heightened CTQ scores were associated with miscategorizing happy faces as fearful ($r=0.40$, $p=0.03$) and miscategorizing neutral faces as angry ($r=0.39$, $p=0.04$), though these effects did not persist after FDR corrections.

Neuroimaging results

Emotion-specific brain activation positively correlated with CTQ

In the whole sample at the whole brain level, we observed higher CTQ total scores significantly associated with greater activation in the inferior parietal cortex (happy), posterior cingulate (angry) the cingulate gyrus (fearful), and the lingual (fearful) gyrus for distinct parts of emotional expression contrasts (see Table 2). No contrasts had activation that was inversely correlated with CTQ scores. The right middle frontal gyrus had a positive correlation of CTQ scores with activation for angry, fearful, sad, and happy, neutral face contrasts, in slightly different but largely overlapping areas (see Figure 2).

MarsBaR ROI analysis for rMFG

Right MFG cluster activity in all emotion conditions other than neutral was significantly correlated with CTQ scores, as displayed in Figure 2, with peak activation near $X=38$ (see Table 3). Activation was positively correlated with CTQ scores for angry ($r=0.37$, $p<0.01$), fearful ($r=0.40$, $p<0.01$), happy ($r=0.30$, $p<0.05$), and sad ($r=0.29$, $p<0.05$) facial expressions. Figure 3 shows relations with other conditions (e.g., rest and neutral), which were not equivalent between HC and rMDD groups.

Discussion

The present study assessed FEP and negative affective bias via a forced-choice categorization paradigm of facial expressions among young adult participants with and without a history of MDD and varying levels of childhood trauma. We evaluated behavioral and neural response patterns for different facial emotions in relation to participants' extent of past childhood trauma across HC and rMDD groups. This study expands upon previous emotion processing research by investigating the relations between childhood trauma and functional activation responses to social-emotional cues, independent of past depression history.

We found that individuals who reported higher levels of childhood trauma (regardless of diagnosis) demonstrated greater right MFG activity (part of DLPFC) during valenced (as opposed to neutral) emotional faces. We also observed across all participants that higher exposure to childhood trauma was related to miscategorization of happy faces as angry. Follow-up tests determined that HC participants with elevated childhood trauma tended to miscategorize neutral faces as angry more often than HC who reported less childhood trauma. Surprisingly, our whole-brain analyses did not reveal a relation between past childhood trauma and activation in the sgACC or the amygdala during exposure to emotional stimuli, but rather within right middle frontal gyrus (8, 9, 11).

Our finding of dimensional relations between trauma and FEP across diagnostic categories are consistent with our prior work examining inhibitory control and trauma in healthy individuals and

TABLE 2 Peak MNI coordinates of brain regions with increased activation associated[§] with greater CTQ, independent of other factors.

Lobe	Region	Emotion	BA	x	y	z	Voxels* (k)	Peak Intensity (Z)
Frontal	Superior/Middle Frontal	Angry	9	38	42	34	51	3.2
		Fearful	9/10	44	40	28	71	3.27
		Happy	10	46	48	12	58	3.38
		Happy	9	28	44	38	128	3.53
		Neutral	9	38	34	42	10**	3.3
		Sad	9	40	40	32	15**	3.01
Limbic	Cingulate Gyrus	Fearful	31	14	-30	44	40	3.31
Occipital/ Limbic	Lingual Gyrus/Posterior Cingulate	Angry	18/19	10	-54	2	177	4.14
Parietal	Inferior Parietal	Happy	40	38	-54	40	106	3.15

Z-values are based upon peak intensity at MNI coordinates listed.

[§]No clusters were detected that show significantly lower activation with increasing CTQ at our voxel cutoff.

*Statistical threshold was set at a cutoff of $k=40$ voxels and $p=0.005$.

**For sad and neutral, cutoff was changed to $k=10$ voxels to accommodate relevant cluster and for transparency and comparison.

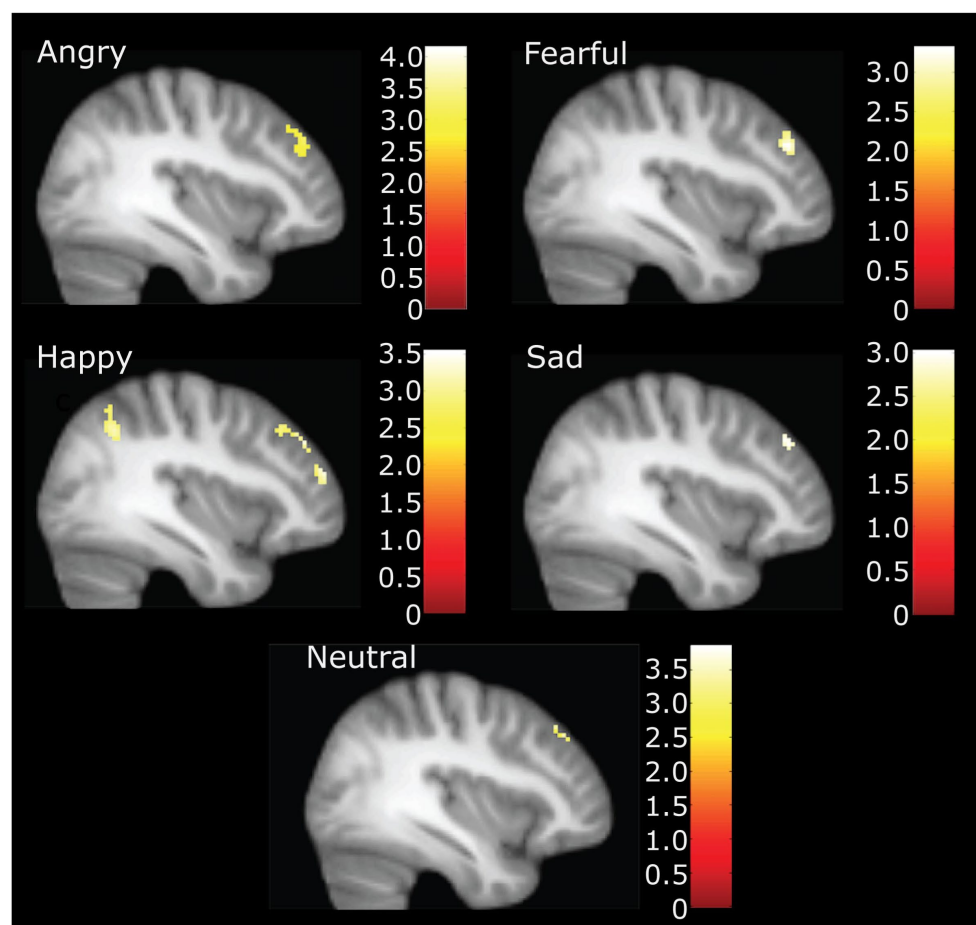


FIGURE 2

Neural activation during accurate categorization for angry, fearful, happy, sad and neutral emotions positively correlated with childhood trauma. Figure highlights right middle frontal gyrus activation at $X = 38$. Happy also demonstrates inferior parietal and other significant frontal clusters. Illustration only at $k = 40$ for angry, fearful, and happy. *For sad and neutral correlations, the voxel threshold was dropped to $k = 10$, $p = 0.005$ to display for comparison.

those with bipolar disorder (56). Additional research is needed to extrapolate potential long-term influences that different types of trauma may have on emotion processing in adulthood, and how these processes may vary across persons with different mental health diagnoses. For example, only longitudinal studies like the ABCD can infer the sequential relations of trauma to brain changes in key processes that may be the foundation for risk for psychopathology.

Our hypothesis, that individuals with more severe childhood trauma would more frequently miscategorize faces as fearful and angry, was partially supported. We found that higher childhood trauma severity was associated with misperceiving happy faces as angry, regardless of diagnostic history. It is possible that abuse and neglect may lead persons to conflate others' happiness and anger, because both emotions are associated with approach-related social behavior [e.g., (57)]. Prior research indicates that patterns of approach-avoidance behavior are associated with emotional valence evoked by environmental stimuli. Approach behaviors are typically linked to positive affect and can be associated with attack behaviors in the context of anger [e.g., (58)]. A further possibility is that a person engaging in abuse may appear happy while executing an angry response, which may cause the victim of abuse to link angry and happy emotions – particularly after repeated exposures (e.g., in cases

where the person engaging in abuse is also a caregiver or loved one). The human brain is also primed to recognize fear-relevant or threat-inducing stimuli like anger more readily than other cues (59), and such a predisposition could be triggered by trauma experiences. In fact, one study found that humans detect angry faces more readily than happy faces among a crowd of people (60).

We hypothesized that childhood trauma would be most strongly associated with anger and fear processing as manifested by heightened amygdala and blunted DLPFC activation, and we did not observe either of these patterns. Amygdala activation appears to have prominent state-dependent (including with active depression) and individual differences effects that can be ascribed to processes other than excessive childhood trauma exposure or trait-based effects of MDD (61–65). Another surprising finding was that results yielded a *positive* rather than *negative* relation between activation within the MFG and childhood trauma. This opposite pattern may be due to the current sample's *lack* of active mood symptoms, such that both blunted DLPFC activation and increased amygdala activation during FEP occurs only during an episode, with associated cognitive burden or loss of functioning. On the other hand, positive relations between activation in MFG and childhood trauma during accurate facial expression perception may demonstrate adaptive compensation or

TABLE 3 Partial Correlations between accuracy and emotion biases on the FEPT with Total Childhood Trauma (CTQ).

	ALL (<i>df</i> = 65)	HC (<i>df</i> = 28)	rMDD (<i>df</i> = 33)
<i>Accuracy</i>			
Neutral	−0.04	0.03	−0.08
Happy	0.05	−0.54***^	0.15
Angry	0.11	0.11	0.16
Fearful	0.03	0.07	−0.01
Sad	0.03	−0.22	0.01
<i>Biases (Errors)</i>			
Neutral as fearful	−0.11	−0.30	−0.15
Neutral as angry	−0.02	0.39*	−0.17
Neutral as happy	0.16	0.27	0.13
Neutral as sad	0.03	0.14	0.01
Neutral no response	0.01	0.13	0.07
Happy as neutral	0.05	0.21	−0.27
Happy as fearful	−0.03	0.40*	−0.14
Happy as angry	0.40***^	0.50***^	0.32
Happy as sad	0.21	0.17	0.26
Happy no response	−0.09	0.38*	−0.13

2 CTQ total scores were truncated at 3 SD. *df*, degrees of freedom, *df* were adjusted after covariates.

* $p \leq 0.05$, ** $p \leq 0.01$.

^Benjamini–Hochberg significance with FDR $q = 0.25$.

suppression of amygdala activation to emotionally salient stimuli. Indeed, Briceño et al. (66) found that those females with active MDD who shifted away from left DLPFC activation toward greater right DLPFC activation had greater emotion detection accuracy. We found that MFG activation was related to all emotionally valenced facial expressions as CTQ scores increased, rather than only fearful and angry faces. The presence of the same pattern, in both active and remitted MDD, could reflect a stable characteristic of trauma associated with brains. That is, activation within rMFG may be linked to how trauma history and emotionally salient stimuli are bound more generally, perhaps requiring more higher-order cognitive processing. While heightened MFG activation for emotional stimuli has been reported in those with active MDD (67–70), there is a paucity of studies of childhood trauma within the context of remitted MDD. Such studies are needed to dissociate whether activation patterns are related to trauma versus symptoms. It is possible that both childhood adversity and active depressive episodes result in elevated DLPFC activation and increased higher-order cognitive processing of emotional expressions, thereby a common pathway (67–70).

While neural results demonstrate group differences in brain activation and trauma histories on trials when participants *correctly* categorized the emotion of a facial expression, it is possible that interesting activation patterns related to childhood trauma may also present in the instances where participants *incorrectly* categorized a face. There was a surprising and interesting relationship where happy faces were more likely to be incorrectly labeled as angry in individuals with higher CTQ scores. Future studies could pursue this with longer versions of the test so that there would be enough errors to reliably model the BOLD signal for errors of different emotions.

A final consideration from this study is that neutral facial expression categorization and rest block conditions may not serve as adequate control condition(s) for FEP studies. Researchers often assume that neutral and rest block conditions capture “normative” activity that would be unrelated to trauma or disease. Many scientists use such designs to establish a baseline against which emotion evocation or FEP conditions can be compared to cancel out unrelated neural activation noise. Our results demonstrated that patterns of neural activation varied systematically with CTQ scores in *both* neutral facial expression trials and at rest (Figure 3). As such, using either neutral or rest block scans as a control condition (e.g., as part of a contrast between an emotion and neutral or rest) would have distorted and potentially hidden our current results with salient emotions. Moreover, our results suggest rest and neutral do not demonstrate activation equivalent relationships with childhood trauma that can be used interchangeably for creation of contrasts of interest. While a byproduct result of the current analyses, these results coalesce with others demonstrating significant differences in connectivity patterns at rest for individuals with childhood trauma [e.g., (71)]. Future studies would be best served by continuing to ensure equivalency in their control conditions across groups within their samples prior to examining contrast conditions.

Although this study design has several strengths, including investigation of childhood trauma in young adults while early in the course of recurrent MDD processes, limitations should be considered. First, we used a retrospective measure of childhood trauma, which may be influenced by environmental factors, symptoms, and poor recall, and therefore potentially limited in their validity (72, 73), although more recent studies suggest that these scores are stable over time in adulthood (74). We controlled for current symptoms through inclusion criteria (remission from depression) and inclusion of covariates diagnosis and recent distress in analyses, yet were unable to examine differential relations with adult trauma exposure. Prospective longitudinal studies, including adjustment for age of first trauma exposure, and measurement of adult traumas would more accurately probe relations between childhood trauma and emotion processing. Sample size and power to detect effects are long-standing difficulties in the field of neuroimaging; while the sample here was adequate to detect a main fixed effect of childhood trauma, the sample size was underpowered to detect emotion-related processing differences across diagnosis or trauma subscales. Analysis of specific types of abuse and neglect independently may reveal differential FEP and neurobiology, as each type is related to different outcomes [e.g., (75)]. A third limitation is that recent life traumas and stressors were not assessed. Future studies focused specifically on the developmental effects of childhood trauma should include a questionnaire to account for the potential influence of recent life stress and trauma occurring post-childhood. In future studies, scientists should recruit a larger sample of participants who have a wider range of childhood trauma severity.

Conclusion

Childhood trauma is a multifaceted developmental experience. Researchers should continue to study distal effects of trauma on social emotional processing in order to hone prevention efforts and better elucidate risk for interpersonal difficulties and adverse health outcomes, including risk for MDD. The present study provides

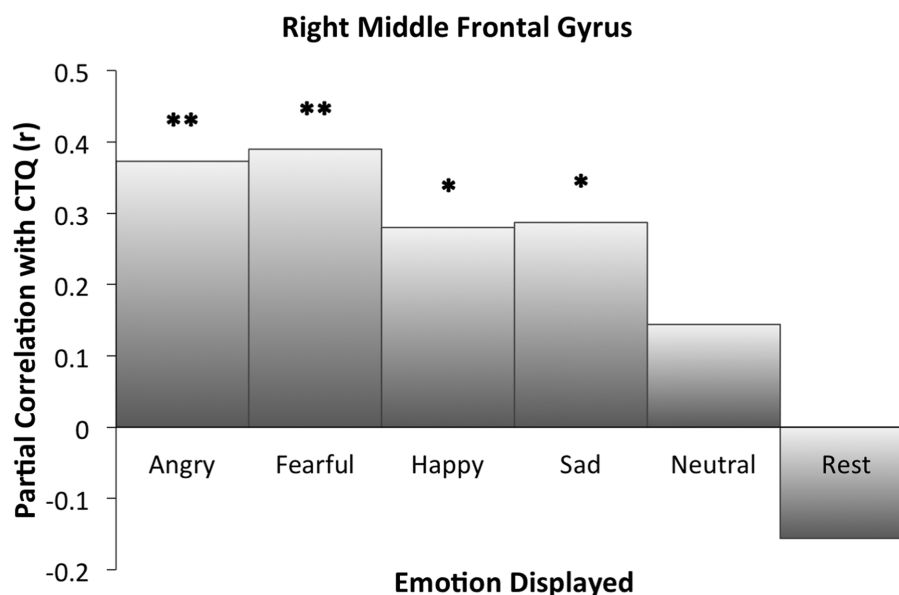


FIGURE 3

Right middle frontal gyrus activation partial correlations with childhood trauma (CTQ). Findings of the ROI analysis in an 8 mm cluster. Significant cluster activation differences occurred in relation to CTQ when correctly identifying angry, fearful, happy, and sad faces. For neutral and rest block conditions, CTQ was not significantly correlated with extracted activation within the cluster. *Indicates significant correlation between childhood trauma and activation for the specified condition. * $p \leq 0.05$. ** $p \leq 0.01$.

evidence that childhood trauma is related to emotion processing, categorization, and biased recognition accuracy as well as differing patterns of neural activation while engaged in emotion processing and categorization. Furthermore, some of these effects differed by individuals' experiences of prior episodes of depression. Additional research is needed to extrapolate potential long-term influences that different types of trauma may have on emotion processing in adulthood, and how these processes may vary across persons with different mental health diagnoses.

Data availability statement

The raw data supporting the conclusions of this article will be made available by the authors, without undue reservation.

Ethics statement

The studies involving human participants were reviewed and approved by University of Michigan (UM) and the University of Illinois at Chicago (UIC). The patients/participants provided their written informed consent to participate in this study. Written informed consent was obtained from the individual(s) for the publication of any identifiable images or data included in this article.

Author contributions

AR, KB, LJ, JS, KR, and SL: conceptualization. AR, KB, and SL: data curation. AR, KB, LJ, JS, and SL: formal analysis and writing – original draft. AR, EK, and SL: funding acquisition. AR, KS, LG, LK,

and SL: investigation. AR, LG, LK, KR, MS, EK, SC, and SL: methodology. KB, KS, LG, LK, and SL: project administration. KR and SL: resources and software. KB, LG, LK, and SL: supervision. KB, MS, EK, SC, and SL: validation. KB, LJ, and SL: visualization. AR, KB, LJ, KS, LG, LK, JS, KR, MS, EK, SC, and SL: writing – review and editing. All authors contributed to the article and approved the submitted version.

Funding

This funding was provided by the National Institute of Mental Health (NIMH), R01 MH091811: Identification of Neurobiological Intermediate Phenotypes in Major Depressive Disorder (MINDS), 07/17/2015, SL and JS was supported by grant 1K23MH112769-01A1 from NIMH. KB was supported by an F31 (MH117856).

Conflict of interest

The authors declare that the research was conducted in the absence of any commercial or financial relationships that could be construed as a potential conflict of interest.

Publisher's note

All claims expressed in this article are solely those of the authors and do not necessarily represent those of their affiliated organizations, or those of the publisher, the editors and the reviewers. Any product that may be evaluated in this article, or claim that may be made by its manufacturer, is not guaranteed or endorsed by the publisher.

References

- Hoppen TH, Chalder T. Childhood adversity as a transdiagnostic risk factor for affective disorders in adulthood: a systematic review focusing on biopsychosocial moderating and mediating variables. *Clin Psychol Rev.* (2018) 65:81–1. doi: 10.1016/j.cpr.2018.08.002
- Watters ER, Aloe AM, Wojciak AS. Examining the associations between childhood trauma, resilience, and depression: a multivariate Meta-analysis. *Trauma Violence Abuse.* (2023) 24:231–4. doi: 10.1177/15248380211029397
- Besette KL, Karstens AJ, Crane NA, Peters AT, Stange JP, Elverman KH, et al. A lifespan model of interference resolution and inhibitory control: risk for depression and changes with illness progression. *Neuropsychol Rev.* (2003) 30:477–8. doi: 10.1007/s11065-019-09424-5
- Nagy SA, Kurtos Z, Nemeth N, Perlaki G, Csernel E, Lakner FE, et al. Childhood maltreatment results in altered deactivation of reward processing circuits in depressed patients: a functional magnetic resonance imaging study of a facial emotion recognition task. *Neurobiol Stress.* (2021) 15:100399. doi: 10.1016/j.ynstr.2021.100399
- Demers LA, Hunt RH, Cicchetti D, Cohen-Gilbert JE, Rogosch FA, Toth SL, et al. Impact of childhood maltreatment and resilience on behavioral and neural patterns of inhibitory control during emotional distraction. *Dev Psychopathol.* (2022) 34:1260–71. doi: 10.1017/S0954579421000055
- Demers LA, Mckenzie KJ, Hunt RH, Cicchetti D, Cowell RA, Rogosch FA, et al. Separable effects of childhood maltreatment and adult adaptive functioning on amygdala connectivity during emotion processing. *Biol Psych Cogn Neurosci Neuroimaging.* (2018) 3:116–4. doi: 10.1016/j.bpsc.2017.08.010
- Hart H, Rubia K. Neuroimaging of child abuse: a critical review. *Front Hum Neurosci.* (2012) 6:52. doi: 10.3389/fnhum.2012.00052
- Marusak HA, Martin KR, Etkin A, Thomason ME. Childhood trauma exposure disrupts the automatic regulation of emotional processing. *Neuropsychopharmacology.* (2015) 40:1250–8. doi: 10.1038/npp.2014.311
- Philip NS, Sweet LH, Tyrka AR, Carpenter SL, Albright SE, Price LH, et al. Exposure to childhood trauma is associated with altered n-back activation and performance in healthy adults: implications for a commonly used working memory task. *Brain Imaging Behav.* (2016) 10:124–5. doi: 10.1007/s11682-015-9373-9
- Schulze L, Schulze A, Renneberg B, Schmahl C, Niedtfeld I. Neural correlates of affective disturbances: a comparative Meta-analysis of negative affect processing in borderline personality disorder, major depressive disorder, and posttraumatic stress disorder. *Biol Psychiatry Cogn Neurosci Neuroimaging.* (2019) 4:220–2. doi: 10.1016/j.bpsc.2018.11.004
- Stuhrmann A, Suslow T, Dannowski U. Facial emotion processing in major depression: a systematic review of neuroimaging findings. *Biol Mood Anxiety Disord.* (2011) 1:10. doi: 10.1186/2045-5380-1-10
- Antypa N, Cerit H, Kruijt AW, Verhoeven FE, Van Der Does AJ. Relationships among 5-HTT genotype, life events and gender in the recognition of facial emotions. *Neuroscience.* (2011) 172:303–3. doi: 10.1016/j.neuroscience.2010.10.042
- Dargis M, Newman J. Altered emotion modulated startle in women with a history of childhood neglect. *Personal Individ Differ.* (2016) 89:187–1. doi: 10.1016/j.paid.2015.10.014
- Nicol K, Pope M, Hall J. Facial emotion recognition in borderline personality: an association, with childhood experience. *Psychiatry Res.* (2014) 218:256–8. doi: 10.1016/j.psychres.2014.04.017
- Russo M, Mahon K, Shanahan M, Solon C, Ramjas E, Turpin J, et al. The association between childhood trauma and facial emotion recognition in adults with bipolar disorder. *Psychiatry Res.* (2015) 229:771–6. doi: 10.1016/j.psychres.2015.08.004
- Young JC, Widom CS. Long-term effects of child abuse and neglect on emotion processing in adulthood. *Child Abuse Negl.* (2014) 38:1369–81. doi: 10.1016/j.chiabu.2014.03.008
- Kessler R, Schmitt S, Sauder T, Stein F, Yuksel D, Grotegerd D, et al. Long-term neuroanatomical consequences of childhood maltreatment: reduced amygdala inhibition by medial prefrontal cortex. *Front Syst Neurosci.* (2020) 14:28. doi: 10.3389/fnsys.2020.00028
- Van Harmelen AL, Van Tol MJ, Demenescu LR, Van Der Wee NJ, Veltman DJ, Aleman A, et al. Enhanced amygdala reactivity to emotional faces in adults reporting childhood emotional maltreatment. *Soc Cogn Affect Neurosci.* (2013) 8:362–9. doi: 10.1093/scan/nss007
- Saariainen A, Keltikangas-Jarvinen L, Jaaskelainen E, Huhtaniska S, Pudas J, Tovar-Perdomo S, et al. Early adversity and emotion processing from faces: a meta-analysis on behavioral and neurophysiological responses. *Biol Psychiatry Cogn Neurosci Neuroimaging.* (2021) 6:692–5. doi: 10.1016/j.bpsc.2021.01.002
- Romund L, Raufelder D, Flemming E, Lorenz RC, Pelz P, Gleich T, et al. Maternal parenting behavior and emotion processing in adolescents-an fMRI study. *Biol Psychol.* (2016) 120:120–5. doi: 10.1016/j.biopsycho.2016.09.003
- Langenecker SA, Bieliauskas LA, Rapport LJ, Zubieta JK, Wilde EA, Berent S. Face emotion perception and executive functioning deficits in depression. *J Clin Exp Neuropsychol.* (2005) 27:320–3. doi: 10.1080/13803390490515720
- Jenkins L, Kassel M, Gabriel L, Gowins JR, Hymen E, Verges A, et al. Amygdala and dorsomedial activity during facial emotion processing in youth with remitted major depression. *Soc Cogn Affect Neurosci.* (2016) 11:736–5. doi: 10.1093/scan/nsv152
- Kohler CG, Hoffman LJ, Eastman LB, Healey K, Moberg PJ. Facial emotion perception in depression and bipolar disorder: a quantitative review. *Psychiatry Res.* (2011) 188:303–9. doi: 10.1016/j.psychres.2011.04.019
- Langenecker SA, Jacobs RH, Passarotti AM. Current neural and behavioral dimensional constructs across mood disorders. *Curr Behav Neurosci Rep.* (2014) 1:144–3. doi: 10.1007/s40473-014-0018-x
- Brown A, Bennet J, Rapee RM, Hirshfeld-Becker DR, Bayer JK. Exploring the stress sensitization theory with temperamentally inhibited children: a population-based study. *BMC Pediatr.* (2020) 20:264. doi: 10.1186/s12887-020-02159-w
- Bouhuys AL, Geerts E, Mersch PP, Jenner JA. Nonverbal interpersonal sensitivity and persistence of depression: perception of emotions in schematic faces. *Psychiatry Res.* (1999) 64:193–3. doi: 10.1016/S0165-1781(96)02930-7
- Joormann J, Gotlib IH. Selective attention to emotional faces following recovery from depression. *J Abnorm Psychol.* (2007) 116:80–5. doi: 10.1037/0021-843X.116.1.80
- Bodenschatz CM, Skopinceva M, Russ T, Suslow T. Attentional bias and childhood maltreatment in clinical depression - an eye-tracking study. *J Psychiatr Res.* (2019) 112:83–8. doi: 10.1016/j.jpsychires.2019.02.025
- Dalili MN, Penton-Voak IS, Harmer CJ, Munafò MR. Meta-analysis of emotion recognition deficits in major depressive disorder. *Psychol Med.* (2015) 45:1135–44. doi: 10.1017/S0033291714002591
- Leppanen JM. Emotional information processing in mood disorders: a review of behavioral and neuroimaging findings. *Curr Opin Psychiatry.* (2006) 19:34–9. doi: 10.1097/01.yco.0000191500.46411.00
- Bhagwagar Z, Cowen PJ, Goodwin GM, Harmer CJ. Normalization of enhanced fear recognition by acute SSRI treatment in subjects with a previous history of depression. *Am J Psychiatry.* (2003) 161:166–8. doi: 10.1176/appi.ajp.161.1.166
- Bouhuys AL, Geerts E, Gordijn MCM. Depressed patients' perceptions of facial emotions in depressed and remitted states are associated with relapse: a longitudinal study. *J Nerv Ment Dis.* (1999) 187:595–2. doi: 10.1097/00005053-199910000-00002
- Gibb BE, Benas JS, Grassia M, Mcgeary J. Children's attentional biases and 5-HTTLPR genotype: potential mechanisms linking mother and child depression. *J Clin Child Adolesc Psychol.* (2009) 38:415–6. doi: 10.1080/15374410902851705
- Dearing KF, Gotlib IH. Interpretation of ambiguous information in girls at risk for depression. *J Abnorm Child Psychol.* (2009) 37:79–91. doi: 10.1007/s10802-008-9259-z
- Platt B, Cohen Kadosh K, Lau JY. The role of peer rejection in adolescent depression. *Depress Anxiety.* (2013) 30:809–1. doi: 10.1002/da.22120
- Cerny BM, Stange JP, Kling LR, Hamlat EJ, O'donnell LA, Deveney C, et al. Self-reported affective biases, but not all affective performance biases, are present in depression remission. *Br J Clin Psychol.* (2019) 58:274–8. doi: 10.1111/bjc.12217
- Nurnberger JI, Blehar MC, Kaufmann CA, York-Cooler C, Simpson SG, Harkavy-Friedman J, et al. Diagnostic interview for genetic studies. Rationale, unique features, and training. *NIMH Genet Initiat ArchGenPsychiatry.* (1994) 51:849–9. doi: 10.1001/archpsyc.1994.03950110009002
- Bernstein DP, Ahluwalia T, Pogge D, Handelsman L. Validity of the childhood trauma questionnaire in an adolescent psychiatric population. *J Am Acad Child Adolesc Psychiatry.* (1997) 36:340–8. doi: 10.1097/00004583-199703000-00012
- Scher CD, Stein MB, Asmundson GJ, McCreary DR, Forde DR. The childhood trauma questionnaire in a community sample: psychometric properties and normative data. *J Trauma Stress.* (2001) 14:843–7. doi: 10.1023/A:1013058625719
- Bernstein DP, Stein JA, Newcomb MD, Walker E, Pogge D, Ahluwalia T, et al. Childhood trauma questionnaire--short form. *Child Abuse Negl.* (2003) 27:169–0.
- Walker EA, Gelfand A, Katon WJ, Koss MP, Von Korff M, Bernstein D, et al. Adult health status of women with histories of childhood abuse and neglect. *Am J Med.* 107:332–9. doi: 10.1016/S0002-9343(99)00235-1
- Briceno EM, Rapport LJ, Kassel MT, Bieliauskas LA, Zubieta JK, Weisenbach SL, et al. Age and gender modulate the neural circuitry supporting facial emotion processing in adults with major depressive disorder. *Am J Geriatr Psychiatry.* (2015) 23:304–3. doi: 10.1016/j.jagp.2014.05.007
- Langenecker SA, Caveney AF, Giordani B, Young EA, Nielson KA, Rapport LJ, et al. The sensitivity and psychometric properties of a brief computer-based cognitive screening battery in a depression clinic. *Psychiatry Res.* (2007) 152:143–4. doi: 10.1016/j.psychres.2006.03.019
- Weisenbach SL, Rapport LJ, Briceno EM, Haase BD, Vederman AC, et al. Reduced emotion processing efficiency in healthy males relative to females. *Soc Cogn Affect Neurosci.* (2014) 9:316–5. doi: 10.1093/scan/nss137
- Jenkins LM, Kendall AD, Kassel MT, Patron VG, Gowins JR, Dion C, et al. Considering sex differences clarifies the effects of depression on facial emotion processing during fMRI. *J Affect Disord.* (2018) 225:129–6. doi: 10.1016/j.jad.2017.08.027

46. Tottenham N, Tanaka JW, Leon AC, McCarry T, Nurse M, Hare TA, et al. The NimStim set of facial expressions: judgments from untrained research participants. *Psychiatry Res.* (2009) 168:242–9. doi: 10.1016/j.psychres.2008.05.006
47. Beck AT, Epstein N, Brown G, Steer RA. An inventory for measuring clinical anxiety: psychometric properties. *J Consult Clin Psychol.* (1988) 56:893–7. doi: 10.1037/0022-006X.56.6.893
48. Beck AT, Steer RA, Brown GK. Beck depression inventory-II. *J San Antonio.* (1996a) 78:490–8.
49. Beck AT, Steer RA, Brown GK. *Manual for the Beck depression inventory - II.* Agra: Psychological Corporation (1996b).
50. Ekman P, Friesen . *Pictures of facial affect.* Palo Alto, CA: C.P. Press (1976).
51. Psychology Software Tools, I. (2007). E-Prime 2.0. Pittsburgh, PA.
52. Cox RW. AFNI: software for analysis and visualization of functional magnetic resonance neuroimages. *Comput Biomed Res.* (1996) 29:162–3. doi: 10.1006/cbmr.1996.0014
53. Jenkinson M, Bannister P, Brady M, Smith S. Improved optimization for the robust and accurate linear registration and motion correction of brain images. *NeuroImage.* (2002) 17:825–1. doi: 10.1006/nimg.2002.1132
54. Tabachnick B, Fidell L. *Using multivariate statistics.* Boston, MA: Pearson Education (2007).
55. Benjamini Y, Hochberg Y. Controlling the false discovery rate: a practical and powerful approach to multiple testing. *J R Stat Soc Ser B Methodol.* (1995) 57:289–0. doi: 10.1111/j.2517-6161.1995.tb02031.x
56. Marshall DF, Passarotti AM, Ryan KA, Kamali M, Saunders EFH, Pester B, et al. Deficient inhibitory control as an outcome of childhood trauma. *Psychiatry Res.* (2016) 235:7–12. doi: 10.1016/j.psychres.2015.12.013
57. Harmon-Jones C, Schmeichel BJ, Mennitt E, Harmon-Jones E. The expression of determination: similarities between anger and approach-related positive affect. *J Pers Soc Psychol.* (2011) 100:172–1. doi: 10.1037/a0020966
58. Lang PJ, Bradley MM. Emotion and the motivational brain. *Biol Psychol.* (2010) 84:437–0. doi: 10.1016/j.biopsycho.2009.10.007
59. Fox E, Lester V, Russo R, Bowles RJ, Pichler A, Dutton K. Facial expressions of emotion: are angry faces detected more efficiently? *Cogn Emot.* (2000) 14:61–92. doi: 10.1080/026999300378996
60. Hansen CH, Hansen RD. Finding the face in the crowd: an anger superiority effect. *J Pers Soc Psychol.* (1988) 54:917–4. doi: 10.1037/0022-3514.54.6.917
61. Gerber AJ, Posner J, Gorman D, Colibazzi T, Yu S, Wang Z, et al. An affective circumplex model of neural systems subserving valence, arousal, and cognitive overlay during the appraisal of emotional faces. *Neuropsychologia.* (2008) 46:2129–39. doi: 10.1016/j.neuropsychologia.2008.02.032
62. Olsavsky AK, Brotman MA, Rutenber JG, Muhrer EJ, Deveney CM, Fromm SJ, et al. Amygdala hyperactivation during face emotion processing in unaffected youth at risk for bipolar disorder. *J Am Acad Child Adolesc Psychiatry.* (2012) 51:294–3. doi: 10.1016/j.jaac.2011.12.008
63. Phan KL, Fitzgerald DA, Nathan PJ, Tancer ME. Association between amygdala hyperactivity to harsh faces and severity of social anxiety in generalized social phobia. *Biol Psychiatry.* (2006) 59:424–9. doi: 10.1016/j.biopsych.2005.08.012
64. Taylor SF, Kang J, Bregge IS, Tso IF, Hosanagar A, Johnson TD. Meta-analysis of functional neuroimaging studies of emotion perception and experience in schizophrenia. *Biol Psychiatry.* (2012) 71:136–5. doi: 10.1016/j.biopsych.2011.09.007
65. Weldon AL, Hagan M, Van Meter A, Jacobs RH, Kassel M, Hazlett KE, et al. Stress response to the functional magnetic resonance imaging environment in healthy adults relates to the degree of limbic reactivity during emotion processing. *Neuropsychobiology.* (2015) 71:85–96. doi: 10.1159/000369027
66. Briceno EM, Weisenbach SL, Rapport LJ, Hazlett EA, Bieliauskas LA, Haase BD, et al. Shifted laterality in inferior frontal activation during emotion processing in women with major depressive disorder. *Psychol Med.* (2013)
67. Lawrence NS, Williams AM, Surguladze S, Giampietro V, Brammer MJ, Andrew C, et al. Subcortical and ventral prefrontal cortical neural responses to facial expressions distinguish patients with bipolar disorder and major depression. *Biol Psychiatry.* (2004) 55:578–7. doi: 10.1016/j.biopsych.2003.11.017
68. Sheline YI, Barch DM, Donnelly J, Ollinger J, Snyder AZ, Mintun MA. Increased amygdala response to masked emotional faces in depressed subjects resolves with antidepressant treatment: an fMRI study. *Biol Psychiatry.* (2001) 50:651–8. doi: 10.1016/S0006-3223(01)01263-X
69. Struyker Boudier H, Teppema L, Cools A, Van Rossum J. (3,4-Dihydroxy-phenylamino)-2-imidazoline (DPI), a new potent agonist at dopamine receptors mediating neuronal inhibition. *J Pharm Pharmacol.* (1975) 27:882–3. doi: 10.1111/j.2042-7158.1975.tb10240.x
70. Surguladze SA, Young AW, Senior C, Brebion G, Travis MJ, Phillips ML. Recognition accuracy and response bias to happy and sad facial expressions in patients with major depression. *Neuropsychology.* (2004) 18:212–8. doi: 10.1037/0894-4105.18.2.212
71. Quinn ME, Stange JP, Jenkins LM, Corwin S, Deldonno SR, Bessette KL, et al. Cognitive control and network disruption in remitted depression: a correlate of childhood adversity. *Soc Cogn Affect Neurosci.* (2018) 13:1081–90. doi: 10.1093/scan/nsy077
72. Hardt J, Rutter M. Validity of adult retrospective reports of adverse childhood experiences: review of the evidence. *J Child Psychol Psychiatry.* (2004) 45:260–3. doi: 10.1111/j.1469-7610.2004.00218.x
73. Widom CS, Raphael KG, Dumont KA. The case for prospective longitudinal studies in child maltreatment research: commentary on Dube, Williamson, Thompson, Felitti, and Anda (2004). *Child Abuse Negl.* (2004) 28:715–2. doi: 10.1016/j.chiabu.2004.03.009
74. Wang X, Ding F, Cheng C, He J, Wang X, Yao S. Psychometric properties and measurement invariance of the childhood trauma questionnaire (short form) across genders, time points and presence of major depressive disorder among Chinese adolescents. *Front Psychol.* (2022) 13:816051. doi: 10.3389/fpsyg.2022.816051
75. Hildyard KL, Wolfe DA. Child neglect: developmental issues and outcomes. *Child Abuse Negl.* (2002) 26:679–5. doi: 10.1016/S0145-2134(02)00341-1

Appendix

Exclusions from current analysis

133 participants were enrolled in the study, yet two were excluded from data collection due to symptoms of schizophrenia or schizotypal disorder. In addition following the collection of data, 60 participants who had participated in the study were excluded from the current analysis for the following reasons: not scanned or fMRI data was unusable (61), excessive head movement during FEPT (31), incomplete or missing questionnaires – study dropout (52), Hamilton Depression Rating (HDRS) score above 7 indicating active depression (40), and conversion to active depressed or bipolar during study timeline (47) software for analysis and visualization of functional magnetic).

Scanner acquisition details

The UM scanner was a 3T Signa (release VH3, General Electric, USA) and used a reverse spiral sequence to acquire 36 slices 3.5 mm thick. The image matrix was 64 x 64 over a 22 cm field of view (FOV) for a 3.44 x 3.44 voxel. TR = 2000 ms, TE = 30 ms. Additionally, 116 high-resolution T1 spoiled gradient echo (SPGR) slices were collected for co-registration purposes, with slice thickness = 1.2 mm, field of view = 26cm, matrix size = 256 x 256.

The UIC scanner was a 3T GE Discovery and acquired images with a gradient-echo axial echo-planar imaging sequence. The image matrix was 64 x 64 over a 22 cm FOV with 3mm slice thickness (0 gap) for a 3.44 x 3.44 voxel. TR = 2000ms, TE = minFul (22.2ms), 90° flip, 44 slices (ascending, interleaved). The 4 initial scans were discarded, resulting in 126 volumes for each of five runs, each lasting 4 minutes 20 seconds. The anatomical scan was a T1SPGR echo, with a 22 cm FOV, 256 x 256 matrix size, 1 mm slice thickness, for a 0.86 x 0.86 voxel size, including 182 slices during a scan time of around 4 minutes.

Frontiers in Psychiatry

Explores and communicates innovation in the field of psychiatry to improve patient outcomes

The third most-cited journal in its field, using translational approaches to improve therapeutic options for mental illness, communicate progress to clinicians and researchers, and consequently to improve patient treatment outcomes.

Discover the latest Research Topics

[See more →](#)

Frontiers

Avenue du Tribunal-Fédéral 34
1005 Lausanne, Switzerland
frontiersin.org

Contact us

+41 (0)21 510 17 00
frontiersin.org/about/contact

